The Dissertation Committee for Bethany Margaret Neilson Certifies that this is the approved version of the following dissertation:

Photoswitching the Donating and Catalytic Properties of N-Heterocyclic Carbenes and the Design of Functional Co-Polymers for Stabilization of Iron Oxide Nanoparticles

Committee:

Christopher W. Bielawski, Supervisor

Keith P. Johnston

C. Grant Willson

Jennifer S. Brodbelt

Jonathan L. Sessler

Photoswitching the Donating and Catalytic Properties of N-Heterocyclic Carbenes and the Design of Functional Co-Polymers for Stabilization of Iron Oxide Nanoparticles

by

Bethany Margaret Neilson, B. S.

Dissertation

Presented to the Faculty of the Graduate School of

The University of Texas at Austin

in Partial Fulfillment

of the Requirements

for the Degree of

Doctor of Philosophy

The University of Texas at Austin

May 2013

Dedication

For my first and favorite chemistry teachers, Bob and Patty Neilson.

Acknowledgements

First and foremost I would like to thank my advisor, Prof. Chris Bielawski, for finding a place for me in his outstanding research group. I am extremely grateful for his commitment and enthusiasm, during both the exciting and the tough times in science.

I am also extremely grateful to all the members of the Bielawski group, both past and present, for their help and support, and for making the lab a great place to spend a lot of time. I give special thanks to Dan Dreyer and Jon Moerdyk for all of the helpful discussions and their willingness to share their chemistry knowledge. I'd especially like to thank Kelly Wiggins for being there during the entire roller coaster of grad school. Finally, a special thanks goes to Aaron Teator for being brave enough to take on the photoswitchable catalysis project.

I also acknowledge and thank my collaborators and co-authors. Specifically I thank Prof. Keith Johnston for the opportunity to be a part of a truly remarkable collaboration. Thanks goes to the members of his group with whom I have worked over the past few years: Ki Youl Yoon, Hitesh Bagaria, Andrew Worthen, and Eric Zheng. I need to also thank Melinda Jue, the undergraduate student who has worked closely with me on this project over the past year.

Apart from the members of the Bielawski and Johnston groups, I am extremely grateful to Prof. Grant Willson and his research group, especially Ryan Deschner, for allowing me to spend several months using the photolysis equipment in their labs. Without their help, and a lot of Ryan's patience, I don't know how I would have learned any of the experimental photochemistry in this dissertation.

Before coming to UT, my path to a Ph.D. in chemistry was influenced by several people who deserve special thanks. The first is Paul Price, my high school chemistry teacher, who introduced me to the fun and frustrating challenges chemistry can provide, and who, even long after I left his classroom, has always managed to be available whenever there's a problem. I would also like to thank my second semester organic professor, Dr. Holly Sebahar, whose enthusiasm made it impossible not to love organic chemistry. I also thank Prof. Stephen Craig for being a wonderful and inspiring undergraduate research advisor, and for introducing me to the excitement of doing research at an extremely high academic level.

Most importantly, I am extremely thankful to my parents, Bob and Patty Neilson, for passing along their passion and talent for chemistry, while never forcing me in that direction. They have multi-tasked to play the roles of supplemental research advisors, counselors, and supportive parents in a way that I don't think anyone else could have successfully done. I also thank my brother, Andy Neilson, for all of his support and wise insights. I would truly not be the chemist or the person that I am without my family's advice and support, and I am extremely proud to become the fourth Neilson Ph.D. chemist!

I am also extremely grateful for all of the friends I have made during my time in Austin who have played a huge role in keeping me sane, especially Kelly Wiggins and Kate Crawford.

Finally, I thank John DeLorbe for his unwavering support and patience, and for being a constant reminder of my ultimate goals.

Photoswitching the Donating and Catalytic Properties of N-Heterocyclic Carbenes and the Design of Functional Co-Polymers for Stabilization of Iron Oxide Nanoparticles

Bethany Margaret Neilson, Ph.D.

The University of Texas at Austin, 2013

Supervisor: Christopher W. Bielawski

In an effort to develop broadly applicable photoswitchable catalysts, we have reported a method for modulating N-heterocyclic carbene (NHC) donicity using light by incorporating a photochromic diarylethene (DAE) into the backbone of a NHC scaffold. UV irradiation of 4,5-dithienylimidazolone or an analogous NHC-Ir$(CO)_2$Cl complex effected a photocyclization between the two thiophene rings, which led to a change in the electron donating ability of the NHC scaffold. Subsequent exposure to visible light reversed the photocyclization reaction. The concept of photo-modulating NHC donicity in this manner enabled photoswitchable NHC organocatalysis. The catalytic activity of a DAE-annulated imidazolium pre-catalyst in transesterification and amidation reactions was successfully switched between the active and nearly inactive states (k_{vis}/k_{UV} = 100) upon alternate UV (λ_{irr} = 313 nm) or visible (λ_{irr} > 500 nm) irradiation. The photoswitchable NHC organocatalysis was later extended to facilitating ring-opening polymerizations of cyclic esters, the rates of which were controlled via external light stimuli. Additionally, a photochromic dithienylethene-annulated N-heterocyclic carbene (NHC)-Rh(I) complex was synthesized and enabled photoswitching of the catalytic activity in series of hydroboration reactions. All of the examples demonstrate extremely

rare instances of photomodulating a catalyst's activity by tuning its electronic properties. Furthermore, by taking advantage of the versatility of NHCs in both organo- and organometallic catalysis, we have developed novel photoswitchable catalysts for a variety of applicable transformations.

Nanoparticles that can be transported in subsurface reservoirs at high salinities and temperatures are expected to have a major impact on enhanced oil recovery and electromagnetic imaging. We have developed an approach that will facilitate nanopaticle transport through porous media at high salinity by adsorbing or grafting rationally designed co-polymers on platform nanoparticles. Notably, co-polymers of acrylic acid with either 2-acrylamido-2-methylpropanesulfonate or styrenesulfonate have been electrostatically adsorbed or covalently grafted onto iron oxide nanoclusters. The presence of sulfonate groups on the iron oxide surface enabled long-term colloidal stability of the particles in extremely concentrated brine (8% wt. NaCl + 2% wt. $CaCl_2$) at elevated temperatures (90 °C) and minimized their adsorption on model mineral surfaces.

Table of Contents

List of Tables

List of Figures

PHOTOSWITCHING THE DONATING AND CATALYTIC PROPERTIES OF N-HETEROCYCLIC CARBENES

Chapter 1: Photoswitchable Catalysis

1.1 INTRODUCTION

In nature the essential functions of living organisms are controlled to an exceptional degree by functional molecular units that undergo changes triggered by external stimuli. The pursuit of similarly modular synthetic molecules that can alter their properties in response to external stimuli is an ongoing area of research, as such systems are expected to enable enhanced control over molecular structure and function. From a synthetic chemist's perspective, the ability to amplify the effect of an external stimulus via incorporation into a catalytic cycle is quite attractive because it would allow an impressive level of control over catalytic function. A number of external stimuli, including acid-base chemistry,[1] mechanical force,[2] redox processes,[3] and light[4] have been utilized in recent years to actively modulate catalytic activity and selectivity.[5] Of these, one of the most powerful and accessible stimuli available is light, as it is non-invasive, offers excellent temporal and spatial resolution, and can be precisely controlled with an appropriate source. Furthermore, using light of carefully chosen wavelengths allows for selective excitation of specific molecular units, resulting in precise reactivity.

Examples of photo-responsive processes in nature, including photosynthesis and vision, clearly illustrate the power of electromagnetic radiation to initiate and regulate complex molecular and biochemical processes. Such examples underscore the need to develop synthetic catalyst systems that can respond to light with similar precision. A number of conceptually different approaches may be used to realize such artificial light-gated systems, including photocatalysis, photoactivated catalysis, and photoswitchable

catalysis. In the process of photocatalysis,[6] an inactive catalyst species is irradiated to generate a photoexcited state which subsequently reacts with a substrate due to its increased energy content (Figure 1.1a). The reaction of the catalyst directly from its photo-excited state[7] is commonly a photo-induced electron transfer step. Another approach is photoactivated or "photocaged" catalysis, in which an inactive catalyst species undergoes a photochemical transformation that endows it with catalytic activity (Figure 1.1b). Notable examples of photoactivated catalysis include photoacid and photobase generators,[8] and metal complexes that may be activated by the dissociation of photolabile ligands.[9,10] In contrast to the two aforementioned concepts, photoswitchable catalysis involves a catalytic species that undergoes a reversible photochemical transformation that alters its instrinsic catalytic ability (Figure 1.1c). The catalyst in its initial state may be active or inactive and the photoinduced transformation may either change the rate at which the catalyst facilitates a given reaction ($A \rightarrow B$; $k_1 \neq k_2$), or may allow the catalyst to promote an orthogonal reaction ($C \rightarrow D$; Figure 1.1c). If the forward and reverse transformations are induced by orthogonal stimuli, i.e. different wavelengths of light, the result is a catalyst that may be toggled between two forms having different reactivities or selectivies via a remote light stimulus. While more difficult to realize, photoswitchable catalysis offers distinct advantages over photocatalysis or photoactivated catalysis, since it offers an additional level of control over the catalytic process.

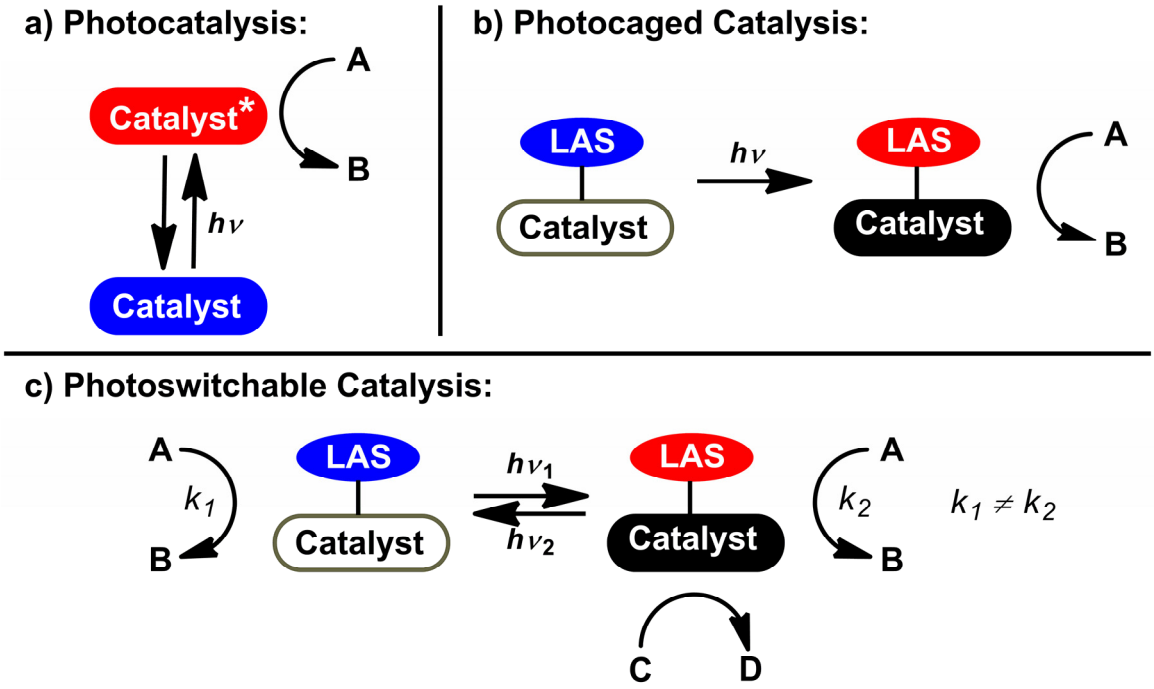

Figure 1.1: Representation of varied approaches to light-mediated catalysis: (a) Photocatalysis involves the reaction of a catalytic species directly from its photoexcited state. (b) In photoactivated catalysis an inactive catalyst species undergoes a photochemical transformation to an active form. (c) Photoswitchable catalysis involves a reversible photochemical transformation that alters the activity and/or selectivity of a given photo-sensitive catalyst.

This chapter aims to highlight the recent advances in the burgeoning field of photoswitchable catalysis, including both heterogenous and homogenous systems. Heterogeneous photoswitchable catalysis has been achieved by employing catalytic materials that undergo significant changes in their surface properties, and therefore their catalytic ability upon exposure to light. The development of homogeneous photoswitchable catalysts has largely involved the incorporation of photochromic[11] groups, which may be reversibly switched between two states having different steric and electronic properties, into catalytically active species (Figure 1.2). Specifically, azobenzene[12] and stilbene[13] moieties, which undergo a reversible photochemical $E \rightarrow Z$

isomerization, have enabled steric switching of catalytic activity. Diarylethenes,[14,15] which undergo an electrocyclic ring-closing reaction in the presence of light, have been utilized for switching of both the steric and electronic properties of catalysts. In addition, spiropyran[16] units can alter catalytic activity due to their photoinduced changes in charge distribution resulting from the ring opening to the merocyanine isomer. The development of a photoswitchable catalyst requires that the photoinduced transformation occur with high efficiency, in both the forward and reverse directions. Additionally, the photosensitive unit should be capable of absorbing light of a different wavelength than would excite the rest of the molecule or the substrates to avoid photodegradation of either the catalyst or substrate. Finally, the photoinduced transformation must have a significant influence over the geometrical or electronic properties of the catalyst in order to translate the outcome of the photochemical transformation into significant catalytic activity differences. A number of unique approaches, described in the following sections, have been reported which have successfully achieved the above requirements and realized efficient photoswitchable catalysts.

a) Azobenzene / stilbene

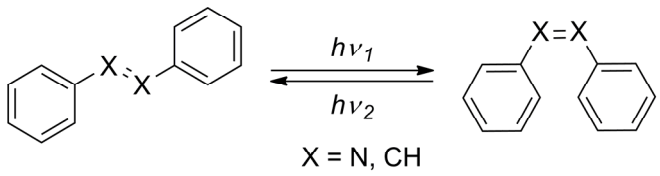

b) Diarylethene

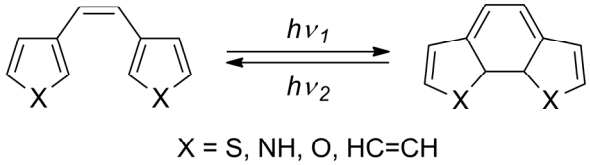

c) Spiropyran

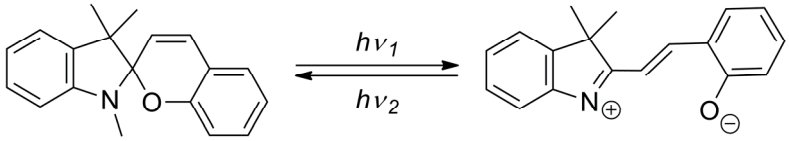

Figure 1.2: Photochromic units, including (a) azobenzene or stilbene, (b) diarylethenes, and (c) spiropyrans, have been incorporated into photoswitchable catalysts.

1.2 HETEROGENEOUS PHOTOSWITCHABLE CATALYSIS

A number of groups have successfully enabled heterogeneous photoswitchable catalysts using the inherent photo-responsive nature of surfaces or by incorporating photoswitchable moieties into heterogenous catalytic materials. A unique example of using light to alter the enzymatic activity of peroxidases was recently reported using cadmium selenide (CdSe) quantum dots (QDs), which are known to facilitate the formation of reactive oxygen species (ROS) in aqueous solutions.[17] The heme-containing peroxidases, horseradish peroxidase, cyctochrome C peroxidase, myoglobin, and CYP152A1, were inactive in the presence of CdSe QDs in the dark, but were activated upon irradiation with 366 nm light. The peroxidase activity could be switched between fast and slow states multiple times over the course of a single oxidation of non-fluorescent N-acetyl-3,7-dihydroxyphenoxazine to the brightly fluorescent product,

resorufin. While further studies to elucidate the detailed activation mechanism are required, the reported method was general for various peroxidases and is expected to be suitable for other oxygen-consuming enzymes.

A second example of photoswitchable heterogenous catalysis took advantage of the reversible, light-induced wettability of TiO_2 surfaces.[18] Upon UV irradiation, water molecules in the air presumably may coordinate with the titanium atoms on the TiO_2 surface, greatly increasing the number of surface hydroxyl groups, and thus the hydrogen bonding capability of the surface (Figure 1.3).[19] A number of hydrogen bond catalyzed organic transformations were investigated, including aldol reactions, epoxide ring-openings, Diels-Alder reactions, and C-C couplings (Figure 1.3), and all were found to give higher yields in the presence of UV irradiation than under ambient light (UV: 33-76%; ambient: 0-34%). The light-induced wettability was confirmed by X-ray diffraction (XRD), Brunauer-Emmet-Teller (BET), and infrared (IR) analysis, as well as contact angle measurements, which indicated that the number of surface hydroxyl groups increased upon UV irradiation, and decreased upon standing in the dark. The reversible wettabilility was then used as a catalytic activity switch in the aldol reaction between benzaldehyde and acetophenone (Figure 1.3). The TiO_2 catalyst could be used to promote the reaction (~60% yield), then separated from the reaction, kept in the dark to attenuate activity (20% yield), then subsequently irradiated with UV light to restore its activity (60% yield). The irradiation/separation process was repeated up to 8 times and gave consistently high activity under UV irradiation (60% yield), but poor activity in the dark (20% yield). The photo-controlled rates of relevant C-C bond forming organic reactions with a heterogeneous catalyst such as TiO_2 offers a convenient, inexpensive, environmentally friendly method, which is expected to find utility in a variety of synthetic efforts.

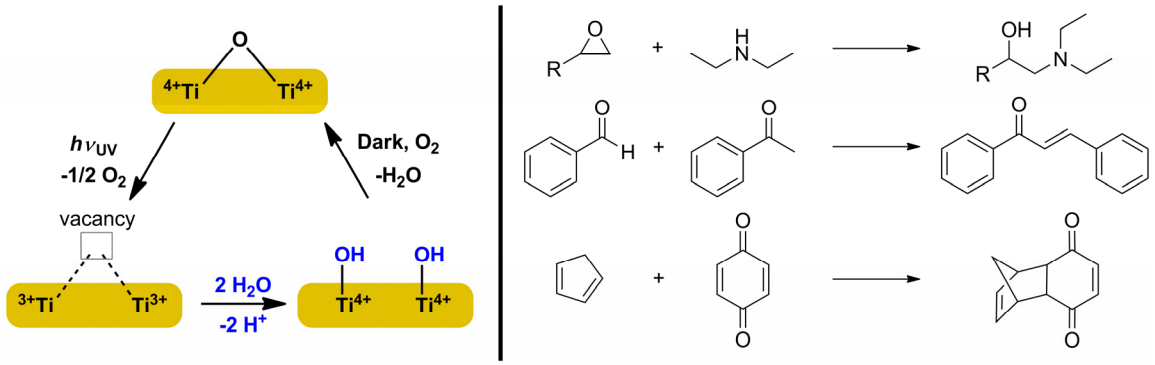

Figure 1.3: The reversible UV-induced surface wettability of TiO_2 enabled control over the rates of a variety of acid-catalyzed reactions, including epoxide ring-openings, aldol reactions, and Diels-Alder reactions.

Willner and co-workers[20] reported a unique example of photoswitchable electrocatalysis and chemiluminescence, which utilized Pt nanoparticles (NPs) for the reduction of H_2O_2. A photochromic nitrospyropyran derivative was tethered to an indium tin oxide (ITO) electrode to form a monolayer that lacked affinity for the negatively charged Pt NPs, and thus was catalytically inactive toward H_2O_2 reduction. Upon UV irradiation of the system, however, the nitrospyropyran underwent a ring-opening reaction to form the positively charged merocyanine species (Figure 1.4). The positively charged monolayer attracted the Pt NPs to the ITO electrode, which activated the electrode toward electrocatalytic H_2O_2 reduction. Subsequent exposure to visible light effected reversion of the merocyanine back to the starting spiropyran, resulting in detachment of the Pt NPs and a reduction in catalytic activity. The ITO electrode could thus be switched between catalytically inactive and active states by exposure to remote light stimuli. The formation of H_2O_2 was detected electrochemically and via addition of luminal, which chemiluminesced upon UV irradiation and H_2O_2 generation. Notably, the electrocatalytic functions of the electrode (i.e. its catalytic activity and

chemiluminescence) could be photoswitched for up to ten cycles without detectable degradation of the electrode.

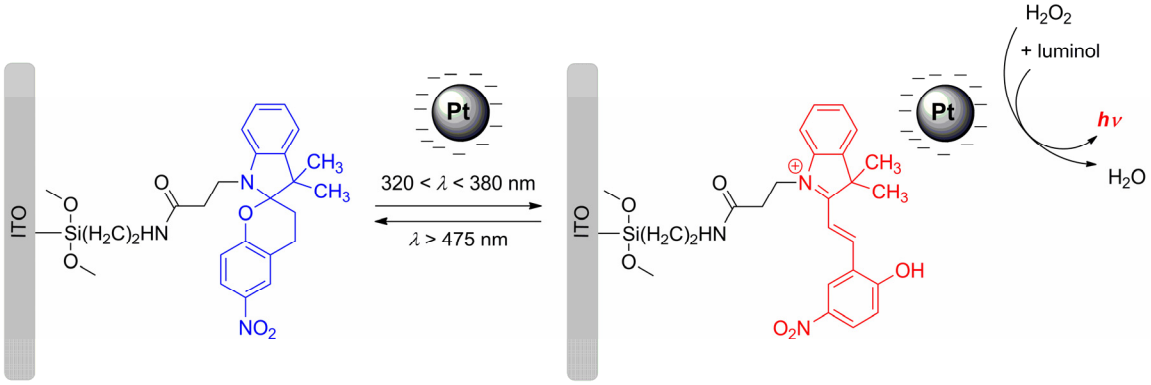

Figure 1.4: The UV-induced ring-opening of a nitrospiropyran triggered attraction of Pt NPs to an ITO electrode, which enable electrocatalytic H_2O_2 reduction.

Gryzbowski and co-workers[21] successfully achieved a photoswitchable catalytic system by appending photochromic azobenzene units to Au NPs. The Au NPs were decorated with a mixed self-assembled monolayer of dodecylamine and azobenzene terminated alkane thiol moieties (Figure 1.5). Under ambient light, when the azobenzene units were in the *E* form, the nanoparticles were readily dispersed in toluene and efficiently catalyzed the hydrosilylation of 4-methoxybenzaldehyde with diphenylsilane. However, upon UV irradiation to effect the isomerization of the azobenene units to their *Z* form, the NPs aggregated,[22] which reduced the solvent-exposed surface area and significantly slowed the rate of hydrosilylation (k_{ON}/k_{OFF} = 90). Subsequent irradiation with visible light resulted in re-dispersion of the particles and restoration of the initial hydrosilylation rate. The catalytic activity could be switched between states of fast and slow reactivity up to three times during the course of a single hydrosilylation reaction. The reversible NP aggregation resulted from the development of an electric dipole as a result of the $E \rightarrow Z$ isomerization of the surface azobenzene moieties, which in a

nonpolar solvent was translated into attractive forces between the NPs. The reversible photo-induced aggregation phenomenon was confirmed by UV-vis spectroscopy, as well as dynamic light scattering and transmission electron microscopy. Taken together, the aforementioned work successfully demonstrates a rare example of photoswitchable catalysis that offers high k_{ON}/k_{OFF} ratios as well as multiple switching cycles.

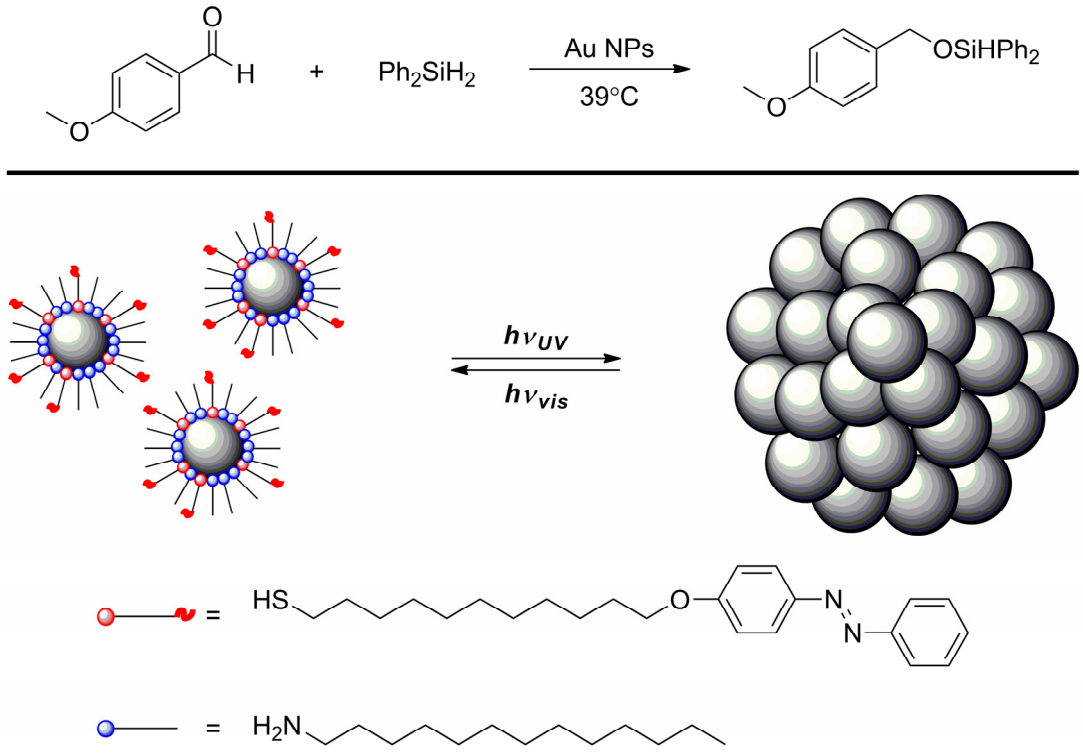

Figure 1.5: Dispersed Au NPs decorated with photochromic azobenzene moieties efficiently catalyzed the hydrosilylation of 4-methoxybenzaldehyde. Upon UV irradiation to effect the $E \rightarrow Z$ isomerization of the surface azobenzene moieties, the particles aggregated, reducing the catalytic activity due to the decreased surface area.

1.3 HOMOGENEOUS PHOTOSWITCHABLE CATALYSIS

Steric Photoswitches

The majority of known photoswitchable catalysts operate based upon the concept of photochemical modulation of the catalyst's steric properties; i.e. the steric bulk surrounding a catalyst's active site. The $E \rightarrow Z$ isomerization of an azobenzene or stilbene moiety.[12,13] has commonly been used to accomplish this, as the isomerization is accompanied by a significant conformational change. The first reported photoswitchable catalyst took advantage of the UV-induced $E \rightarrow Z$ isomerization of azobenzene[12] in conjuction with an ester hydrolysis catalyst β-cyclodextrin (Figure 1.6).[23] By capping the β-cyclodextrin with an azobenzene moiety, the rate of hydrolysis of *p*-nitrophenylacetate could be modulated by exposure of the reaction mixture to UV irradiation. The *E*-azobenzene cap appended to the β-cyclodextrin in the initial catalyst ***E*-1** effectively blocked one end of the β-cyclodextrin, and thus prevented strong binding of the ester substrate in the β-cyclodextrin cavity, which inhibited the hydrolysis reaction. Upon UV irradiation, however, the catalyst was converted to the *Z* form ***Z*-1**, which deepened the β-cyclodextrin cavity, promoted substrate binding and allowed more efficient hydrolysis. The photochemical $E \rightarrow Z$ isomerization resulted in a 5-fold increase in the rate of hydrolysis of *p*-nitrophenylacetate, and the authors claim that the reversible nature of the isomerization via application of heat or visible light (440 nm) enabled on-off control of the catalytic activity. Ueno and coworkers later demonstrated that connecting the azobenzene to the β-cyclodextrin via a histidine spacer facilitated similar photoswitchable catalytic hydrolysis of *p*-nitrophenylacetate and Boc-alanine-*p*-nitrophenyl ester due to the differences in steric bulk and binding affinities of the *E*-azobenzene and *Z*-azobenzene moieties ($k_E/k_Z \leq 16$).[24] Furthermore, azobenzene moieties

were later tethered to Au NPs and used in conjuction with β-cyclodextrin to demonstrate a heterogeneous photoswitchable catalytic system for ester hydrolysis.[25]

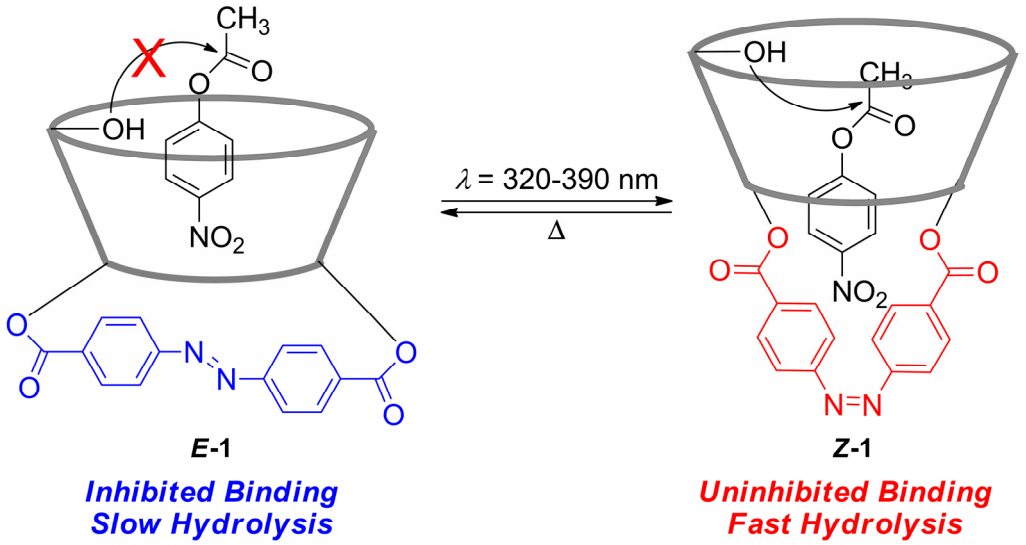

Figure 1.6: Capping β-cyclodextrin with an azobenzene moiety enabled photoswitchable catalytic ester hydrolysis via the reversible $E \rightarrow Z$ isomerization which resulted in a deeper cavity and enhanced substrate binding affinity.

In 1995 Rebek and coworkers[26,27] reported another photoswitchable supramolecular catalyst system which relied on the $E \rightarrow Z$ isomerization of azobenzene. The connection of two carbazole-based adenine receptors by an azobenzene moiety enabled control over the rate of the coupling reaction between aminoadenosine **3** and the adenosine-derived ester **4** (Figure 1.7). The disparity in the rates between the ***E*-2** and ***Z*-2** catalysts arose because both receptor units must be in close proximity to one another for sufficient adenine binding to occur. When the catalyst was in the extended *E* form the receptor units were too far apart to allow for sufficient adenine binding, giving rise to a much smaller coupling rate than the folded *Z* catalyst ($k_Z/k_E \leq 50$), which facilitated efficient substrate binding.

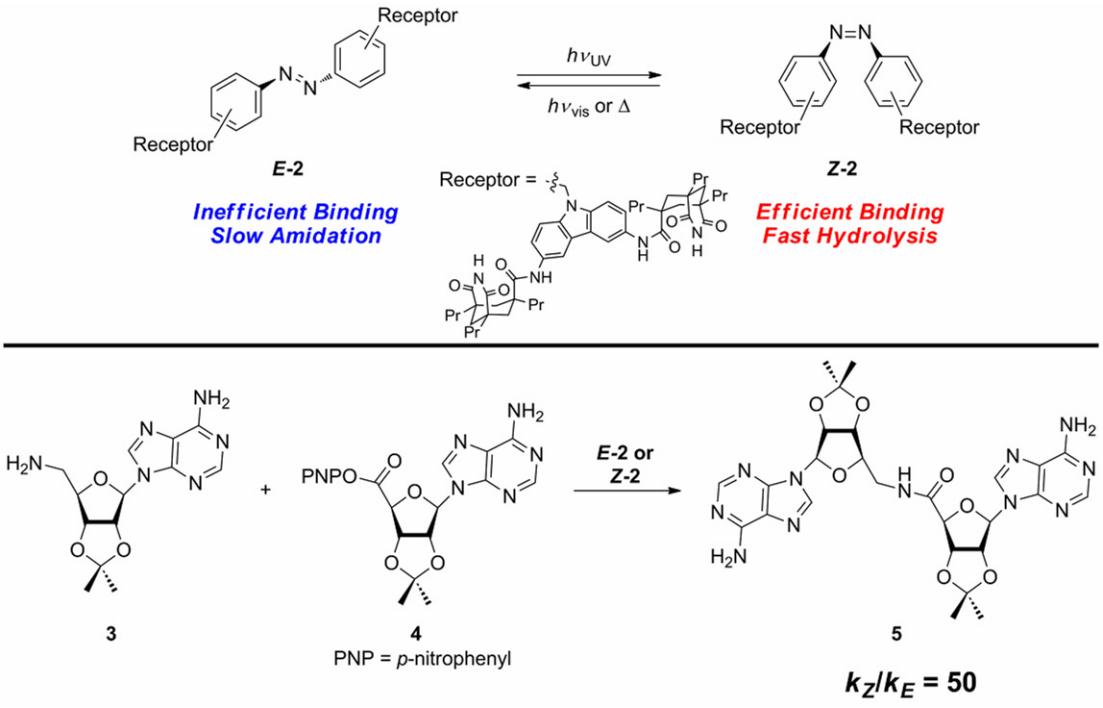

Figure 1.7: Carbazole-based adenine receptor units were linked by a photochromic azobenzene moiety. Upon photochemical isomerization of catalyst ***E*-2** to ***Z*-2** the rate of the coupling reaction between **3** and **4** was significantly enhanced.

In a similar manner to azobenzene, the reversible photoisomerization of stilbene was employed in photoswitchable supramolecular catalysis. Inoue and co-workers[28] demonstrated that the coordination of 2-stilbazole to metalloporphyrins could be reversibly tuned by UV or visible irradiation due to the differences in sterics between the *E* and *Z* isomers of stilbazole. Given that aluminum porphyrins will catalyze the reaction of carbon dioxide with epoxides only when a nitrogen-containing base is coordinated to the aluminum center, the ability to photochemically tune the binding was expected to dictate the catalytic activity. Due to unfavorable steric interactions between the porphyrin ring system and the bulky *t*-butyl groups, *E*-3,5-di-*t*-butyl-2-stilbazole was unable to efficiently bind the aluminum center in methoxyaluminum 5,10,15,20-

tetraphenylporphine, resulting in a very low yield in the reaction of propylene oxide with CO_2 (2% conversion in 18 h; Figure 1.8). On the other hand, with *Z*-3,5-di-*t*-butyl-2-stilbazole, which was expected to bind readily to the Al porphyrin, the formation of propylene carbonate was significantly accelerated (23% in 18 h). The system could alternately be exposed to UV or visible light during the course of the reaction to remotely tune the rate.

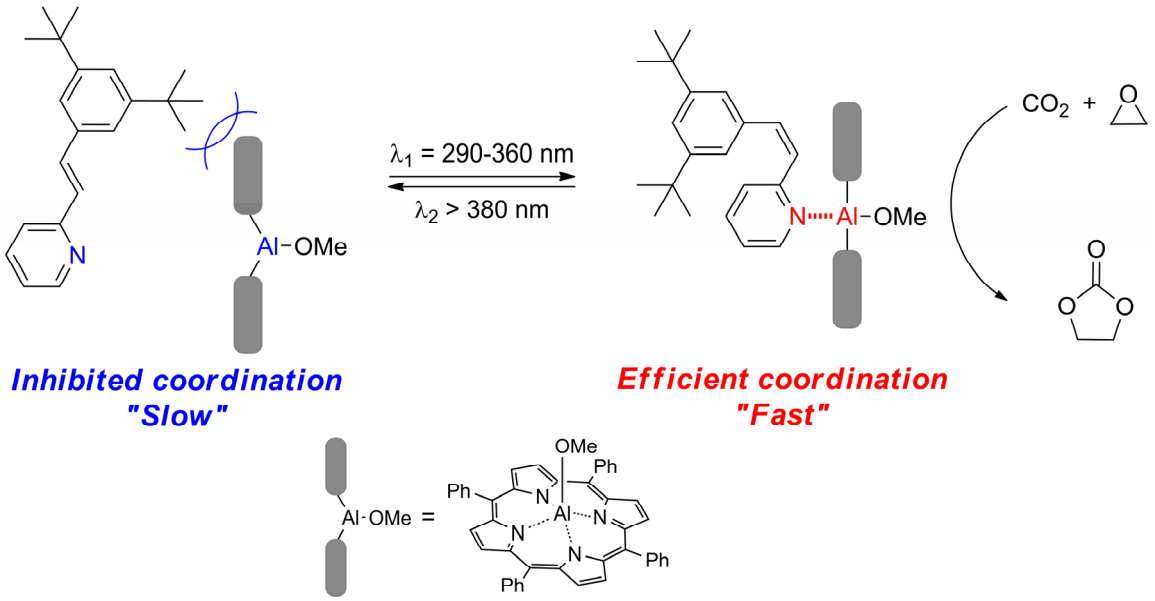

Figure 1.8: Unfavorable steric interactions between the porphyrin ring system and the bulky *t*-butyl groups in *E*-3,5-di-*t*-butyl-2-stilbazole prohibited efficient N-Al binding, which decreased the yield of the reaction between CO_2 and ethylene oxide.

The next example of photoswitching the activity of a supramolecular catalyst using the $E \rightarrow Z$ isomerization of azobenzene was reported nearly a decade later by Cacciapaglia and Mandolini[29] for the ethanolysis of anilide derivatives. A photochromic bis-crown ether complex **6** was synthesized and shown to undergo a reversible $E \rightarrow Z$ isomerization in the presence of bound Ba^{2+}. Efficient ethanolysis requires two metal

ions: one to serve as a binding unit for the carboxylate group, and the other to deliver the alkoxide to the amide carbonyl. Both Ba^{2+} ions must be in sufficiently close proximity to bind a single substrate, which is only feasible for catalyst ***Z*-6** formed upon UV irradiation of the inactive catalyst ***E*-6** (Figure 1.9). The reversibility of the isomerization allowed the ethanolysis activity to be switched between fast and slow states multiple times over the course of a single reaction ($k_Z/k_E \leq 5$).

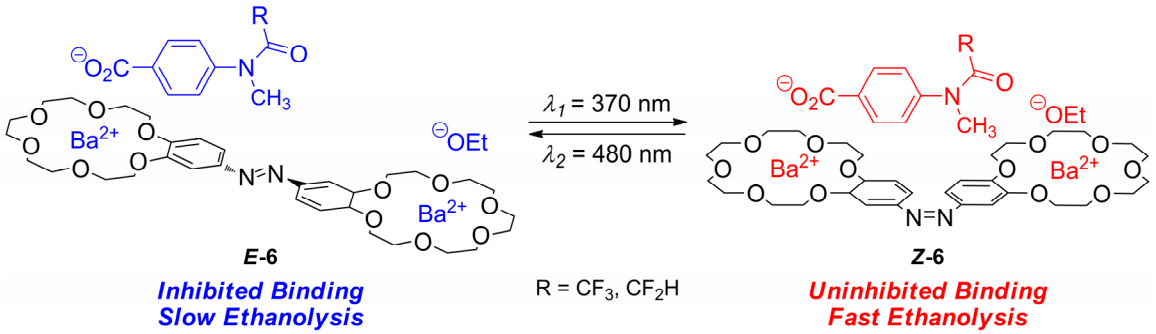

Figure 1.9: A photoswitchable bis-crown ether ligand facilitated external modulation of the rate of anilide ethanolysis.

Hecht and co-workers[30] later moved away from photoswitchable supramolecular catalysis and adapted the concept of photo-reversible steric shielding by incorporating an azobenzene unit directly into a piperidine base catalyst. In the elegantly designed, conformationally restricted, N-alkylated piperidine, the lone pair of electrons on the piperidine nitrogen may be reversibly blocked by the azobenzene substituents (Figure 1.10). The shielding was optimized by introduction of structural restrictions including the predominance of the chair conformation with the N-alkyl substituent in the equatorial position, the spiro junction which fixed the position of the azobenzene moiety, and the steric bulk of the 3,5-disubstituted phenylazo group. The resting catalyst ***E*-7** featured a sterically inaccessible basic site and exhibited a fairly low basicity in titration experiments with trifluoromethanesulfonic acid. However, UV irradiation effected an

isomerization to form ***Z*-7**, which left the basic site accessible and significantly increased the catalyst's basicity (pK_a(***Z*-7c**) – pK_a(***E*-7c**) = 0.7). As a result, ***E*-7c** displayed negligible catalytic activity in the aza-Henry reaction between *p*-nitrobenzaldehyde and nitroethane, while ***Z*-7c** formed upon UV irradiation efficiently promoted the reaction (k_Z/k_E = 35.5). The effective blocking of the catalyst's active site was further demonstrated by X-ray crystallography,[31] which clearly showed the preferred chair conformation and the position of the azobenzene blocking substituent, which effectively shielded the N lone pair in the *E*-isomer but left the basic site accessible in the *Z*-isomer. Additional analyses, including NMR experiments using residual dipolar couplings and DFT calculations, were also employed to provide further evidence for the fixed conformation of the catalyst and illustrate that the catalysis results were indeed a result of the proposed photoswitchable steric shielding.[31] In a subsequent study the piperidine catalyst was immobilized on silica to facilitate heterogeneous photoswitchable catalysis.[32]

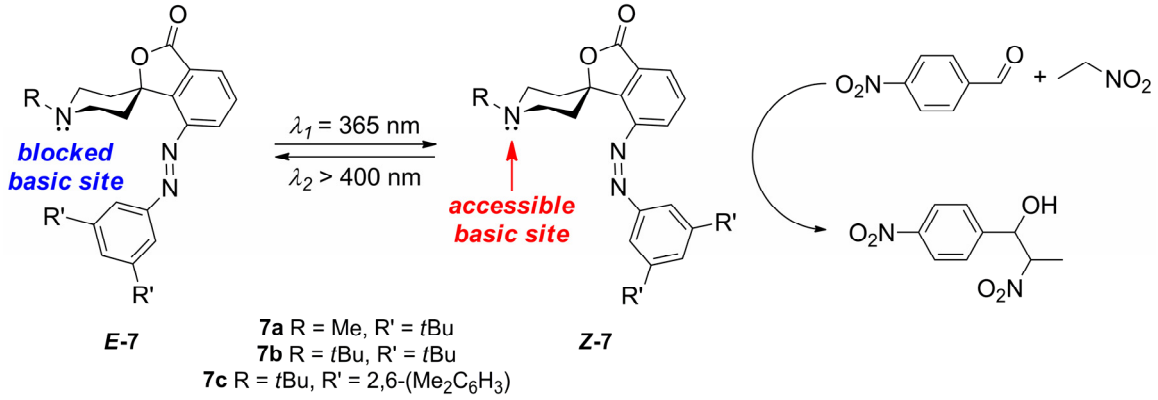

Figure 1.10: An azobenzene annulated piperidine catalyzed the Henry reaction in its *Z* form, however the more stable *E* form displayed significantly reduced activity due to steric shielding of the basic site.

Hecht's employment of the azobenzene isomerization in a photoswitchable base catalyst was followed by a photoswitchable acid catalyst. Imahori and co-workers[33]

developed an azobenzene-tethered bis(trityl alcohol) for use in the acid-catalyzed Morita-Baylis-Hillman (MBH) reaction (Figure 1.11). Similar to the aforementioned adenine binding and bis-Ba^{2+}-crown ether examples, the photoswitchable acid catalyst relies on cooperative bifunctional catalysis, which can be disrupted by altering the conformation of the catalyst such that the two required active sites are no longer in sufficient proximity. Linking two trityl alcohol moieties to an azobenzene core resulted in a cooperative bifunctional catalyst that could be photochemically switched between its inactive *E* form and the active *Z* isomer. The catalyst ***Z*-8**, generated by UV irradiation of ***E*-8**, promoted the MBH reaction of 2-cyclopenten-1-one and 3-phenylpropanal with a 25% increase in reaction yield over its isomer ***E*-8**. As a control, the reaction catalyzed by trityl alcohol proceeded with negligible conversion, indicating that both trityl alcohol units were needed to promote the reaction, which indicated that the photochemically induced change in spatial arrangement was responsible for the observed reactivity differences.

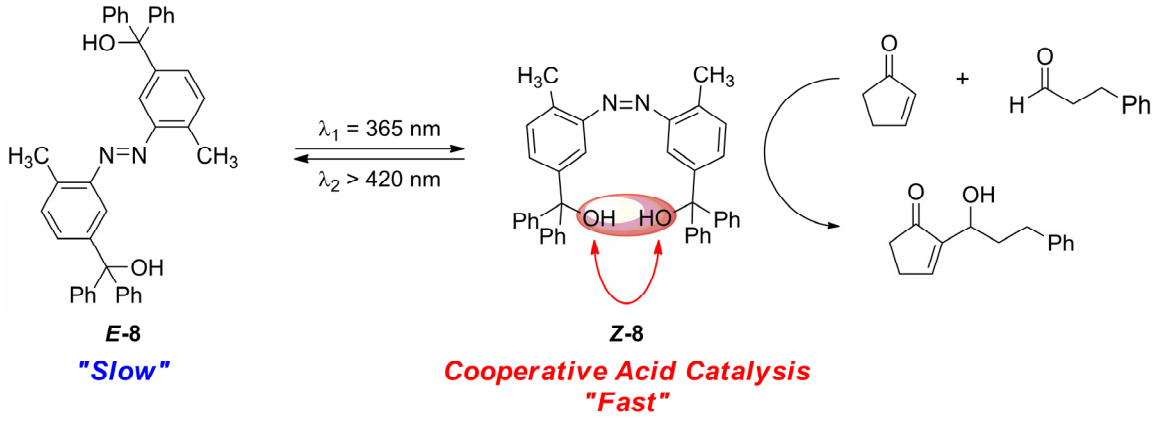

Figure 1.11: The azobenzene core of a bis(trityl alcohol) acid catalyst allowed photo-control over the rate of an MBH reaction due to disruption of the cooperative functional groups needed for catalysis.

While the cis-trans isomerization of azobenzene and stilbene moieties has been widely used as a steric photoswitch for a variety of catalysts, Branda and coworkers[34]

recently took advantage of a dithienylethene photocyclization to alter the steric properties of a copper(I) cyclopropanation catalyst. A chiral bis(oxazoline) dithienylethene ligand was developed, which in its open form (**9o**) was capable of chelating a Cu(I) atom in the chiral pocket between the two oxazoline moieties to facilitate the enantioselective cyclopropanation of styrene (30-50% *ee*; Figure 1.12). Upon UV irradiation, however, the bis(oxazoline) ligand underwent an electrocyclic ring-closing to form **9c**, in which the oxazoline moieties were too far apart to chelate a copper atom. Thus, when the photocyclized ligand **9c** was used in the cyclopropanation reaction, negligible enantioselectivity was observed (5 % *ee*). Subsequent irradiation with visible light (434 nm) effected the cycloreversion to **9o** and restored the enantioselectivity, thus demonstrating the first example of photoswitching stereoselectivity in a catalytic reaction.

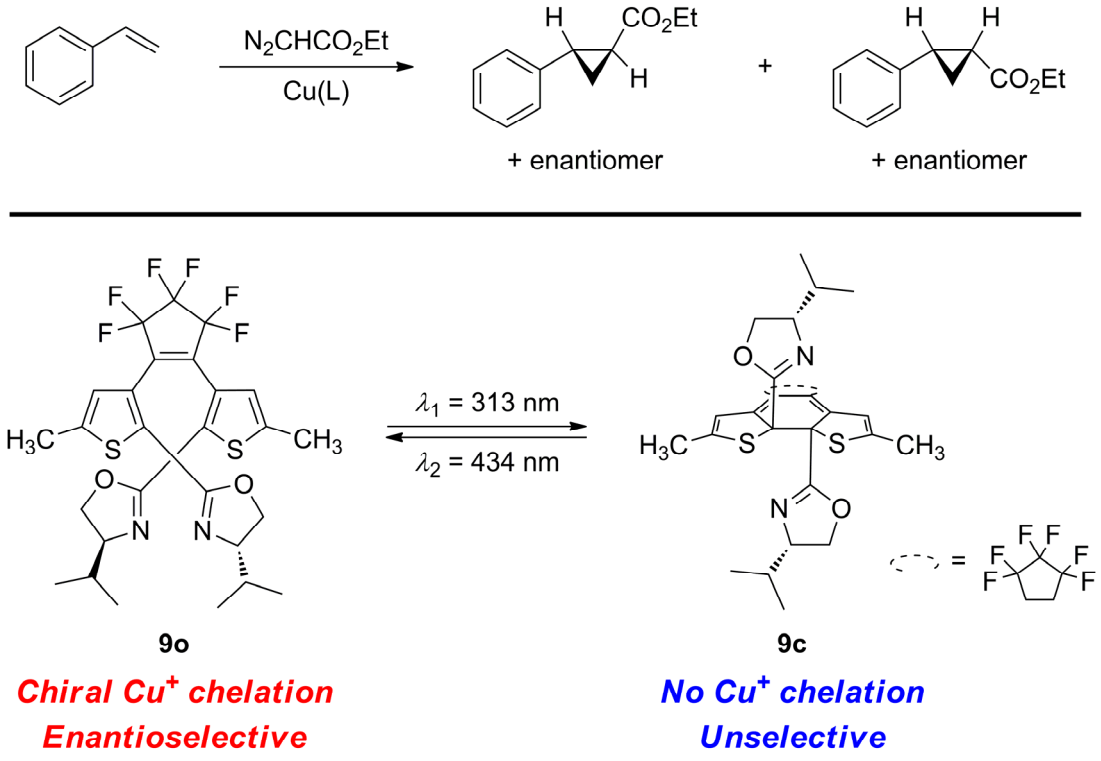

Figure 1.12: Chelation of a Cu(I) atom in the chiral pocket of **9o** facilitated stereoselective cyclopropanation; UV irradiation to form **9c** disrupted the chelation and decreased the stereoselectivity.

Electronic Photoswitches

While a number of photoswitchable catalysts have successfully employed changes in steric properties to alter catalytic activities, the ability to photomodulate the electronic properties of a catalyst active site is expected to enable remote tuning of catalyst selectivity as well as activity. Diarylethenes hold significant promise in this field, as their photocyclization results in a complete redistribution in electron density when exposed to UV irradiation, which is reversed upon treatment with visible light. The resulting changes in electronic properties have led to differences in a variety of chemical properties,[35] including acidity,[36] basicity,[37] hydrogen bonding ability,[38] ligand coordination,[39] and

propensity to undergo cycloaddition chemistry.[40] Only in a few instances, however, have such photoinduced electronic changes been harnessed in catalytic applications.

An early example of photoswitching catalytic activity via electronic modulation was reported by Branda and co-workers.[41] Drawing inspiration from the use of light to control biochemical processes, a photoresponsive mimic of the biologically active form of vitamin B_6, pyridoxal 5′-phosphate (PLP) was developed. The action of PLP is dependent upon the electronic connection of the aldehyde and pyridinium functional groups, which allows for enhancement of the acidity of the α-hydrogen on the aldimine generated by condensation of an amino acid with PLP via stabilization of the conjugate base via contribution from the quinonoid resonance structure (Figure 1.13). A photoresponsive PLP analogue was developed by replacing the PLP core ring with a photochromic diarylethene unit, where in the ring-open form **10o**, the pyridinium and aldehyde units were electronically isolated from each other, which precluded any catalytic activity. However upon UV irradiation to form the ring-closed isomer **10c**, the redistribution in electron density resulted in a fully conjugated structure in which the pyridinium and aldehyde groups were electronically connected. The ring closed isomer **10c** was therefore able to form the stabilizing quionoid structure upon condensation with an amino acid followed by deprotonation of the aldimine α-hydrogen. It was thereby possible to switch the catalyst between its inactive form **10o** and its active form **10c** by alternating exposure to UV and visible light. Treatment of L-alanine with **10o** resulted in no reaction, however upon UV irradiation to form **10c** an immediate surge in the rate of racemization was observed, which could again be attenuated by subsequent exposure to visible light.

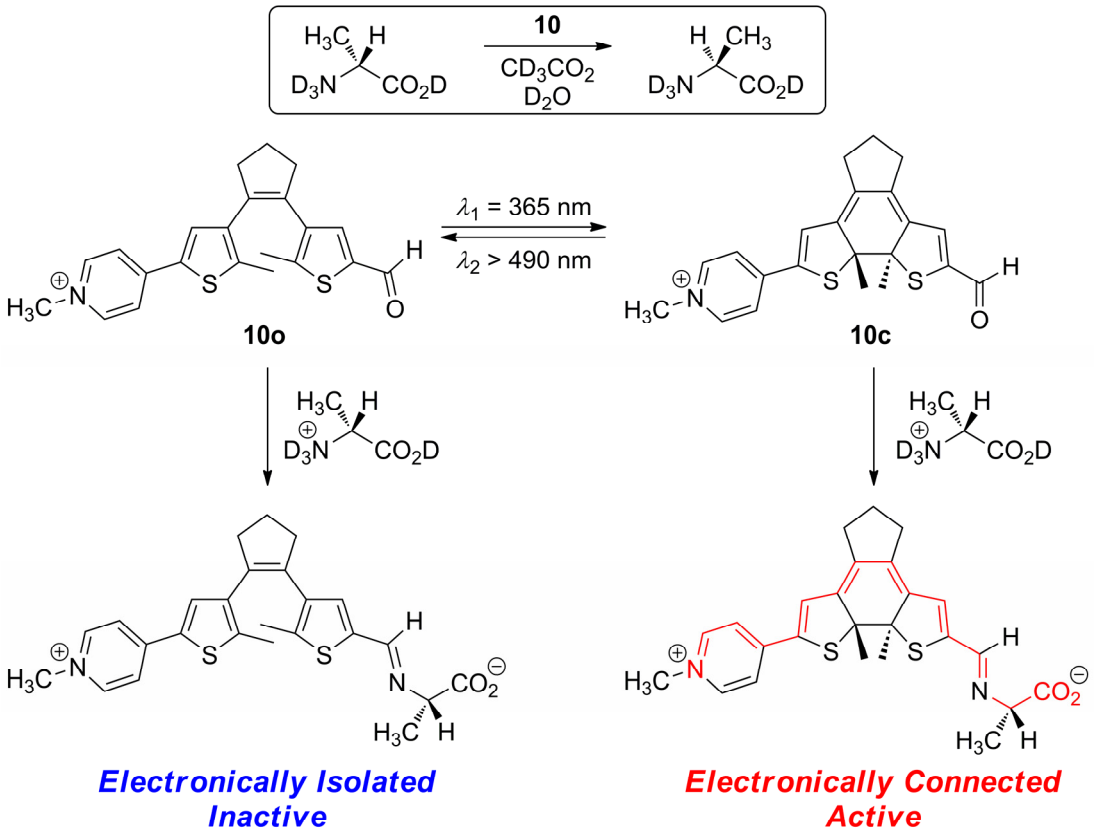

Figure 1.13: A photoresponsive PLP mimic was developed by connecting the aldehyde and pyridinium moieties with a DTE. The reversible changes in conjugation upon irradiation with UV or visible light allowed the photoswitchable racemization of L-alanine.

1.4 Conclusions and Outlook

In summary, the field of photoswitchable catalysis has seen rapid development over the past three decades. A variety of conceptually different approaches have been taken to reversibly control reactions using light. For example, heterogeneous photoswitchable catalysis has been realized using inherently photosensitive surfaces such as TiO_2 and CdSe. The attachment of photochromic moieties to surfaces is also capable of rendering them photoswitchable, a concept that may be extended to a wide variety of solid materials. Additionally, a number of photoswitchable homogeneous catalyst

systems have been realized by capitalizing on the drastic steric changes resulting from the photochemical $E \rightarrow Z$ isomerization of azobenzene and stilbene derivaties. Photochromic diarylethene moieties have also been incorporated into catalytic systems to facilitate switching of both stereochemistry through steric changes, and catalytic activity via alteration of a catalyst's electronic properties.

While a number of notable accomplishments have been made, the burgeoning field of photoswitchable catalysis faces several remaining challenges. The practical utility of photoswitchable catalysts will be promoted by development of catalytic species that may be converted with high fidelity between two significantly sterically or electronically different states, in order to maximize the k_{ON}/k_{OFF} ratios. Moreover, the design of versatile and broadly applicable catalysts is still desirable, given that many of the known photowitchable catalysts are only able to mediate one or a small number of transformations. Synthetically relevant reactions such as C-C bond formations, metathesis reactions, and polymerizations catalyzed by homogeneous metal catalysts, nucleophilic organocatalysts, and/or general acid/base catalysts are all attractive targets. An ideal photoswitchable catalyst would facilitate useful transformations with broad substrate scope, and would be able to alter both activity and, perhaps more importantly, selectivity upon exposure to light. The ability to remotely fine-tune a catalyst's intrinsic chemo-, regio-, and/or stereoselectivity with spatial and temporal control would undoubtedly be extremely powerful. Such photoswitchable catalysts are expected to provide unprecedented control over polymer microstructure as well as simplify multi-step syntheses of complex small molecules. A possible approach to this attractive, while daunting, challenge would be to develop photoswitchable ligands[40] that may act as photoswitchable organocatalysts or enable photomodulation of a ligated catalytic metal center.[42] While potentially problematic due to the often low photochemical conversions

and photodegradation, the use of photochromic metal complexes as photoswitchable catalysts would vastly expand the scope of possible reactions as well as allow potential for tuning selectivity as well as reactivity. If properly designed, however, a photochromic ligand may facilitate the development of robust, multi-functional photoswitchable catalysts that will lead to the development of otherwise unattainable materials with sophisticated structures and advanced functions.

1.5 REFERENCES

[1] (a) Blanco, V.; Carlone, A.; Hänni, K. D.; Leigh, D. A.; Lewandowski, B. *Angew. Chem. Int. Ed.* **2012**, *51*, 5166-5169. (b) Yoon, H. J.; Junpei, K.; Kim, J.-H.; Mirkin, C. A. *Science* **2010**, *330*, 66-69. (c) Schmittel, M.; De, S.; Pramanik, S. *Angew. Chem. Int. Ed.* **2012**, *51*, 3822-3826. (d) Balof, S. L.; P'Pool, S. J.; Berger, N. J.; Valente, E. J.; Shiller, A. M.; Schanz, H.-J. *Dalton Trans.* **2008**, *42*, 5791-5799. (e) Balof, S. L.; Yu, B.; Lowe, A. B.; Ling, Y.; Zhang, Y.; Schanz, H.-J. *Eur. J. Inorg. Chem.* **2009**, *13*, 1717-1722.

[2] (a) Wiggins, K. W.; Hudnall, T. W.; Tennyson, A. G.; Bielawski, C. W. *J. Mater. Chem.* **2011**, *21*, 8355-8359. (b) Tennyson, A. G.; Wiggins, K. M.; Bielawski, C. W. *J. Am. Chem. Soc.* **2010**, *132*, 16631-16636. (c) Karthikeyan, S.; Potisek, S. L.; Piermattei, A.; Sijbesma, R. P. *J. Am. Chem. Soc.* **2008**, *130*, 14968-14969.

[3] (a) Allgeier, A. M.; Mirkin, C. A. *Angew. Chem. Int. Ed.* **1998**, *37*, 894-908. (b) Lorkovic, I. M.; Duff, R. R.; Wrighton, M. S. *J. Am. Chem. Soc.* **1995**, *117*, 3617. (c) Gregson, C. K. A.; Gibson, V. C.; Long, N. J.; Marshall, E. L.; Oxford, P. J.; White, A. J. P. *J. Am. Chem. Soc.* **2006**, *128*, 7410. (d) Broderick, E. M.; Guo, N.; Vogel, C. S.; Xu, C.; Sutter, J. R.; Miller, J. T.; Meyer, K.; Mehrkhodavandi, P.; Diaconescu, P. L. *J. Am. Chem. Soc.* **2011**, *133*, 9278. (e) Broderick, E. M.; Guo, N.; Wu, T.; Vogel, C. S.; Xu, C.; Sutter, J.; Miller, J. T.; Meyer, K.; Cantat, T.; Diaconescu, P. L. *Chem. Commun.* **2011**, *47*, 9897.

[4] Stoll, R. S.; Hecht, S. *Angew. Chem. Int. Ed.* **2010**, *49*, 5054-5075.

[5] For reviews on switchable catalysts, see: (a) Lüning, U. *Angew. Chem. Int. Ed.* **2012**, *51*, 8163-8165. (b) Leibfarth, F. A.; Mattson, K. M.; Fors, B. P. Collins, H. A.; Hawker, C. J. *Angew. Chem. Int. Ed.* **2013**, *52*, 199-210.

[6] *Photocatalysis*; Bignozzi, C. A., Ed.; Topics in Current Chemistry 303; Springer: Berlin, Germany, 2011.

[7] For selected reviews on photocatalysis, see: (a) Narayanam, J. M. R.; Stephenson, C. R. J. *Chem. Soc. Rev.* **2011**, *40*, 102-113. (b) Salomon, R. G. *Tetrahedron*, **1983**,

39, 485-575. (c) Hennig, H. *Coord. Chem. Rev.* **1999**, *182*, 101-123. (d) Serpone, N.; Salinaro, A.; Emeline, A.; Ryabchuk, V. *J. Photochem. Photobiol. A* **2000**, *130*, 83-94. (e) Fagnoni, M.; Dondi, D.; Ravelli, D.; Albini, A. *Chem. Rev.* **2007**, *107*, 2725-2756. (f) Parnom, V. N. *Catal. Today* **1997**, *39*, 137-144. (g) Ravelli, D.; Dondi, D.; Fagnoni, M.; Albini, A. *Chem. Soc. Rev.* **2009**, *38*, 1999-2011.

[8] Shirai, M.; Tsunooka, M. *Prog. Polym. Sci.* **1996**, *21*, 1-45.

[9] For representative examples of photo-activation of metal catalysts via CO dissociation, see: (a) Schroeder, M. A.; Wrighton, M. S. *J. Am. Chem. Soc.* **1976**, *98*, 551-558. (b) Graff, J. L.; Sanner, R. D.; Wrighton, M. S. *J. Am. Chem. Soc.* **1979**, *101*, 273-275. (c) Krausz, P.; Garnier, F.; Dubois, J. E. *J. Am. Chem. Soc.* **1975**, *97*, 437-438.

[10] (a) van der Schaaf, P.; Hafner, A. *Angew. Chem. Int. Ed.* **1996**, *35*, 1845-1847. (b) Hafner, A.; Mühlebach A.; van der Schaaf, P. *Angew. Chem. Int. Ed.* **1997**, *36*, 2121-2124.

[11] (a) H. Durr, H. Bouas-Laurent, Eds. *Photochromism: Molecules and Systems*; Elsevier: Amsterdam, The Netherlands, **2003**. (b) Special Issue: "Photochromism: Memories and Switches" (Ed. M. Irie), *Chem Rev.* **2000**, *100*, 1683.

[12] Bandara, H. M. D.; Burdette, S. C. *Chem. Soc. Rev.* **2012**, *41*, 1809-1825.

[13] Papper, V.; Likhtenshtein, G. I. *J. Photoch. Photobio. A* **2001**, *140*, 39-52.

[14] Irie, M. *Chem Rev.* **2000**, *100*, 1685-1716.

[15] (a) Matsuda, K.; Irie, M. *J. Photochem. Photobio. C: Photochem Rev.* **2004**, 169. (b) Tian, H.; Yang, S. *Chem. Soc. Rev.* **2004**, *33*, 85. (c) Tian, H.; Wang, S. *Chem. Commun.* **2007**, 781. (d) Yun, C.; You, J.; Kim, J.; Huh, J.; Kim, E.; *J. Photochem. Photobio. C: Photochem Rev.* **2009**, *10*, 111. (e) Yam, V. W.-W.; Lee, J. K.; Ko, C.; Zhu, N. *J. Am. Chem. Soc.* **2009**, *131*, 912.

[161] Berkovic, G.; Krongauz, V.; Weiss, V. *Chem. Rev.* **2000**, *100*, 1741-1753.

[17] Fruk, L.; Rajendran, V.; Spengler, M.; Niemeyer, C. M. *ChemBioChem.* **2007**, *8*, 2195-2198.

[18] Niu, F.; Zhai, J.; Jiang, L.; Song, W.-G. *Chem. Commun.* **2009**, 4738-4740.

[19] Wang, R.; Hashimoto, A.; Fujishima, M.; Chikuni, M.; Kojima, E.; Kitamura, A.; Shimohigoshi, M.; Watanabe, T.; *Nature*, **1997**, *388*, 431-432. (b) Feng, X.-J.; Zhai, J.; Lian, L. *Angew. Chem. Int. Ed.* **2005**, *44*, 5115-5118. (c) Caputo, C.; Nobile, C.; Kipp, T.; Blasi, L.; Grillo, V.; Carlino, E.; Manna, L.; Cingolani, R.; Cozzoli, P. D.; Athanassiou, A. *J. Phys. Chem. C.* **2008**, *112*, 701-714.

[20] Niazov, T.; Shlyahovsky, B.; Willner, I. *J. Am. Chem. Soc.* **2007**, *129*, 6374-6375.

[21] Wei, Y.; Han, S.; Kim, J.; Soh, S.; Grzybowski, B. A. *J. Am. Chem. Soc.* **2010**, *132*, 11018-11020.

[22] (a) Klajn, R.; Bishop, K. J. M.; Gryzbowski, B. A. *P. Natl. Acad. Sci. USA*, **2007**, *104*, 10305-10309. (b) Klajn, R.; Wesson, P. J.; Bishop, K. J. M.; Gryzbowski, B. A. *Angew. Chem. Int. Ed.* **2009**, *48*, 7035-7039.

[23] Ueno, A.; Takahashi, K.; Osa, T. *J. Chem. Soc., Chem. Commun*. **1981**, *3*, 94–96.

[24] Lee, W.-S.; Ueno, A. *Macromol. Rapid Commun.* **2001**, *22*, 448–450.

[25] Zhu, L.; Yan, H.; Ang, C. Y.; Nguyen, K. T.; Li, M.; Zhao, Y. *Chem. Eur. J.* **2012**, *18*, 13979-13983.

[26]Würthner, F.; Rebek Jr., J. *J. Chem. Soc. Perkin Trans. 2*, **1995**, *9*, 1727-1734.

[27]Würthner, F. Rebek Jr., J. *Angew. Chem. Int. Ed.* **1995**, *34*, 446-448.

[28] Sugimoto, H.; Kimura, T.; Inoue, S. *J. Am. Chem. Soc.* **1999**, *121*, 2325-2326.

[29] Cacciapaglia, R.; Di Stefano, S.; Mandolini, L. *J. Am. Chem. Soc.* **2003**, *125*, 2224-2227.

[30] Peters, M. V.; Stoll, R. S.; Kühn, A.; Hecht, S. *Angew. Chem. Int. Ed.* **2008**, *47*, 5968-5972.

[31] Stoll, R. S.; Peters, M. V.; Kühn, A.; Heiles, S.; Goddard, R.; Bühl, M.; Thiele, C. M.; Hecht, S. *J. Am. Chem. Soc.* **2009**, *131*, 357-367.

[32] Stoll, R. S.; Hecht, S.; *Org. Lett.* **2009**, *11*, 4790-4793.

[33] Imahori, T.; Yamaguchi, R.; Kurihara, S. *Chem. Eur. J.* **2012**, *18*, 10802-10807.

[34] Sud, D.; Norsten, T. B.; Branda, N. R. *Angew. Chem. Int. Ed.* **2005**, *44*, 2019-2021.

[35] Samachetty, H. D.; Branda, N. R. *Pure Appl. Chem.* **2006**, *78*, 2351-2359.

[36] (a) Odo, Y.; Matsuda, K.; Irie, M. *Chem. Eur. J.* **2006**, *12*, 4283-4288. (b) Lemieux, V.; Spantulescu, D. M.; Baldridge, K. K.; Branda, N. R. *Angew. Chem. Int. Ed.* **2008**, *120*, 5112-5115. (c) Kawai, S. H.; Gilat, S. L.; Lehn, J.-M. *Eur. J. Org. Chem.* **1999**, 2359-2366.

[37] Samachetty, H. D.; Branda, N. R. *Chem. Commun.* **2005**, 2840-2842.

[38] Herder, M.; Pätzel, M.; Grubert, L.; Hecht, S. *Chem. Commun.* **2011**, *47*, 460-462.

[39] Sud, D.; McDonald, R.; Branda, N. R. *Inorg. Chem.* **2005**, *44*, 5960-5962.

[40] (a) Lemieux, V.; Gauthier, S.; Branda, N. R. *Angew. Chem. Int. Ed.* **2006**, *45*, 6820-6824. (b) Sud, D.; Wigglesworth, T. J.; Branda, N. R. *Angew. Chem. Int. Ed.* **2007**, *46*, 8017-8019. (c) Tanaka, Y.; Ishisaka, T.; Inagaki, A.; Koike, T.; Lapinte, C.; Akita, M. *Chem. Eur. J.* **2010**, *16*, 4762-4776. (d) Uchida, K.; Inagaki, A.; Akita, M,; *Organometallics*, **2007**, *26*, 5030-5041.

[41] Wilson, D.; Branda, N. R. *Angew. Chem. Int. Ed.* **2012**, *51*, 5431-5434.

[42] For reviews on photochromic metal complexes, see: (a) Akita, M. *Organometallics* **2011**, *30*, 43-51. (b) Kuma, S.; Nishihara, H. *Dalton Trans.* **2008**, 3260-3271. (c) Guerchais, V.; Ordronneau, L.; Bozec, H. L. *Coord. Chem. Rev.* **2010**, *254*, 2533-2545. (d) Ko, C.-C.; Yam, V.-W.-W. *J. Mater. Chem.* **2010**, *20*, 2063-2070.

Chapter 2: Photoswitchable *N*-Heterocyclic Carbenes: Using Light to Modulate Electron Donating Properties

2.1 Introduction

N-heterocyclic carbenes (NHCs) are a robust and well-studied class of ligands used to support a broad range of catalytically-active transition metals.[1] The performance of these catalysts is strongly dependent on the electron donating properties of the NHC ligands,[2] and an ability to modulate this donicity using external stimuli should enable access to switchable catalysts with controlled activities and selectivities.[3] We envisioned incorporating a photochromic[4] diarylethene (DAE)[5] into the backbone of a NHC scaffold[6] to facilitate the remote photomodulation and monitoring of the carbene's donating ability. For example, as illustrated in Figure 2.1, the bonding pattern of an imidazol-2-ylidene scaffold properly outfitted with thiophenes at the 4- and 5-positions should change upon photoinduced electrocyclic ring-closing. Considering that the product of this reaction extends the conjugation of the nitrogen atoms adjoining the carbenoid nucleus,[7] less electron density should be available for donation into the π^* orbital of the C=X moiety and thus result in a stronger bond.[8] While photocyclization phenomena have been widely exploited in molecular switches[5] and modulating chemical reactivity,[9] they have rarely been used to control the electron donating ability of ligands.[10] Herein we report the first example of photochemically tuning the electronic structure and donating properties of a photochromic NHC scaffold embedded within chalcogen (X = O, S) and metal (X = $Ir(CO)_2Cl$) adducts.

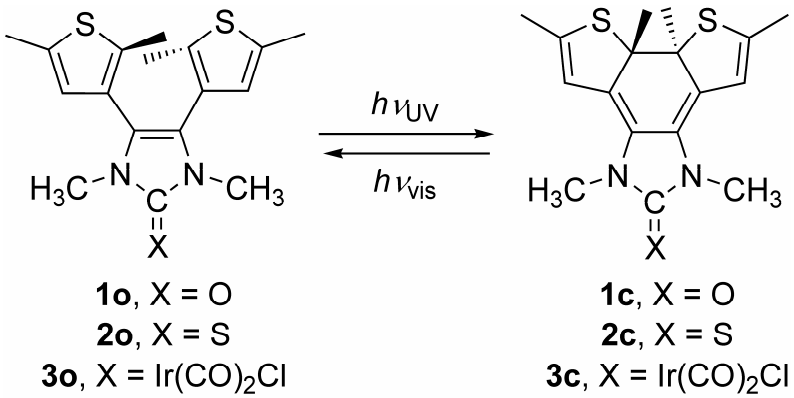

Figure 2.1: Photochromism of various NHC-adducts. The notation **o** and **c** refers to the open- and ring-closed isomers, respectively.

2.2 RESULTS AND DISCUSSION

The 4,5-diarylimidazolones,[11] **1** and **2**, were prepared as shown in Figure 2.2. Acylation of commercially-available 2,5-dimethylthiophene with aluminum trichloride and oxalyl chloride in the presence of pyridine afforded diketone **4**,[12] which was reduced to the α-hydroxy ketone **5** using zinc metal and sodium chloride in refluxing methanol/H_2O (1:1 v/v).[13] Subsequent condensation of 5 with 1,3-dimethylurea in refluxing acetic acid afforded **1o**. Thiourea **2o** was also prepared from **4**, which underwent formylative cyclization under aqueous acidic conditions to afford imidazole **6**.[8] Subsequent methylation with CH_3I in acetonitrile using K_2CO_3 as a base gave known[6] imidazolium salt **7** which was then deprotonated with NaH and catalytic sodium tert-butoxide in the presence of elemental sulfur to yield **2o**.[14] Notably, the syntheses of **1** and **2** avoided the use of metal-catalyzed aryl-aryl cross-coupling chemistry that is commonly used to prepare photochromic DAEs.[5,6,9]

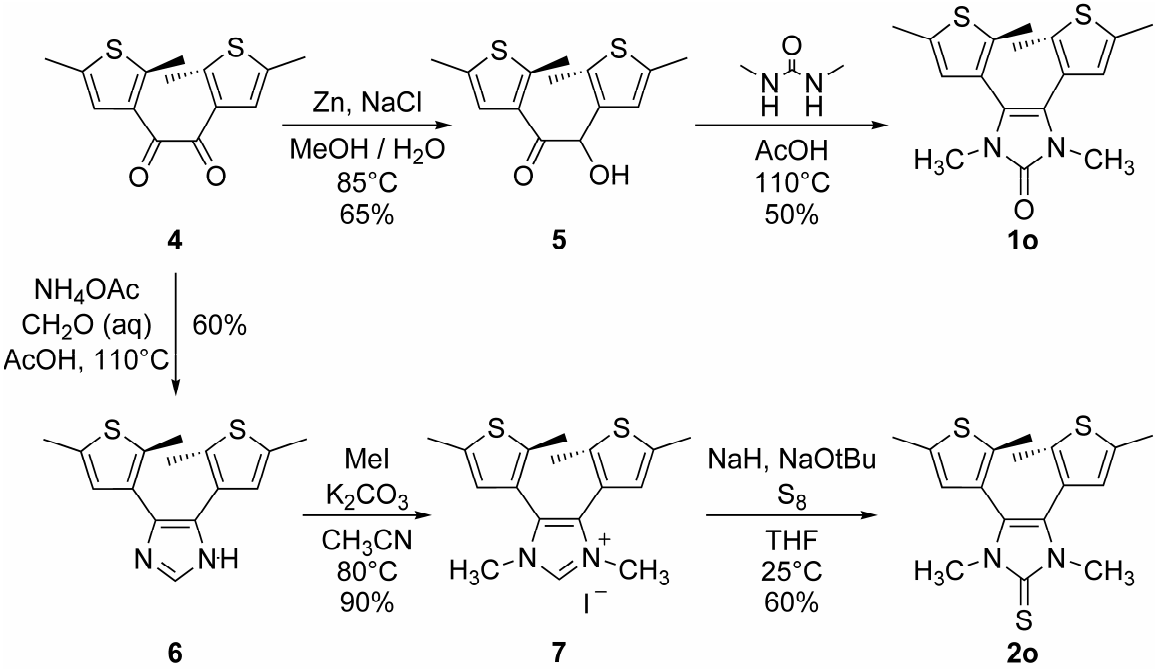

Figure 2.2: Synthesis of urea **1o** and thiourea **2o**.

The UV-vis spectra of **1o** and **2o** acquired in acetonitrile exhibited intense absorptions between 210 nm and 300 nm which were assigned to the $n \rightarrow \pi^*$ and $\pi \rightarrow \pi^*$ transitions of the N-heterocycle and thiophene systems, respectively.[6] UV irradiation (λ_{irr} = 280 nm) of a colorless solution of **1o** in acetonitrile resulted in the development of a bright orange color, concomitant with a decrease in the intensity of the absorption band centered at 214 nm and the appearance of a new band at 476 nm (Figure 2.3). Similarly, irradiation of **2o** under the same conditions resulted in the appearance of a new absorption band at 521 nm and the development of a red color. Collectively, these spectral changes were consistent with the disruption of aromaticity in the thiophene rings in the aforementioned substrates and the formation of an extended π-conjugated system.[5, 6] Moreover, the isosbestic points observed at 255 nm for **1o** and 289 nm for **2o** suggested to us that the cyclization reactions proceeded without noticeable side reactions.

Compounds **1o** and **2o** reached their photostationary states after 10 and 4 min of irradiation and were comprised of 75% **1c** and 74% **2c**, respectively.[15] Subsequent irradiation of these solutions with visible light (λ_{irr} > 500 nm) resulted in decoloration and attenuation of the broad, low energy absorption bands. The initial UV-vis spectra were nearly completely restored (>90% conversion), indicating that the closed isomers returned to their ring-opened precursors with minimal decomposition.[16] Additionally, the cyclizations were confirmed by ^{1}H NMR spectroscopic analysis of the mixtures, which showed the expected upfield shifts of the signals assigned to the thiophenes (i.e., from δ = 6.4 ppm in **1o** to 5.9 ppm in **1c**, and from δ = 6.6 ppm in **2o** to 6.2 ppm in **2c**; $CDCl_3$).

Once the expected photocyclization processes were confirmed, the effect of the cyclization reaction on the $C_{carbenoid}$=X bonds in **1o** and **2o** was investigated using IR spectroscopy (Figure 2.3). Prior to the irradiation of **1o**, a signal was observed at 1688 cm^{-1} and was assigned to the urea C=O stretching frequency (ν_{CO}). Upon irradiation at 280 nm, a new band appeared at 1716 cm^{-1}, which was attributed to the ν_{CO} of **1c**. The 28 cm^{-1} shift to higher frequency reflected a significant difference in the electronic character of the two isomers.[17] Thus, while the thiophene rings in **1o** are electronically isolated, photocyclization enabled delocalization of the nitrogen lone pairs into the dihydrothiophene π-systems of **1c** and afforded a stronger C=O bond. Due to vibrational coupling effects,[18] only a small difference in the thiourea C=S stretching frequency (< 2 cm^{-1}) was observed when the IR spectra of **2o** and **2c** were compared.

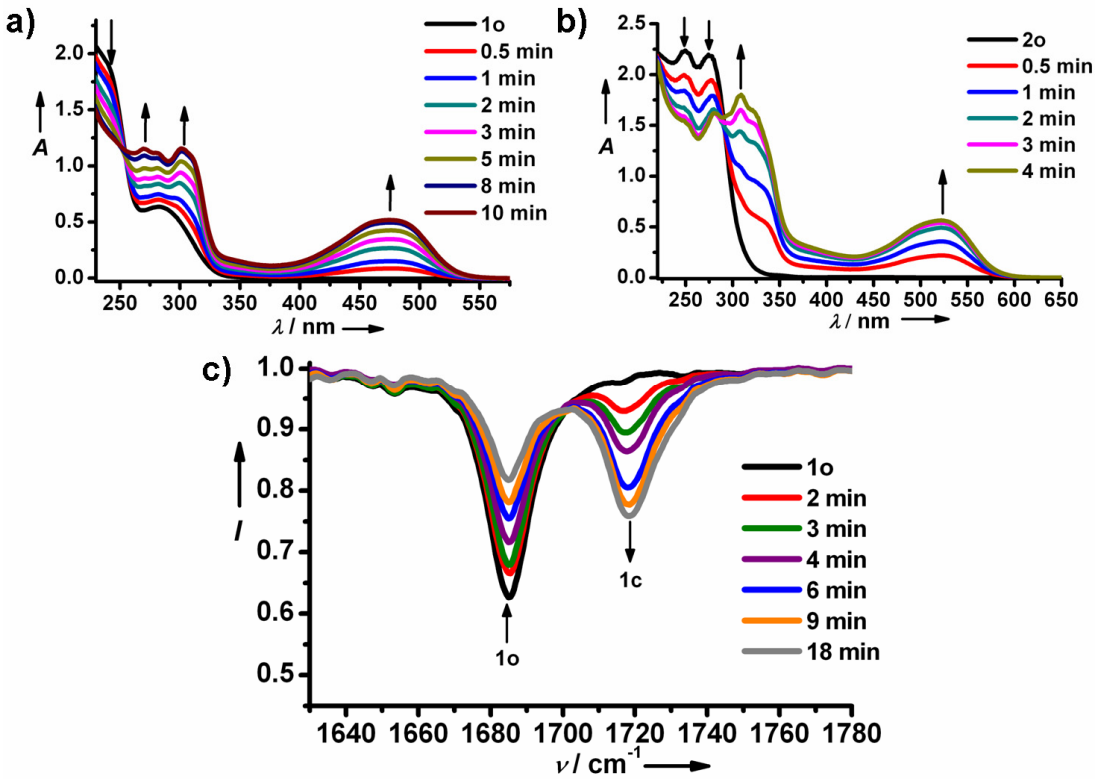

Figure 2.3: (a) UV-vis spectral changes of **1o** in acetonitrile ($[\mathbf{1o}]_0 = 1 \times 10^{-4}$ M) upon UV irradiation ($\lambda_{irr} = 280$ nm). The spectra were recorded after irradiation for 0, 0.5, 1, 2, 3, 5, 8, and 10 min (indicated). (b) UV-vis spectral changes of **2o** in acetonitrile ($[\mathbf{2o}]_0 = 1 \times 10^{-4}$ M) upon UV irradiation ($\lambda_{irr} = 280$ nm). The spectra were recorded after irradiation for 0, 0.5, 1, 2, 3, and 4 min (indicated). (c) Normalized infrared spectral changes of the carbonyl stretching frequency upon photochemical conversion of **1o** (1688 cm^{-1}) to **1c** (1716 cm^{-1}) in acetonitrile ($[\mathbf{1o}]_0 = 1.0 \times 10^{-2}$ M). The reaction was facilitated by 280 nm light in a CaF_2 IR solution cell, and spectra were recorded after 0, 1, 2, 3, 4, 5, 6, 7, 9, 12 (not shown), and 18 min of irradiation (indicated). The arrows indicate the evolution of the spectral changes over time.

In addition to demonstrating a photoinduced redistribution of electron density in the imidazolone ring of **1o** in situ, we also isolated and characterized the photocyclized product **1c**. After UV irradiation ($\lambda_{irr} = 280$ nm) in acetonitrile, the photocyclized urea **1c** was separated from its mixture with **1o** by column chromatography and isolated in 62% yield. The UV-vis, ^{1}H NMR and IR spectra of **1c** were consistent with the observed

spectral changes described above, and the ^{13}C NMR spectrum of **1c** featured a signal at δ = 67.8 ppm ($CDCl_3$), which was assigned to the sp^3 carbon nuclei adjacent to the sulfur atoms in the dihydrothiophene moieties. Upon isolation and storage in the dark, **1c** was found to be stable in the solid state and in solutions of chloroform, toluene, and hexanes at room temperature for > 24 h, or for weeks at –20 °C (< 5% decomposition was observed by ^1H NMR spectroscopy). In acetonitrile, **1c** cleanly reverted back to **1o** upon exposure to visible light (λ_{irr} > 500 nm) for 3 min, or upon standing in ambient light for 3 h.[19]

The structures of **1o** as well as **1c** were also confirmed by single crystal X-ray diffraction analysis.[20] The solid state structure of **1c** is to the best of our knowledge the first example of an isolated, photocyclized DAE containing a heterocyclic linker. As shown in Figure 2.4, the changes in bond lengths and angles from **1o** to **1c** were consistent with the aforementioned photocyclization reaction. For example, the C_2 symmetric thiophene rings in **1o** were twisted with respect to the imidazolone ring and featured an interplanar torsion angle of 57.3(3)º. In contrast, the dihydrothiophene rings in **1c** were significantly more planar with respect to the imidazolone ring and featured an interplanar torsion angle of 16.40(12)º, due to the formation of the bond between C6 and C7. The C6–C7 distance in **1c** (1.53(2) Å) was consistent with that of a C–C single bond, whereas the analogous distance in **1o** was significantly longer (3.23 Å). Additionally, the hybridization state of C6 and C7 changed from sp^2 in **1o** to sp^3 in **1c**, as evidenced by the sum of the bond angles around C7 (**1o**, 360º; **1c**, 324º[21]). As expected for a photochemical electrocyclic ring closing of a 1,3,5-hexatriene,[22] the C14 and C15 methyl groups in **1c** adopted a *trans* configuration.[23] Finally, the aforementioned increase in ν_{CO} induced by the photocyclization reaction may be further rationalized by comparing the C2–C4 and C2–C3 distances measured in the solid state structures of **1o**

and **1c**. In the latter, each nitrogen atom is formally conjugated to a dihydrothiophene moiety which effectively attenuates donation into the carbonyl's π*-orbital.[24]

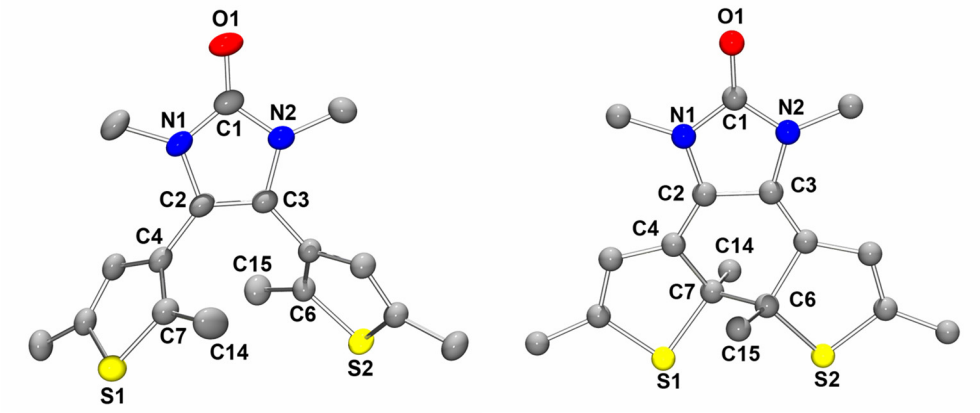

Figure 2.4: POV-ray representations of urea **1o** (left) and its cyclized derivative **1c** (right) showing ellipsoids at 50% probability. Hydrogen atoms have been omitted for clarity. Key distances (Å), angles (º), and torsions (º) with errors expressed in parentheses: **1o**, N1-C1, 1.379(3); N2-C1, 1.363(3); C1-O1, 1.233(2); N1-C2, 1.402(2); C2-C4, 1.466(3); C4-C7, 1.367(3); C2-C3, 1.361(3); N1-C1-N2, 106.29(16); N1-C2-C4, 122.56(17); C3-C2-C4, 130.37(17); C4-C7-S1, 110.80(15); C14-C7-S1, 120.60(16); C3-C2-C4-C7, 57.3(3). **1c**, N1-C1, 1.386(8); N2-C1, 1.377(9); C1-O1, 1.228(8); N1-C2, 1.395(8); C2-C4, 1.356(9); C4-C7, 1.556(16); C2-C3, 1.439(9); C7-C6, 1.53(2); N1-C1-N2, 107.4(6); N1-C2-C3, 131.6(6); C3-C2-C4, 122.4(6); C4-C7-S1, 99.4(10); C14-C7-S1, 109.7(10); C3-C2-C4-C7, -16.4(12).

Having demonstrated the ability of the DAE photocyclization to alter the bonding character of a NHC-chalcogen adduct, we sought to extend the concept to altering the ligand donating ability of a NHC contained within a metal complex. With NHC precursor **7** in hand, the [Ir(cod)Cl] (cod = 1,5-cis,cis-cyclooctadiene) complex **9** was synthesized via transmetallation from the silver complex **8**,[6] obtained by deprotonation of **7** with silver oxide (Figure 2.5).[25] Bubbling 1 atm of carbon monoxide into a dichloromethane solution of **9** afforded the carbonyl complex **3o**, which was used to evaluate the change in NHC donicity by monitoring the $\Delta\nu_{CO}$ upon irradiation.[26]

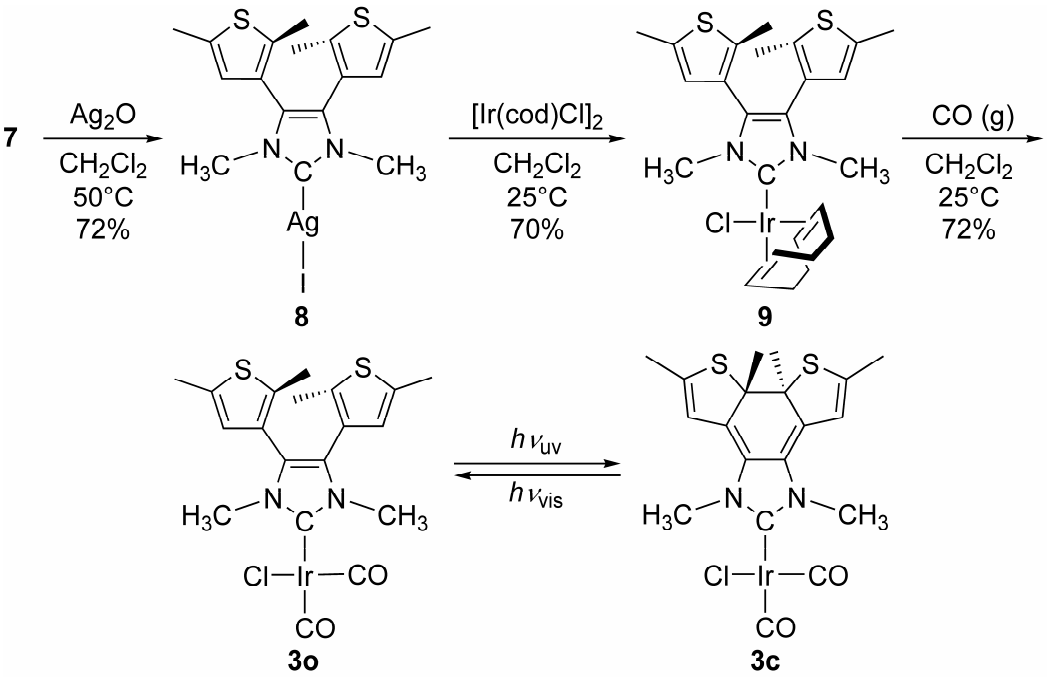

Figure 2.5: Synthesis and photochromism of complex **3**.

UV irradiation (λ_{irr} = 297 nm) of a cyclohexane[27] solution of **3o** resulted in a decrease in intensity of the high energy absorption centered at 227 nm and the appearance of a new band at 545 nm in the UV-vis spectrum, consistent with the spectral changes expected for the photocyclization process shown in Figure 2.5.[28] The cyclization was confirmed by ^{1}H NMR spectroscopy, wherein a signal was observed at δ = 5.38 ppm (C_6D_6) and attributed to the newly formed dihydrothiophene. Prior to irradiation, the IR spectrum of **3o** exhibited two signals at 2066 cm^{-1} and 1978 cm^{-1}, which were assigned to the νCOs of the carbonyl ligands. Upon irradiation, two new bands appeared at 2072 cm^{-1} and 1986 cm^{-1} and were assigned to the νCOs of **3c**. The formation of these signals was concomitant with a decrease in the intensity of the analogous νCOs of **3o** (Figure 2.6). Subsequent irradiation with visible light (λ_{irr} > 500 nm) resulted in reversion of **3c** to the starting material **3o**, as evidenced by the disappearance of the peaks at 2072 cm^{-1} and

1986 cm^{-1} and an increase in the intensity of the signals previously observed at 2066 cm^{-1} and 1978 cm^{-1}.[29] The Tolman electronic parameters (TEPs),[26] as calculated from these IR data,[26a] revealed that the ligand donating ability of the NHC in **3o** (TEP = 2049 cm^{-1}) falls within the range of known NHCs while that of **3c** (2055 cm^{-1}) approaches that of typical phosphines. In other words, the 6 cm^{-1} shift in TEP upon irradiation indicates that the photocyclization of **3o** to **3c** significantly decreases the ability of the NHC to donate electron density to the metal center. Since TEP values have been tied to activities of various catalysts,[2] the ability to photochemically alter a ligand's TEP may now be extended to the photomodulation of catalytic activity.

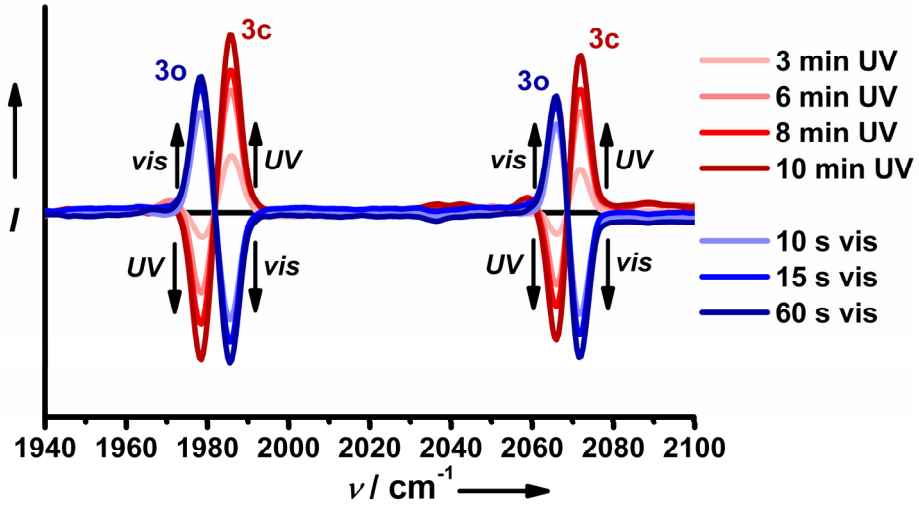

Figure 2.6: (red) Normalized infrared difference spectra showing the shift in the νCO*s* upon the photochemical conversion of **3o** (2066 cm^{-1} and 1978 cm^{-1}) to **3c** (2072 cm^{-1} and 1986 cm^{-1}) in cyclohexane solution ($[\mathbf{3o}]_0 = 1.0 \times 10^{-2}$ M). The reaction was promoted by 297 nm light in a quartz cuvette. Aliquots were transferred to a CaF_2 IR solution cell and spectra were recorded after 0, 3, 6, 8, and 10 min of irradiation (indicated). (blue) Normalized infrared difference spectra showing the shift in the νCO*s* upon the photochemical reversion of **3c** (2072 cm^{-1} and 1986 cm^{-1}) to **3o** (2066 cm^{-1} and 1978 cm^{-1}) in cyclohexane solution ($[\mathbf{3o}]_0 = 1.0 \times 10^{-2}$ M). After 10 min of UV irradiation, the sample was irradiated with visible light ($\lambda_{irr} > 500$ nm) in a quartz cuvette. Aliquots were transferred to a CaF_2 IR solution cell and spectra were recorded after 10, 15 and 60 s of irradiation (indicated). The arrows indicate the evolution of the spectral changes over time.

2.3 Conclusions

In conclusion, we report the first example of photochemically switching the electron donating properties of an NHC by exploiting a photochromic DAE integrated with the backbone of an imidazol-2-ylidene. The chalcogen-NHC adducts **1o** and **2o** were found to undergo photoinduced electrocyclic ring closure, as determined by NMR, IR, and UV-vis spectroscopy, as well as X-ray crystallography for the former. Upon photocyclization of **1o**, the donation of electron density from the nitrogen atoms to the carbonyl moiety was reduced, as evidenced by an increase in the measured νCO. Similarly,

a significant change in the ν_{CO}-derived TEP of the NHC ligand contained within the $Ir(CO)_2Cl$ complex **3o** was measured upon irradiation. Collectively, these data establish a new approach to remotely changing the donating properties of NHCs and potentially the electronic characteristics of other heteroatomic systems.[30] In a broader perspective, the results described herein are expected to guide the discovery and development of NHC-based catalysts with photoswitchable activities, selectivities, and other functions.

2.4 EXPERIMENTAL

2.4.1 Materials and Methods

Unless otherwise specified, all reagents were purchased from commercial sources and used without further purification. Solvents were dried and degassed using a Vacuum Atmospheres Company solvent purification system. $[Ir(cod)Cl]_2$ (cod = 1,5-cis,cis-cyclooctadiene) was synthesized according to a literature procedure.[31] ^1H and ^{13}C NMR spectra were recorded using a Varian 300 or 400 MHz spectrometer. Chemical shifts δ (in ppm) are referenced to tetramethylsilane using the residual solvent as an internal standard. For ^1H NMR: $CDCl_3$, 7.24 ppm; DMSO-d_6, 2.50 ppm; C_6D_6, 7.15 ppm. For ^{13}C NMR: $CDCl_3$, 77.0 ppm; DMSO-d_6, 39.5 ppm; C_6D_6, 128.0 ppm. Coupling constants (*J*) are expressed in hertz (Hz). FT-IR spectra were recorded using Perkin-Elmer Spectrum BX system in the solid state in KBr or in acetonitrile, cyclohexane, or dichloromethane solution in a Perkin-Elmer CaF_2 IR solution cell. Melting points were obtained with a Mel-Temp apparatus and are uncorrected. Mass spectra (MS, ESI or CI) were obtained with a VG analytical ZAB2-E or a Karatos MS9 instrument and are reported as m/z (relative intensity). UV-vis spectra were acquired using a Perkin-Elmer Lambda 35 UV-vis Spectrometer in 6Q Spectrosil quartz cuvettes (Starna) with 1.0 cm path lengths and 3.0 mL sample solution volumes. Beer's law measurements were performed using 10, 20,

30, and 40 μM sample concentrations. Photochemical reactions monitored by UV-vis spectroscopy were performed in the same quartz cuvettes using 4.0 mL sample solution volumes at substrate concentrations of 0.1 mM or 0.033 mM. The irradiation source for photochemical reactions was a Newport/Oriel 66942 200-500W Hg Arc lamp housing equipped with a 350 W Hg lamp, a Newport 6117 liquid filter, a Newport 71445 electronic safety shutter, and a Newport 71260 filter holder. The source was powered by a Newport 669910 power supply and mounted on a Newport XL48 optical rail with a Newport 13950 shielded cuvette holder placed at a distance of 8 cm from the end of the source. The irradiation wavelength for the photocyclization reactions was obtained using a 280 nm bandpass filter (Andover Corporation). For the cycloreversion reaction, visible light was obtained using a long-pass edge filter (> 500 nm) (Andover Corporation). Elemental analyses were performed at Midwest Microlab, LLC (Indianapolis, IN). Deconvolution of infrared spectroscopic peaks was performed using PeakFit, Version 4.12 (SeaSolve Software Inc.).

2.4.2 Syntheses

1,2-Bis-(2,5-dimethyl-thiophen-3-yl)-ethanedione (4). An oven-dried 500 mL three-necked round bottom flask equipped with an addition funnel, N_2 inlet adaptor, rubber septum, and a stir bar was evacuated and refilled with N_2 (3×). The reaction flask was then charged with 6.0 g (44.9 mmol) of aluminum trichloride, which was suspended in 50 mL of CH_2Cl_2. The resulting suspension was cooled in a -18 °C NaCl/ice bath and 1.8 mL (22.3 mmol) of pyridine in 10 mL of CH_2Cl_2 was added via the addition funnel, followed by 5.0 g (44.6 mmol) of 2,5-dimethylthiophene 25 mL in CH_2Cl_2. At -18 °C, 3.4 g (26.8 mmol) of oxalyl chloride in 25 mL of CH_2Cl_2 was added dropwise to the reaction mixture over a period of 80 min. After the addition was complete, the temperature of the

ice bath was allowed to warm to 5 °C over 90 min, and the reaction mixture was then poured into 200 mL of ice water. The organic layer was separated and the aqueous layer was extracted with 3 × 200 mL portions of chloroform. The combined organic layers were neutralized by washing with water (200 mL) followed by 2 × 200 mL portions of a saturated aqueous solution of K_2CO_3. The organic layer was dried over Na_2SO_4 and the solvent was removed under reduced pressure. The resulting crude, dark orange oil was purified by column chromatography on silica gel, eluting with a 10:1 v/v mixture of hexanes and ethyl acetate, to afford 2.17 g (35% yield) of desired product as a yellow-orange solid. Spectral data matched literature values.[32] mp 64-65 °C. ^{1}H NMR (400 MHz, $CDCl_3$): δ 2.36 (s, 6H), 2.70 (s, 6H), 6.89 (s, 2H). ^{13}C NMR (100 MHz, $CDCl_3$) δ 14.9, 15.9, 126.8, 131.7, 136.2, 151.7, 189.16. UV-vis (CH_2Cl_2): λ_{abs} = 270 nm (ε = 14553 dm^3 mol^{-1} cm^{-1}). HRMS (*m/z*): Calcd. for $C_{14}H_{14}O_2S_2$ $[M+Na]^+$, 301.0333; Found, 301.0329.

1,2-Bis-(2,5-dimethyl-thiophen-3-yl)-2-hydroxy-ethanone (5). A three-necked round bottom flask equipped with a reflux condenser, N_2 inlet adaptor, rubber septum and stir bar was charged with 2.0 g (7.2 mmol) of **4**, 5.1 g (76 mmol) of zinc metal, and 4.5 g (76 mmol) of sodium chloride. To this flask was added 50 mL of methanol and 50 mL of deionized water, and the resulting mixture was heated to reflux under N_2 for 18 h. The reaction mixture was cooled to room temperature and poured into 200 mL of deionized water. The resulting precipitate was collected on a frit of medium porosity, dissolved in ethyl acetate and then filtered through the frit into a clean collection flask to remove the excess zinc metal. The ethyl acetate filtrate was then dried over Na_2SO_4 and the solvent was removed under reduced pressure. The resulting yellow solid was washed with cold hexanes and collected via filtration to yield 1.3 g of the desired product as a pale yellow powder (65% yield). Spectral data matched literature values.[33] mp 133-135 °C. ^{1}H NMR

(400 MHz, $CDCl_3$): δ 2.30 (d, *J* = 4.8, 6H), 2.49 (s, 3H), 2.69 (s, 3H), 4.39 (d, *J* = 5.6, 1H) 5.49 (d, *J* = 6.0, 1H), 6.29 (s, 1H), 6.65 (s, 1H). ^{13}C NMR (100 MHz, $CDCl_3$) δ 13.0, 15.0, 15.1, 16.2, 70.9, 124.2, 124.9, 131.6, 134.4, 135.1, 135.6, 136.9, 150.7, 194.2. UV-vis (CH_2Cl_2): λ_{abs} = 270 nm (ε = 14553 dm^3 mol^{-1} cm^{-1}). HRMS (*m/z*): Calcd. for $C_{14}H_{16}O_2S_2$ $[M-H]^+$, 279.0513; Found, 279.0515.

1,3-Dimethyl-4,5-bis(2,5-dimethyl-thiophen-3-yl)-imidazol-2-one (1o). A three-necked round bottom flask fitted with a reflux condenser, N_2 inlet adaptor, rubber septum and stir bar was charged with 1.0 g (3.6 mmol) of **5** and 1.0 g (11.3 mmol) of 1,3-dimethylurea. The reaction flask was then evacuated and refilled with N_2 (3×), after which 5 mL of deoxygenated acetic acid was added. The reaction mixture was heated to reflux for 12 h under an atmosphere of N_2 and then cooled to room temperature. Deionized water (50 mL) was added to the cooled reaction mixture, which was extracted with 3 × 50 mL portions of chloroform. The combined organic layers were washed with 100 mL portions of a saturated aqueous solution of $NaHCO_3$ (3×), dried over Na_2SO_4, and the residual solvent was removed under reduced pressure. Purification by column chromatography on silica eluting with 1:9 v/v 2-propanol/ethyl acetate afforded 600 mg (50% yield) of the desired product as a beige powder. mp 170-172 °C. ^1H NMR (400 MHz, $CDCl_3$): δ 1.87 (s, 6H), 2.36 (s, 6H), 3.13 (s, 6H), 6.39 (s, 2H). ^{13}C NMR (100 MHz, $CDCl_3$) δ 13.7, 15.2, 28.6, 116.6, 125.3, 126.2, 136.2, 136.5, 153.7. IR (KBr): ν 3348, 3040, 2910, 1688, 1572, 1442, 1380, 1241, 1148, 1108, 1009, 882, 745, 685, 591, 496, 407 cm^{-1}. UV-vis (CH_3CN): λ_{abs} = 214 nm (ε = 21605 dm^3 mol^{-1} cm^{-1}), 240 nm (ε = 17630 dm^3 mol^{-1} cm^{-1}), 282 nm (ε = 5979 dm^3 mol^{-1} cm^{-1}). HRMS (*m/z*): Calcd. for $C_{17}H_{20}N_2OS_2$ $[M+H]^+$, 333.1095; Found, 333.1092. Anal. Calcd. for $C_{17}H_{20}N_2OS_2$: C, 61.41; H, 6.06; N, 8.43; Found: C, 61.13; H, 5.93; N, 8.45.

Photocyclized Urea 1c. A solution of **1o** (34 mg, 0.16 mmol) in 24 mL of acetonitrile was prepared under inert nitrogen atmosphere in a glove box. Successive 4 mL portions of the solution were transferred to a quartz cuvette, removed from the glove box and irradiated for 3 h each. The 4 mL portions were combined and the solvent removed under reduced pressure to afford a mixture of **1o** and **1c**, as determined by ^{1}H NMR spectroscopy ($CDCl_3$). The two isomers were separated by column chromatography (SiO_2, 1:1 v/v ethyl acetate/hexanes) to afford 21 mg of **1c** (62% yield). ^{1}H NMR (400 MHz, $CDCl_3$): δ 1.97 (s, 6H), 2.07 (s, 6H), 3.17 (s, 6H), 5.92 (s, 2H). ^{13}C NMR (100 MHz, $CDCl_3$) δ 17.9, 27.5, 29.0, 67.7, 113.9, 120.9, 122.9, 143.4, 156.1. IR (KBr): ν 2904, 1716, 1606, 1440, 1389, 1330, 1255, 1119, 1059, 862, 801, 743, 630, 575 cm^{-1}. UV-vis (CH_3CN): λ_{abs} = 269 nm (ε = 13797 dm^3 mol^{-1} cm^{-1}), 282 nm (ε = 13070 dm^3 mol^{-1} cm^{-1}), 302 nm (ε = 14830 dm^3 mol^{-1} cm^{-1}), 476 nm (ε = 7178 dm^3 mol^{-1} cm^{-1}).

4,5-Bis(2,5-dimethyl-3-thienyl)-imidazole (6). A round bottom flask fitted with a reflux condenser and a stir bar was charged with 480 mg (1.7 mmol) of **4** in 20 mL of glacial acetic acid. To the reaction flask was added 2.9 g of ammonium acetate (37.6 mmol) and 0.7 mL of aqueous formaldehyde (37% w/w). The reaction mixture was heated to reflux for 26 h, then cooled to room temperature, diluted with 30 mL of deionized water and concentrated ammonium hydroxide was added until a pH = 7 was reached. The aqueous mixture was extracted with 100 mL portions of dichloromethane (3×) and the combined organic layers were washed with 100 mL portions of saturated, aqueous potassium carbonate (3×). The organic layer was dried over sodium sulfate and the solvent was removed under reduced pressure. The resulting yellow solid was washed with diethyl ether to yield 296 mg (60% yield) of the desired product as a beige power. Spectral data matched literature values.[8a] mp 202 ºC (dec.) ^{1}H NMR (400 MHz, DMSO-d_6): δ 1.95 (s, 6H), 2.08 (d, J = 4.8 6H), 2.32 (d, J = 18 6H), 6.51 (s, 1H), 6.59 (s, 1H),

7.70 (s, 1H), 12.17 (s, 1H). ^{13}C NMR (100 MHz, $CDCl_3$) δ 13.9, 14.3, 15.3, 55.4, 122.3, 127.6, 128.6 131.4, 132.7, 133.4, 134.0, 134.4, 135.4, 135.6. UV-vis (CH_3CN): λ_{abs} = 230 nm (ε = 19705 dm^3 mol^{-1} cm^{-1}), λ_{abs} = 272 nm (ε = 10354 dm^3 mol^{-1} cm^{-1}). HRMS (*m/z*): Calcd. for $C_{15}H_{16}N_2S_2$ $[M+H]^+$, 289.0833; Found, 289.08277.

4,5-Bis(2,5-dimethyl-3-thienyl)-1,3-dimethylimidazolium Iodide (7). A 30 mL vial was charged with 200 mg (0.7 mmol) of **6** and 600 mg K_2CO_3 in 15 mL of CH_3CN. After adding iodomethane (0.3 mL, 4.8 mmol) dropwise, the vial was sealed with a Teflon-lined cap and the resulting mixture was stirred at 80 °C for 24 h. The reaction mixture was then cooled to room temperature, filtered through a plug of Celite, and the filtrate was concentrated under reduced pressure. The resulting residue was taken up into 20 mL of dichloromethane and the insoluble salts were removed by filtration. The filtrate was concentrated under reduced pressure and the residue was washed with diethyl ether. The desired product was was collected via vacuum filtration as a cream colored powder (275 mg, 90% yield). Spectral data matched literature values.[6a] mp 221 ºC (dec.) ^{1}H NMR (400 MHz, $CDCl_3$): δ 1.9 (s, 6H), 2.39 (s, 6H), 3.83 (s, 6H), 6.49 (s, 2H), 10.42 (s, 1H). ^{13}C NMR (100 MHz, $CDCl_3$) δ 14.2, 15.5, 35.2, 120.8, 125.6, 128.5, 138.0, 138.8, 140.4. UV-vis (CH_3CN): λ_{abs} = 244.8 nm (ε = 31955 dm^3 mol^{-1} cm^{-1}). HRMS (*m/z*): Calcd. for $C_{17}H_{22}IN_2S_2$ $[M-I-H]^+$, 317.1146; Found, 317.1146.

3-Dimethyl-4,5-bis(2,5-dimethyl-thiophen-3-yl)-imidazol-2-thione (2o). A 30 mL vial was charged with 90 mg of **6** dissolved in tetrahydrofuran under N_2 in a glove box. Sodium hydride (6 mg, 95% in mineral oil) and catalytic sodium *tert*-butoxide were added, followed by 20 mg of elemental sulfur. The reaction mixture was stirred at room temperature for 16 h, then removed from the glove box and filtered through a 0.2 μm PTFE filter. The filtrate was concentrated under reduced pressure and the residue washed with 20 mL of hexanes. The remaining salts were removed by filtration and the filtrate

was concentrated under reduced pressure. Purification by column chromatography on silica eluting with 1:9 v/v ethyl acetate/hexanes followed by ethyl acetate afforded 40 mg (60% yield) of the desired product. mp 172-174 °C. ^{1}H NMR (400 MHz, $CDCl_3$): δ 1.86 (s, 6H), 2.37 (s, 6H), 3.49 (s, 6H), 6.41 (s, 2H); ^{13}C NMR (100 MHz, $CDCl_3$): δ 161.8, 137.7, 136.9, 125.9, 124.1, 123.5, 33.2, 15.2, 13.7. UV-vis (CH_3CN): λ_{abs} = 247.47 nm (ε = 7749 dm^3 mol^{-1} cm^{-1}), λ_{abs} = 275.61 nm (ε = 7620 dm^3 mol^{-1} cm^{-1}). IR (KBr): 2935, 2908, 2850, 1569, 1438, 1389, 1377, 1242, 1167, 1145, 1102, 1002, 883, 848, 538, 494 cm^{-1}. HRMS (*m/z*): Calcd. for $C_{17}H_{20}N_2S_3$ $[M+1]^+$, 348.0789; Found, 349.0822. Anal. Calcd. for $C_{17}H_{20}N_2S_3$: C, 58.58; H, 5.78; N, 8.04; Found: C, 58.39; H, 5.69; N, 7.95.

[Ag{4,5-Bis(2,5-dimethyl-3-thienyl)-1,3-dimethylimidazolylidene}I] (8): A 40 mL vial equipped with a stir bar was charged with 200 mg (0.45 mmol) of **6** and 25 mL of dichloromethane under N_2 in a glove box. To the solution was added 50 mg (0.22 mmol) of silver oxide and 3 Å molecular sieves. The reaction vial was sealed with a Telfon-lined cap, removed from the glove box and heated to 50 °C overnight in the dark. The reaction mixture was filtered to remove the molecular sieves while hot and the filter cake was washed with hot dichloromethane and methanol. The filtrate was concentrated under reduced pressure, and the resulting residue was triturated in diethyl ether. The product was collected by vacuum filtration to afford 180 mg (72% yield) of the desired product as a tan solid. mp 146 °C (dec). ^{1}H NMR (400 MHz, $CDCl_3$): δ 1.93 (s, 6H), 2.38 (s, 6H), 3.67 (s, 6H), 6.44 (s, 2H). Characterization of this compound via ^{13}C NMR spectroscopy was not possible due to its poor solubility. HRMS (*m/z*): Calcd. for $C_{17}H_{20}N_2S_2I^{107}Ag$, 549.9164; Found, 549.9156; Calcd. for $C_{17}H_{20}N_2S_2I^{109}Ag$, 551.9160; Found, 551.9151.

[Ir{4,5-Bis(2,5-dimethyl-3-thienyl)-1,3-dimethylimidazolylidene}(cod)Cl] (9): A 40 mL vial with a stir bar was charged with 180 mg (0.3 mmol) of **7** and 10 mL of

dichloromethane under N_2 in a glove box. To the mixture was added a solution of 100 mg (0.15 mmol) of $[Ir(cod)Cl]_2$ in 10 mL of dichloromethane. The reaction mixture was stirred at room temperature for 6 h during which time the solution turned bright yellow and a white precipitate formed. The reaction mixture was removed from the glove box and filtered through a 0.2 μm PTFE filter. The filtrate was concentrated under reduced pressure which produced a yellow film. Purification of residue using column chromatography (SiO_2; 3:1 v/v hexanes:ethyl acetate as the eluent) afforded 150 mg (70% yield) of the desired product as a bright yellow powder. mp 181 °C (dec). ^{1}H NMR (400 MHz, $CDCl_3$): δ 1.58-1.89 (m, br, 10H), 2.20 (t, br, J = 4.8, 6H), 2.34 (s, 6H), 2.97 (s, 2H), 3.77 (s, 6H), 4.56 (s, 2H), 6.39 (s, 2H). ^{13}C NMR (100 MHz, $CDCl_3$): δ 179.9, 137.3, 136.5, 127.0, 126.0, 124.4, 83.9, 51.3, 35.6, 33.5, 29.5, 15.1, 13.6. UV-vis (CH_3CN): λ_{abs} = 270 nm (ε = 12877 dm^3 mol^{-1} cm^{-1}), λ_{abs} = 374.6 nm (ε = 956 dm^3 mol^{-1} cm^{-1}), λ_{abs} = 419 nm (ε = 1098 dm^3 mol^{-1} cm^{-1}), λ_{abs} = 482 nm (ε = 301 dm^3 mol^{-1} cm^{-1}). HRMS (*m/z*): Calcd. for $C_{25}H_{32}N_2S_2ClIr$ $[M]^+$, 652.1325; Found, 652.1317. Anal. Calcd. for $C_{25}H_{32}N_2S_2ClIr$: C, 46.03; H, 4.94; N, 4.29; Found: C, 45.88; H, 4.88; N, 3.98.

[Ir{4,5-Bis(2,5-dimethyl-3-thienyl)-1,3-dimethylimidazolylidene}$(CO)_2$Cl] (3o): A round bottom flask equipped with a stir bar was charged with 75 mg (0.12 mmol) of **9** dissolved in 15 mL of dichloromethane and fitted with a rubber septum. Carbon monoxide (1 atm) was bubbled through the solution from a balloon with an attached needle for 1 h while stirring at room temperature. The dichloromethane was removed under reduced pressure and the resulting yellow film was washed with cold pentanes to remove the residual 1,5-cyclooctadiene. The product was subsequently collected as a pale yellow powder by vacuum filtration (50 mg, 72% yield). mp 170 °C (dec). ^{1}H NMR (400 MHz, $CDCl_3$): δ 1.93 (s, 6H), 2.38 (s, 6H), 3.71 (s, 6H), 6.45 (s, 2H); ^{13}C NMR (100 MHz, $CDCl_3$): δ 181.8, 173.8, 168.6, 138.5, 137.6, 128.5, 126.3, 123.9, 36.9, 15.6, 14.2.

UV-vis (cyclohexane): λ_{abs} = 237 nm (ε = 21114 dm^3 mol^{-1} cm^{-1}), λ_{abs} = 261 nm (ε = 15208 dm^3 mol^{-1} cm^{-1}), λ_{abs} = 332 nm (ε = 2002 dm^3 mol^{-1} cm^{-1}), λ_{abs} = 373 nm (ε = 2926 dm^3 mol^{-1} cm^{-1}). IR (KBr): ν_{CO} 2065, 1983 cm^{-1}. IR (cyclohexane) ν_{CO} 2066, 1978 cm^{-1}. HRMS (*m/z*): Calcd. for $C_{19}H_{23}N_2O_2S_2Cl^{191}Ir$ $[M]^+$, 601.0489; Found, 601.0496. Anal. Calcd. for $C_{19}H_{23}N_2O_2S_2ClIr$: C, 37.90; H, 3.68; N, 4.65; Found: C, 37.82; H, 3.55; N, 4.48.

Photocyclized Ir Complex 3c. A solution of **3o** (14 mg, 0.023 mmol) in 23 mL of deoxygenated cyclohexane was prepared under an atmosphere of nitrogen, sealed with a rubber septum, and 1 atm of carbon monoxide was bubbled through the solution from a balloon with an attached needle for 15 min. Successive 4 mL portions of the solution were transferred to a quartz cuvette under an atmosphere of nitrogen and irradiated for 1 h each. The 4 mL portions were combined and the solvent removed under reduced pressure to afford a mixture of **3o**, **3c** and the remainder being an unidentified decomposition products (relative ratios = 3:1:1), as determined by ^{1}H NMR spectroscopy (C_6D_6). ^{1}H NMR (400 MHz, C_6D_6): δ 1.92 (s, 9H), 2.2 (d, *J* = 13.2, 3H), 2.59 (d, *J* = 18.8, 1.5H), 2.76 (d, *J* = 19.2, 1H), 3.03 (s, 1H), 3.19 (d, *J* = 4.4, 6H), 3.46 (s, 6H), 5.38 (s, 0.5H), 5.45, (s, 0.5H), 5.92 (s, 2H). ^{13}C NMR (100 MHz, C_6D_6): δ 182.8, 174.9, 169.8, 167.5, 138.3, 137.2, 133.4, 130.7, 129.0, 126.4, 124.2, 117.9, 114.9, 111.5, 68.0, 39.2, 36.4, 34.4, 30.2, 29.3, 24.2, 23.3, 22.7, 17.7, 14.7, 13.5, 11.1. UV-vis (cyclohexane): λ_{abs} = 235, 326, 370, 548 nm. IR (cyclohexane): ν_{CO} = 2066, 1979 cm^{-1}.

Reversion of Photocyclized Ir Complex 3c to 3o. A solution of the product mixture described above in C_6D_6 (33 mM) was allowed to stand at room temperature under ambient light for 18 h. ^{1}H NMR (400 MHz, C_6D_6): δ 1.92 (s, 9H), 2.59 (d, *J* = 18.8, 1.5H), 2.76 (d, *J* = 19.2, 1H), 3.03 (s, 1H), 3.46 (s, 6H), 5.45, (s, 0.5H), 5.92 (s, 2H). IR (cyclohexane): ν_{CO} = 2066, 1978 cm^{-1}.

2.4.3 Additional Spectroscopic Data

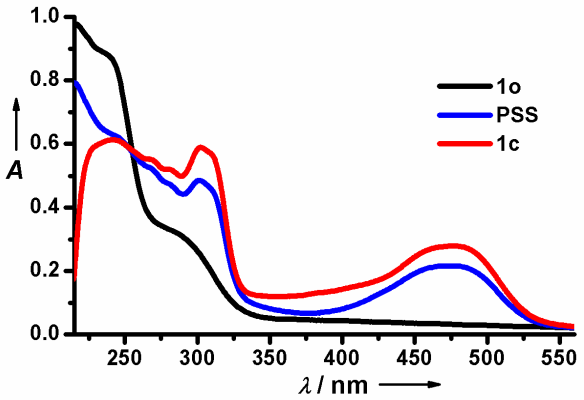

Figure 2.7: UV-vis spectra acquired in acetonitrile of **1o** (4×10^{-5} M), **1c** (4×10^{-5} M), and a 1 : 3 molar mixture of **1o** : **1c** at the photostationary state (PSS) after irradiating **1o** for 10 min ($[\mathbf{1o}]_0 = 4 \times 10^{-5}$ M).

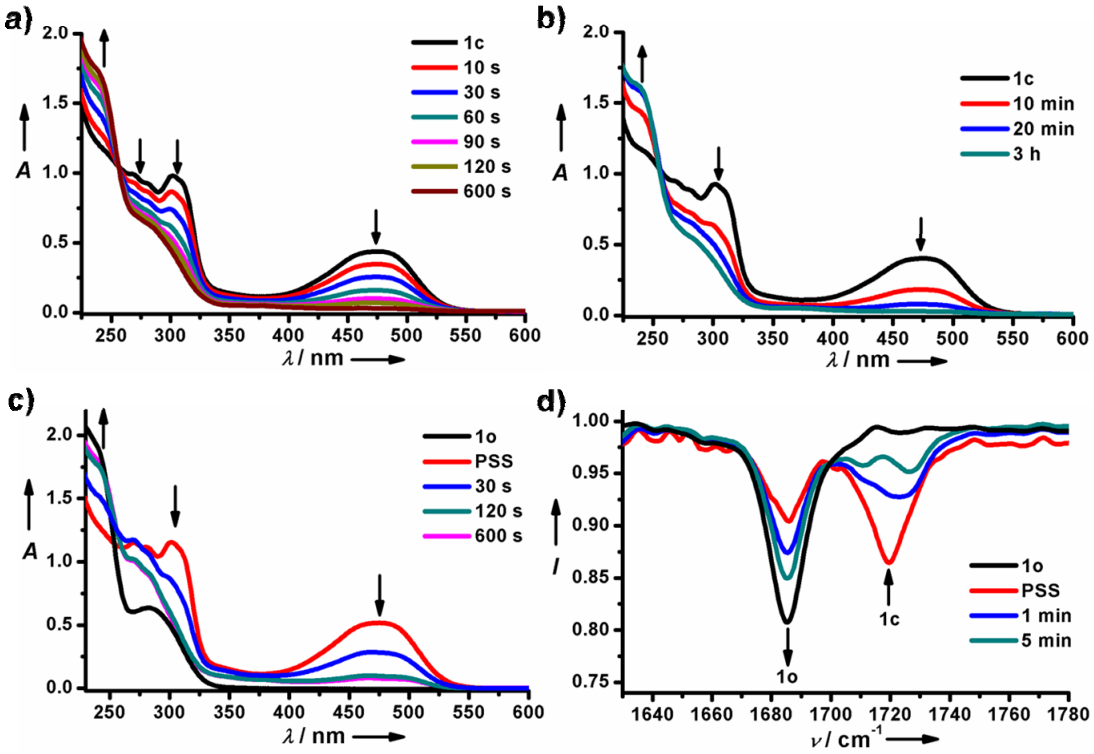

Figure 2.8: a) UV-vis spectral changes of **1c** in acetonitrile ($[\mathbf{1c}]_0 = 1 \times 10^{-4}$ M) upon visible light irradiation (> 500 nm). The spectra were recorded after irradiation for 0 s, 30 s, 60 s, 90 s, 120 s, and 600 s (indicated). b) UV-vis spectral changes of **1c** in acetonitrile ($[\mathbf{1c}]_0 = 1 \times 10^{-4}$ M) upon standing at room temperature in ambient light for 10 min, 30 min, and 3 h (indicated). c) UV-vis spectra of **1o** in acetonitrile ($[\mathbf{1o}]_0 = 1 \times 10^{-4}$ M), the photostationary state (PSS), and the PSS upon visible light irradiation (> 500 nm). The spectra were recorded after visible light irradiation of the sample in the PSS for 30 s, 120 s, and 600 s (indicated). d) Normalized IR spectra of **1o** in acetonitrile ($[\mathbf{1o}]_0 = 4.5 \times 10^{-4}$ M), the PSS, and spectral changes of the PSS upon visible light irradiation. The spectra were recorded after irradiation of the sample in the PSS (> 500 nm) for 1 min and 5 min (indicated). The arrows indicate the evolution of the spectral changes over time.

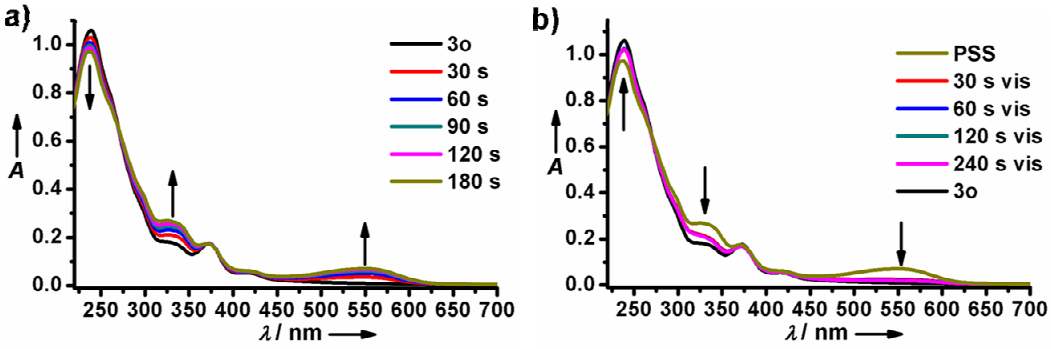

Figure 2.9: a) UV-vis spectral changes of **3o** in cyclohexane ($[\mathbf{3o}]_0 = 33 \times 10^{-5}$ M) upon irradiation at 297 nm. The spectra were recorded after irradiation for 0 s, 30 s, 60 s, 90 s, 120 s, and 180 s (indicated). b) UV-vis spectra of **3o** in cyclohexane ($[\mathbf{3o}]_0 = 33 \times 10^{-5}$ M), the PSS, and spectral changes of the PSS upon visible light irradiation (> 500 nm). The spectra were recorded after irradiation of the sample in the PSS for 30 s, 60 s, 120 s, and 240 s (indicated). The arrows indicate the evolution of the spectral changes over time.

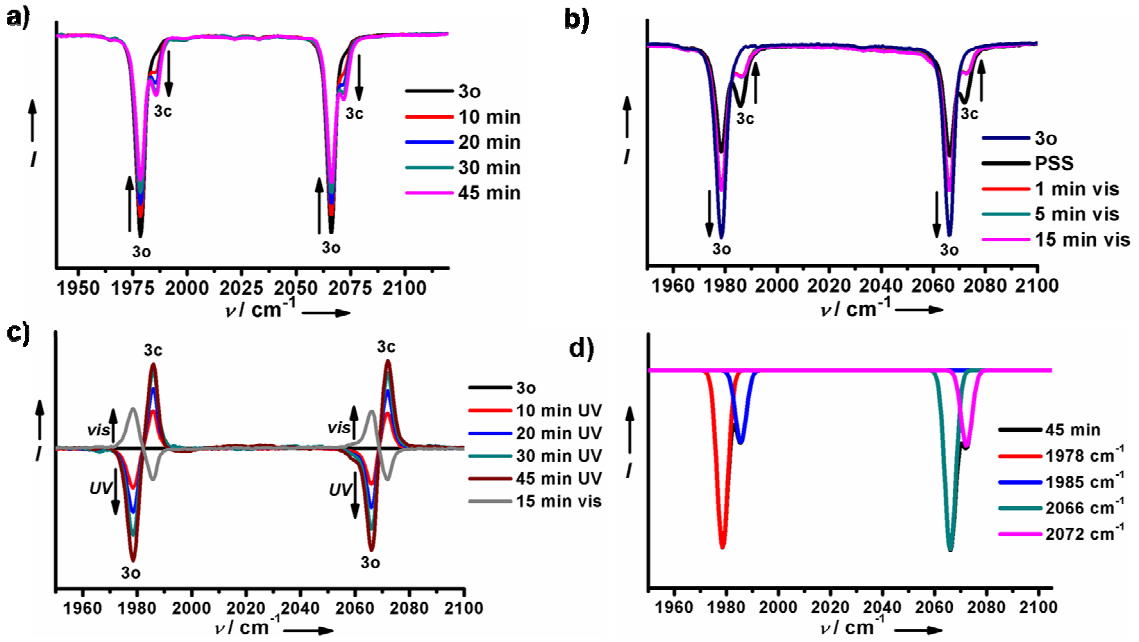

Figure 2.10: a) Normalized infrared spectra of **3o** in cyclohexane ($[\mathbf{3o}]_0 = 1 \times 10^{-4}$ M) upon irradiation at 297 nm in a quartz cuvette. Aliquots were transferred to a CaF_2 IR solution cell and the spectra were recorded after irradiation for 0, 10, 20, 30, and 45 min (indicated). b) Normalized infrared spectra of **3o** in cyclohexane ($[\mathbf{3o}]_0 = 1 \times 10^{-4}$ M), the PSS, and spectral changes of the PSS upon visible light irradiation in a quartz cuvette. Aliquots were transferred to a CaF_2 IR solution cell and the spectra were recorded after visible light irradiation of the sample in the PSS (> 500 nm) for 1, 5, and 15 min (indicated). c) Normalized infrared difference spectrum showing the shift in carbonyl stretching frequency upon photochemical conversion of **3o** (2066 cm^{-1} and 1978 cm^{-1}) to **3c** (2072 cm^{-1} and 1986 cm^{-1}) in cyclohexane solution ($[\mathbf{3o}]_0 = 1.0 \times 10^{-2}$ M). The reaction was promoted by 297 nm light in a quartz cuvette. Aliquots were transferred to a CaF_2 IR solution cell and spectra were recorded after 0, 10, 20, 30, and 45 min of irradiation (indicated). d) Peak deconvolution of the normalized infrared spectrum of the PSS in cyclohexane ($[\mathbf{3o}]_0 = 1 \times 10^{-4}$ M) after irradiation at 297 nm for 45 min; see Table 2.1 for integrated peak areas. The arrows indicate the evolution of the spectral changes over time.

Compound / Peak	Integrated Peak Area	
	10 min (λ_{irr} = 297 nm)	45 min (λ_{irr} = 297 nm)[a]
3o / 1978 cm^{-1}	0.8023	0.7106
3c / 1986 cm^{-1}	0.1977	0.2894
3o / 2066 cm^{-1}	0.8347	0.7034
3c / 2072 cm^{-1}	0.1653	0.2966

Table 2.1: Integrated peak areas obtained via peak deconvolution of the normalized IR spectra.[a] The deconvoluted spectra after 45 min of UV irradiation are shown in Figure 2.11.

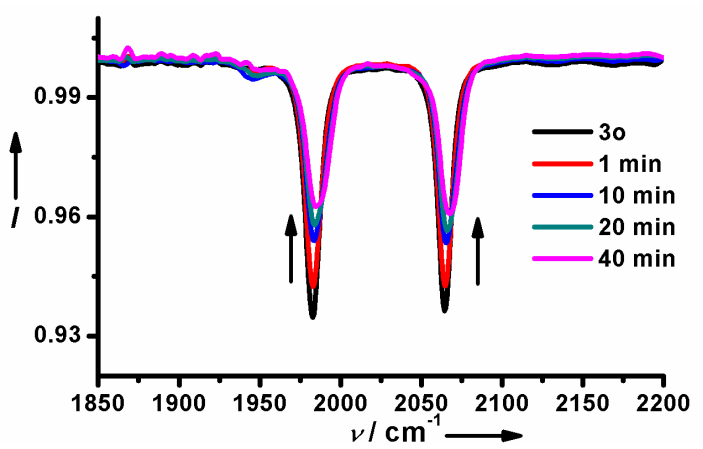

Figure 2.11: Normalized infrared spectra of **3o** in acetonitrile ([**3o**]$_0$ = 1 × 10^{-4} M) upon irradiation at 297 nm in a CaF_2 IR solution cell. Spectra were recorded after irradiation for 0, 10, 20, and 40 min (indicated). Similar results were observed in dichloromethane.

2.5 Acknowledgements

Portions of this chapter were reproduced with permissions from Neilson, B. M.; Lynch, V. M.; Bielawski, C. W. *Angew. Chem. Int. Ed.* **2011**, *50*, 10322-10326. Copyright © 2011 WILEY-VCH Verlag GmbH & Co. KGaA, Weinheim. I thank

Vincent M. Lynch for contributing the X-ray crystallography data, and Christopher Bielawksi for help in writing the original manuscript.

2.6 REFERENCES

[1] For reviews on NHCs and their coordination chemistry see: (a) Hahn, F. E.; Jahnke, M. C. *Angew. Chem. Int. Ed.* **2008**, *47*, 3122-3172. (b) Herrmann, W. A.; *Angew. Chem. Int. Ed.* **2002**, *41*, 1290-1309. (c) Bourissou, D.; Guerret, O.; Gabbaï, F. P.; Bertrand, G. *Chem. Rev.* **2000**, *100*, 39-91. (d) Herrmann, W. A.; Köcher, C. *Angew. Chem. Int. Ed.* **1997**, *36*, 2162-2187. (e) Díez-González, S.; Marion, N.; Nolan, S. P. *Chem. Rev.* **2009**, *109*, 3612-3676. (f) Dröge, T.; Glorius, F. *Angew. Chem. Int. Ed*. **2010**, *49*, 6940-6952.

[2] For studies of tuning the donicity of NHC's as a means to influence catalytic reactions, see: (a) Khramov, D. M.; Rosen, E. L.; Er, J. A. V.; Vu, P. D.; Lynch, V. M.; Bielawski, C. W. *Tetrahedron*, **2008**, *64*, 6853-6862. (b) Sanderson, M. D.; Kamplain, J. W.; Bielawski, C. W. *J. Am. Chem. Soc.* **2006**, *128*, 12614-15615. (c) Khramov, D. M.; Lynch, V. M.; Bielawski, C. W. *Organometallics*, **2007**, *26*, 6042. (d) Benhamou, L.; Vujkovic, N.; César, V.; Gornitzka, H.; Lugan, N.; Lavigne, G. *Organometallics* **2010**, *29*, 2616-2630. (e) Süβner, M.; Plenio, H. *Chem. Commun.* **2005**, *43*, 5417-5419. (f) Sashuk, V.; Peeck, L. H.; Plenio, H. *Chem. Eur. J.* **2010**, *16*, 3983-3993. (g) Hudnall, T. W.; Moerdyk, J. P.; Bielawski, C. W. *Chem. Comm.* **2010**, *46*, 4288-4290. (h) Moerdyk, J. P.; Bielawski, C. W. *Organometallics* **2011**, *30*, 2278-2284. (i) Fürstner, A.; Alcarazo, M.; Krause, H.; Lehmann, C. W. *J. Am. Chem. Soc.* **2007**, *129*, 12676-12677. (j) Hudnall, T. W.; Tennyson, A. G.; Bielawksi, C. W. *Organometallics*, **2010**, *29*, 4569-4578. (k) O'Brien, C. J.; Kantchev, E. A. B.; Chass, G. A.; Niloufar, H.; Hopkinson, A. C.; Organ, M. G., Setiadi, D. H.; Tang, T.; Fan, D. *Tetrahedron,* **2005**, 61, 9723-9735.

[3] For examples of switchable NHCs and related catalysts see: (a) Tennyson, A. G.; Lynch, V. M.; Bielawski, C. W. *J. Am. Chem. Soc.* **2010**, *132*, 9420-9429. (b) Süβner, M.; Plenio, H. *Angew. Chem. Int. Ed.* **2005**, *44*, 6885-6888. (c) Rosen, E. L.; Varnado Jr., C. D.; Tennyson, A. G.; Khramov, D. M.; Kamplain, J. W.; Sung, D. H.; Cresswell, P. T.; Lynch, V. M.; Bielawski, C. W. *Organometallics*, **2009**, *28*, 6695-6706. (d) Peeck, L. H.; Leuthäusser, S.; Plenio, H. *Organometallics* **2010**, *29*, 4339-4345. (e) Balof, S. L.; P'Pool, S. J.; Berger, N. J.; Valente, E. J.; Shiller, A. M.; Schanz, H.-J. *Dalton Trans.* **2008**, *42*, 5791-5799. (f) Balof, S. L.; Yu, B.; Lowe, A. B.; Ling, Y.; Zhang, Y.; Schanz, H.-J. *Eur. J. Inorg. Chem.* **2009**, *13*, 1717-1722. (g) P'Pool, S. J.; Schanz, H.-J. *J. Am. Chem. Soc.* **2007**, *129*, 14200-14212.

[4] (a) Durr, H.; Bouas-Laurent, H.; Eds. *Photochromism: Molecules and Systems*; Elsevier: Amsterdam, The Netherlands, **2003**. (b) Special Issue: "Photochromism: Memories and Switches" (Ed. M. Irie), *Chem Rev.* **2000**, *100*, 1683.

[5] (a) Irie, M.; *Chem Rev*. **2000**, *100*, 1685-1716. (b) Matsuda, K.; Irie, M. *J. Photochem. Photobio. C: Photochem Rev.* **2004**, 169-182. (c) Tian, H.; Yang, S.; *Chem. Soc*. *Rev*. **2004**, *33*, 85-97. (d) Tian, H.; Wang, S. *Chem. Commun.* **2007**, 781-792. (e) Yun, C.; You, J.; Kim, J.; Huh, J.; Kim, E. *J. Photochem. Photobio. C: Photochem Rev.* **2009**, *10*, 111-129. (f) Akita, M. *Organometallics*, **2011**, *30*, 43-51.

[6] For an investigation of the photophysical properties of metal complexes supported by 1,3-dimethyl-4,5-dithienylimidazolylidenes, see: (a) Yam, V. W.-W.; Lee, J. K.; Ko, C.; Zhu, N. *J. Am. Chem. Soc.* **2009**, *131*, 912-913. (b) Lee, P. H.-M.; Ko, C.-C.; Zhu, N.; Yam, V. W.-W. *J. Am. Chem. Soc.* **2007**, *129*, 6058-6059.

[7] (a) Siamaki, A. R.; Black, D. A.; Arndtsen, B. A. *J. Org. Chem.* **2008**, *73*, 1135-1138.

[8] In support of this hypothesis, ring-opened 4,5-dithienylimidazolium salts were found to be more electrophilic than their ring-closed isomers; see: (a) Duan, G. Zhu, N.; Yam, V. W.-W. *Chem. Eur. J.* **2010**, *16*, 13199-13209. (b) Nakashima, T.; Goto, M.; Kawai, S.; Kawai, T. *J. Am. Chem. Soc.* **2008**, *130*, 14570-14575.

[9] (a) Odo, Y.; Matsuda, K.; Irie, M. *Chem. Eur. J.* **2006**, *12*, 4283-4288. (b) Lemieux, V.; Spantulescu, M. D.; Baldridge, K. K.; Branda, N. R. *Angew. Chem. Int. Ed.* **2008**, *47*, 5034-5037. (c) Samachetty, H. D.; Branda, N. R. *Chem. Commun.* **2005**, 2840. (d) Sud, D.; Norsten, T. B.; Branda, N. R. *Angew. Chem. Int. Ed.* **2005**, *44*, 2019-2021. (e) Herder, M.; Pätzel, M.; Grubert, L.; Hecht, S. *Chem. Commun.* **2011**, *47*, 460-462. (f) Kawai, S. H.; Gilat, S. L.; Lehn, J. M. *Eur. J. Org. Chem.* **1999**, 2359-2366. (g) Lemieux, V.; Gauthier, S.; Branda, N. R. *Angew. Chem. Int. Ed.*, **2006**, *45*, 6820-6824. (h) Sud, D.; Wigglesworth, T. J.; Branda, N. R. *Angew. Chem. Int. Ed.*, **2007**, *46*, 8017-8019. (i) Samachetty, H. D.; Lemieux, V.; Branda, N. R. *Tetrahedron*, **2008**, *64*, 8292-8300. (j) Stoll, R. S.; Hecht, S. *Angew. Chem. Int. Ed.* **2010**, *49*, 5054-5075. (k) Hirose, T.; Matsuda, K.; Irie, M. *J. Org. Chem.* **2006**, *71*, 7499-7508. (l) Hirose, T.; Irie, M.; Matsuda, K. *Adv. Mat.* **2008**, *20*, 2137-2141; m) Singer, M.; Jäschke, A. *J. Am. Chem. Soc.* **2010**, *132*, 8372-8277.

[10] (a) Sud, D.; McDonald, R.; Branda, N. R. *Inorg. Chem.* **2005**, *44*, 5960-5962. (b) Tanaka, Y.; Inagaki, A.; Akita, M. *Chem. Commun.* **2007**, 1169-1171. (c) Motoyama, K.; Koike, T.; Akita, M. *Chem. Commun.* **2008**, 5812-5314. (d) Tanaka, Y.; Inagaki, A.; Koike, T.; Lapinte, C.; Akita, M. *Chem.-Eur. J.* **2010**, *16*, 4762-4776. (e) Uchida, K.; Inagaki, A.; Akita, M. *Organometallics*, **2007**, *26*, 5030-5041.

[11] For other examples of photochromic 4,5-diarylimidazolones, see: M. M. Krayushkin, S. N. Ivanov, A. Y. Martynkin, B. V. Lichitsky, A. A. Dudinov, L.

G. Vorontsova, Z. A. Starikova, B. M. Uzhinov, *Russ. Chem. Bull. Int. Ed*., **2002**, *51*, 1731-1736.

[12] Belen'kii, L. I.; Shirinyan, V. Z.; Gromova, G. P.; Kolotaev, A. V.; Strelenko, Y. A.; Tandura, S. N.; Shumskii, A. N.; Krayushkin, M. M. *Chem. Het. Cmpds.* **2003**, *39*, 1570-1578.

[13] Toda, F.; Tanaka, K.; Tange, H. *J. Chem. Soc. Perkin Trans. I*, **1989**, 1555-1556.

[14] Benac, B. L.; Burgess, E. M.; Arduengo, A. J. *Org. Synth.* **1986**, *64*, 92.

[15] The conversion of the photocyclization reaction involving **1** was determined using the molar absorptivities of **1o** and **1c**. The conversion of the reaction involving **2** was determined using the molar absorptivity of **2c**, as obtained from a combination of quantitative ^{1}H NMR and UV-vis spectroscopy.

[16] Based on the extinction coefficient for the absorbance measured at 240 nm, greater than 90% of the mixture returns to **1o**; see Figure 2.8.

[17] Urea **1o** exhibited a υ_{CO} typical of amides while that of **1c** was more characteristic of aliphatic ketones. See: E. Pretsch, P. Buhlmann, M. Badertscher, *Structure Determination of Organic Compounds: Tables of Spectral Data*, 4th ed., Springer-Verlag: Berlin, Germany, **2009,** pp 310-324.

[18] (a) Rao, C. N. R.; *Chemical Applications of Infrared Spectroscopy*, Academic Press: New York, **1963**, pp 298-303. (b) Davies, M.; Jones, J.; *J. Chem. Soc.* **1958**, 955-958.

[19] See Figure 2.8 for UV-vis spectral data for the photocycloreversion of isolated **1c** to **1o**.

[20] See Appendix A for additional details of the X-ray diffraction analysis.

[21] The sum of the following angles was calculated to be 324º: C4-C7-C14, C14-C7-S1, C4-C7-S1.

[22] R. B. Woodward, R. Hoffman, *The Conservation of Orbital Symmetry*, Verlag Chemie GmbH, Weinheim, **1970**.

[23] The structure of **1c** was slightly disordered due to the existence of two enantiomers in the sample, with one having the *S,S* configuration at C6 and C7 and the other having the *R,R* configuration at the same atoms. See Supporting Information for additional discussion. Similar disorder has been observed in previously reported structures of ring-closed perfluorocyclopentene-based dithienylethenes; see: (a) Kobatake, S.; Yamada, M.; Yamada, T.; Irie, M. *J. Am. Chem. Soc.* **1999**, *121*, 8450-8456 (b) Morimoto, M.; Irie, M. *J. Am. Chem. Soc.* **2010**, *132*, 14172-14178. (c) Choi, H.; Lee, H.; Kang, Y.; Kim, E.; Kang, S.-O.; Ko, J. *J. Org. Chem.* **2005**, *70*, 8291-8297. (d) Irie, M. Lifka, T. Kobatake, S. Kato, N. *J. Am. Chem. Soc.* **2000**, *122*, 4871-4876. (e) Kobatake, S. Shibata, K. Uchida, Irie, K. M. *J. Am. Chem. Soc.* **2000**, *122*, 12135-12141. (f) Irie, M.; Kobatake, S.;

Horichi, M. *Science*, **2001**, *291*, 1769-1772. (g) Morimoto, M.; Kobatake, S.; Irie, M. *Chem. Eur. J.* **2003**, *9*, 621-627.)h) Morimoto, M.; Kobatake, S.; Irie, M. *Photochem. Photobiol. Sci.* **2003**, *2*, 1088-1094. (i) Kodani, T.; Matsuda, K.; Yamada, T.; Kobatake, S.; Irie, M. *J. Am. Chem. Soc.* **2000**, *122*, 9631-9637.

[24] Nearly identical percent buried volumes ($\%V_{bur}$) were calculated for **1o** (30.1%) and **1c** (30.2%). The calculations were performed using the web application Sam*V*ca with Bondi radii scaled by 1.17, R = 3.5 Å for the sphere radius, d = 2.10 Å for the distance between C1 and O1, and s = 0.05 Å for the mesh spacing. See: Poater, A.; Cosenza, B.; Correa, A.; Giudice, S.; Ragone, F.; Scarano, V.; Cavallo, L. *Eur. J. Inorg. Chem.* **2009**, *13*, 1759-1766.

[25] (a) Chianese, A. R.; Li, X.; Janzen, M. C.; Faller, J. W.; Crabtree, R. H. *Organometallics*, **2003**, *22*, 1663-1667. (b) Wang, H. M. J.; Lin, I. J. B. *Organometallics*, **1998**, *17*, 972-975.

[26] (a) Kelly III, R. A.; Clavier, H.; Giudice, S.; Scott, N. M.; Stevens, E. D. Bordner, I Samardjiev, Hoff, J. C. D.; Cavallo, L.; Nolan, S. P. *Organometallics*, **2008**, *27*, 202-210. (b) Tolman, C. A. *Chem. Rev.* **1977**, *77*, 313-348.

[27] Decarbonylation was observed by IR spectroscopy when **3o** was irradiated in acetonitrile or dichloromethane; see: Figure 2.11.

[28] See Figure 2.9 for the UV-vis spectral data accompanying the cyclization of **3o** to **3c**.

[29] The conversion of **3o** to **3c** was calculated to be 18% by IR spectroscopy after 10 min of irradiation at 297 nm. After 45 min of irradiation, the conversion was calculated to be 29% by IR spectroscopy (see Figure 2.10 and Table 2.1). These conversions are in accord with other reported photochromic DAE-containing metal complexes; see: (a) Kume, S.; Nishihara, H. *Dalton Trans.* **2008**, *25*, 3260-3271. (b) Tan, W.; Zhou, J.; Li, F.; Yi, T.; Tian, H. *Chem. Asian. J.* **2011**, *6*, 1263-1268. (c) reference 6a.

[30] The results reported herein demonstrate that the bonding characteristics of carbamides may be modulated using only electronics as opposed to stereoelectronic approaches, see: (a) Chan, C.; Heid, R.; Zheng, S.; Guo, J.; Zhou, B.; Furuuchi, T.; Danishefsky, S. J. *J. Am. Chem. Soc.* **2005**, *127*, 4596-4598. (b) Clayden,J.; Moran, W. *Angew. Chem. Int. Ed.* **2006**, *45*, 7118-7120. (c) Tani, K.; Stoltz, B. M. *Nature*, **2006**, *441*, 731-734; (d) Szostak, M.; Yao, L.; Day, V. W.; Powell, D. R.; Aubé, J. *J. Am. Chem. Soc.* **2010**, *132*, 8836-8837. (e) Hudnall, T. W.; Bielawski, C. W. *J. Am. Chem. Soc.* **2009**, *131*, 16039-16041.

[31] Yang, D.; Long, Y.; Wang, H.; Zhang, Z. *Org. Lett.* **2008**, *10*, 4723-4726.

[32] Belen'kii, L. I.; Shirinyan, V. Z.; Gromova, G. P.; Kolotaev, A. V.; Strelenko, Y. A.; Tandura, S. N.; Shumskii, A. N.; Krayushkin, M. M. *Chem. Het. Cmpds.* **2003**, *39*, 1570-1578.

[33] Anjos, T.; Charlton, A.; Coles, S. J.; Croft, A. K.; Hurshouse, M. B.; Kalaji, M.; Murphy, P. J.; Roberts-Bleming, S. J. *Macromolecules*, **2009**, *42*, 2505-2515.

Chapter 3: Photoswitchable Organocatalysis: Using Light to Modulate the Catalytic Activities of N-Heterocyclic Carbenes

3.1 INTRODUCTION

Photoswitchable catalysis is a burgeoning field of study that utilizes photochemical processes to alter the courses of chemically-catalyzed transformations.[1] Although many known[2] photochromic moieties may be reversibly switched between states that feature different steric and/or electronic properties,[3] examples of using photochromism to modulate catalytic reactions are scarce.[4] Following Ueno's seminal report of an azobenzene-capped β-cyclodextrin which was used to modulate the hydrolysis of *p*-nitrophenyl acetate in 1981 (Figure 1.6a),[4e] Cacciapaglia and Mandolini described a phototunable "butterfly" crown ether that facilitated the ethanolysis of anilides (Figure 1.9b).[4f] Most recently, Hecht reported an elegantly designed piperidine that enabled photoswitchable control over the Henry reaction (Figure 1.10c).[4a-c] In all of these and other examples, however, the catalytic activity was modulated through reversible steric shielding that resulted from a photochemically-induced isomerization reaction.[4] Indeed, as recently noted by Hecht, "no example of successful reactivity switching by a photochrome-mediated electronic modulation of a catalyst's active site has been described to date."[1] Catalysts with photoswitchable electronic structures are expected to be broadly applicable while enabling precise control over intrinsic chemo- and/or regioselectivities.

To realize such a photoswitchable catalyst, we were drawn to the photochromic diarylethenes (DAEs),[5] which were recently shown by our group[6] and others[7] to alter the electron density at the C2 position of imidazolium salts and related N-heterocyclic carbene (NHC)[8] adducts. As NHCs and their complexes are known to catalyze a variety of useful synthetic transformations,[9] we envisioned that such photoinduced changes in

electronic properties may be used to modulate the activities of NHC-based catalysts.[10] Herein, we report a DAE-annulated NHC organocatalyst and demonstrate that its activity may be switched through the remote photomodulation of electronic structure.

3.2 Results and Discussion

Considering that the previously reported photochromic DAE annulated NHC adducts and precursors required high energy radiation (λ_{irr} < 290 nm) to undergo cyclization,[6, 7] we targeted a derivative that would isomerize under relatively mild conditions. As shown in Figure 3.1, NHC precursor **1·HPF$_6$** features phenyl substituents at the 5- and 5′-positions of the thiophene rings, which extend the conjugation length of the dithienyl backbone, and therefore was expected to undergo electrocyclic ring-closure upon exposure to relatively low energy radiation.

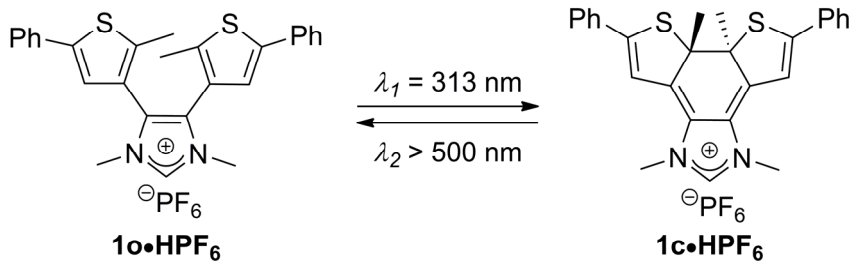

1o•HPF$_6$ **1c•HPF$_6$**

Figure 3.1: Photochromism of NHC precursor **1·HPF$_6$**.

The synthesis of the open form of the aforementioned salt (**1o·HPF$_6$**) is summarized in Figure 3.2. Acylation of commercially available 2-methyl-5-phenyl-thiophene with acetic anhydride and tin (IV) chloride afforded 3-acetyl-2-methyl-5-phenylthiophene **2**, which was then oxidized with selenium dioxide. The resulting glyoxal monohydrate **3** was coupled with one equivalent of 2-methyl-5-phenylthiophene in the presence of tin (IV) chloride to give known[11] α-hydroxy ketone **4**. Oxidation of **4** with copper (II) acetate and ammonium nitrate in refluxing acetic acid afforded diketone

5, which was formylatively cyclized to give imidazole **6**. Finally, methylation with iodomethane under basic conditions followed by anion metathesis[12] afforded imidazolium salt **1o·HPF$_6$**, as evidenced in part by the appearance of diagnostic ^{1}H (δ = 8.6 ppm) and ^{13}C (δ = 142 ppm; $CDCl_3$) NMR signals which corresponded to the proton and carbon nuclei at the C2 position, respectively.

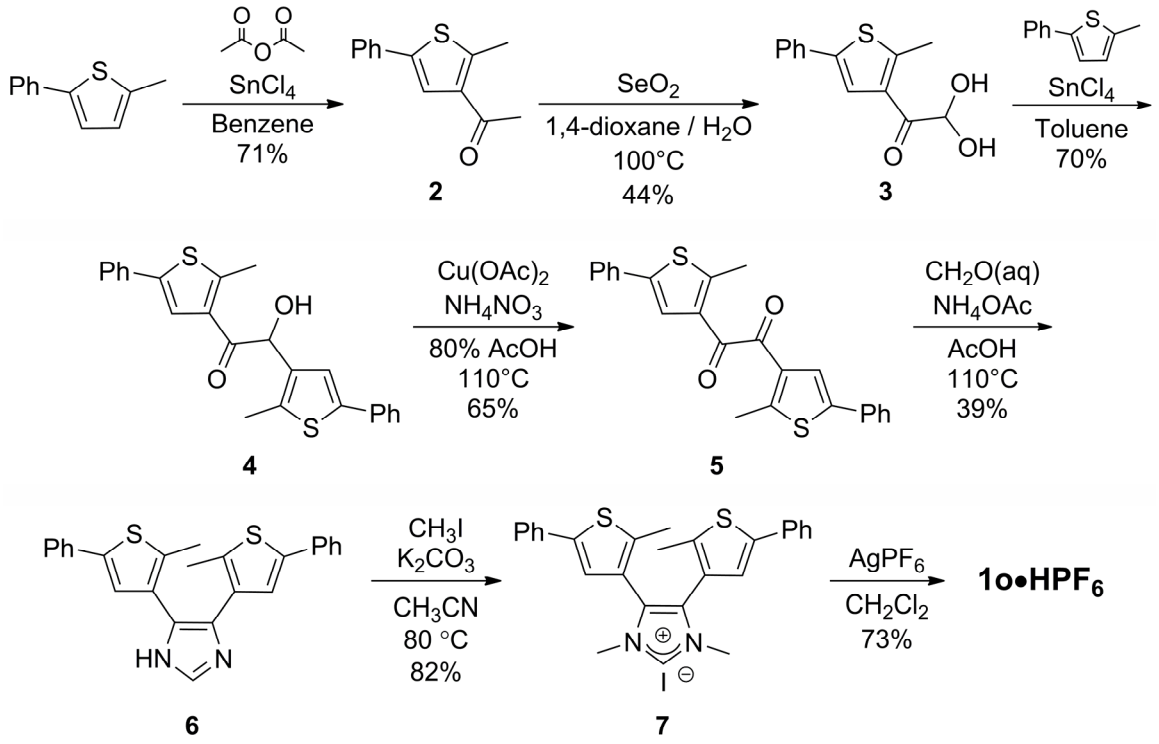

Figure 3.2: Synthesis of **1o·HPF$_6$**.

The UV-vis spectrum of **1o·HPF$_6$** in benzene, tetrahydrofuran, or acetonitrile exhibited intense absorption bands between 275 and 325 nm, which were assigned to the $n \rightarrow \pi^*$ and $\pi \rightarrow \pi^*$ transitions of the N-heterocycle and thiophene systems, respectively. Due to the phenyl groups in the 5 and 5′-positions of the thiophene moieties, the absorption spectrum of **1o·HPF$_6$** was bathochromically shifted when compared to previously reported 4,5-dithienyl N-heterocycles.[6, 7a] As a result, exposing a solution of

1o·HPF$_6$ in benzene to relatively low energy radiation (λ_{irr} = 313 nm vs. 280 nm[6]) resulted in a color change from pale yellow to bright blue. Concomitant with this color change, a decrease in the intensity of the absorption band centered at 292 nm and the appearance of a new band at 670 nm was observed (Figure 3.3a). The spectroscopic changes reached a steady state after 240 s of UV exposure and reflected an 88% conversion of **1o·HPF$_6$** to its ring-closed isomer **1c·HPF$_6$** upon measurement (see Figure 3.1).[5,13a] Moreover, an isosbestic point was observed at 309 nm which indicated that the cyclization proceeded without appreciable side reactions. Subsequent irradiation of the UV exposed solutions with visible light (λ_{irr} > 500 nm) resulted in the attenuation of the broad, low energy absorption bands. After 300 s of irradiation, the UV-vis spectrum of **1o·HPF$_6$** was nearly completely restored (>95% conversion),[13a] which suggested to us that the ring-closed product **1c·HPF$_6$** reverted back to the starting material (Figure 3.3b).

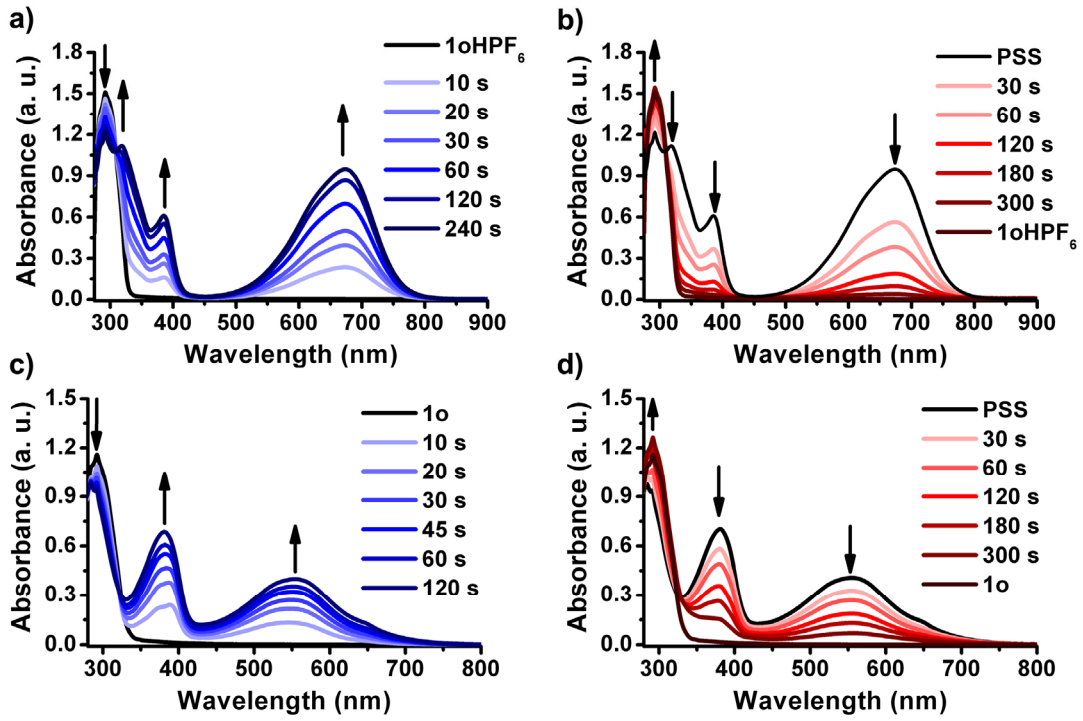

Figure 3.3: (a) UV-vis spectral changes of **1o·HPF$_6$** in C_6H_6 upon UV irradiation (λ_{irr} = 313 nm). (b) UV-vis spectra in C_6H_6 of **1o·HPF$_6$**, the photostationary state (PSS) reached after UV irradiation (λ_{irr} = 313 nm) of **1o·HPF$_6$** for 240 s, and spectral changes of the PSS upon visible irradiation (λ_{irr} > 500 nm). (c) UV-vis spectral changes of **1o** (generated in situ by treatment of **1o·HPF$_6$** with 1.0 equivalent of NaHMDS) in C_6H_6 upon UV irradiation (λ_{irr} = 313 nm). (d) UV-vis spectra in C_6H_6 of 1o, the photostationary state (PSS) reached after UV irradiation of **1o** for 120 s, and spectral changes of the PSS upon visible irradiation (λ_{irr} > 500 nm). In all cases, the initial concentration of **1o** was 4 × 10^{-5} M and the spectra were recorded after irradiation for the indicated amount of time. The arrows indicate the evolution of the spectral changes over time.

The photocyclizations were further confirmed by ^{1}H NMR spectroscopy. After irradiation of **1o·HPF$_6$** in CD_3CN at 313 nm for 45 min ([**1o·HPF$_6$**]$_0$ = 1 × 10^{-3} M), the signals assigned to the thiophene protons shifted upfield from δ 7.3 ppm to 6.9 ppm, and a significant upfield shift of the signal assigned to the proton at the C2 position in **1o·HPF$_6$** from 8.6 ppm to 8.1 ppm was observed. Integration of these signals indicated

that 81% of **1o·HPF$_6$** converted to **1c·HPF$_6$**. Exposure of the UV treated solution to ambient light for 4 h reversed the aforementioned chemical shifts (> 95% conversion).

Considering that catalytically active NHCs may be generated by exposing imidazolium salts to base, subsequent efforts focused on investigating the photochemical behavior of **1o·HPF$_6$** under basic conditions. Although the free NHC **1o** was not isolable, its formation was observed in situ by NMR spectroscopy upon treatment of **1o·HPF$_6$** with one equivalent of KOtBu or NaHMDS, as evidenced by the loss of the imidazolium ^{1}H NMR signal at 8.82 ppm and the appearance of a ^{13}C NMR signal assigned to the carbenoid nucleus at 201.9 ppm (C_6D_6). Similar to that of its imidazolium precursor, the UV-vis spectrum of **1o** exhibited an intense absorption centered at 291 nm in benzene. Upon UV irradiation, a decrease in the intensity of this band was observed concomitant with the appearance of new bands at 378 nm and 554 nm, as well as an isosbestic point at 321 nm (Figure 3.3c). Measurement of these signals revealed that > 99% of **1o** converted to its ring-closed isomer **1c** after 120 s of UV irradiation.[13b] As further confirmation of the forward cyclization reaction, the ^{1}H NMR signals assigned to the thiophene protons shifted upfield from δ 7.0 ppm to 6.7 ppm after irradiation of **1o** in C_6D_6 at 313 nm ([**1o**]$_0$ = 1 × 10^{-3} M), with the conversion of **1o** to **1c** reaching 71% after 1 h of irradiation. Additionally, a new ^{13}C NMR resonance was observed at δ 66.6 ppm after irradiation of **1o** in C_6D_6 and assigned to the sp^3 carbon nuclei adjacent to the sulfur atoms in **1c**. Subsequent irradiation with visible light for 300 s reversed the observed UV-vis spectral changes, and the spectrum of **1o** was nearly restored (85% conversion), indicating that **1c** had undergone photocycloreversion (Figure 3.3d). Together, these results suggested to us that **1** underwent a similar reversible photochemical process as its precursor **1·HPF$_6$**.

Having demonstrated that **1o·HPF$_6$** and **1o** underwent similar reversible photocyclizations, our attention shifted towards exploring the photoinduced

isomerizations as a means to modulate catalytic activity. Our attention was directed toward transesterification and amidation reactions as imidazolium salts in the presence of base have been shown to catalyze these useful transformations.[14] Moreover, Nolan and others have shown that the catalytic activities observed in these reactions are sensitive to changes in the electronic structure of the NHC organocatalyst.[14c]

In a preliminary experiment, **1o** was found to promote the transesterification of allyl alcohol and vinyl acetate (Figure 3.4). A 35% conversion[15] to the expected ester product was observed after 1 h by ^{1}H NMR spectroscopy upon treatment of a THF solution containing equimolar quantities of the aforementioned alcohol and ester starting materials (initial concentration of each: 0.1 M) to **1o** (1 mol%; prepared in situ by treating **1o·HPF$_6$** with one equivalent of KO*t*Bu) at room temperature. To determine if exposure to UV irradiation would influence the aforementioned condensation reaction, a freshly prepared solution of **1o** in THF ([**1o**]$_0$ = 1 × 10^{-3} M) was divided in half: one half was placed in a quartz cuvette sealed with a Teflon-lined septum cap and the other half was transferred to a flask and sealed with a rubber septum. The solution in the quartz cuvette was then subjected to UV irradiation (λ_{irr} = 313 nm) for 1 h while the other solution was kept in ambient light over the same period of time, after which equimolar amounts of vinyl acetate and allyl alcohol were added to each reaction vessel separately. Aliquots were then periodically removed from each mixture, diluted with methanol to quench the reaction and analyzed by gas chromatography using *n*-octane as an internal standard. Inspection of these data revealed that the reaction kept in ambient light proceeded with a second order rate constant, k_{vis}, of 5 ± 1 × 10^{-4} mol^{-1}·s^{-1} whereas the reaction that had been subjected to UV irradiation exhibited only negligible conversion to product (< 3% by GC; k_{UV} = 4 ± 1 × 10^{-5} mol^{-1}·s^{-1}). The 10-fold decrease in reactivity suggested to us that photocyclization occurred upon UV irradiation and the corresponding changes in the

electronic structure of **1** significantly attenuated its catalytic activity.[16] Moreover, the differences in reactivity were consistent with Nolan's observation that imidazol-2-ylidene catalysts were more active than their relatively electron deficient imidazolin-2-ylidene analogues in similar transesterification reactions.[17]

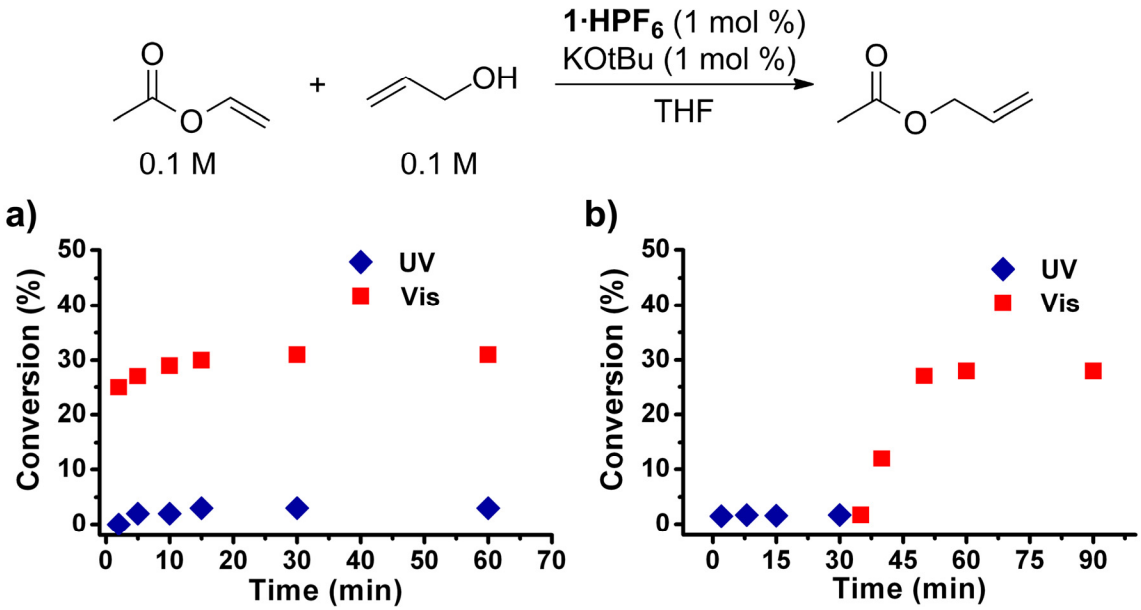

Figure 3.4: Plots of reaction conversion versus time for the condensation of vinyl acetate and allyl alcohol catalyzed by **1** (prepared in situ from **1·HPF$_6$** and KO*t*Bu) in THF. The reactions were monitored over time by GC using *n*-octane as an internal standard. (a) Two reactions were run concurrently with one vessel exposed to UV irradiation (λ_{irr} = 313 nm) for 1 h prior to substrate addition (blue diamonds) and one kept under ambient conditions (red squares). (b) A single reaction vessel was exposed to UV irradiation (λ_{irr} = 313 nm) for 1 h prior to substrate addition. The contents of the vessel were then stirred under UV light for 30 min (blue diamonds) prior to exposure to visible light (λ_{irr} > 500 nm) (red squares).

Since **1o** and **1c** may be interconverted by exposure to light of different wavelengths, we sought to explore the potential of switching the catalytic activity over the course of a condensation reaction. When vinyl acetate and allyl alcohol were added to a THF solution of **1c**, no conversion was observed by GC for at least 30 min while the

reaction vessel was irradiated with UV light. However, the rate of product formation significantly increased (Figure 3.4b) upon subsequent exposure to visible light ($\lambda_{irr} > 500$ nm), consistent with the formation of the catalytically active **1o** from **1c**. Unfortunately, multiple switching cycles were precluded by the relatively slow photocyclization and condensation kinetics.[15] Regardless, the result constituted the first example of using light to activate a latent NHC-based organocatalyst.[1, 18]

Next, efforts were directed towards exploring photoswitchable amidation reactions, which were envisioned to be better suited for photoswitching as they generally proceed with consistently higher conversions and longer reaction times than analogous transesterification reactions.[14e] Initial studies showed that when ethyl acetate and 2-aminoethanol were added to **1o** (2.5 mol%; prepared in situ from **1o·HPF$_6$** and 0.9 equivalents of NaHMDS), a 61% conversion to the expected amide was observed by ^{1}H NMR spectroscopy after 21 h. Using similar comparative kinetics experiments as described above for the transesterification reactions, the aforementioned amidation reaction performed under ambient light proceeded with a second order rate constant of $k_{vis} = 5 \pm 4 \times 10^{-4}$ mol^{-1}·s^{-1} whereas an analogous reaction exposed to UV light was relatively slow ($k_{UV} = 5 \pm 4 \times 10^{-6}$ mol^{-1}·s^{-1}; $k_{vis/UV} = 100$); see Figure 3.5a.[19] The disparate rates enabled the photomodulation of the reaction kinetics over the course of a single amidation reaction. As shown in Figure 3.5b, after exposure to ambient light for 2h ($k_{vis} = 6 \pm 5 \times 10^{-4}$ mol^{-1}·s^{-1}), the vessel containing an identical mixture to that described above was subjected to UV irradiation for 1 h which effectively stopped the reaction. After a further 3 h in the dark, during which no conversion was observed, exposure to visible light ($\lambda_{irr} > 500$ nm) resulted in a significant restoration of the catalytic activity ($k = 1.3 \pm 0.5 \times 10^{-4}$ mol^{-1}·s^{-1}). The initial reaction rate was not fully restored likely due to photochemical fatigue of the catalyst upon prolonged UV irradiation. However, since

only a minor portion of the catalyst underwent decomposition,[20] it was possible to switch the catalytic activity over multiple timescales. A reaction duplicate to that described above was kept under ambient light for 30 min before being exposed to UV irradiation for 30 min, which effectively stopped the reaction. The reaction conversion remained stagnant while the reaction vessel was kept in the dark for a further 1 h, however the catalytic activity was restored upon subsequent exposure to visible light (see Figure 3.9). Collectively, these results suggested to us that the photocyclization process intrinsic to **1** was responsible for the changes in catalytic activity, which was consistent with our previous observation that the dithienylethene photocyclization decreases the electron density at the C2 position of the NHC.[6] Furthermore, since we have previously shown that there is minimal change in the steric properties of related photochromic NHCs upon photocyclization,[6] these results demonstrate that photo-induced changes in electronic structure may be used to reversibly tune the activity of a catalytic species.

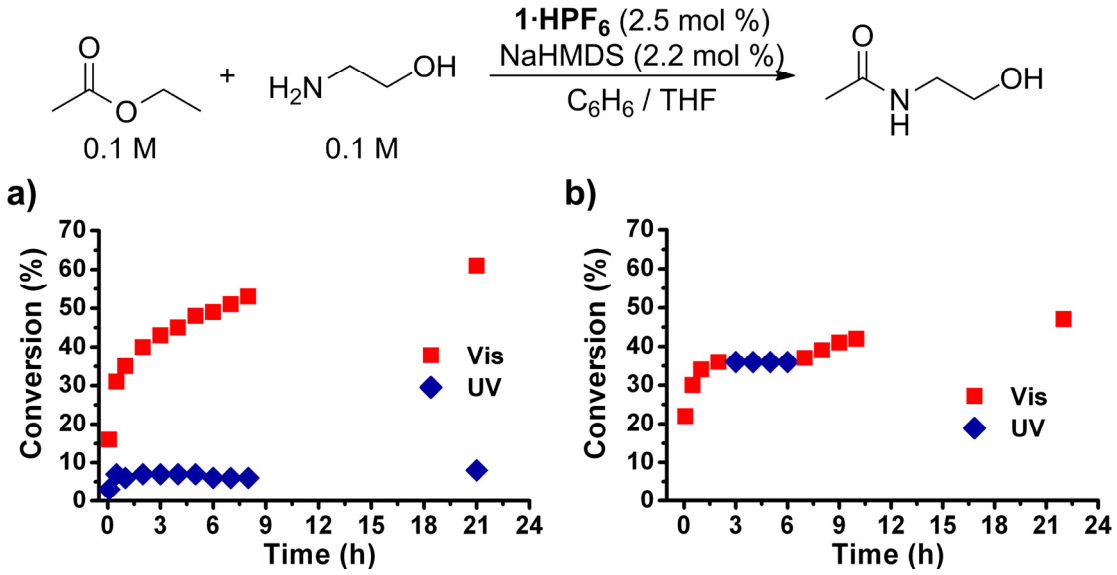

Figure 3.5: Plots of reaction conversion versus time for the condensation of ethyl acetate and 2-aminoethanol catalyzed by **1** (prepared in situ from **1·HPF$_6$** and NaHMDS) in 3:1 C_6H_6 : THF (v/v). The reactions were monitored over time by GC using *n*-octane as an internal standard. (a) Two reactions were run concurrently with one vessel exposed to UV irradiation (λ_{irr} = 313 nm) for 1 h prior to substrate addition (blue diamonds) and one kept under ambient conditions (red squares). (b) A single reaction was allowed to proceed in ambient light for 2 h (red squares), then subjected to UV irradiation (blue diamonds) (λ_{irr} = 313 nm) for 1 h and kept in the dark for a further 3 h prior to exposure to visible light (λ_{irr} > 500 nm) (red squares). For experiments where the reaction was switched over different timescales, see Figure 3.10.

To gain additional insight into the photoswitchable NHC reactivity, the identities of the active and inactive adducts of the amidation catalyst were probed using ^{13}C NMR spectroscopy. Since low concentrations were required for the photocyclization reactions, an analogue of **1o·HPF$_6$** that was isotopically labeled with a ^{13}C atom at the C2 position was used. The labeled precatalyst, **1o·HPF$_6$***, was synthesized via an analogous route to that employed for **1o·HPF$_6$** with the exception that $^{13}CH_2O$ was used in the formylative cyclization step (see Figure 3.8). Upon treatment of **1o·HPF$_6$*** with one equivalent of NaHMDS in C_6D_6, a ^{13}C NMR signal was observed at 201.9 ppm (Figure 3.6a), as

expected for the in situ formation of the free NHC **1o***. The addition of equimolar quantities of 2-aminoethanol and ethyl acetate to **1o*** (2.5 mol%) in C_6D_6 resulted in the formation of an imidazolium species,[21] as evidenced by the upfield shift of the C2 ^{13}C NMR signal from 201.9 ppm to 138.6 ppm (Figure 3.6b). UV irradiation of the mixture ($[\mathbf{1o}]_0 = 2.5 \times 10^{-3}$ M; $\lambda_{irr} = 313$ nm) for 1 h resulted in a further upfield shift of the signal assigned to the C2 atom (Figure 3.6c). The new resonance was observed at 93.3 ppm and identified as an NHC-alcohol adduct,[22, 23] the formation of which may have been facilitated by the decreased electron density at the C2 position caused by the photocyclization reaction. Visible light irradiation reversed these spectroscopic changes and caused the signal at 93.3 ppm to shift downfield to 138.6 ppm, consistent with reversion to the imidazolium species (Figure 3.6d).[24] In combination with the results from the catalysis experiments described above, the ^{13}C NMR data suggested to us that the resting state of the active catalyst was an imidazolium species, which converted to a NHC-alcohol adduct upon UV irradiation and effectively suspended the catalytic cycle (Figure 3.7). Moreover, the 20-fold restoration in activity observed upon visible light irradiation demonstrated that the photocyclized adduct may be converted back to an imidazolium species that then re-engages the catalytic cycle.[25] Together, these results support the conclusion that the catalyst was reversibly switched with high fidelity between active and inactive adducts via photoinduced changes in electronic structure. Moreover, given that the transesterification reactions discussed above involve analogous alcohol and ester substrates, a similar photoswitching mechanism may be operative.

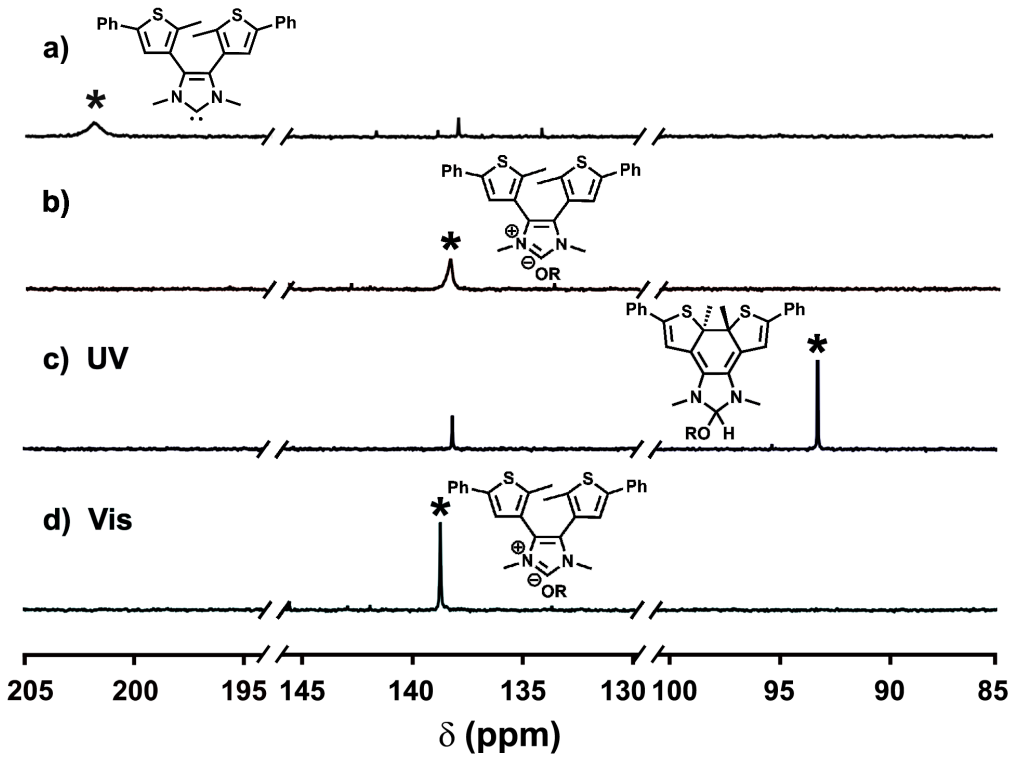

Figure 3.6: Quantitative ^{13}C NMR spectra collected sequentially in C_6D_6 over the course of the following experiment: A sample of (a) **1o** labeled at the C2 position with a ^{13}C atom (i.e., **1o***; $[\mathbf{1o^*}]_0 = 1.0 \times 10^{-2}$ M) (b) was treated with equimolar quantities of 2-aminoethanol and ethyl acetate, (c) then exposed to UV irradiation for 1 h ($\lambda_{irr} = 313$ nm; $[\mathbf{1o^*}]_0 = 2.5 \times 10^{-3}$ M), and finally (d) irradiated with visible light for an additional 2 h ($\lambda_{irr} > 500$ nm, $[\mathbf{1o^*}]_0 = 1.0 \times 10^{-2}$ M).

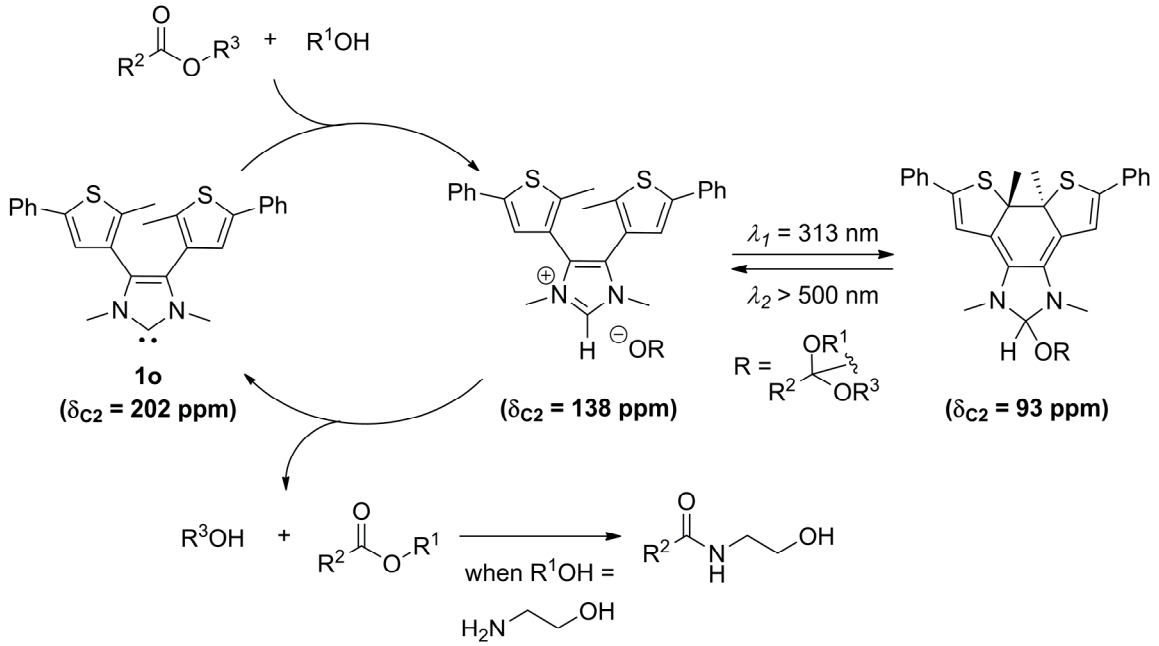

Figure 3.7: Proposed mechanism of photoswitchable NHC catalyzed condensation reactions.

3.3 CONCLUSIONS

In summary, we report a rare[26] example of a photoswitchable catalyst that operates via the remote photomodulation of its electronic structure. By incorporating a dithienylethene moiety into the backbone of a NHC precursor, the activity of the corresponding organocatalyst was remotely tuned via exposure to UV or visible light. The rates of NHC-catalyzed transesterification and amidation reactions were attenuated by one to two orders of magnitude upon exposure to UV light, while subsequent exposure to visible light restored the catalytic activity. Given the vast array of reactions catalyzed by NHCs and NHC-supported metal complexes, the ability to remotely modulate catalyst electronic properties using light is expected to endow a broad range of catalysts with the ability to finely tune intrinsic chemo-, regio-, and stereoselectivities. Such catalysts are envisioned to find applications that range from the preparation of polymeric materials

with sophisticated microstructures to facilitating the multi-step syntheses of complex small molecules.

3.4 EXPERIMENTAL

3.4.1 Materials and Methods

Unless otherwise specified, reagents were purchased from commercial sources and used without further purification. Vinyl acetate, allyl alcohol, ethyl acetate, and 2-aminoethanol were dried over 4Å molecular sieves and bubbled with dry N_2 prior to use. All syntheses were performed under ambient conditions unless specified otherwise. Solvents were dried and degassed using a Vacuum Atmospheres Company solvent purification system. ^{1}H and ^{13}C NMR spectra were recorded using a Varian 400 MHz spectrometer. Chemical shifts δ (in ppm) are referenced to tetramethylsilane using the residual solvent as an internal standard. For ^{1}H NMR: $CDCl_3$, 7.24 ppm; CD_3CN, 1.95 ppm; CD_3OD, 3.30 ppm; DMSO-d_6, 2.50 ppm; C_6D_6, 7.15 ppm. For ^{13}C NMR: $CDCl_3$, 77.0 ppm; DMSO-d_6, 39.5 ppm; CD_3OD, 49.0 ppm; C_6D_6, 128.0 ppm. Quantitative ^{13}C NMR spectra were recorded on a Varian 600 MHz spectrometer using decoupled Nuclear Overhauser Effects with a relaxation delay of 5× the measured T_1 relaxation time. Coupling constants (*J*) are expressed in hertz (Hz). Melting points were obtained with an Opti-Melt Automated Melting Point System MPA100 apparatus and are uncorrected. Mass spectra (MS, ESI or CI) were obtained with a VG analytical ZAB2-E or a Karatos MS9 instrument and are reported as m/z (relative intensity). UV-vis spectra were acquired using a Perkin-Elmer Lambda 35 UV-vis Spectrometer in 6Q Spectrosil quartz cuvettes (Starna) with 1.0 cm path lengths and 3.0 mL sample solution volumes. Beer's law measurements were performed using 10, 20, 30, and 40 μM sample concentrations. The photochemical reactions were performed in the same quartz cuvettes using 4.0 mL

sample solution volumes. The irradiation source for photochemical reactions was a Newport/Oriel 66942 200-500W Hg Arc lamp housing equipped with a 350 W Hg lamp, a Newport 6117 liquid filter, a Newport 71445 electronic safety shutter, and a Newport 71260 filter holder. The source was powered by a Newport 669910 power supply and mounted on a Newport XL48 optical rail with a Newport 13950 shielded cuvette holder placed at a distance of 8 cm from the end of the source. The irradiation wavelength for the photocyclization reactions was obtained using a 313 nm bandpass filter (Andover Corporation). A long-pass edge filter (> 500 nm) (Andover Corporation) was used to introduce visible light. Elemental analyses were performed at Midwest Microlab, LLC (Indianapolis, IN). Gas chromatography (GC) was performed on an Agilent 6850 gas chromatograph (HP-1 column, L = 30 m, I.D. = 0.32 mm) equipped with a flame ionization detector (FID). For reactions between allyl alcohol and vinyl acetate, the GC oven temperature was held at 30 °C for 5 min, then increased to 100 °C at 10 °C min^{-1}. For reactions between 2-aminoethanol and ethyl acetate, the GC oven temperature was held at 40 °C for 3 min, then increased to 100 °C at 10 °C min^{-1} and finally increased to 250 °C at 20 °C min^{-1}. The internal standard *n*-octane was used to aid in measuring reaction conversions.

3.4.2 Syntheses

3-acetyl-2-methyl-5-phenylthiophene (2): Compound **2** was prepared according to a modified literature procedure.[27] An oven-dried Schlenk flask equipped with a magnetic stir bar was charged with 3.00 g (17.2 mmol) of 2-methyl-5-phenylthiophene, and the flask was evacuated and refilled with N_2 three times. The reaction flask was kept under static vacuum and 150 mL of dry toluene was added via a cannula. After cooling the reaction vessel to 0 °C in an ice bath, 1.62 mL (17.2 mmol) of acetic anhydride was

added via syringe under an atmosphere of N_2. At the same temperature, 2.4 mL (20.5 mmol) of tin(IV) chloride was added dropwise via a N_2 purged syringe. The reaction mixture was stirred for 2 h in the ice bath, and then poured into a mixture of 100 g of ice and 100 mL of 0.5 M HCl. The organic layer was separated and washed with 150 mL of deionized water, then dried over sodium sulfate and concentrated under reduced pressure. Purification of the resulting brown residue by column chromatography on silica gel eluting with a 2:1 v/v mixture of hexanes and dichloromethane followed by dichloromethane yielded 2.7 g (71% yield) of the desired product as a pale yellow solid. mp 70-71 °C. ^{1}H NMR (400 MHz, $CDCl_3$): δ 2.52 (s, 3H), 2.74 (s, 3H), 7.28 (t, *J* = 7.6, 1H), 7.37 (t, *J* = 7.6, 2H), 7.51 (s, 1H), 7.54 (dd, *J* = 7.6, 2H). ^{13}C NMR (100 MHz, $CDCl_3$) δ 16.2, 29.7, 124.1, 125.5, 127.6, 128.9, 133.4, 136.8, 139.3, 148.3. HRMS (*m/z*): Calcd. for $C_{13}H_{12}OS$ $[M]^+$, 216.0609; Found, 216.0608. Anal. Calcd. for $C_{13}H_{12}OS$: C, 72.19; H, 5.59; Found: C, 72.21; H, 5.56.

1,2-bis(2′-methyl-5′-phenylthien-3′-yl)-glyoxal monohydrate (3): A three-necked round bottom flask equipped with a reflux condenser, N_2 inlet and magnetic stir bar was charged with 2.67 grams (10.6 mmol) of 2-methyl-3-acetyl-5-phenylthiophene **2**, 1.36 grams (12.3 mmol) of SeO_2, 0.5 mL of deionized water, and 11.5 mL of 1,4-dioxane. The mixture was heated at reflux for 48 h under an atmosphere of nitrogen. The mixture was cooled to room temperature and filtered through Celite, and the filtrate was concentrated under reduced pressure. The resulting orange residue was washed with cold ethyl acetate and 1.35 g of the desired product was collected on a frit by vacuum filtration as a pale yellow powder (44% yield). The product was isolated as a mixture of the glyoxal monohydrate **3** and the corresponding glyoxal compound (85:15 molar ratio). mp 128 °C (dec). ^{1}H NMR (400 MHz, $CDCl_3$): δ 2.77 (s, 3H), 2.82 (s, 0.7H), 5.14 (d, *J* = 10.3, 1H), 6.12 (d, *J* = 10, 1H), 7.31 (t, *J* = 7.6, 1.3H), 7.39 (t, *J* = 7.6, 2.5H), 7.54 (dd, *J*

= 8, 2.5H), 7.88 (s, 1H), 7.98 (s, 0.18H), 9.53 (s, 0.15H). ^{13}C NMR (100 MHz, $CDCl_3$) δ 16.4, 89.9, 123.9, 125.4, 127.7, 128.7, 131.3, 132.9, 139.9, 153.7, 187.4, 189.9. HRMS (*m/z*): Calcd. for $C_{13}H_{10}O_2S$ $[M\text{-}H_2O]^+$, 230.0402; Found, 230.0400.

1,2-bis(2′-methyl-5′-phenylthien-3′-yl)-2-hydroxy-1-ethanone (4): Compound **4** was prepared according to a modified literature procedure.[11] An oven-dried Schlenk flask with a stir bar was charged with 1.1 g (4.4 mmol) of **3**, 0.9 g (5.2 mmol) of 2-methyl-5-phenylthiophene and 70 mL of dry toluene under an atmosphere of N_2. The reaction mixture was cooled to 0 °C in an ice bath, and 0.6 mL (5.2 mmol) of tin (IV) chloride was added dropwise. The reaction mixture was stirred in the ice bath for 3 h, and then poured into 100 mL of ice water. The mixture was extracted with ethyl acetate (3 × 75 mL) and the combined organic layers were washed with deionized water (2 × 150 mL) and brine (2 × 150 mL). After removing the residual solvent under reduced pressure, the resulting orange residue was washed with cold ethyl acetate to give 1.25 g (70% yield) of the desired product as a beige powder. Spectral data were in agreement with literature values.[11]

1,2-bis-(2′-methyl-5′-phenylthien-3′-yl)-ethanedione (5): A round bottom flask with a stir bar was charged with 1.1 g (2.7 mmol) of the α-hydroxy ketone **4** in 50 mL of glacial acetic acid, 98 mg (0.54 mmol) of copper (II) acetate, and 540 mg (6.75 mmol) of NH_4NO_3. The mixture was heated to reflux for 24 h, then cooled to room temperature and poured into 50 mL of ice water. To the mixture was added concentrated ammonium hydroxide until a pH = 7 was observed. The mixture was extracted with ethyl acetate (3 × 50 mL) and the combined organic layers were washed with deionized water (3 × 100 mL), saturated aqueous K_2CO_3 (3 × 100 mL), and brine (2 × 100 mL). The solvent was removed under reduced pressure and the resulting brown residue was passed through a short column of silica gel aided with dichloromethane eluent. The residual solvent was

removed under reduced pressure and the resulting orange oil was recrystallized from hot ethyl acetate to yield 0.95 g (65% yield) of the desired product as a beige solid. mp 161 °C (dec). ^{1}H NMR (400 MHz, $CDCl_3$): δ 2.82 (s, 6H), 7.27 (t, *J* = 7.6, 2H), 7.35 (t, *J* = 8, 4H), 7.47 (s, 2H 7.51 (dd, *J* = 7.2, 4H),). ^{13}C NMR (100 MHz, $CDCl_3$) δ 16.6, 124.8, 126.1, 128.3, 129.3, 133.1, 133.3, 141.0, 153.1. HRMS (*m/z*): Calcd. for $C_{24}H_{18}O_2S_2$ $[M]^+$, 402.0749; Found, 402.0748. Anal. Calcd. for $C_{24}H_{18}O_2S_2$: C, 71.61; H, 4.51; Found: C, 70.71; H, 4.56.

1,2-bis-(2′-methyl-5′-phenylthien-3′-yl) imidazole (6): A round bottom flask equipped with a reflux condenser and stir bar was charged with 300 mg (0.74 mmol) of diketone **5**, 50 mL of glacial acetic acid, 0.3 mL of aqueous formaldehyde (37% w/v in H_2O, 3.7 mmol), and 1.2 g (15.5 mmol) of ammonium acetate. The mixture was stirred at 110 °C for 48 h, then cooled to room temperature and poured into 100 mL of ice water. Concentrated ammonium hydroxide was added dropwise until a pH = 7 was observed. The mixture was extracted with ethyl acetate (3 × 50 mL) and the combined organic layers were washed with deionized water (2 × 100 mL), saturated aqueous K_2CO_3 (3 × 100 mL), and brine (1 × 100 mL). After washing the resulting residue with cold ethyl acetate, 120 mg (39% yield) of the desired product was collected via filtration as a beige solid. mp 190 °C (dec). ^{1}H NMR (400 MHz, CD_3OD): δ 2.11 (s, 6H), 7.22 (t, *J* = 6.8, 2H), 7.24 (s, 2H), 7.32 (t, *J* = 7.6, 4H), 7.52 (d, *J* = 7.2, 4H), 7.82 (s, 1H). ^{13}C NMR (100 MHz, CD_3OD) δ 14.1, 125.7, 126.2, 128.4, 129.9, 132.2, 135.5, 136.4, 137.1, 141.7. HRMS (*m/z*): Calcd. for $C_{25}H_{21}N_2S_2$ $[M+H]^+$, 413.1141; Found, 413.1142. Anal. Calcd. for $C_{25}H_{20}N_2S_2$: C, 72.78; H, 4.89; N, 6.79; Found: C, 72.41; H, 4.89; N, 6.72.

1,2-bis-(2′-methyl-5′-phenylthien-3′-yl)-1,3-dimethylimidazolium Iodide (7): A 40 mL vial with a stir bar was charged with 100 mg (0.24 mmol) of imidazole **6**, 123 mg (0.89 mmol) of K_2CO_3, 10 mL of CH_3CN and 75 μL of iodomethane (1.2 mmol),

sealed with a Teflon-lined cap, and heated to 80 °C for 16 h. The reaction mixture was cooled to room temperature and filtered through Celite. After the filtrate was concentrated under reduced pressure, the residue was taken up into dichloromethane. The remaining K_2CO_3 was removed by a second filtration through Celite and the dichloromethane was removed from the filtrate under reduced pressure. The residue was triturated in diethyl ether and 113 mg (82% yield) of the desired product was isolated by filtration as a pale yellow powder. mp 206 °C (dec). ^{1}H NMR (400 MHz, $CDCl_3$): δ 2.15 (s, 6H), 3.94 (s, 6H), 7.14 (s, 2H), 7.29 (t, *J* = 7.4, 2H), 7.36 (t, *J* = 7.6, 4H), 7.50 (d, *J* = 7.2, 4H), 10.43 (s, 1H). ^{13}C NMR (100 MHz, $CDCl_3$) δ 14.4, 35.1, 121.9, 123.1, 125.5, 128.1, 129.0, 132.9, 138.2, 141.8, 142.9. HRMS (*m/z*): Calcd. for $C_{27}H_{25}N_2S_2$ $[M+1-I]^+$, 441.14537; Found, 441.1454. Anal. Calcd. for $C_{27}H_{25}IN_2S_2$: C, 57.04; H, 4.43; N, 4.93; Found: C, 57.73; H, 4.73; N, 4.54.

1,2-bis-(2′-methyl-5′-phenylthien-3′-yl)-1,3-dimethylimidazolium Hexafluorophosphate (1o·HPF$_6$): A 20 mL vial equipped with a stir bar was charged with 100 mg (0.18 mmol) of **7** dissolved in 10 mL of dichloromethane. To the vial was added 45.5 mg (0.18 mmol) of silver hexafluorophosphate dissolved in 2 mL of dichloromethane. A white precipitate formed immediately, and the reaction was stirred at room temperature for a further 15 min. The mixture was then filtered through a 0.2 μm PTFE filter and the filtrate was concentrated and dried under reduced pressure to yield 75 mg (73% yield) of the desired product as a pale yellow powder. mp 221 °C (dec). ^{1}H NMR (400 MHz, $CDCl_3$): δ 2.13 (s, 6H), 3.81 (s, 6H), 7.11 (s, 2H), 7.29 (t, *J* = 7.6, 2H), 7.37 (t, *J* = 7.6, 4H), 7.50 (d, *J* = 7.6, 4H), 8.87 (s, 1H). ^{13}C NMR (100 MHz, $CDCl_3$) δ 13.9, 34.5, 122.0, 123.2, 125.6, 128.1, 128.2, 129.1, 133.1, 137.7, 142.0, 142.8. UV-vis (C_6H_6): λ_{abs} = 293 nm (ε = 24894 dm^3 mol^{-1}). HRMS (*m/z*): Calcd. for $C_{27}H_{25}N_2S_2$ [M+1-

$PF_6]^+$, 441.14537; Found, 441.1455. Anal. Calcd. for $C_{27}H_{25}F_6N_2PS_2$: C, 55.28; H, 4.30; N, 4.78; Found: C, 55.33; H, 4.34; N, 4.44.

1,2-bis-(2′-methyl-5′-phenylthien-3′-yl)-1,3-dimethylimidazolylidene (1o): Under an atmosphere of N_2 in a glove box, a 8 mL vial equipped with a stir bar was charged with 11.0 mg (0.02 mmol) of **1o·HPF$_6$**. In a separate 8 mL vial, 6 mg (0.033 mmol) of NaHMDS was dissolved in 2 mL of C_6D_6, and 1 mL of the base solution was added to the vial containing **1o·HPF$_6$**. The mixture was stirred at room temperature for 30 min and then transferred to an NMR tube or reaction vessel. The free NHC **1o** was not isolated, but was characterized in situ. ^{1}H NMR (400 MHz, C_6D_6): δ 1.83 (s, 6H), 3.55 (s, 6H), 6.99 (m, 4H), 7.08 (t, J = 7.6, 4H), 7.45 (d, J = 7.6, 4H). ^{13}C NMR (100 MHz, C_6D_6) δ 13.6, 33.9, 122.6, 123.7, 125.8, 129.3, 133.7, 142.1, 142.9, 201.9. UV-vis (C_6H_6): λ_{abs} = 291 nm.

Synthesis of ^{13}C labeled NHC 1o*. The ^{13}C labeled NHC **1o*** was synthesized using an analogous route to that employed for **1o** with the exception that ^{13}C-enriched formaldehyde solution was used in the formylative cyclization of **5** to give the labeled imidazole **6***. Subsequent alkylation, anion metathesis, and in situ deprotonation yielded **1o***.

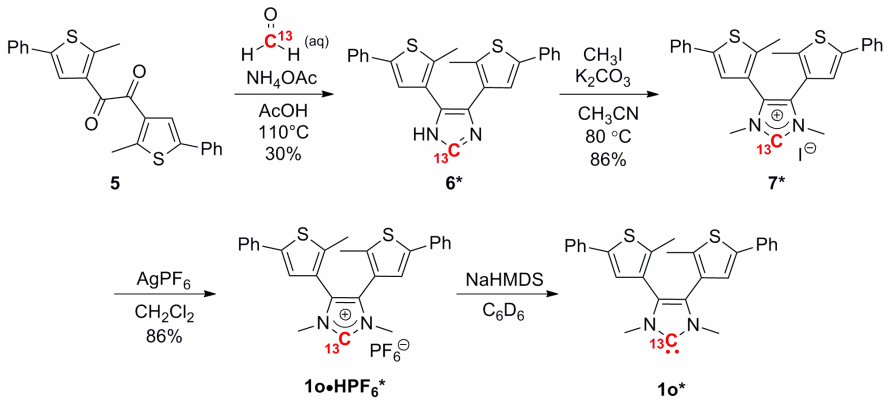

Figure 3.9: Synthesis of **1o***.

1,2-bis-(2′-methyl-5′-phenylthien-3′-yl)-2-^{13}C-imidazole (6*): ^{1}H NMR (400 MHz, CD_3OD): δ 2.13 (s, 6H), 7.23 (t, *J* = 7.6, 2H), 7.25 (s, 2H), 7.33 (t, *J* = 8, 4H), 7.53 (d, *J* = 8, 4H), 7.82 (d, *J* = 207, 1H). ^{13}C NMR (100 MHz, CD_3OD): δ 136.4.

1,2-bis-(2′-methyl-5′-phenylthien-3′-yl)-1,3-dimethyl-2-^{13}C-imidazolium iodide (7*): ^{1}H NMR (400 MHz, $CDCl_3$): δ 2.15 (s, 6H), 3.95 (s, 6H), 7.17 (s, 2H), 7.27 (t, *J* = 7.6, 2H), 7.35 (t, *J* = 8, 4H), 7.50 (d, *J* = 7.2, 4H), 10.39 (d, *J* = 220, 1H). ^{13}C NMR (100 MHz, $CDCl_3$): δ 138.1.

1,2-bis-(2′-methyl-5′-phenylthien-3′-yl)-1,3-dimethyl-2-^{13}C-imidazolium hexafluoro-phosphate (1o·HPF$_6$*): ^{1}H NMR (400 MHz, $CDCl_3$): δ 2.13 (s, 6H), 3.81 (s, 6H), 7.13 (s, 2H), 7.29 (t, *J* = 8, 2H), 7.37 (t, *J* = 8, 4H), 7.50 (d, *J* = 8, 4H), 8.86 (d, *J* = 220, 1H). ^{13}C NMR (100 MHz, $CDCl_3$): δ 137.6. HRMS (*m/z*): Calcd. for $C_{27}H_{25}N_2S_2$ $[M+1-PF_6]^+$, 442.14872; Found, 442.14850.

1,2-bis-(2′-methyl-5′-phenylthien-3′-yl)-1,3-dimethylimidazol-2-^{13}C-ylidene (1o*): ^{1}H NMR (400 MHz, C_6D_6): δ 1.81 (s, 6H), 3.63 (s, 6H), 6.94 (s, 2H), 7.01 (t, *J* = 8, 2H), 7.08 (t, *J* = 8, 4H), 7.45 (d, *J* = 4, 4H). ^{13}C NMR (100 MHz, C_6D_6): δ 13.8, 37.0, 124.5, 125.8, 127.1, 129.2, 134.2, 138.9, 141.7, 150.9, 201.9.

3.4.3 Procedures for Photochemical and Catalysis Experiments

Photochemical Experiments with 1o*. Under an inert N_2 atmosphere in a glove box, 2 mg (0.012 mmol) of NaHMDS in 1 mL of C_6D_6 was added to a 5.8 mg (0.01 mmol) sample of **1o·HPF$_6$*** in an 8 mL vial. The solution was allowed to stir at room temperature for 1 h, then transferred to an NMR tube and analyzed by ^{13}C NMR spectroscopy. Under an inert atmosphere, the solution was then diluted further with 3 mL of C_6D_6 and transferred to a quartz cuvette ([**1o***] = 1 × 10^{-3} M). The cuvette was then either removed from the glove box and irradiated directly (λ_{irr} = 313 nm) for 1 h, or 2-

aminoethanol and/or ethyl acetate were added in stoichiometric (0.01 mmol) or superstoichiometric (0.4 mmol) quantities along with 0.1 mL of THF under inert atmosphere prior to irradiation (λ_{irr} = 313 nm). The UV-treated solution was concentrated under reduced pressure to a volume of approximately 1 mL prior to ^{13}C NMR analysis. Subsequent visible light irradiation was carried out directly in the NMR tube using the concentrated sample at approximately [**1***] = 4.0×10^{-3} M and the irradiated sample was analyzed again by ^{13}C NMR spectroscopy.

Transesterification of Vinyl Acetate and Allyl Alcohol: Under an atmosphere of N_2 in a glove box, a vial equipped with a magnetic stir bar was charged with 5.8 mg (0.01 mmol) of **1o·HPF$_6$**, 2 mg (0.01 mmol) of KOtBu, and 10 mL of THF. The solution was stirred at room temperature for 30 min, after which a 4 mL portion was transferred to a quartz cuvette equipped with a stir bar and a second 4 mL portion was transferred to a 10 mL round bottom flask equipped with a stir bar. The cuvette was then sealed with a Teflon-lined septum cap, and the round bottom flask was sealed with a rubber septum secured with a copper wire. The two reaction vessels were removed from the glove box and the solution in the quartz cuvette was irradiated with UV light (λ_{irr} = 313 nm) with stirring for 1 h, while the solution in the round bottom flask was stirred under ambient light. After 1 h, 65 μL (0.4 mmol) of *n*-octane (internal standard) was added to each vessel via a N_2 purged syringe, followed by 37 μL (0.4 mmol) of vinyl acetate and 27 μL (0.4 mmol) of allyl alcohol. The reaction in the cuvette was kept under UV irradiation and the reaction in the round bottom flask was kept under ambient light throughout the course of the reaction. Aliquots were removed after given amounts of time, diluted with wet methanol to quench the reaction and analyzed by GC. For the photoswitching experiments described in the main text, a single reaction was set up as described above in

a quartz cuvette and irradiated with UV or visible light after the indicated amounts of time.

Amidation of Ethyl Acetate with 2-Aminoethanol: Under an atmosphere of N_2 in a glove box, a vial equipped with a magnetic stir bar was charged with 11 mg (0.02 mmol) of **1o·HPF$_6$**. A solution of 16 mg (0.02 mmol) of NaHMDS in 10 mL of THF was prepared, and 2 mL of that solution was added to the vial containing **1o·HPF$_6$**. The catalyst solution was diluted with 6 mL of benzene and then stirred at room temperature for 15 min. A 4 mL portion of the catalyst solution was transferred to a quartz cuvette equipped with a stir bar and a second 4 mL portion was transferred to a 10 mL round bottom flask with a stir bar. The cuvette was then sealed with a Teflon-lined septum cap, and the round bottom flask was sealed with a rubber septum secured with a copper wire. The two reaction vessels were removed from the glove box and the solution in the quartz cuvette was irradiated with UV light (λ_{irr} = 313 nm) with stirring for 1 h, while the solution in the round bottom flask was stirred under ambient light. After 1 h, 63 μL (0.4 mmol) of *n*-octane (internal standard) was added to each vessel via a N_2 purged syringe, followed by 33.5 μL (0.4 mmol) of ethyl acetate and 24 μL (0.4 mmol) of 2-aminoethanol. The reaction in the cuvette was kept under UV light for the first 2 h, while the reaction in the round bottom flask was kept under ambient light throughout the course of the reaction. Aliquots were removed after given amounts of time, diluted into wet methanol to quench the reaction and analyzed by GC. For the photoswitching experiments described in the main text, a single reaction was set up as described above in a quartz cuvette and irradiated with UV or visible light after the indicated amounts of time.

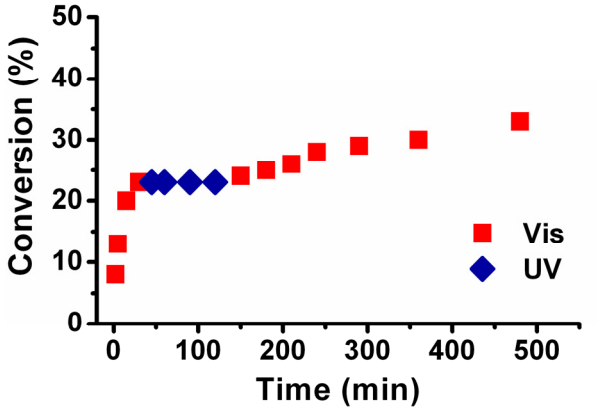

Figure 3.9: Plot of reaction conversion versus time for the condensation of ethyl acetate and 2-aminoethanol catalyzed by **1** (prepared in situ from **1·HPF$_6$** and 0.9 equiv. of NaHMDS) in 3:1 C_6H_6 : THF (v/v). The reaction was monitored over time by GC using *n*-octane as an internal standard. A single reaction was set up, allowed to react under ambient light for 30 min (red squares), then exposed to UV light (blue diamonds) (λ_{irr} = 313 nm) for 30 min and finally kept in the dark for 1 h prior to exposure to visible light (λ_{irr} > 500 nm) (red squares).

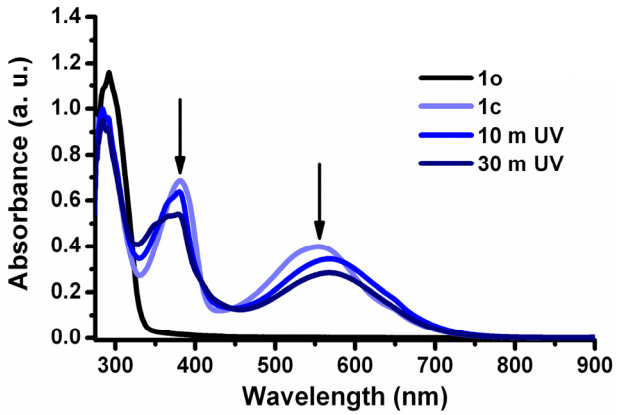

Figure 3.10: UV-vis spectra of **1o**, **1c**, and the spectral changes of **1c** upon prolonged UV irradiation (λ_{irr} = 313 nm) in benzene ([**1o**]$_0$ = 4 × 10^{-5} M). The spectra were recorded after irradiation for 0 (**1o**), 2 (**1c**), 10 and 30 min (indicated).

3.5 ACKNOWLEDGEMENTS

Portions of this chapter were reprinted with permission from Neilson, B. M.; Bielawski, C. W. *J. Am. Chem. Soc.* **2012**, *134*, 12693-12699. Copyright 2012 American Chemical Society. I am grateful to Steve Sorey for his help with the quantitative ^{13}C NMR experiments, and to Christopher Bielawski for help in writing the original manuscript.

3.6 REFERENCES

[1] Stoll, R. S.; Hecht, S. *Angew. Chem. Int. Ed.* **2010**, *49*, 5054-5075.

[2] (a) H. Durr, H. Bouas-Laurent, Eds. *Photochromism: Molecules and Systems*; Elsevier: Amsterdam, The Netherlands, **2003**. (b) Special Issue: "Photochromism: Memories and Switches" (Ed. M. Irie), *Chem Rev.* **2000**, *100*, 1683.

[3] (a) Russew, M.-M.; Hecht, S. *Adv. Mat.* **2010**, *22*, 3348-3360. (b) Guerchais, V.; Ordronneau, L.; Bozec, H. L. *Coord. Chem. Rev.* **2010**, *254*, 2533-2545. (c) Kuma, S.; Nishihara, H. *Dalton Trans.* **2008**, 3260-3271. (d) Ko, C.-C.; Yam, V.-W.-W. *J. Mat. Chem.* **2010**, *20*, 2063-2070. (e) Kobatake, S.; Irie, M. *Annu. Rep. Prog. Chem., Sect. C.* **2003**, *99*, 277-313. (f) Matsuda, K.; Irie, M. *J. Photochem. Photobio. C: Photochem Rev.* **2004**, *5*, 169-182. (g) Tian, H.; Yang, S. *Chem. Soc. Rev*. **2004**, *33*, 85-97. (h) Tian, H.; Wang, S. *Chem. Commun.* **2007**, *8*, 781-792. (i) Yun, C.; You, J. ; Kim, J.; Huh, J.; Kim, E. *J. Photochem. Photobio. C: Photochem Rev.* **2009**, *10*, 111-129. (j) Akita, M. *Organometallics*, **2011**, *30*, 43-51.

[4] (a) Peters, M. V.; Stoll, R. S.; Kühn, A.; Hecht, S. *Angew. Chem. Int. Ed.* **2008**, *47*, 5968-5972. (b) Stoll, R. S.; Peters, M. V.; Kühn, A.; Heiles, S.; Goddard, R.; Bühl, M.; Thiele, C. M.; Hecht, S. *J. Am. Chem. Soc.* **2009**, *131*, 357-367. (c) Stoll, R. S.; Hecht, S. *Org. Lett.* **2009**, *11*, 4790-4793. (d) Wei, Y.; Han, S.; Kim, J.; Soh, S.; Grzybowski, B. A. *J. Am. Chem. Soc.* **2010**, *132*, 11018-11020. (e) Ueno, A.; Takahashi, K.; Osa, T. *J. C. S. Chem. Comm.* **1981**, *3*, 94-96. (f) Cacciapaglia, R.; Di Stefano, S.; Mandolini, L. *J. Am. Chem. Soc.* **2003**, *125*, 2224-2227. (g) Sugimoto, H.; Kimura, T.; Inoue, S. *J. Am. Chem. Soc.* **1999**, *121*, 2325-2326. (h) Lee, W.-S.; Ueno, A. *Macromol. Rapid. Commun.* **2001**, *22*, 448-450. (i) Keiper, S.; Vyle, J. S. *Angew. Chem. Int. Ed.* **2006**, *45*, 3306-3309.

[5] Irie, M. *Chem Rev*. **2000**, *100*, 1685-1716.

[6] Neilson, B. M.; Lynch, V. M.; Bielawski, C. W.; *Angew. Chem. Int. Ed.* **2011**, *50*, 10322-10326.

[7] (a) Yam, V. W.-W.; Lee, J. K.-W.; Ko, C.-C.; Zhu, N. *J. Am. Chem. Soc.* **2009**, *131*, 912-913. (b) Lee, P. H.-M.; Ko, C.-C.; Zhu, N.; Yam, V. W.-W. *J. Am. Chem. Soc.* **2007**, *129*, 6058-6059. (c) Duan, G.; Zhu, N.; Yam, V. W.-W. *Chem. Eur. J.* **2010**, *16*, 13199-13209. (d) Nakashima, T.; Goto, M.; Kawai, S.; Kawai, T. *J. Am. Chem. Soc.* **2008**, *130*, 14570-14575.

[8] For reviews on NHCs and their coordination chemistry, see: (a) Hahn, F. E.; Jahnke, M. C. *Angew. Chem. Int. Ed.* **2008**, *47*, 3122-3172. (b) Herrmann, W. A. *Angew. Chem. Int. Ed.* **2002**, *41*, 1290-1309; (c) Bourissou, D.; Guerret, O.; Gabbaï, F. P.; Bertrand, G. *Chem. Rev.* **2000**, *100*, 39-91. (d) Herrmann, W. A.; Köcher, C. *Angew. Chem. Int. Ed. Engl.* **1997**, *36*, 2162-2187. (e) Díez-González, S.; Marion, N.; Nolan, S. P. *Chem. Rev.* **2009**, *109*, 3612-3676. (f) Dröge, T.; Glorius, F. *Angew. Chem. Int. Ed*. **2010**, *49*, 6940-6952.

[9] For reviews on NHC-based organocatalysts, see: (a) Zeitler, K. *Angew. Chem. Int. Ed.* **2005**, *44*, 7506-7510. (b) Enders, D.; Niemeier, O.; Henseler, A. *Chem. Rev.* **2007**, *107*, 5606-5655. (c) Marion, N.; Díez-González, S.; Nolan, S. P. *Angew. Chem. Int. Ed.* **2007**, *46*, 2988-3000. (d) Nair, V.; Vellalath, S.; Babu, B. P. *Chem. Soc. Rev.* **2008**, *37*, 2691-2698. (e) Nair, V.; Menon, R. S.; Biju, A. T.; Sinu, C. R.; Paul, R. R.; Jose, A.; Vellalath, S. *Chem. Soc. Rev.* **2011**, *40*, 5336-5346. (f) Biju, A. T.; Kuhl, N.; Glorius, F. *Acc. Chem. Res.* **2011**, *44*, 1182-1195.

[10] For studies on tuning the electron donating properties of NHCs as a means to influence catalytic reactions, see: (a) Khramov, D. M.; Rosen, E. L.; Er, J. A. V.; Vu, P. D.; Lynch, V. M.; Bielawski, C. W. *Tetrahedron*, **2008**, *64*, 6853-6862. (b) Benhamou, L.; Vujkovic, N. V.; César, V.; Gornitzka, H.; Lugan, N.; Lavigne, G. *Organometallics* **2010**, *29*, 2616-2630. (c) Süβner, M.; Plenio, H. *Chem. Commun.* **2005**, *43*, 5417-5419. (d) Sashuk, V.; Peeck, L. H.; Plenio, H. *Chem. Eur. J.* **2010**, *16*, 3983-3993. (e) Moerdyk, J. P.; Bielawski, C. W. *Organometallics* **2011**, *30*, 2278-2284. (f) Fürstner, A.; Alcarazo, M.; Krause, H.; Lehmann, C. W. *J. Am. Chem. Soc.* **2007**, *129*, 12676-12677. (g) O'Brien, C. J.; Kantchev, E. A. B.; Chass, G. A.; Niloufar, H.; Hopkinson, A. C.; Organ, M. G., Setiadi, D. H.; Tang, T. Fan, D. *Tetrahedron,* **2005**, 61, 9723-9735. (h) Balof, S. L.; P'Pool, S. J.; Berger, N. J.; Valente, E. J.; Shiller, A. M.; Schanz, H.-J. *Dalton Trans.* **2008**, *42*, 5791-5799. (i) Balof, S. L.; Yu, B.; Lowe, A. B.; Ling, Y.; Zhang, Y.; Schanz, H.-J. *Eur. J. Inorg. Chem.* **2009**, *13*, 1717-1722. (j) César, V.; Tourneux, J.-C.; Vujkovic, N.; Brousses, R.; Lugan, N.; Lavigne, G. *Chem. Commun.* **2012**, *48*, 2349-2351.

[11] Lemieux, V.; Spantulescu, M. D.; Baldridge, K. K.; Branda, N. R. *Angew. Chem. Int. Ed.* **2008**, *47*, 5034-5037.

[12] UV irradiation of the imidazolium iodide **7** resulted in decomposition; as such, the PF_6 anion was substituted for the iodide anion.

[13] (a) The conversions of the forward and reverse cyclizations were measured using the molar extinction coefficient for the absorbance of **1c·HPF$_6$** centered at 670 nm (ε = 24684 dm^3 mol^{-1}), as determined from a combination of ^{1}H NMR and UV-vis spectroscopy. (b) A similar procedure was used to determine the interconversion of **1o** and **1c** (**1c**: ε = 9767 dm^3 mol^{-1}).

[14] (a) Nyce, G. W.; Lamboy, J. A.; Connor, E. F.; Waymouth, R. M.; Hedrick, J. L. *Org. Lett.* **2002**, *4*, 3587-3590. (b) Grasa, G. A.; Kissling, R. M.; Nolan. S. P. *Org. Lett.* **2002**, *4*, 3583-3586. (c) Grasa, G. A.; Güveli, T.; Singh, R.; Nolan. S. P. *J. Org. Chem.* **2003**, *68*, 2812-2819. (d) Singh, R.; Kissling, R. M.; Letellier, M.-A.; Nolan. S. P. *J. Org. Chem.* **2004**, *69*, 209-212. (e) Movassaghi, M.; Schmidt, M. A. *Org. Lett.* **2005**, *7*, 2453-2456.

[15] Similar conversions (11-31%) in analogous NHC-catalyzed transesterifications of vinyl esters have been observed as a result of undesired catalyst deactivation pathways, see: Pignataro, L.; Papalia, T.; Slawin, A. M. Z.; Goldup, S. M. *Org. Lett.* **2009**, *11*, 1643-1646.

[16] When a control reaction was performed in the absence of **1o** under ambient light, a background reaction was observed with the KO*t*Bu acting as the catalyst (31% conversion after 1 h). However when an analogous was exposed to UV light, no significant reduction of catalytic activity was observed (26% conversion after 1 h), indicating that UV irradiation alone did not impede the reaction. Similarly, UV irradiation did not alter the catalytic activity when 1,3-dimesitylimidazolinylidene (SIMes), an NHC-based organocatalyst which lacks a photochromic moiety, was used in lieu of **1o** (conversion after 1 h: 39 % under ambient light; 58% under UV light).

[17] Nolan reported that unsaturated NHCs were significantly more active transesterification catalysts than their saturated analogues; see reference 14c. While no formal change in unsaturation occurs upon conversion of **1o** to **1c**, the disruption of the endocyclic double bond in **1o** upon photocyclization has a similar effect on the nucleophilicity of the NHC, which was reflected by the reduction in reaction rate observed under UV irradiation and in accord with the previous demonstration that the electron donating ability of the NHC was reduced upon photocyclization, see reference 6.

[18] For other examples of light-activated latent catalysts, see: (a) Sun, X.; Gao, J. P.; Wang, Z. Y. *J. Am. Chem. Soc.* **2008**, *130*, 8130-8131. (b) Ben-Asuly, A.; Aharoni, A.; Diesendruck, C. E.; Vidavsky, Y.; Goldberg, I.; Straub, B. F.; Lemcoff, N. G. *Organometallics* **2009**, *28*, 4652-4655. (c) Hafner, A.; Muhlengach, A.; van der Schaaf, P. A. *Angew. Chem. Int Ed.* **1997**, *36*, 2121-2124. (d) Keitz, B. K.; Grubbs, R. H. *J. Am. Chem. Soc.* **2009**, *131*, 2038-2039. (e) Wang, D.; Wurst K.; Knolle, W.; Decker, U.; Prager, L.; Naumov, S.; Buchmeiser, M. R. *Angew. Chem. Int. Ed.* **2008**, *47*, 3267-3270.

[19] When a control reaction was performed in the absence of **1o**, a background reaction was observed with NaHMDS acting as the catalyst (44% conversion after 4 h) under ambient light. However, no attenuation of cataytic activity was observed under UV light (53% conversion after 4 h). When imidazolium salts without photochromic moieties, such as 1,3-dimesitylimidazolium chloride or 1,3-dimesityl-imidazolinium chloride, were used the precatalyst, no significant conversion to product was observed under ambient light or UV irradiation after 4 h.

[20] Decomposition (29%) of **1c** was observed by UV-vis spectroscopy upon prolonged UV irradiation (> 0.5 h, $[\mathbf{1o}]_0 = 4 \times 10^{-5}$ M); see Figure 3.11.

[21] The observed results were consistent with the formation of an imidazolium alkoxide intermediate, as proposed in a previous report of NHC-catalyzed amidation reactions; see reference 14e.

[22] (a) Trnka, T. M.; Morgan, J. P.; Sanford, M. S.; Wilhelm, T. E.; Scholl, M.; Choi, T.-L.; Ding, S.; Day, M. W.; Grubbs, R. H. *J. Am. Chem. Soc.* **2003**, *125*, 2546-2558. (b) Csihony, S.; Culkin, D. A.; Sentman, A. C.; Dove, A. P.; Waymouth, R. M.; Hedrick, J. L. *J. Am. Chem. Soc.* **2005**, *127*, 9079-9084.

[23] When a stoichiometric quantity of 2-aminoethanol was added to **1o*** (generated in situ), a signal assigned to the C2 nucleus of the NHC was observed at 165 ppm and in agreement with a proton transfer reaction. Upon UV irradiation, the signal shifted upfield to 102 ppm, which was consistent with the formation of a NHC-alcohol adduct. Visible light irradiation reversed the spectral changes, which suggested to us that the decreased electron density at the C2 position upon photocyclization resulted in the reversible formation of a NHC-alcohol adduct.

[24] UV irradiation of **1o*** was performed out in 4 mL of C_6D_6 in a quartz cuvette ($[\mathbf{1o^*}]_0 = 2.5 \times 10^{-3}$ M). Prior to NMR analysis, the solution was concentrated under reduced pressure to a volume of approximately 1 mL ($[\mathbf{1o^*}] = 1.0 \times 10^{-2}$ M). The visible light irradiation was carried out directly on the concentrated sample in the NMR tube.

[25] Using quantitative ^{13}C NMR analysis of **1o*** versus *p*-xylene as an internal standard, a small amount (13%) of the catalyst was observed to decompose to insoluble byproduct(s) after UV irradiation ($[\mathbf{1o^*}]_0 = 2.5 \times 10^{-3}$ M; $\lambda_{irr} = 313$ nm for 1 h) followed by visible irradiation ($\lambda_{irr} > 500$ nm for 2 h) ($[\mathbf{1c^*}] = 1.0 \times 10^{-2}$ M). The observed photochemical fatigue may account for the inability to restore the initial reaction rate after irradiation; see Appendix C.

[26] During the preparation of this manuscript, an elegant example of photomodulating deuterium exchange reactions using a pyridinium catalyst electronically linked to a DAE scaffold was reported, see: Wilson, D.; Branda, N. R. *Angew. Chem. Int. Ed.* **2012**, *51*, 5431-5434.

[27] Iwamoto, O.; Sugiyama, H.; Hara, T. Fulgimide Derivatives. U. S. Patent 5,359,085, October 25, 1994.

Chapter 4: Photoswitchable NHC-Promoted Ring-Opening Polymerizations

4.1 INTRODUCTION

Externally-regulated polymerizations offer the potential to achieve unsurpassed control over the structures and properties of synthetic macromolecular materials.[1] Light is an ideal stimulus for controlling polymerization reactions because it is non-invasive, chromophore selective, and provides excellent spatial and temporal control.[2] Over the past few years, a number of successful photoswitchable polymerizations have been developed. In a seminal contribution, Manners reported[3] the photo-controlled living ring-opening polymerization (ROP) of ferrocenophane monomers via reversible photo-induced metal-ligand bond dissociation. More recently, reversible photo-induced bixanthene dissociation and electron transfer processes were reported by Yang[4] and Hawker,[5] respectively, as methods to control living radical polymerizations.[6] However, of the reported examples,[3-6] none have involved the use of a photoswitchable organocatalyst to effect ring-opening polymerizations (ROPs)[7] of cyclic esters.[8,9] Such a photoswitchable ROP catalyst is expected to offer a new level of control over the synthesis of biologially and industrially relevant polyesters, and may enable the development of novel materials with sophisticated macromolecular architectures and advanced functions.

N-heterocyclic carbenes (NHCs)[10] have been shown by Waymouth and Hedrick[11] to be efficient organocatalysts for facilitating the ROP of cyclic esters. Recently, we reported[12] that the intrinsic catalytic activities displayed by NHCs in transesterification[13] and transamidation[14] reactions may be photo-modulated via annulation to a photochromic diarylethene. As shown in Figure 4.1, cyclization of the NHC precatalyst **1o•HPF$_6$** was found to reduce the electron density at the corresponding carbene nucleus[15] and resulted in a catalytically inactive species upon UV irradiation. Subsequent exposure to visible

light reversed the cyclization reaction and regenerated an active catalyst.[12] Given this initial success, we envisioned that photoswitchable NHCs could be extended to gain control over ROPs.

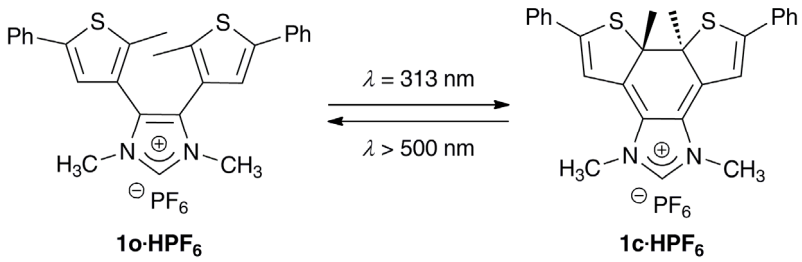

Figure 4.1: Photochromism of NHC precatalyst **1o•HPF$_6$**.

4.2 Results and Discussion

In an initial experiment, **1o•HPF$_6$**[12] (0.01 mmol) was treated with NaHMDS (0.0095 mmol) in THF followed by ε-caprolactone (2 mmol) and benzyl alcohol (BnOH; 0.02 mmol) (Eq. 4.1). After 1 h at room temperature, complete conversion (> 95%) of ε-caprolactone to the corresponding polymer was observed by ^{1}H NMR spectroscopy. Gel permeation chromatography (GPC) of the resulting material revealed that the polymer with a number average molecular weight (M_n) of 15,900 Da and polydispersity index (PDI) of 1.15 was formed.[16] Although the measured molecular weight was higher than its theoretical value ($M_{n(theor)}$ = 11,400 Da),[17] the narrow PDI was consistent with a controlled chain growth process.[7]

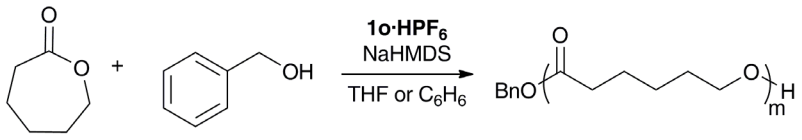

Eq. 4.1

To determine if UV irradiation would affect the rate of the aforementioned polymerization, a solution of **1o** was freshly prepared by treatment of **1o•HPF$_6$** with 0.95

equiv of NaHMDS in C_6H_6 and then equally divided into two quartz cuvettes. One of the cuvettes was exposed to UV irradiation for 1 h, while the other was kept in ambient light. ε-Caprolactone (1.0 M) and BnOH (0.01 M) were then added to each reaction vessel. After 1 h, an aliquot was removed from each cuvette and quenched by exposure to methanol. Upon concentration and dissolution in $CDCl_3$, ^1H NMR spectroscopic analysis of each aliquot revealed that the reaction in ambient light had reached complete conversion to polymer (> 95%), while the mixture exposed to UV radiation did not react (< 5% conversion). The lack of reactivity observed upon exposure to UV light was consistent with the reduced catalytic activity of **1c** compared with **1o**.[12]

Unfortunately, the polymerization of ε-caprolactone in ambient light was too fast to accurately measure at a practical temperature (> 95% conversion in 5 min; 25 °C), even at lower concentrations and catalyst loadings. However, the photoswitchable nature of **1** was demonstrated by a photo-gated[2] chain extension experiment. First, a reaction mixture similar to that described above (2 mmol ε-caprolactone; 0.5 mol% **1**, 1.0 mol% BnOH) was allowed to react in ambient light for 30 min, during which time it reached complete conversion (> 95% by ^1H NMR spectroscopy) and formed a polymer with a M_n of 12,500 Da ($M_{n(theor)}$ = 11,414 Da[17]) and a PDI of 1.57. The same reaction vessel was then irradiated with UV light for 1 h, after which a second equivalent of ε-caprolactone (2 mmol) was added. The reaction vessel was kept under UV irradiation for a further 3 h, during which time neither the monomer conversion nor the molecular weight of the polymer increased, consistent with the formation of the inactive photocyclized catalyst **1c**. Subsequent exposure to visible light, however, resulted in a significant increase in the M_n of the resulting polymer to 19,000 Da (PDI = 1.31; $M_{n(theor)}$ = 16,000 Da), and ^1H NMR analysis revealed that 40% of the second monomer fraction had undergone polymerization. The observed increase in molecular weight coupled with the enhanced

monomer conversion suggested to us that the inactive catalyst **1c** underwent the photocycloreversion to regenerate the active catalyst **1o**, which facilitated polymer growth.[12] Collectively these results demonstrated a rare example of a latent photo-activated ROP.[8]

Subsequent attention was shifted to δ-valerolactone, which was expected to polymerize more slowly than its seven-membered analogue on account of its lower ring-strain and thus provide greater control over the reaction. After an initial experiment revealed that **1o** efficiently catalyzed the polymerization of δ-valerolactone (Eq. 4.2),[18] a comparative kinetics experiment was conducted to determine if UV irradiation would affect the rate of the polymerization. A freshly prepared solution of **1o** (0.016 mmol **1o•HPF$_6$** and 0.015 mmol NaHMDS) and the internal standard durene (1 mmol) in benzene (4.0 mL) was divided evenly into two quartz cuvettes, which were then each sealed with teflon-lined septum caps. One of the cuvettes was then exposed to UV irradiation (λ = 313 nm) for 1 h with stirring, while the second cuvette was stirred in ambient light. The monomer, δ-valerolactone (2 mmol), and BnOH (0.016 mmol), were then added via N_2 purged syringes to each reaction vessel. Aliquots were periodically removed from each reaction, diluted into methanol, filtered through 0.2 μm PTFE and analyzed by gas chromatography (GC). Inspection of these data revealed that the reaction in ambient light proceeded with a pseudo-first order rate constant, k_{amb}, of $1.2 \pm 0.5 \times 10^{-3}$ s^{-1}, while the reaction conducted in UV radiation was significantly slower ($k_{UV} = 2.0 \pm 1.0 \times 10^{-5}$ s^{-1}; $k_{amb}/k_{UV} = 59$; Fig. 4.2a).[19]

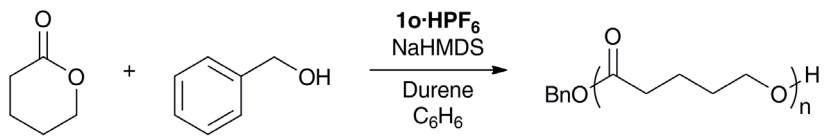

Eq. 4.2

The disparity in the rates of the ROP of δ-valerolactone in ambient versus UV light, coupled with the reversiblity of the photocyclization of the catalyst, enabled the rate of the polymerization to be photoswitched over time. First, when the polymerization of δ-valerolactone (2 mmol) with BnOH (0.012 mmol) and **1o** (0.3 mol%) was allowed to proceed in ambient light, a rate constant, k_{amb}, of $8.0 \pm 3.0 \times 10^{-4}$ s^{-1} was measured. Subsequent exposure to UV light to effect the photocyclization to **1c** (λ = 313 nm) resulted in a significant decrease in the rate constant ($k_{UV} = 7.0 \pm 2.0 \times 10^{-6}$ s^{-1}; k_{amb}/k_{UV} = 114; Fig. 4.2b). Alternatively, when the reaction was initially subjected to UV irradiation, negligible reactivity was observed ($k_{UV} = 2.0 \pm 1.0 \times 10^{-5}$ s^{-1}), however subsequent irradiation with visible light ($\lambda > 500$ nm) triggered the polymerization ($k_{vis} = 3.5 \pm 1.0 \times 10^{-4}$ s^{-1}; k_{vis}/k_{UV} = 17; Fig. 4.2c).[20] By alternating exposure to UV and visible light, the reactivity could be switched between slow and fast states. For example, the polymerization rate was initially suppressed by UV irradiation, restored upon exposure to visible light, and again attenuated upon a second exposure to UV light ($k_{UV}' = k_{UV} = 1.1 \pm 0.9 \times 10^{-5}$ s^{-1}; k_{vis}/k_{UV}' = 32; Fig. 4.2d).[21]

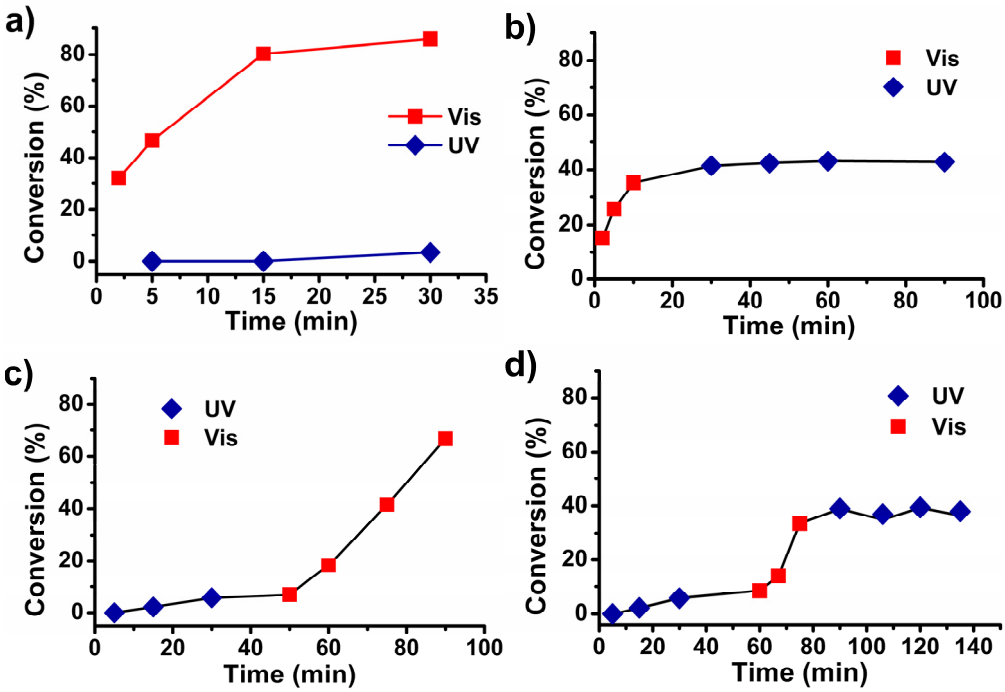

Figure 4.2: Plots of reaction conversion versus time for the ROP of δ-valerolactone catalyzed by **1** (prepared in situ from **1·HPF$_6$** and NaHMDS) in C_6H_6. The reactions were monitored over time by GC using durene as an internal standard. Conditions: [δ-valerolactone]$_0$ = 0.5 M; [BnOH]$_0$/[**1o**]$_0$ = 4; [δ-valerolactone]$_0$/[**1o**] = 250, unless otherwise noted. (a) Two reactions were run concurrently with one irradiated with UV light (λ_{irr} = 313 nm) for 1 h prior to substrate addition (blue diamonds) and the other kept in ambient light (red squares). (b) A single reaction vessel was allowed to proceed in ambient light for 10 min prior to UV exposure (blue diamonds). For this experiment, [δ-valerolactone]$_0$/[**1o**] = 333. (c) A single reaction vessel was exposed to UV irradiation for 1 h prior to substrate addition and then was kept in UV light for 30 min (blue diamonds) prior to visible light irradiation (λ_{irr} > 500 nm) (red squares). (d) A single reaction was exposed to UV irradiation for 1 h prior to substrate addition, then kept in UV light for 30 min (blue diamonds) prior to visible light irradiation (red squares). After 45 min the reaction was exposed to UV radiation (blue diamonds).

A proposed catalytic cycle for the photoswitchable ROP of δ-valerolactone is given in Figure 4.3. In accord with the mechanism proposed for NHC-promoted ROPs[7,11a] and previously reported ^{13}C NMR experiments,[12] **1o** facilitates the ring-opening of the

ester to form the resting state of the active catalyst. The corresponding imidazolium alkoxide can then turn over to form product or, upon UV irradiation, is converted to a NHC-alcohol adduct that is catalytically inactive due to the decreased electron density at the carbenoid center.[15] The catalytic activity is then restored by exposure to visible light to effect the cycloreversion, which regenerates the active imidazolium species and re-engages the catalytic cycle.

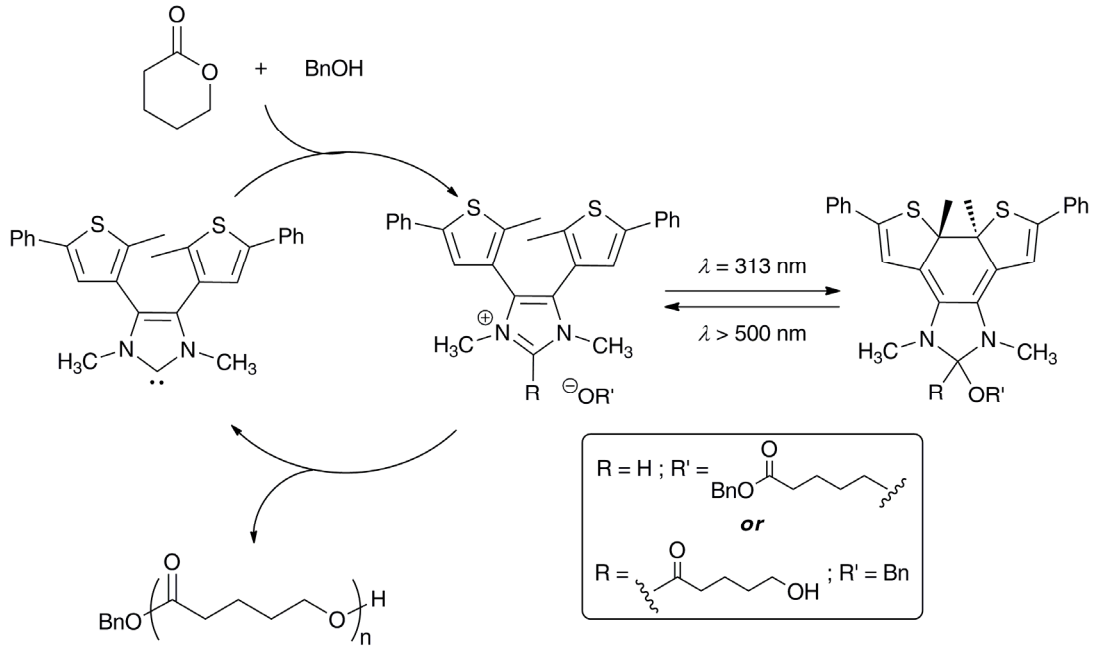

Figure 4.3: Proposed catalytic cycle for the photoswitchable ring-opening polymerizations catalyzed by **1o**.

4.3 CONCLUSIONS

In summary, we have developed a photoswitchable ROP of cyclic esters using a photochromic NHC catalyst. The ROP of ε-caprolactone and δ-valerolactone were promoted by the NHC **1o** in ambient light, however UV irradiation to form the photocyclized catalyst **1c** resulted in significant attenuation of the polymerization activity (k_{amb}/k_{UV} = 59 for δ-valerolactone). Moreover, the ROP of δ-valerolactone was reversibly

activated and deactivated through alternate exposure to visible and UV light. To the best of our knowledge, **1o** is the first example of a photoswitchable ROP organocatalyst, as well as the first photoswitchable NHC-based polymerization catalyst. Given the versatility of NHC organocatalysts for various ROP and other polymerizations,[7,11] we believe that the method may be extended to a wide variety of monomers and offers significant potential for the development of novel polymers and copolymers[22] with sophisticated architectures.

4.4 EXPERIMENTAL

Materials and Methods

Unless otherwise specified, reagents were purchased from commercial sources and used without further purification. Benzyl alcohol, ε-caprolactone and δ-valerolactone were stirred over CaH_2 under an atmosphere of dry N_2 for 18 h, then were distilled under vacuum and degassed by the freeze-pump-thaw method prior to use. Compound **1o·HPF$_6$** was prepared via the previously reported method.[12] Benzene and tetrahydrofuran were dried and degassed using a Vacuum Atmospheres Company solvent purification system. ^{1}H and ^{13}C NMR spectra were recorded using a Varian 400 MHz spectrometer. Chemical shifts δ (in ppm) for ^{1}H NMR are referenced to tetramethylsilane using the residual solvent as an internal standard: $CDCl_3$, 7.24 ppm. The photochemical reactions were performed in 6Q Spectrosil quartz cuvettes (Starna) with 1.0 cm path lengths and 3.0 mL sample solution volumes. The irradiation source for photochemical reactions was a Newport/Oriel 66942 200-500W Hg Arc lamp housing equipped with a 350 W Hg lamp, a Newport 6117 liquid filter, a Newport 71445 electronic safety shutter, and a Newport 71260 filter holder. The source was powered by a Newport 669910 power supply and mounted on a Newport XL48 optical rail with a Newport 13950 shielded cuvette holder

placed at a distance of 8 cm from the end of the source. The irradiation wavelength for the photocyclization reactions was obtained using a 313 nm bandpass filter (Andover Corporation). A long-pass edge filter (> 500 nm) (Andover Corporation) was used to introduce visible light. Gas chromatography (GC) was performed on an Agilent 6850 gas chromatograph (HP-1 column, L = 30 m, I.D. = 0.32 mm) equipped with a flame ionization detector (FID). The GC oven temperature was held at 40 °C for 3 min, then increased to 100 °C at 10 °C min^{-1} and finally increased to 250 °C at 20 °C min^{-1}. The internal standard durene was used to aid in measuring reaction conversions. Gel permeation chromatography (GPC) was performed using THF as the eluent on a Viscotek GPCmax Solvent/Sample Module, two fluorinated polystyrene columns (IMBHW-3078 and I-MBLMW-3078) thermostatted at 24 °C arranged in series, and a Viscotek VE 3580 Refractive Index Detector. Molecular weight and polydispersity data are reported relative to polystyrene standards in THF.

Ring-opening polymerization of ε-caprolactone: Under an atmosphere of N_2 in a glove box, a vial equipped with a magnetic stir bar was charged with 17.4 mg (0.03 mmol) of **1o·HPF$_6$** and 5.0 mL of C_6H_6. A solution of 27 mg (0.15 mmol) of NaHMDS in 5 mL of C_6H_6 was prepared, and 1 mL of that solution was added to the vial containing **1o·HPF$_6$**. The catalyst solution was then stirred at room temperature for 20 min before it was filtered through a 0.2 μm PTFE filter into a clean vial. Each of 2 quartze cuvettes was then charged with 2.0 mL (0.5 mol%) of the catalyst solution and 2.0 mL of C_6H_6. The cuvettes were then sealed with Teflon-lined septum caps and removed from the glove box. The solution in one cuvette was irradiated with UV light (λ_{irr} = 313 nm) with stirring for 1 h, while the solution in the other cuvette was stirred under ambient light. After 1 h, 0.22 mL (2 mmol) of ε-caprolactone was added to each cuvette followed by 2.1 μL of benzyl alcohol. The reaction in the cuvette was kept under UV light, while the

reaction in the round bottom flask was kept under ambient light throughout the course of the reaction. Aliquots (0.3 mL) were removed after given amounts of time, diluted into 1.0 mL of methanol to quench the reaction and concentrated under reduced pressure. The residue from each aliquot was then redissolved in $CDCl_3$ and analyzed by ^1H NMR and/or was redissolved in THF and analyzed by GPC. For the chain extension experiment described in the main text, a single reaction was set up as described above in a quartz cuvette and after 30 min in ambient light was irradiated with UV light. After 1 h of UV irradiation a second equivalent of monomer (0.22 mL) was added and the reaction was kept under UV irradiation for a further 3 h prior to irradiation with visible light.

Ring-opening polymerization of δ-valerolactone: Under an atmosphere of N_2 in a glove box, a vial equipped with a magnetic stir bar was charged with 12 mg (0.02 mmol) of **1o·HPF$_6$** and 4.0 mL of C_6H_6. A solution of 17.5 mg (0.095 mmol) of NaHMDS in 5 mL of C_6H_6 was prepared, and 1 mL of that solution was added to the vial containing **1o·HPF$_6$**. The catalyst solution was then stirred at room temperature for 20 min before it was filtered through a 0.2 μm PTFE filter into a clean vial. In a separate vial, 402 mg (3 mmol) of the internal standard durene was dissolved in 3.0 mL of C_6H_6. Each of 2 quartz cuvettes was then charged with 1.0 mL of the durene solution (1 mmol) and either 1.5 mL (0.3 mol%) or 2.0 mL (0.4 mol%) of the catalyst solution. The total volume of the solution in each cuvette was then brought to 4.0 mL by addition of C_6H_6. The cuvettes were then sealed with Teflon-lined septum caps and removed from the glove box. The solution in one cuvette was irradiated with UV light (λ_{irr} = 313 nm) with stirring for 1 h, while the solution in the other cuvette was stirred under ambient light. After 1 h, 0.2 mL (2 mmol) of δ-valerolactone was added to each cuvette followed by 0.1 mL (0.024 mmol; 1.2 mol%) or 0.13 mL (0.0032 mmol; 1.6 mol%) of a previously prepared solution of 25 μL of benzyl alcohol in C_6H_6. The reaction in the cuvette was

kept under UV light, while the reaction in the round bottom flask was kept under ambient light throughout the course of the reaction. Aliquots (0.1 mL) were removed after given amounts of time, diluted into 1.0 mL of methanol to quench the reaction and precipitate the polymer product. Each aliquot was filtered through a 0.2 μm PTFE filter and analyzed by GC. For the photoswitching experiments described in the main text, a single reaction was set up as described above in a quartz cuvette and irradiated with UV or visible light after the indicated amounts of time.

4.5 REFERENCES

[1] Leibfarth, F. A.; Mattson, K. M.; Fors, B. P. Collins, H. A.; Hawker, C. J. *Angew. Chem. Int. Ed.* **2013**, *52*, 199-210.

[2] Stoll, R. S.; Hecht, S. *Angew. Chem. Int. Ed.* **2010**, *49*, 5054-5075.

[3] Tanabe, M.; Vandermeulen, G. W. M.; Chan, W. Y.; Cyr, P. W.; Vanderark, L.; Rider, D. A.; Manners, I. *Nature Chem.* **2006**, *6*, 467-470.

[4] Zheng, X.; Yue, M.; Yang, P.; Li, Qi, Yang, W.; *Polym. Chem.* **2012**, *3*, 1982-1986.

[5] Fors, B. P.; Hawker, C. J. *Angew. Chem. Int. Ed.* **2012**, *51*, 8850-8853.

[6] For additional examples of photoswitchable controlled radical polymerizations, see: (a) Kwak, Y.; Matyjaszewski, K. *Macromolecules*, **2010**, *43*, 5180-5183. (b) Mosnáček, J.; Ilčíková, M. *Macromolecules*, **2012**, *45*, 5859-5865. (c) Zhou, H.; Johnson, J. A. *Angew. Chem. Int. Ed.* **2013**, *52*, 2235-2238. (d) Zhang, G.; Song, I. Y.; Ahn, K. H.; Park, T.; Choi, W. *Macromolecules*, **2011**, *44*, 7594-7599.

[7] Kamber, N. E.; Jeong, W.; Waymouth, R. M.; Pratt, R. C.; Lohmeijer, B. G. G.; Hedrick, J. L. *Chem. Rev.* **2007**, *107*, 5813-5840.

[8] For an elegant example of a latent photo-activated organocatalyst for ROP, see: Sun, X.; Gao, J. P.; Wang, Z. Y. *J. Am. Chem. Soc.* **2008**, *130*, 8130-8131.

[9] For an example of a photo-activated and thermally-deactivated ring-opening metathesis polymerization, see: Ben-Asuly, A.; Aharoni, A.; Diesendruck, C. E.; Vidavsky, Y.; Goldberg, I.; Straub, B. F.; Lemcoff, N. G. *Organometallics* **2009**, *28*, 4652-4655.

[10] For reviews on NHC-based organocatalysts, see: (a) Zeitler, K. *Angew. Chem. Int. Ed.* **2005**, *44*, 7506-7510. (b) Enders, D.; Niemeier, O.; Henseler, A.; *Chem. Rev.* **2007**, *107*, 5606-5655. (c) Marion, N.; Díez-González, S.; Nolan, S. P. *Angew. Chem. Int. Ed.* **2007**, *46*, 2988-3000. (d) Nair, V.; Vellalath, S.; Babu, B. P. *Chem.*

Soc. Rev. **2008**, *37*, 2691-2698. (e) Nair, V.; Menon, R. S.; Biju, A. T.; Sinu, C. R.; Paul, R. R.; Jose, A.; Vellalath, S. *Chem. Soc. Rev.* **2011**, *40*, 5336-5346. (f) Biju, A. T.; Kuhl, N.; Glorius, F. *Acc. Chem. Res.* **2011**, *44*, 1182-1195.

[11] (a) Connor, E. F.; Nyce, G. W.; Myers, M.; Möck, A.; Hedrick, J. L. *J. Am. Chem. Soc.* **2002**, *124*, 914-915. (b) Nyce, G. W.; Glauser, T.; Connor, E. F.; Möck, A.; Waymouth, R. M. Hedrick, J. L. *J. Am. Chem. Soc.* **2003**, *125*, 3046-3056. (c) Kamber, N. E.; Jeong, W.; Gonzalez, S.; Hedrick, J. L.; Waymouth, R. M. *Macromolecules* **2009**, *42*, 1634-1649.

[12] Neilson, B. M.; Bielawksi, C. W. *J. Am. Chem. Soc.* **2012**, *134*, 12693-12699.

[13] (a) Nyce, G. W.; Lamboy, J. A.; Connor, E. F.; Waymouth, R. M.; Hedrick, J. L. *Org. Lett.* **2002**, *4*, 3587-3590. (b) Grasa, G. A.; Kissling, R. M.; Nolan, S. P. *Org. Lett.* **2002**, *4*, 3583-3586. (c) Grasa, G. A.; Güveli, T.; Singh, R.; Nolan, S. P. *J. Org. Chem.* **2003**, *68*, 2812-2819. (d) Singh, R.; Kissling, R. M.; Letellier, M.-A.; Nolan, S. P. *J. Org. Chem.* **2004**, *69*, 209-212.

[14] Movassaghi, M. Schmidt, M. A. *Org. Lett.* **2005**, *7*, 2453-2456.

[15] Neilson, B. M.; Lynch, V. M.; Bielawski, C. W. *Angew. Chem. Int. Ed.* **2011**, *50*, 10322-10326.

[16] Molecular weight and polydispersity data are reported relative to polystyrene standards in THF.

[17] The theoretical molecular weight was based on the initial ratio of ε-caprolactone to BnOH.

[18] Conditions: [δ-valerolactone]0 = 0.5 M; [BnOH]0/[**1o**]0 = 4; [δ-valerolactone]0/[**1o**] = 250; 25 °C; 30 min; 93% conversion; Mn = 7,400 Da; PDI = 1.16; Mn(theor) = 5900 Da.

[19] All reported rate constants (*k*amb, *k*UV, *k*vis, *k*UV′) were obtained from the average of at least three separate experiments.

[20] We have previously shown that approximately 13% of the catalyst **1o** decomposes during the course of a UV (λirr = 313 nm; 1 h) and visible (λirr > 500 nm; 2 h) irradiation cycle; see reference 12.

[21] When a control reaction was performed in the absence of **1o** under ambient light, a background reaction was observed with the NaHMDS acting as the catalyst (> 95% conversion in 5 min). However when an analogous reaction was exposed to UV (λ_{irr} = 313 nm) or visible (λ_{irr} > 500 nm) light, no significant alteration of catalytic activity was observed (conversion after 5 min: > 95 % in UV or visible light), indicating that light alone did not impede or promote the reaction. Similarly, UV irradiation did not alter the catalytic activity when 1,3-dimethylimidazolium hexafluorophosphate, an NHC-based organocatalyst which

lacks a photochromic moiety, was used in lieu of **1o** (conversion after 5 min: > 95 % in ambient, UV, or visible light).

[22] When an equimolar mixture of ε-caprolactone (1 mmol) and δ-valerolactone (1 mmol) was added to a solution of **1o** (0.01 mmol) and BnOH (0.04 mmol) in benzene (4.0 mL), complete consumption of both monomers was observed by 1H NMR spectroscopy after 5 min in ambient light. After precipitation from methanol, GPC analysis of the resulting polymer revealed a Mn of 14,300 Da and a PDI of 1.59, which was in good agreement with the theoretical molecular weight of the expected copolymer (Mn(theor) = 11,300 Da). When an identical reaction was performed in UV light (λ_{irr} = 313 nm) negligible conversion of either monomer was observed (< 5% conversion).

Chapter 5: Remotely Tuning Hydroboration Activity via a Photoswitchable Rh(I) Catalyst

5.1 INTRODUCTION

Developments in homogenous organometallic catalysis have historically focused on improving catalytic activity and/or selectivity through ligand development. Once a ligand is chosen, however, the coordination environment of the catalyst active site typically dictates a fixed rate and selectivity for a given reaction. This restriction limits the versatility of state-of-the-art catalysts as well as the degree of control maintained over the course of the reaction. Recent efforts to address this issue have involved the development of "switchable catalysts,"[1] in which reduction/oxidation processes,[2] acid-base chemistry,[3] or light[4] is utilized to actively modify catalytic activity or selectivity.

Photochemical stimuli are particularly attractive for switching the intrinsic properties exhibited by catalysts, as such methods are typically non-invasive and use an inexpensive, renewable stimulus. Despite these advantages, very few photoswitchable catalysts are known (see Chapter 1).[5] To the best of our knowledge, however, the utilization of photo-induced changes in electronics to alter the outcomes of transition metal catalyzed transformations has not been realized.[6,7] Adding a photoswitchable feature to metal-based catalysts is expected to endow them with enhanced control over their intrinsic activities and selectivities.

A promising method for photochemically tuning the electronic properties of metal complexes involves the use of ligands which feature photochromic[8] diarylethene (DAE)[9] moieties.[10,11] We[12] and others[13] have established that the UV-induced cyclization of a DAE properly annulated to a N-heterocyclic carbene (NHC)[14] scaffold significantly decreases the electron donating ability of the NHC moiety[15] in both organic and organometallic adducts. Considering that the product of the photocyclization reaction

extends the conjugation of the nitrogen atoms adjoining the carbenoid nucleus, less electron density should be available for donation into the carbene center, resulting in a decrease in the ligand's overall donating ability. We recently demonstrated that photoswitchable DAE annulated NHCs may be used to tune the rates of NHC-promoted transesterification and amidation reactions.[16] Given this initial success and the large number of reactions facilitated by NHC-supported metal complexes,[14,15] we sought to photomodulate catalytic activity via changes in ligand donicity and realize a new concept in organometallic catalysis. Herein we report the first photochromic DAE-annulated NHC-Rh(I) complex and demonstrate that its catalytic activity may be tuned using light.

5.2 Results and Discussion

Considering that NHC-Rh(I) complexes are active catalysts for a wide variety of transformations,[17] we focused our attention on complex **1**, which featured a photochromic DAE-annulated NHC ligand (Figure 5.1). We envisioned that the UV-induced photocyclization of the ring-open isomer **1o** to the ring-closed form **1c** would alter the electronic properties of the complex, and subsequently its catalytic activity. The synthesis of the photochromic NHC- Rh(I) complex **1** is summarized in Figure 5.3. The known imidazolium iodide salt **2**[16] was treated with 0.5 equiv of silver (I) oxide in dichloromethane over 3 Å molecular sieves at 50 °C to afford the silver complex **3** in 90% yield. Subsequent transmetallation of **3** with 0.5 equiv of $[Rh(cod)Cl]_2$ (cod = 1,5-cis,cis-cyclooctadiene) in dichloromethane afforded the desired Rh complex **1o** in 75% yield. The formation of **1o** was evidenced by the characteristic ^{1}H NMR signals observed at 5.0 and 3.4 ppm, corresponding to the olefinic protons of the Rh-coordinated cyclooctadiene ligand, and by the doublet observed at 183 ppm in the ^{13}C NMR spectrum which was assigned as the Rh-coordinated carbenoid nucleus ($CDCl_3$).[18,15a]

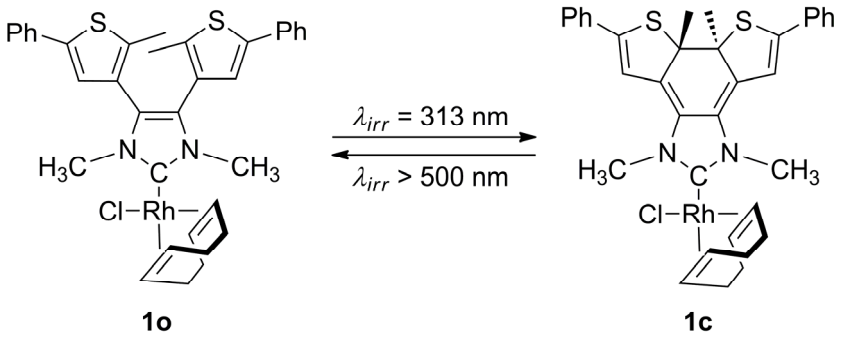

Figure 5.1: Reversible photocyclization of complex **1**.

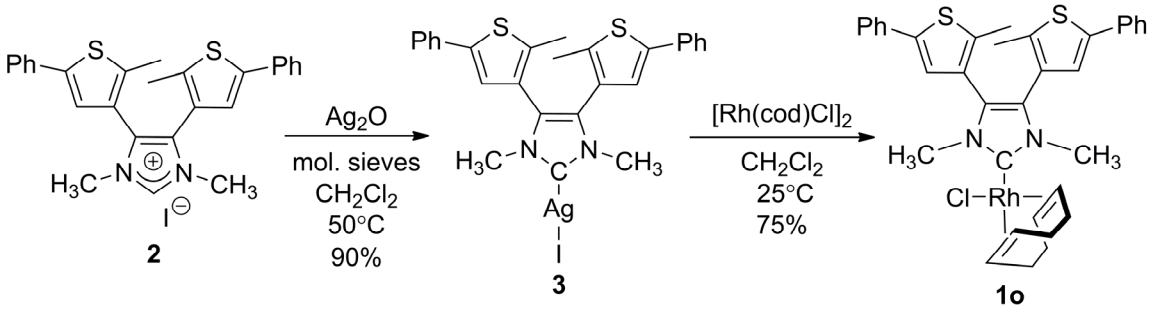

Figure 5.2: Synthesis of photochromic complex **1**.

The UV-vis profile of **1o** in cyclohexane or benzene featured an intense absorbance centered at 285 nm corresponding to the $n \rightarrow \pi^*$ and $\pi \rightarrow \pi^*$ transitions of the N-heterocycle and phenylthiophene systems, respectively. Upon UV irradiation (λ_{irr} = 313 nm), the pale yellow solution of **1o** underwent a color change to bright blue, concomitant with a decrease in the intensity of the absorption band centered at 285 nm and the appearance of new bands at 391 and 630 nm (Figure 5.3a). The development of the lower energy bands upon UV irradiation was consistent with an increase in π-conjugation and the formation of the ring-closed isomer **1c**. After 2 min of UV exposure, the spectroscopic changes reached a steady state, reflecting a 62% conversion of **1o** to its ring-closed isomer **1c**.[19] When the UV exposed solution was subsequently irradiated with visible light (λ_{irr} > 500 nm), the low energy absorption bands were attenuated and, after 1

min of irradiation, the UV-vis spectrum of **1o** was restored (98% conversion) (Figure 5.3b). The presence of an isosbestic point at 311 nm in the data for both the forward and reverse reactions indicated that the cyclization/cycloreversion process occurred without significant side reactions.

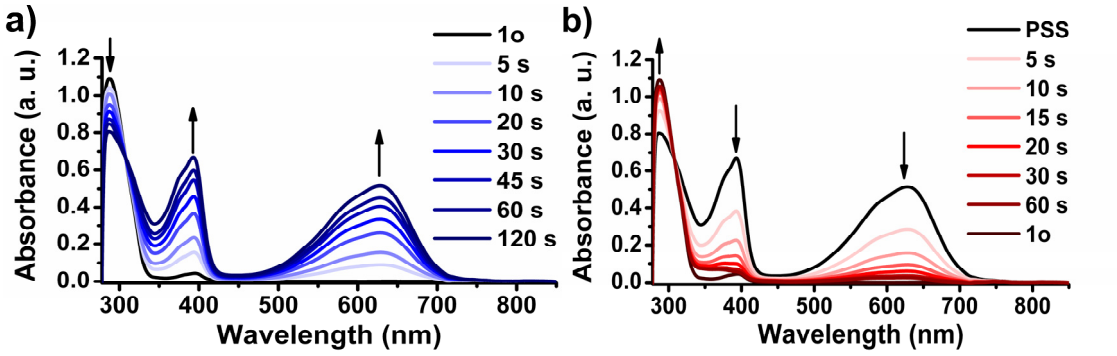

Figure 5.3: (a) UV-vis spectral changes of **1o** in C_6H_6 ($[\mathbf{1o}]_0 = 3.3 \times 10^{-5}$ M) upon UV irradiation (λ_{irr} = 313 nm). (b) UV-vis spectrum of **1o** in C_6H_6, the spectrum of the photostationary state (PSS) that was reached after UV irradiation of **1o** for 120 s, and the spectral changes of the PSS upon exposure to visible light (λ_{irr} > 500 nm). The arrows indicate the evolution of the spectral changes over time.

The photocyclization of **1o** was further confirmed by NMR spectroscopy. After UV irradiation of **1o** in cyclohexane[20] or benzene for 2 h ($[\mathbf{1o}]_0 = 1 \times 10^{-3}$ M), the solvent was removed under reduced pressure and the resulting blue solid was redissolved in $CDCl_3$. Subsequent ^{1}H NMR spectroscopic analysis revealed that the signals assigned to the thiophene protons shifted upfield from δ 6.9 ppm to 6.5 ppm ($CDCl_3$), indicative of the loss of aromaticity upon photocyclization to **1c**. Integration of these signals revealed that 73% of **1o** converted to **1c** in benzene. Moreover, a slight downfield shift of the signal assigned to the protons of the cyclooctadiene olefin in the position trans to the NHC ligand was observed from 5.5 ppm to 5.6 ppm ($CDCl_3$; see Figures A20-21; Appendix E), which was indicative of a decrease in the electron donating ability of **1c**

compared with **1o**.[15a] Exposure of the UV treated solution to ambient light for 2 h reversed the aforementioned chemical shifts (>95% conversion), which suggested to us that **1c** underwent complete cycloreversion to regenerate **1o**. The ^{13}C NMR spectrum provided additional evidence for the photocyclization, as a new signal was observed at 68 ppm (C_6D_6), which was assigned to the sp^3 carbon nuclei adjacent to the sulfur atoms in the newly formed dihydrothiophene rings in **1c**. Furthermore, a shift in the ^{13}C NMR resonance corresponding to the carbenic carbon from 183 ppm to 211 ppm (C_6D_6) was observed upon UV irradiation. The observed shift further underscored the change in electron density at the carbenic carbon upon photocyclization, and was consistent with disrupting the endocyclic double bond in the NHC backbone of **1o** to form **1c** (Figures A22-A23, Appendix E).[21]

Having demonstrated that **1o** underwent the photocyclization in a reversible manner and with high fidelity, subsequent efforts were shifted toward utilizing the photochromic Rh complex in catalytic reactions. Attention was initially focused on the hydroboration of olefins and alkynes[22] since these reactions are widely utilized in organic synthesis, often catalyzed by Rh(I) species,[23] and sensitive to minute changes in electron density at the metal center.[15a] In an initial experiment, treatment of 1-octene (0.10 M) with pinacolborane (0.11 M) in C_6D_6 in the presence of **1o** (1 mol%) at room temperature resulted in 91% conversion of 1-octene to the corresponding linear hydroboration product after 16 h, as observed by ^1H NMR spectroscopy and gas chromatography (GC) (Figure 5.4). To determine if exposure to UV irradiation would affect the hydroboration reaction, a freshly prepared solution of **1o** in C_6H_6 ($[\mathbf{1o}]_0 = 1 \times 10^{-3}$ M) was divided in half and placed in two separate quartz cuvettes, both of which were then sealed with Teflon-lined septum caps. The solution in one of the cuvettes was then subjected to UV irradiation (λ_{irr} = 313 nm) for 2 h while the other cuvette was kept in ambient light over the same period

of time. Mesitylene (0.10 M) was subsequently added as an internal standard followed by 1-octene (0.10 M) and pinacolborane (0.11 M) to each reaction vessel separately. Aliquots were then periodically removed from each reaction mixture, diluted with wet THF to quench the reaction and analyzed by GC. Each reaction was performed in triplicate.

Inspection of the data recorded from the aforementioned experiments revealed that the reaction in ambient light proceeded with a second order rate constant, k_{vis}, of 1.9 ± 0.5 × 10^{-3} $mol^{-1} \cdot s^{-1}$.[24] In contrast, the reaction that had been conducted under UV irradiation was significantly slower, with a rate constant, k_{UV}, of 7.8 ± 2.1 × 10^{-4} $mol^{-1} \cdot s^{-1}$ (Figure 5.4; Table 5.1). The observed 2.4-fold decrease in activity upon irradiation suggested to us that the photocyclized catalyst **1c** was less active for facilitating the hydroboration reaction than the ring-open isomer **1o**.

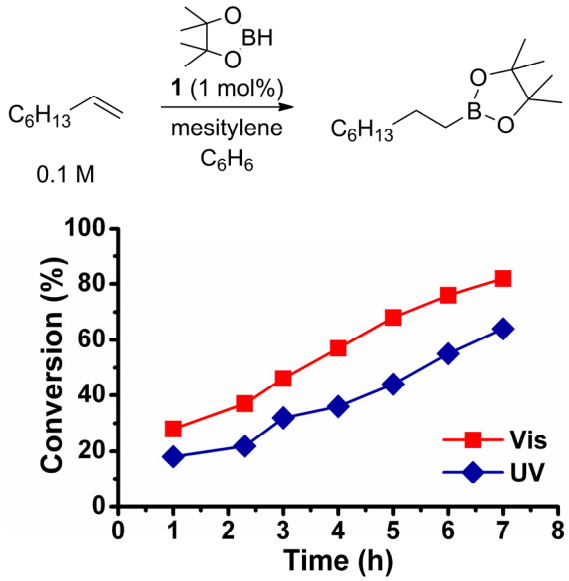

Figure 5.4: Plots of the percent conversion versus time for the hydroboration of 1-octene with pinacolborane catalyzed by **1** in C_6H_6. The reactions were monitored over time by GC using mesitylene as an internal standard. Two reactions were run concurrently with one vessel kept under ambient light (red squares), and one exposed to UV irradiation (λ_{irr} = 313 nm) for 2 h prior to the addition of substrate (blue diamonds). The UV-treated reaction was kept under UV irradiation for the first 4 h of the reaction and then was kept in the dark.

We subsequently sought to employ the photochromic Rh complex **1** to catalyze the hydroboration of other olefinic substrates. When styrene (0.10 M) and pinacolborane (0.11 M) were added to a solution of **1o** ($[\mathbf{1o}]_0 = 1 \times 10^{-3}$ M) in C_6D_6, the complete loss of the starting material and conversion to the linear (L), branched (B), and E-olefin (E) products[23d,g] in a molar ratio of L:B:E = 0.5 : 1.0 : 0.9 was observed by ^{1}H NMR spectroscopy and GC after 8 h at room temperature (Figure 5.5). Using similar comparative kinetics experiments to those described above for 1-octene, the hydroboration of styrene with pinacolborane proceeded in ambient light with a rate constant, k_{vis}, of 2.3 ± 0.2 × 10^{-3} $mol^{-1}\cdot s^{-1}$, while the catalytic activity was significantly attenuated in UV light (k_{UV} = 2.5 ± 0.6 × 10^{-4} $mol^{-1}\cdot s^{-1}$; k_{vis}/k_{UV} = 9.3) (Figure 5.5a; Table

5.1). The disparity in the rates enabled photoswitching of the catalytic activity over the course of a single reaction. After exposure to ambient light for 1 h (k_{vis} = 1.8 ± 0.9 × 10^{-3} $mol^{-1}·s^{-1}$), a freshly prepared solution identical to that described above was exposed to UV irradiation for a further 4 h, during which the reaction rate was significantly attenuated (kUV = 2.3 ± 0.5 × 10^{-4} mol-1·s^{-1}; k_{vis}/k_{UV} = 7.8). Subsequent exposure to visible light to facilitate the cycloreversion of the catalyst restored the catalytic activity (k_{vis} = 1.6 ± 0.5 × 10^{-3} $mol^{-1}·s^{-1}$) (Figure 5.5b). Collectively, these results suggested to us that the reversible photocyclization within the NHC ligand of **1** altered the propensity of the Rh center to facilitate the hydroboration reaction, and enabled remote tuning of its catalytic activity.

To verify that the rate attenuation observed under UV irradiation was a result of the photoinduced change in the structure of the catalyst, a series of control experiments was performed. When the hydroboration reaction between styrene and pinacolborane was conducted in the absence of catalyst **1**, negligible conversion was observed under ambient light (k_{vis}, = 5.0 × 10^{-6} $mol^{-1}·s^{-1}$) or UV irradiation (k_{UV}, = 5.0 × 10^{-6} $mol^{-1}·s^{-1}$), indicating that the latter alone was not responsible for the decrease in activity (Figure 5.9; Table 5.1). Moreover, a significant reduction in activity was not observed under UV irradiation compared with ambient light (k_{vis}, = 6.0 × 10^{-2} $mol^{-1}·s^{-1}$; k_{UV}, = 1.9 × 10^{-1} $mol^{-1}·s^{-1}$; k_{vis}/k_{UV} = 0.3) (Figure 5.10; Table 5.1) when the reaction was performed using chloro(η^4-1,5-cyclooctadiene)(1-methyl-3-methylimidazole-2-ylidene)rhodium(I), a structurally related NHC-Rh(I) complex which lacks a photochromic dithienylethene moiety, as the catalyst. Collectively, the results of these control experiments suggested to us that the decrease in rate upon UV exposure was unique to complex **1** and was due to the photocyclization of **1o** to **1c**.

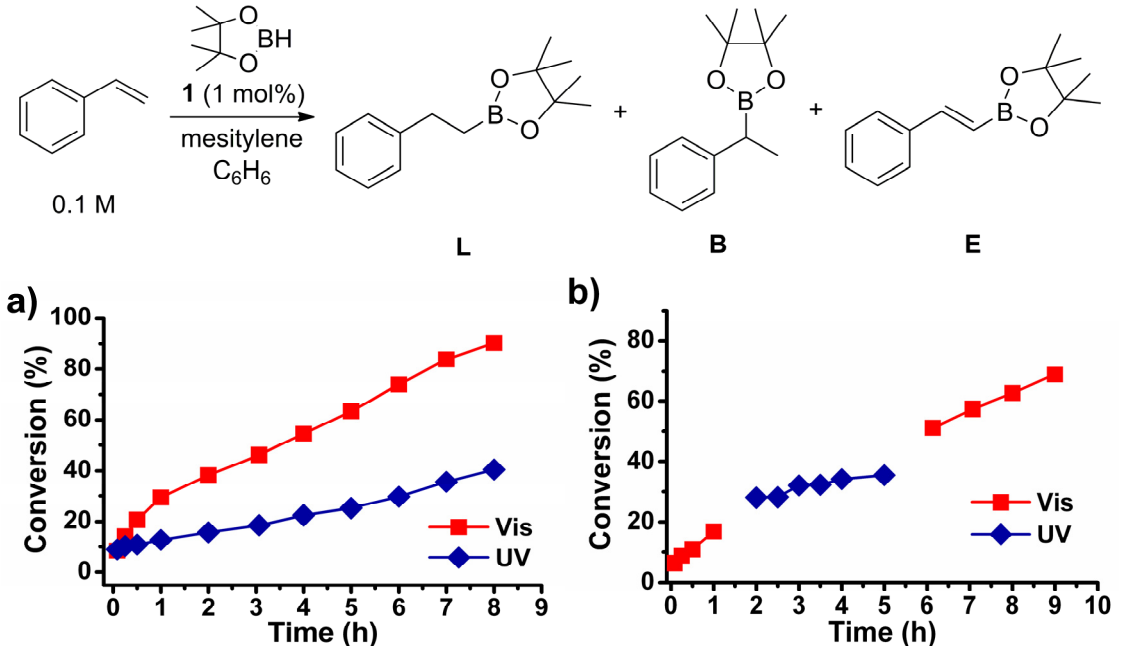

Figure 5.5: Plots of the percent conversion versus time for the hydroboration of styrene with pinacolborane catalyzed by **1** in C_6H_6. The reactions were monitored over time by GC using mesitylene as an internal standard. (a) Two reactions were run concurrently with one vessel kept under ambient light (red squares), and one exposed to UV irradiation (λ_{irr} = 313 nm) (blue diamonds) for 2 h prior to the addition of substrate. The reaction vessel exposed to UV was irradiated for the first 4 h of the reaction and then was kept in the dark. (b) A single reaction was allowed to proceed in ambient light for 1 h (red squares), subjected to UV irradiation (blue diamonds) (λ_{irr} = 313 nm) for 2 h and then kept in the dark for a further 2 h prior to exposure to visible light (λ_{irr} > 500 nm) (red squares).

In an effort to expand the substrate scope of the photo-controlled hydroboration reaction and to determine if the electronic properties of the substrate would affect the rate disparity, attention next turned toward substituted styrene derivatives. The hydroboration of 4-chlorostyrene with pinacolborane was significantly faster in ambient light (k_{vis} = 8.4 ± 4.0 × 10^{-4} $mol^{-1}·s^{-1}$) than under UV irradiation (k_{UV} = 1.3 ± 0.8 × 10^{-4} $mol^{-1}·s^{-1}$; k_{vis}/k_{UV} = 6.7), as was the reaction between 4-methoxystyrene and pinacolborane (k_{vis} = 5.7 ± 3.0 × 10^{-4} $mol^{-1}·s^{-1}$; k_{UV} = 7.4 ± 1.7 × 10^{-5} $mol^{-1}·s^{-1}$; k_{vis}/k_{UV} = 7.7) (see Figures 5.11-5.12; Table

5.1). The observed decreases in activity upon UV exposure were in good agreement with the aforementioned results observed with styrene and suggested to us that the method is not limited by the electronic properties of the olefin starting material. Moreover, the aforementioned results indicated that the rate-determining step of the hydroboration mechanism was not significantly affected by the electronic character of the substrate (see below).

Since we previously demonstrated that the rates of Rh(I) promoted alkyne hydroborations were sensitive to the electron donating character of the NHC ligated to the metal center,[15a] subsequent efforts focused on alkynes. The hydroboration of phenylacetylene with pinacolborane with **1o** in C_6H_6 primarily resulted in the formation of poly(phenylacetylene)[25] (> 80%) rather than the desired olefin hydroboration products. Alternatively, when *t*-butylacetylene (0.10 M) was treated with pinacolborane (0.11 M) in the presence of **1o** ($[\mathbf{1o}]_0 = 1 \times 10^{-3}$ M), a 67% conversion to the *E*-olefin product was observed after 13 h, as evidenced by ^{1}H NMR spectroscopic analysis of the crude reaction mixture (Figure 5.6). To explore the effect of UV irradiation on the reaction outcome, a comparative kinetics experiment analogous to those described above for the olefinic substrates was performed. Under ambient light the hydroboration of *t*-butylacetylene with pinacolborane proceeded with a rate constant k_{vis}, of $3.3 \pm 0.6 \times 10^{-4}$ $mol^{-1} \cdot s^{-1}$, while the reaction exposed to UV proceeded more slowly ($k_{vis} = 9.0 \pm 1.0 \times 10^{-5}$ $mol^{-1} \cdot s^{-1}$; $k_{UV}/k_{vis} = 3.7$; Figure 5.6; Table 5.1). These results were consistent with the disparate rates observed with the analogous olefins, and suggested to us that the alkyne hydroboration proceeded via a similar mechanism (see below). Furthermore, the aforementioned results demonstrated that the photocyclization of **1o** to **1c** is an effective method for modulating hydroboration rates for a wide variety of substrates.

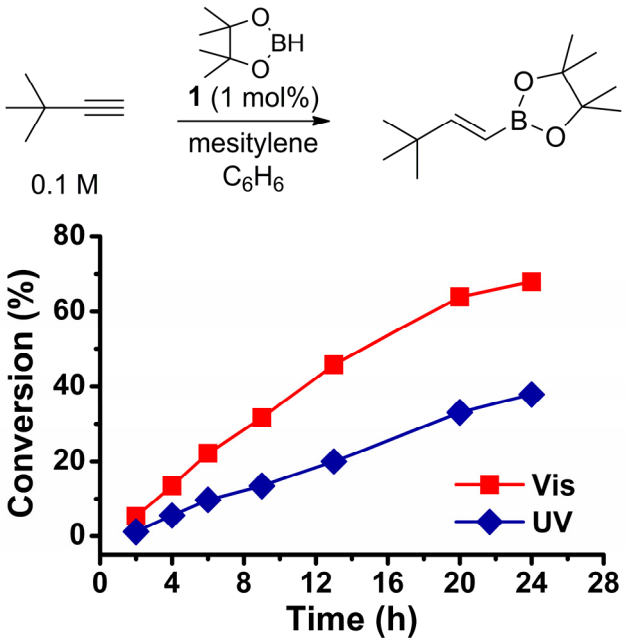

Figure 5.6: Plots of the percent conversion versus time for the hydroboration of *t*-butylacetyelene with pinacolborane catalyzed by **1** in C_6H_6. The reactions were monitored over time by GC using mesitylene as an internal standard. Two reactions were run concurrently with one vessel exposed to UV irradiation (λ_{irr} = 313 nm) for 2 h prior to the addition of substrate and throughout the reaction (blue diamonds) and one was kept under ambient light (red squares).

Substrate[a]	**Catalyst**	k_{vis} ($mol^{-1} \cdot s^{-1}$)	k_{UV} ($mol^{-1} \cdot s^{-1}$)	k_{UV}/k_{vis}
1-octene	**1**	$1.9 \pm 0.5 \times 10^{-3}$	$7.8 \pm 2.1 \times 10^{-4}$	2.4
styrene	**1**	$2.3 \pm 0.2 \times 10^{-3}$	$2.5 \pm 0.6 \times 10^{-4}$	9.3
	---[b]	5.0×10^{-6}	5.0×10^{-6}	1
	(IMe)Rh(cod)Cl[c]	1.9×10^{-1}	6.0×10^{-2}	0.3
4-chlorostyrene	**1**	$8.4 \pm 4.0 \times 10^{-4}$	$1.3 \pm 0.8 \times 10^{-4}$	6.7
4-methoxystyrene	**1**	$5.7 \pm 3.0 \times 10^{-4}$	$7.4 \pm 1.7 \times 10^{-5}$	7.7
t-butylacetylene	**1**	$3.3 \pm 0.6 \times 10^{-4}$	$9.0 \pm 1.0 \times 10^{-5}$	3.7

Table 5.1: Summary of the 2nd order rate constants measured for various hydroboration reactions catalyzed by **1**. [a] Reactions were performed with 0.1 M substrate and 0.11 M pinacolborane in benzene with 1 mol% catalyst. [b] Reaction was performed without a catalyst. [c] (IMe)Rh(cod)Cl = chloro(η^4-1,5-cyclooctadiene)(1,3-dimethylimidazol-2-ylidene)rhodium(I).

A proposed catalytic cycle for the hydroboration reactions catalyzed by **1** is given in Figure 5.7. Since the overall hydroboration rate was attenuated upon UV irradiation to form catalyst **1c** (which features a less electron donating NHC ligand), the rate-determining step must be inhibited by the presence of a more electron deficient Rh center. Of the four general steps of the hydroboration cycle, the reductive elimination step should be slower in the presence of a less donating ligand. Furthermore, the rate of the reductive elimination would not be significantly affected by the electronic properties of the olefin substituents, which is supported by the observation that the substituted styrene derivatives gave similar rate disparities as styrene. Collectively and consistent with previous reports,[26] the results described above suggest to us that the rate-determining step of the catalytic cycle is the reductive elimination. The decrease in the hydroboration rate observed upon UV irradiation reflects that the photocyclization of **1o** to **1c** decreased

the donating ability of the NHC ligand in **1**, and thus the propensity of the complex to undergo reductive elimination. Given that *t*-butylacetylene exhibited a similar decrease in rate upon UV irradiation, a similar mechanism may be operative for the hydroboration of alkynes substrates.

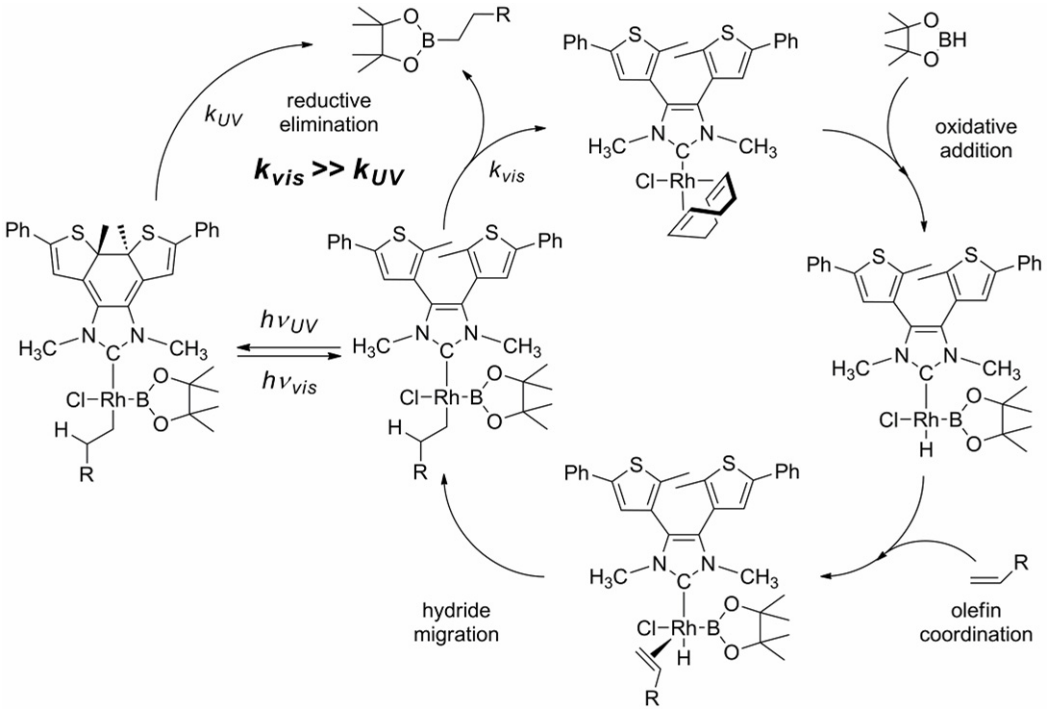

Figure 5.7: Proposed catalytic cycle for the photoswitchable hydroboration catalyzed by **1**. [a] The photocyclized complex may be generated during any step of the catalytic cycle, however for clarity it is only shown at the reductive elimination step. [b] The alkyne substrate is expected to coordinate to the Rh center and undergo the subsequent steps in a manner analogous to the olefins, but is not shown for clarity.

5.3 CONCLUSIONS

In summary, we have developed a photochromic NHC-Rh(I) complex and demonstrated that the UV-induced electrocyclic ring-closing reaction within the NHC ligand decreased the electron donating ability of the NHC. The photo-induced ring-closing was reversed upon exposure to visible light, resulting in the first Rh complex that

was switched with high fidelity between two electronic states via a remote light stimulus. While the open form of the catalyst (**1o**) efficiently facilitated the hydroboration of both olefins and alkynes, the catalytic activity was significantly attenuated upon UV irradiation to the ring-closed isomer (**1c**). Remarkably, the hydroboration of styrene was reduced by nearly an order of magnitude upon UV irradiation, which was sufficient to enable remote photomodulation of the catalytic activity over the course of the reaction, and demonstrated the first example of using photo-induced changes in electronic structure to modulate the activity of a transition metal catalyst. The attenuated reactivity of **1c** compared with **1o** may be attributed to the decrease in donicity of the NHC upon photocyclization, which inhibited the rate-determining reductive elimination step of the hydroboration mechanism.

Given that the outcomes of a wide variety of transformations catalyzed by NHC-supported metal complexes are dependent on the electron donating properties of the NHC ligand,[15] the method described above is expected to be extended and generalized to hydrosilylations,[27] hydrogenations, cross-couplings, metathesis and other reactions. Furthermore, in addition to expanding the scope of photoswitchable catalysis, this system offers new opportunities in tandem homogeneous catalysis.[28] While the photocyclized catalyst **1c** is less electron rich and relatively ineffective for hydroboration reactions, the complex is structurally robust and remains soluble, characteristics which may enable it to facilitate reactions that are orthogonal to the hydroboration chemistry promoted by its counterpart **1o**. Such an ability to alter catalytic activity by remotely photomodulating the electronic state of the catalyst is expected to facilitate multi-step synthesis of complex small- and macromolecules.

5.4 EXPERIMENTAL

5.4.1 Materials and Methods

Unless otherwise specified, reagents were purchased from commercial sources and used without further purification. Styrene, 4-chlorostyrene, 4-methoxystyrene, 1-octene, phenylacetylene, *t*-butylacetylene were dried over 4Å molecular sieves and bubbled with dry N_2 before use. All syntheses were performed under ambient conditions unless specified otherwise. Solvents were dried and degassed using a Vacuum Atmospheres Company solvent purification system. ^{1}H and ^{13}C NMR spectra were recorded using a Varian 400 MHz spectrometer. Chemical shifts δ (in ppm) are referenced to tetramethylsilane using the residual solvent as an internal standard. For ^{1}H NMR: $CDCl_3$, 7.24 ppm; C_6D_6, 7.15 ppm. For ^{13}C NMR: $CDCl_3$, 77.0 ppm; C_6D_6, 128.0 ppm. Coupling constants (*J*) are expressed in hertz (Hz). Melting points were obtained with an Opti-Melt Automated Melting Point System MPA100 apparatus and are uncorrected. Mass spectra (MS, ESI or CI) were obtained with a VG analytical ZAB2-E or a Karatos MS9 instrument and are reported as m/z (relative intensity). UV-vis spectra were acquired using a Perkin-Elmer Lambda 35 UV-vis Spectrometer in 6Q Spectrosil quartz cuvettes (Starna) with 1.0 cm path lengths and 3.0 mL sample solution volumes. Beer's law measurements were performed using 10, 20, 30, and 40 μM sample concentrations. The photochemical reactions were performed in the same quartz cuvettes using 4.0 mL sample solution volumes. The irradiation source for photochemical reactions was a Newport/Oriel 66942 200-500W Hg Arc lamp housing equipped with a 350 W Hg lamp, a Newport 6117 liquid filter, a Newport 71445 electronic safety shutter, and a Newport 71260 filter holder. The source was powered by a Newport 669910 power supply and mounted on a Newport XL48 optical rail with a Newport 13950 shielded cuvette holder placed at a distance of 8 cm from the end of the source. The irradiation

wavelength for the photocyclization reactions was obtained using a 313 nm bandpass filter (Andover Corporation). A long-pass edge filter ($\lambda >$ 500 nm) (Andover Corporation) was used to introduce visible light. Elemental analyses were performed on a Thermo Flash 2000 Organic Elemental Analyzer. Gas chromatography (GC) was performed on an Agilent 6850 gas chromatograph (HP-1 column, L = 30 m, I.D. = 0.32 mm) equipped with a flame ionization detector (FID). The GC oven temperature was held at 40 °C for 3 min then increased to 100 °C at 10 °C min^{-1} and finally increased to 250 °C at 20 °C min^{-1}. The internal standard mesitylene was used to aid in measuring reaction conversions.

5.4.2 Syntheses

[Ag{4,5-bis(2′-methyl-5′-phenylthien-3′-yl)-1,3-dimethylimidazolylidene}I] (3): Under an atmosphere of nitrogen in a glove box, a 30 mL vial with a stir bar was charged with 200 mg (0.35 mmol) of 1,2-bis-(2′-methyl-5′-phenylthien-3′-yl)-1,3-dimethylimidazolium iodide **2,**[16] 40 mg (0.17 mmol) of Ag_2O, 3 Å molecular sieves, and 25 mL of CH_2Cl_2. The vial was sealed with a Teflon-lined cap, covered with aluminum foil, removed from the glove box and heated to 50 °C for 16 h. The reaction mixture was filtered through a frit of coarse porosity while hot and the filter cake was washed thoroughly with 250 mL of CH_2Cl_2. The filtrate was concentrated under reduced pressure, the residue was triturated in diethyl ether and 214 mg (90% yield) of the desired product was collected by filtration as a beige powder. mp 124 °C (dec). UV-vis (CH_2Cl_2): λ_{abs} = 291 nm (ε = 20936 dm^3 mol^{-1}). ^{1}H NMR (400 MHz, $CDCl_3$): δ 2.06 (s, 6H), 3.80 (s, 6H), 7.08 (s, 2H), 7.35 (m, br, 6H), 7.49 (m, br, 4H). Characterization of this compound via ^{13}C NMR spectroscopy was not possible due to its poor solubility. HRMS (*m/z*): Calcd.

for $C_{27}H_{24}N_2S_2I^{107}Ag$ $[M\text{-}I]^+$, 547.0432; Found, 547.0436; Calcd. for $C_{27}H_{24}N_2S_2I^{109}Ag$ $[M\text{-}I]^+$, 549.0428; Found, 549.0452.

Chloro(η^4-1,5-cyclooctadiene)(4,5-bis(2′-methyl-5′-phenylthien-3′-yl)-1,3-dimethylimidazolylidene)rhodium(I) (1o): Under an atmosphere of nitrogen in a glove box, a 30 mL vial with a stir bar was charged with 309 mg (0.46 mmol) of Ag complex **2**, 112 mg (0.23 mmol) of $[Rh(cod)Cl]_2$, and 20 mL of CH_2Cl_2. The vial was sealed with a foil-lined cap and stirred at room temperature for 1 h, during which a white precipitate formed. The vial was removed from the glove box, after which the reaction mixture was passed through a 0.2 μm PTFE filter and the filtrate was concentrated under reduced pressure at room temperature. The resulting yellow residue was purified by column chromatography on silica gel eluting with a 3:1 v/v mixture of hexanes and acetone to afford 237 mg (75% yield) of the desired product. mp 151 °C (dec). UV-vis (C_6H_6): λ_{abs} = 284 nm (ε = 33314 dm^3 mol^{-1}), λ_{abs} = 394 nm (ε = 1580 dm^3 mol^{-1}). ^{1}H NMR (400 MHz, $CDCl_3$): δ 1.98 (d, *J* = 8.8, 8H), 2.43 (m, *J* = 12 4H), 3.41 (s, 2H), 4.01 (s, 6H), 5.05 (s, 2H), 7.03 (s, 2H), 7.25 (t, *J* = 8, 2H), 7.34 (t, *J* = 8, 4H), 7.49 (d, *J* = 8, 4H). ^{13}C NMR (100 MHz, $CDCl_3$) δ 14.1, 28.9, 30.8, 32.9, 36.2, 67.8, 68.0, 98.6, 98.7, 123.8, 125.4, 125.8, 127.4, 127.6, 128.9, 133.6, 141.4, 182.9, 183.4. HRMS (*m/z*): Calcd. for $C_{35}H_{36}N_2RhS_2$ $[M\text{-}Cl]^+$, 651.16395; Found, 651.13706. Anal. Calcd. for $C_{35}H_{36}ClN_2S_2Rh$: C, 61.18; H, 5.28; N, 4.08. Found: C, 60.78; H, 5.38; N, 3.75.

5.4.3 Additional Spectral Data

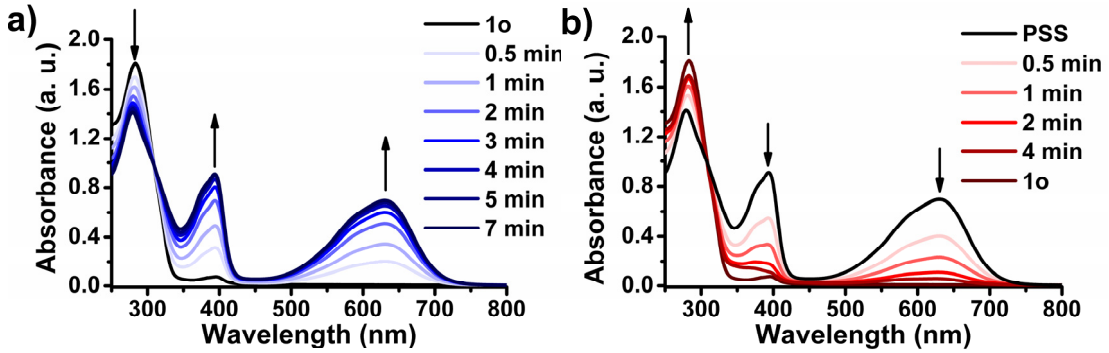

Figure 5.8. (a) UV-vis spectral changes of **1o** in cyclohexane ($[\mathbf{1o}]_0 = 3.3 \times 10^{-5}$ M) upon UV irradiation (λ_{irr} = 313 nm). (b) UV-vis spectrum in cyclohexane of **1o**, the photostationary state (PSS) reached after UV irradiation of **1o** for 120 s, and the spectral changes of the PSS upon visible irradiation (λ_{irr} > 500 nm). The arrows indicate the evolution of the spectral changes over time.

5.4.3 Procedures for Catalysis Experiments

Hydroboration of 1-octene with pinacolborane: Under an atmosphere of N_2 in a glove box, a vial was charged with 5.5 mg (0.008 mmol) of **1o** and 4 mL of C_6H_6. A 2 mL portion of the catalyst solution was added to each of two quartz cuvettes equipped with magnetic stir bars and 2 mL of C_6H_6 was added to each cuvette. The cuvettes were then sealed with Teflon-lined septum caps and removed from the glove box. The solution in one cuvette was irradiated with UV light (λ_{irr} = 313 nm) with stirring for 2 h while the solution in the second cuvette was stirred under ambient light. After 2 h, 56 μL (0.4 mmol) of mesitylene (internal standard) was added to each cuvette via a N_2 purged syringe, followed by 62 μL (0.4 mmol) of 1-octene and 64 μL (0.44 mmol) of pinacolborane. The UV-treated reaction vessel was kept under UV irradiation for the first 4 h of the reaction, then was kept in the dark. The second reaction vessel was kept under ambient light throughout the course of the reaction. Aliquots were removed after given amounts of time, diluted with wet methanol to quench the reaction and analyzed by GC.

Hydroboration of styrene with pinacolborane catalyzed by 1: Under an atmosphere of N_2 in a glove box, a vial was charged with 5.5 mg (0.008 mmol) of **1o** and 4 mL of C_6H_6. A 2 mL portion of the catalyst solution was added to each of two quartz cuvettes equipped with magnetic stir bars and 2 mL of C_6H_6 was added to each cuvette. The cuvettes were then sealed with Teflon-lined septum caps and removed from the glove box. The solution in one cuvette was irradiated with UV light (λ_{irr} = 313 nm) with stirring for 2 h while the solution in the second cuvette was stirred under ambient light. After 2 h, 56 μL (0.4 mmol) of mesitylene (internal standard) was added to each cuvette via a N_2 purged syringe, followed by 46 μL (0.4 mmol) of styrene and 64 μL (0.44 mmol) of pinacolborane. The UV-treated reaction vessel was kept under UV irradiation for the first 4 h of the reaction, then was kept in the dark. The second reaction vessel was kept under ambient light throughout the course of the reaction. Aliquots were removed after given amounts of time, diluted with wet THF to quench the reaction and analyzed by GC. For the photoswitching experiments described in the main text, a single reaction was set up as described above in a quartz cuvette and irradiated with UV or visible light after the indicated amounts of time.

Hydroboration of styrene with pinacolborane without catalyst: A set of two reactions with styrene and pinacolborane identical to that described above for the comparative kinetics was set up without catalyst **1**. The reaction mixture in one cuvette was irradiated with UV light (λ_{irr} = 313 nm) while the solution in the second cuvette was stirred under ambient light for 2 h prior to addition of the substrates and throughout the course of the reaction. Negligible activity (6% conversion after 8 h; $k = 5 \times 10^{-6}$ $mol^{-1} \cdot s^{-1}$) was observed under ambient light or UV irradiation.

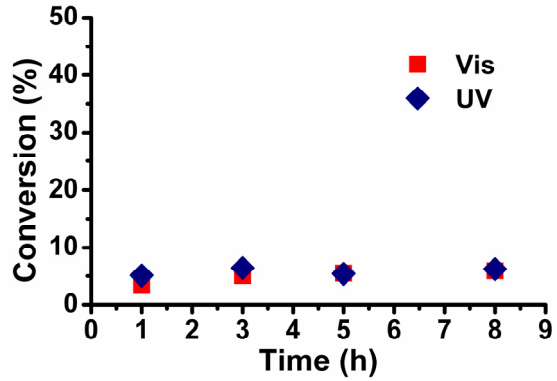

Figure 5.9: Plot of reaction conversion versus time for the hydroboration of styrene with pinacolborane in the absence of **1** in benzene. The reactions were monitored over time by GC using mesitylene as an internal standard. Two reactions were run concurrently with one vessel exposed to UV irradiation (λ_{irr} = 313 nm) for 2 h prior to substrate addition (blue diamonds) and one kept under ambient light (red squares).

Hydroboration of styrene with pinacolborane catalyzed by chloro(η^4-1,5-cyclooctadiene)(1-methyl-3-methylimidazole-2-ylidene)rhodium(I): A set of two reactions with styrene and pinacolborane identical to that described above for the comparative kinetics was set up with 1.38 mg (0.004 mmol) of chloro(η^4-1,5-cyclooctadiene)(1-methyl-3-methylimidazole-2-ylidene)rhodium(I) (IMeRh(cod)Cl) as the catalyst. The reaction mixture in one cuvette was irradiated with UV light (λ_{irr} = 313 nm) while the solution in the second cuvette was stirred under ambient light for 2 h prior to addition of the substrates and throughout the course of the reaction. Similar activities were observed in ambient light (97% conversion after 2 h; $k_{vis} = 0.6 \times 10^{-2}$ mol^{-1}·s^{-1}) and under UV irradiation (99% conversion after 2 h; $k_{UV} = 1.9 \times 10^{-1}$ mol^{-1}·s^{-1}).

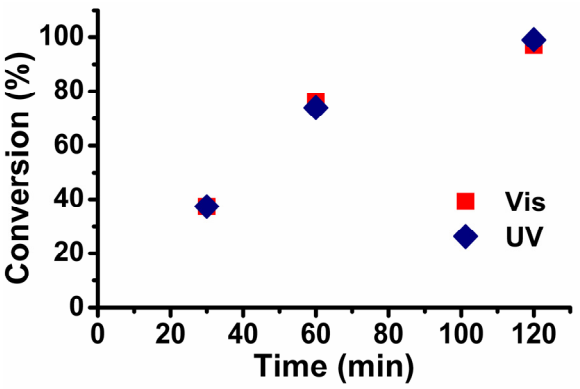

Figure 5.10: Plot of reaction conversion versus time for the hydroboration of styrene with pinacolborane catalyzed by IMeRh(cod)Cl in benzene. The reactions were monitored over time by GC using mesitylene as an internal standard. Two reactions were run concurrently with one vessel exposed to UV irradiation (λ_{irr} = 313 nm) for 2 h prior to substrate addition (blue diamonds) and one kept under ambient light (red squares).

Hydroboration of styrene derivatives with pinacolborane: These reactions were set up as described above for the comparative hydroboration kinetics using 0.004 mmol **1o**, 0.4 mmol 4-chlorostyrene or 4-methoxystyrene, 0.44 mmol of pinacolborane, and 0.4 mmol of mesitylene (internal standard). The reaction mixture in one cuvette was irradiated with UV light (λ_{irr} = 313 nm) while the solution in the second cuvette was stirred under ambient light for 2 h prior to addition of the substrates and throughout the course of the reaction.

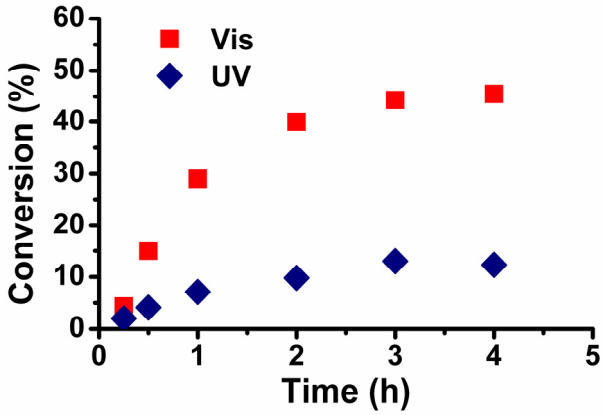

Figure 5.11: Plot of reaction conversion versus time for the hydroboration of 4-methoxystyrene with pinacolborane catalyzed by **1** in benzene. The reactions were monitored over time by GC using mesitylene as an internal standard. Two reactions were run concurrently with one vessel exposed to UV irradiation (λ_{irr} = 313 nm) for 2 h prior to substrate addition (blue diamonds) and one kept under ambient light (red squares).

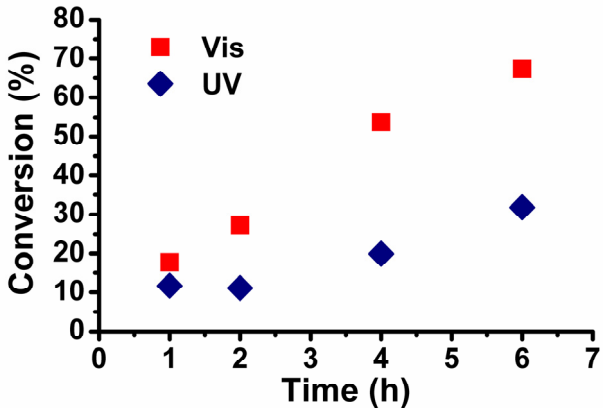

Figure 5.12: Plot of reaction conversion versus time for the hydroboration of 4-chlorostyrene with pinacolborane catalyzed by **1** in benzene. The reactions were monitored over time by GC using mesitylene as an internal standard. Two reactions were run concurrently with one vessel exposed to UV irradiation (λ_{irr} = 313 nm) for 2 h prior to substrate addition (blue diamonds) and one kept under ambient light (red squares).

Hydroboration of *t*-butylacetylene with pinacolborane: The reactions were set up as described above for the comparative hydroboration kinetics with 0.004 mmol **3o**,

0.4 mmol 4 *t*-butylacetyelene, 0.44 mmol of pinacolborane, and 0.4 mmol of mesitylene (internal standard). The reaction mixture in one cuvette was irradiated with UV light (λ_{irr} = 313 nm) while the solution in the second cuvette was stirred under ambient light for 2 h prior to addition of the substrates and throughout the course of the reaction.

5.6 REFERENCES

[1] (a) Lüning, U. *Angew. Chem. Int. Ed.* **2012**, *51*, 8163-8165. (b) Leibfarth, F. A.; Mattson, K. M.; Fors, B. P. Collins, H. A.; Hawker, C. J. *Angew. Chem. Int. Ed.* **2012**, *51*, 2-14.

[2] (a) Allgeier, A. M.; Mirkin, C. A. *Angew. Chem. Int. Ed.* **1998**, *37*, 894-908. (b) Lorkovic, I. M.; Duff, R. R.; Wrighton, M. S. *J. Am. Chem. Soc.* **1995**, *117*, 3617. (c) Gregson, C. K. A.; Gibson, V. C.; Long, N. J.; Marshall, E. L.; Oxford, P. J.; White, A. J. P. *J. Am. Chem. Soc.* **2006**, *128*, 7410. (d) Broderick, E. M.; Guo, N.; Vogel, C. S.; Xu, C.; Sutter, J. R.; Miller, J. T.; Meyer, K.; Mehrkhodavandi, P.; Diaconescu, P. L. *J. Am. Chem. Soc.* **2011**, *133*, 9278. (e) Broderick, E. M.; Guo, N.; Wu, T.; Vogel, C. S.; Xu, C.; Sutter, J.; Miller, J. T.; Meyer, K.; Cantat, T.; Diaconescu, P. L. *Chem. Commun.* **2011**, *47*, 9897.

[3] (a) Blanco, V.; Carlone, A.; Hänni, K. D.; Leigh, D. A.; Lewandowski, B. *Angew. Chem. Int. Ed.* **2012**, *51*, 5166-5169. (b) Yoon, H. J.; Junpei, K.; Kim, J.-H.; Mirkin, C. A. *Science* **2010**, *330*, 66-69. (c) Schmittel, M.; De, S.; Pramanik, S. *Angew. Chem. Int. Ed.* **2012**, *51*, 3822-3826. (d) Balof, S. L.; P'Pool, S. J.; Berger, N. J.; Valente,E. J.; Shiller, A. M.; Schanz, H.-J. *Dalton Trans.* **2008**, *42*, 5791-5799. (e) Balof, S. L.; Yu, B.; Lowe, A. B.; Ling, Y.; Zhang, Y.; Schanz, H.-J. *Eur. J. Inorg. Chem.* **2009**, *13*, 1717-1722.

[4] Stoll, R. S.; Hecht, S. *Angew. Chem. Int. Ed.* **2010**, *49*, 5054-5075.

[5] (a) Peters, M. V.; Stoll, R. S.; Kühn, A.; Hecht, S. *Angew. Chem. Int. Ed.* **2008**, *47*, 5968-5972. (b) Stoll, R. S.; Peters, M. V.; Kühn, A.; Heiles, S.; Goddard, R.; Bühl, M.; Thiele, C. M.; Hecht, S. *J. Am. Chem. Soc.* **2009**, *131*, 357-367. (c) Stoll, R. S.; Hecht, S. *Org. Lett.* **2009**, *11*, 4790-4793. (d) Ueno, A.; Takahashi, K.; Osa, T. *J. C. S. Chem. Comm.* **1981**, 94-96. (e) Cacciapaglia, R.; Di Stefano, S.; Mandolini, L. *J. Am. Chem. Soc.* **2003**, *125*, 2224-2227. (f) Sugimoto, H.; Kimura, T.; Inoue, S. *J. Am. Chem. Soc.* **1999**, *121*, 2325-2326. (g) Lee, W.-S.; Ueno, A. *Macromol. Rapid. Commun.* **2001**, *22*, 448-450. (h) Keiper, S.; Vyle, J. S. *Angew. Chem. Int. Ed.* **2006**, *45*, 3306-3309. (i) Wang, J.; Feringa, B. L. *Science* **2011**, *331*, 1429-1432. (j) Berryman, O. B.; Sather, A. C.; Lledó, A. Rebek Jr., J. *Angew. Chem. Int. Ed.* **2011**, *50*, 9400-9403. (k) Sud, D.; Norsten, T. B.; Branda, N. R. *Angew. Chem. Int. Ed.* **2005**, *44*, 2019-2021. (l) Wilson, D.; Branda, N. R. *Angew. Chem. Int. Ed.* **2012**, *51*, 5431-5434. (m) Würthner, F.;

Rebek Jr., J. *J. Chem. Soc. Perkin Trans. 2* **1995**, *9*, 1727-1734. (n) Niu, F.; Zhai, J.; Jiang, L.; Song, W.-G. *Chem. Commun.* **2009**, *31*, 4738-4740. (o) Imahori, T.; Yamaguchi, R.; Kurihara, S.*Chem. Eur. J.* **2012**, *18*, 10802-10807.

[6] For selected examples of photo-activated or photo-deactivated organometallic catalysts, see: (a) Ben-Asuly, A.; Aharoni, A.; Diesendruck, C. E.; Vidavsky, Y.; Goldberg, I.; Straub, B. F.; Lemcoff, N. G. *Organometallics* **2009**, *28*, 4652-4655. (b) Liu, G.; Wang, J. *Angew. Chem. Int. Ed.* **2010**, *49*, 4425-4429. (c) Hafner, A.; Muhlengach, A.; van der Schaaf, P. A. *Angew. Chem. Int Ed.* **1997**, *36*, 2121-2124. (d) Keitz, B. K.; Grubbs, R. H. *J. Am. Chem. Soc.* **2009**, *131*, 2038-2039. (e) Wang, D.; Wurst K.; Knolle, W.; Decker, U.; Prager, L.; Naumov, S.; Buchmeiser, M. R. *Angew. Chem. Int. Ed.* **2008**, *47*, 3267-3270.

[7] For examples of photoswitchable organometallic catalysts that use changes in steric properties to alter catalytic reactions, see references 5e, 5f and 5k.

[8] (a) Durr, H.; Bouas-Laurent, H. Eds. *Photochromism: Molecules and Systems;* Elsevier: Amsterdam, The Netherlands, **2003**. (b) Special Issue: "Photochromism: Memories and Switches" (Ed. M. Irie), *Chem Rev.* **2000**, *100*, 1683.

[9] Irie, M. *Chem Rev*. **2000**, *100*, 1685-1716.

[10] For reviews on photochromic metal complexes, see: (a) Akita, M. *Organometallics* **2011**, *30*, 43-51. (b) Kuma, S.; Nishihara, H. *Dalton Trans.* **2008**, 3260-3271. (c) Guerchais, V.; Ordronneau, L.; Bozec, H. L. *Coord. Chem. Rev.* **2010**, *254*, 2533-2545. (d) Ko, C.-C.; Yam, V.-W.-W. *J. Mater. Chem.* **2010**, *20*, 2063-2070.

[11] For examples of tuning the electronic properties of photochromic ligands within transition metal complexes, see: (a) Tanaka, Y.; Ishisaka, T.; Inagaki, A.; Koike, T.; Lapinte, C.; Akita, M. *Chem. Eur. J.* **2010**, *16*, 4762-4776. (b) Uchida, K.; Inagaki, A.; Akita, M, *Organometallics*, **2007**, *26*, 5030-5041. (c) Sud, D.; McDonald, R.; Branda, N. R. *Inorg. Chem.* **2005**, *44*, 5060-5962.

[12] Neilson, B. M.; Lynch, V. M.; Bielawski, C. W. *Angew. Chem. Int. Ed.* **2011**, *50*, 10322-10326.

[13] (a) Yam, V. W.-W.; Lee, J. K.-W.; Ko, C.-C.; Zhu, N. *J. Am. Chem. Soc.* **2009**, *131*, 912-913. (b) Lee, P. H.-M.; Ko, C.-C.; Zhu, N.; Yam, V. W.-W. *J. Am. Chem. Soc.* **2007**, *129*, 6058-6059. (c) Duan, G.; Zhu, N.; Yam, V. W.-W. *Chem. Eur. J.* **2010**, *16*, 13199-13209; (d) Nakashima, T.; Goto, M.; Kawai, S.; Kawai, T. *J. Am. Chem. Soc.* **2008**, *130*, 14570-14575.

[14] For selected reviews on NHCs and their coordination chemistry, see: (a) Hahn, F. E.; Jahnke, M. C. *Angew. Chem. Int. Ed.* **2008**, *47*, 3122-3172. (b) Herrmann, W. A. *Angew. Chem. Int. Ed.* **2002**, *41*, 1290-1309. (c) Bourissou, D.; Guerret, O.; Gabbaï, F. P.; Bertrand, G. *Chem. Rev.* **2000**, *100*, 39-91. (d) Herrmann, W. A.; Köcher, C. *Angew. Chem. Int. Ed. Engl.* **1997**, *36*, 2162-2187. (e) Díez-González,

S.; Marion, N.; Nolan, S. P. *Chem. Rev.* **2009**, *109*, 3612-3676. (f) Dröge, T.; Glorius, F. *Angew. Chem. Int. Ed*. **2010**, *49*, 6940-6952.

[15] For studies on tuning the electron donating properties of NHCs as a means to influence catalytic reactions, see: (a) Khramov, D. M.; Rosen, E. L.; Er, J. A. V.; Vu, P. D.; Lynch, V. M.; Bielawski, C. W. *Tetrahedron*, **2008**, *64*, 6853-6862. (b) Benhamou, L.; Vujkovic, N. V.; César, V.; Gornitzka, H.; Lugan, N.; Lavigne, G. *Organometallics* **2010**, *29*, 2616-2630. (c) Süβner, M.; Plenio, H. *Chem. Commun.* **2005**, *43*, 5417-5419. (d) Sashuk, V.; Peeck, L. H.; Plenio, H. *Chem. Eur. J.* **2010**, *16*, 3983-3993. (e) Moerdyk, J. P.; Bielawski, C. W. *Organometallics* **2011**, *30*, 2278-2284. (f) Fürstner, A.; Alcarazo, M.; Krause, H.; Lehmann, C. W. *J. Am. Chem. Soc.* **2007**, *129,* 12676-12677. (g) O'Brien, C. J.; Kantchev, E. A. B.; Chass, G. A.; Niloufar, H.; Hopkinson, A. C.; Organ, M. G.; Setiadi, D. H.; Tang, T.; Fan, D. *Tetrahedron,* **2005**, 61, 9723-9735. (h) César, V.; Tourneux, J.-C.; Vujkovic, N.; Brousses, R.; Lugan, N.; Lavigne, G. *Chem. Commun.* **2012**, *48*, 2349-2351.

[16] Neilson, B. M.; Bielawksi, C. W. *J. Am. Chem. Soc.* **2012**, *134*, 12693-12699.

[17] For reviews on NHC-Rh(I) catalysts, see: (a) Praetorius, J. M.; Crudden, C. M. *Dalton Trans.* **2008**, 4079-4094. (b) Veige, A. S. *Polyhedron*, **2008**, *27*, 3177-3189. (c) Gil, W.; Trzeciak, A. M. *Coord. Chem. Rev.* **2011**, *255*, 473-483.

[18] (a) Khramov, D. M.; Lynch, V. M.; Bielawski, C. W. *Organometallics* **2007**, *26*, 6042-6049. (b) Herrmann, W. A.; Elison, M.; Fischer, J.; Köcher, C.; Artus, G. R. J. *Chem. Eur. J.* **1996**, *2*, 772-780.

[19] The conversions of the forward and reverse cyclizations were measured using the molar extinction coefficient for the absorbance of **1c** centered at 634 nm (ε = 30193 $dm^3 \cdot mol^{-1}$), as determined from a combination of ^1H NMR and UV-vis spectroscopy.

[20] For spectral data recorded after irradiation of **1o** in cyclohexane, see Appendix E.

[21] The shift in the ^{13}C NMR resonance corresponding to the carbenic carbon from 183 ppm in **1o** to 211 ppm in **1c** was consistent with previously reported values for the analogous saturated and unsaturated Rh-NHC complexes, see Appendix E, reference 18b and: Coleman, A. W.; Hithcock, P. B.; Lappert, M. F.; Maskell, R. K.; Müller, J. H. *J. Organomet. Chem.* **1985**, *296*, 173-196.

[22] For reviews on the hydroboration of olefins and alkynes, see: (a) Burgess, K.; Ohlmeyer, M. J. *Chem. Rev.* **1991**, *91*, 1179-1191. (b) Beletskaya, I.; Pelter, A. *Tetrahedron* **1997**, *53*, 4957-5026. (c) Carroll, A.-M.; O'Sullivan, T. P.; Guiry, P. J. *Adv. Synth. Catal.* **2005**, *347*, 609-631. (d) Crudden, C. M.; Edwards, D. *Eur. J. Org. Chem.* **2003**, *24*, 4695-4712.

[23] For representative examples of Rh(I) catalyzed hydroboration of alkenes and alkynes, see: (a) Männig, D.; Nöth, H. *Angew. Chem. Int. Ed.* **1985**, *24*, 878-879.

(b) Ohmura, T.; Yamamoto, Y.; Miyaura, N. *J. Am. Chem. Soc.* **2000**, *122*, 4990-4991. (c) Pereira, S.; Srebnik, M. *Tet. Lett.* **1996**, *37*, 3283-3286. (d) Pereira, S.; Srebnik, M. *J. Am. Chem. Soc.* **1996**, *118*, 909-910. (d) Crudden, C. M.; Hleba, Y. B.; Chen, A. C. *J. Am. Chem. Soc.* **2004**, *126*, 9200-9201. (f) Grasa, G. A.; Moore, Z.; Martin, K. L.; Stevens, E. D.; Nolan, S. P.; Paquet, V.; Lebel, H. *J. Organomet. Chem.* **2002**, *658*, 126-131. (g) Murata, M.; Watanabe, S.; Masuda, Y. *Tetrahedron Lett.* **1999**, *40*, 2585-2588.

[24] For a detailed description of the kinetic analyses, see Appendix D.

[25] Rh(I) complexes are known to promote polymerization of aryl substituted substrates such as phenylacetylene; see for example: (a) Gil, W.; Lis, T.; Trzeciak, A. M.; Ziółkowski, J. J. *Inorg. Chim. Acta* **2006**, *359*, 2835-2841. (b) Tabata, M.; Yang, W.; Yokota, K. *Polym. J.* **1990**, *22*, 1105-1107. (c) Kishimoto, Y.; Miyatake, T.; Ikariya, T.; Noyori, R. *Macromolecules* **1996**, *29*, 5054-5055. (d) Goldberg, Y.; Alper, H. *J. Chem. Soc. Chem. Commun.* **1994**, 1209-1210.

[26] For mechanistic studies of Rh(I)-mediated hydroborations, see: (a) Evans, D. A.; Fu, G. C.; Anderson, B. A. *J. Am. Chem. Soc.* **1992**, *114*, 6679-6685. (b) Burgess, K.; van der Donk, W. A.; Jarstfer, M. B.; Ohlmeyer, M. J. *J. Am. Chem. Soc.* **1991**, *113*, 6139-6144. (c) Evans, D. A.; Fu, G. C. *J. Org. Chem.* **1990**, *55*, 2280-2282. (d) Musaev, D. G.; Mebel, A. M.; Keiji, M. *J. Am. Chem. Soc.* **1994**, *116*, 10693-10702. (e) Widauer, C.; Grüntzmacher, H.; Ziegler, T. *Organometallics* **2000**, *19*, 2097-2107.

[27] NHC-Rh(I) catalysts including **1o**, **1c**, chloro(η^4-1,5-cyclooctadiene)(1-methyl-3-methylimidazole-2-ylidene)rhodium(I), and chloro(η^4-1,5-cyclooctadiene)(1-methyl-3-methybenzimidazole-2-ylidene)rhodium(I) were found to efficiently promote the hydrosilylation of *t*-butylacetylene with dimethylphenylsilane under UV irradiation (λ_{irr} = 313 nm), but were inactive in the dark or under ambient light. The observed activation was presumably due to UV-promoted dissociation of the cyclooctadiene ligand, which facilitated the rate-determining oxidative addition of the silane and enhanced the overall reaction rate. For a mechanistic study of Rh(I) catalyzed hydrosilylation, see: Sakaki, S.; Sumimoto, M.; Fukuhara, M.; Sugimoto, M.; Fujimoto, H.; Matsuzaki, S. *Organometallics*, **2002**, *21*, 3788-3802.

[28] For reviews on tandem catalysis, see: (a) Fogg, D. E.; dos Santos, E. N. *Coord. Chem Rev.* **2004**, *248*, 2365-2379 (b) Wasilke, J.-C.; Obrey, S. J.; Baker, R. T.; Bazan, G. S. *Chem Rev.* **2005***, 105*, 1001-1020. (c) Shindoh, N.; Takemoto, Y.; Takasu, K. *Chem. Eur. J.* **2009**, *15*, 12168-12179.

DESIGN OF FUNCTIONAL CO-POLYMERS FOR EMULSIFICATION OR STABILIZATION OF IRON OXIDE NANOPARTICLES

Chapter 6: Effect of Adsorbed Amphiphilic Copolymers on the Interfacial Activity of Superparamagnetic Nanoclusters and Emulsification of Oil in Water

6.1 INTRODUCTION

Nanoparticles (NPs) may be used to stabilize Pickering emulsions and foams via adsorption at the interfaces between two liquids.[1-8] While conventional surfactants or polymers are typically used to lower oil/water interfacial tension (γ), Pickering emulsions with micron size droplets are often formed with a relatively small reduction of interfacial tension[9-11]. There have been a number of interesting studies using NPs as well as mixtures of particles and surfactants to effect interfacial surface tension reduction.[5,12-14] Adsorbed NPs with surfactant or homopolymer coatings at oil/water interfaces can lower interfacial tension because the surfactant or polymer segments block contact between the oil and water phases.[10, 15] Despite their importance in many industrial applications including food, cosmetics, pharmaceuticals, and oil recovery, there is limited understanding of how polymer-stabilized NPs adsorb at interfaces and lower γ.[10, 15, 16] Furthermore, while amphiphilic copolymers have been investigated as stabilizers on various inorganic NP cores, the resulting reduction in γ and subsequent increase in surface pressure ($\prod = \gamma_0 - \gamma$) has not been reported to the best of our knowledge.[16] The use of amphiphilic copolymers on the NP surfaces may have the potential to raise the interfacial adsorption of the particles and also reduce γ more effectively than homopolymer coatings.

While aqueous dispersions of NPs with polymer coatings have been widely studied,[17-20] relatively few studies have examined their adsorption at oil/water

interfaces,[16, 21] and particularly, how they reduce γ.[15] The adsorption may be controlled by tuning the concentration and hydrophilicity/hydrophobicity of a low molecular weight or polymeric stabilizer on the NP surface.[4,16,22,23] For example, Zhou et al. formed ~ 80 μm oil droplets using 1 % wt. unmodified iron oxide (IO) NPs, but did not report changes in the interfacial tension.[21] Silica particles stabilized with grafted polymer coatings such as poly(styrenesulfonate) (PSS)[10] and poly(2-(dimethylamino)ethyl methacrylate) (PDMAEMA)[15] produced stable oil/water emulsions. Specifically, silica NPs stabilized with grafted PSS[10] reduced γ by ~5 and 15 mN/m at concentrations of 0.04 and 1 % wt., respectively. Silica particles stabilized with grafted PDMAEMA[15] reduced γ by 38 mN/m at a relatively high NP concentration of 2 % wt.. Iron NPs functionalized with a poly(methacrylic acid)-*b*-(methyl methacrylate)-*b*-(styrenesulfonate) triblock copolymer stabilized oil/water emulsions however the reduction in γ was not reported.[16] Thus, it remains a significant challenge to design sub-100 nm NPs with polymer stabilizers to achieve large reduction of interfacial tension at oil/water interface. Such particles are expected to enhance formation and stabilization of small droplets (~ 10 μm) of oil in water at low NP concentrations (< 0.3 % wt.).

Recently, magnetic IO particles have found utility in biomedical applications[20,24-29] including imaging, therapy, drug delivery, *in vitro* cell separation, as well as in the oil industry for imaging of subsurface reservoirs.[28,30-34] Moreover, magnetic NPs have been adsorbed at an oil/water interface and oscillated with an electromagnetic field to generate acoustic waves[35] which may then be analyzed to determine the oil saturation of a reservoir. By judiciously designing the interfacial properties of stabilizers on the NP surface, magnetic NPs can be effective for stabilizing Pickering emulsions of oil and water.[21,23,4] Additionally, we have shown that nanoclusters composed of 5-10 nm primary particles offer advantages over solid nanospheres for stabilization of emulsions.[37]

Because nanoclusters are porous, they occupy a larger area at the oil/water interface than do nanospheres, and therefore a smaller mass of nanoclusters is required to stabilize an emulsion.

A wide variety of stabilizers may be used during synthesis of nanoclusters to control the size and colloidal stability based on the approach of Massart et al.[38] Magnetic NPs have been stabilized with adsorbed polymeric ligands or surfactants,[39] including polyelectrolytes,[40, 41] block copolymers,[42, 43] poly(acrylic acid)[44, 45] and poly(acrylic acid)-based co-polymers[17,46], biopolymers,[28] or small polar molecules such as citric acid (CA).[16,41] Polyelectrolyte molecules simultaneously provide steric stabilization in addition to electrostatic repulsion, resulting in so-called electrosteric stabilization.[41] For example, Ditsch et al. used random copolymers of acrylic acid, styrenesulfonic acid, and vinylsulfonic acid to stabilize IO nanoclusters of controlled size over a wide range of different pH values and salinities. The attachment of the polymer to the NP surface must not interfere with the inorganic crystal structure and surface properties or it may degrade the saturation magnetization. It is therefore desirable for the polymer coating to provide control over the crystallinity during the NP synthesis.

Herein we report the surface pressure (reduction in interfacial tension) at the dodecane/water interface for a rationally designed series of copolymer-coated superparamagnetic IO nanoclusters as a function of the polymer structure. Both block and random copolymers of poly(acrylic acid) (PAA) and poly(butyl acrylate) (PBA) were synthesized with varying lengths of hydrophilic and hydrophobic blocks and used to stabilize IO nanoclusters. The objective was to demonstrate that NPs with non-covalently adsorbed amphiphilic copolymer stabilizers produce very large reductions in interfacial tension (surface pressures of 27.6 mN/m) at low NP concentrations of only 0.27 % wt.. To our knowledge, significant surface pressures have not been reported at such low

concentrations with homopolymer stabilizers.[10,15] Sub-100 nm IO nanoclusters with shells composed of poly(acrylic acid-*b*-butyl acrylate) (PAA-*b*-PBA) stabilized 10-57 μm oil droplets in water at low NP concentrations (0.27 % wt.) and over a broad range of pH conditions. The high surface pressures resulting from efficient NP adsorption at the oil/water interface and the interactions of the polymer shells with the oil and water phases were found to favor the formation and stabilization of oil/water emulsions with small droplets. Furthermore, the polymers enabled controlled NP synthesis to produce Fe_3O_4 nanoclusters with sizes below 100 nm (determined by DLS) and with less than 20% organic content adsorbed on the particle surface (determined by TGA) in order to maintain high saturation magnetization.

6.2 NP DISPERSIONS IN AQUEOUS MEDIA

The size of nanoclusters may be controlled by synthesis in one step in the presence of the final stabilizer[44,45,47] or multiple steps.[17] The single step method was used to form IO nanoclusters consisting of primary NPs, which were nucleated and grown by co-precipitation of Fe(II) and Fe(III) chlorides under alkaline conditions[47-49] in the presence of PAA-*b*-PBA or PAA-*co*-PBA copolymers. Upon nucleation, the carboxylate groups of the PAA coordinated with the iron, facilitating polymer adsorption and consequently stabilization of both the primary particles and the nanoclusters.[45] The presence of the polymer coating on the IO surface was confirmed by thermogravimetric analysis (TGA), which revealed a loss of 13.0 – 28.2 % wt. of organic material (Table 6.1). As the length of the PBA hydrophobic block increased, the adsorption of polymer on the IO increased as the greater hydrophobicity enhanced the tendency of the polymer to leave water. Given the hydrophobicity of the PBA group, it is likely that block

copolymers formed hemi-micelles on the NP surface, as seen in a previous study, which resulted in adsorption of a larger amount of organic material (28.2 % wt.) on the NPs.[50]

Type of polymer stabilizer	**DLS D50 value** (nm) ± std. dev.	**TGA** (weight % loss)	**Electrophoretic Mobility** [(μ/s)/(V/cm)] ± std. dev.	**Zeta Potential** (mV) ± std. dev.
PAA coated NPs	61 ± 6	14.0 %	-3.03 ± 0.11	-39.7 ± 1.50
PAA_{114}-*b*-PBA_{26} coated NPs	81 ± 2	13.0 %	-4.11 ± 0.25	-55.61 ± 3.33
PAA_{114}-*b*-PBA_{38} coated NPs	82 ± 3	19.5 %	-3.41 ± 0.05	-46.17 ± 0.71
PAA_{114}-*b*-PBA_{67} coated NPs	71 ± 3	28.2 %	-2.99 ± 0.13	-40.55 ± 1.82
PAA_{133}-*co*-PBA_{44} coated NPs	151 ± 3	14.4 %	-3.33 ± 0.11	-45.07 ± 1.54

Table 6.1: Percentage weight loss obtained from TGA and zeta potential measurement of polymer stabilized IO NPs at pH = 8.

The morphologies of PAA-*b*-PBA and PAA-*co*-PBA copolymer coated IO particles were characterized by transmission electron microscopy (TEM), which revealed that small primary particles had aggregated to form nanoclusters (Figure 6.1). The nanoclusters with 60-140 nm diameters were composed of the primary crystals with sizes of 3–10 nm, which occurs commonly with co-precipitation of iron-chloride salts in alkaline media.[47-49,51] Similar morphologies and aggregation behavior were previously reported for PAA-coated IO nanoclusters.[44,45]

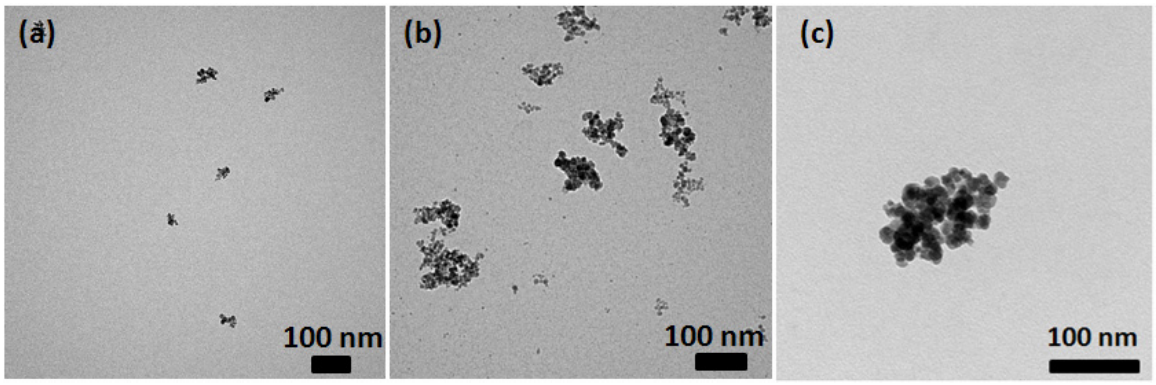

Figure 6.1: TEM images of (a) PAA coated NPs (b) PAA_{114}-*b*-PBA_{26} coated NPs (c) PAA_{133}-*co*-PBA_{64} coated NPs.

The hydrodynamic diameters of the nanoclusters dispersed in water at pH = 8 were investigated by dynamic light scattering (DLS) (Figure 6.2). Average D_{50} values (50% of the clusters by volume are below this diameter) of 70-85 nm were observed for the PAA-*b*-PBA stabilized nanoclusters (Table 6.1). The cluster diameter was modestly smaller (D_{50} = 61 nm) for clusters stabilized with PAA homopolymer. Among the three block copolymers, the cluster size was smallest for the one with the largest hydrophobic block. Relatively narrow size distributions were observed for the nanoclusters stabilized by the block copolymers, exemplifying the controlled process of cluster formation under these conditions. Much larger diameters, 120-160 nm, were observed for the PAA-*co*-PBA coated particles (Figure 6.2) indicating somewhat weaker passivation during growth.

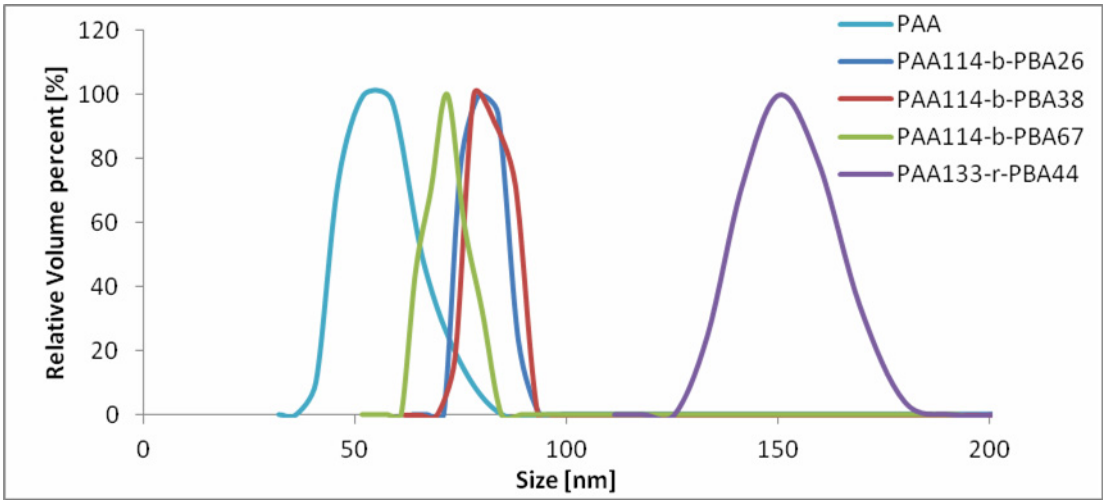

Figure 6.2: Volume fraction based distributions by DLS of PAA_{114}-*b*-PBA_n, PAA-*co*-PBA, and PAA coated IO nanoclusters at pH = 8.

The magnetization curves for the IO nanoclusters with PAA-*b*-PBA or PAA-*co*-PBA copolymer stabilizers revealed superparamagnetic behavior without hysteresis (Figure 6.3). The saturation magnetization values were between 60-86 emu/g Fe, compared to a theoretical magnetization value for magnetite of 92–100 emu/g.[46] The modest decrease in magnetization was influenced by the polymer coordination with the iron cations which attenuates the net charge on the particle surface.[52] The saturation magnetization was highest for pure PAA, and lower for the block copolymers, however it did not decrease as a monotonic function of the amount of PBA. The observed reduction in saturated magnetization is likely a result of the increase in contact areas between IO and polymer with longer PBA blocks, which leads to a larger number of inactive spins on the surface. However, in nanoclusters the polymer coats primarily the outer surface of the cluster and not all of the surface area of the primary particles, which prevents the polymer shell from significantly lowering the magnetization.[46]

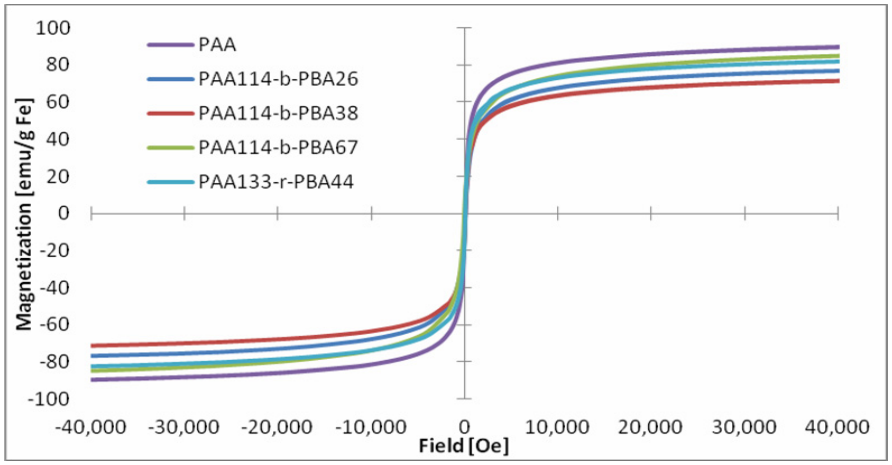

Figure 6.3: SQUID measurement of PAA$_{114}$-*b*-PBA$_n$,, PAA, and PAA-*co*-PBA coated IO nanoclusters at pH = 8.

6.3 Oil-Water Interfacial Tension and NP Adsorption Energy

The interfacial activity of IO nanoclusters with various coatings was studied by measuring the equilibrium interfacial tension γ of a pendant water droplet at the dodecane interface as shown in Table 6.2.

Type of NPs[a]	γ (mN/m)[b]	***a*** (nm)	ΔE (kT)[c]
Citrate coated NP's	no change	50	N/A
PAA coated NPs	no change	31	N/A
PAA$_{114}$-*b*-PBA$_{26}$ coated NPs	25.2	41	-3.9×10^4
PAA$_{114}$-*b*-PBA$_{38}$ coated NPs	28.0	41	-3.5×10^4
PAA$_{114}$-*b*-PBA$_{67}$ coated NPs	30.3	36	-2.4×10^4
PAA$_{133}$-*co*-PBA$_{44}$ coated NPs	28.2	76	-1.2×10^5

Table 6.2: NP size, interfacial tension and adsorption energy of a single particle to the dodecane/water interface. [a] Measured at pH = 8. [b] Determined from equation 1.

The interfacial tension of the bare dodecane/water interface without any stabilizer was measured to be γ_o = 52.8 mN/m. In the case of PAA_{114}-*b*-PBA_{67} polymer, the interfacial tension was 27.85 mN/m at 0.125 % wt. and 26.71 mN/m at 0.25 % wt.. However, for the polymer coated NPs, the total PAA_{114}-*b*-PBA_{67} concentration was 0.076 % wt.. Therefore, it appears that the polymer has a significant effect on the reduction in interfacial tension when associated with the NPs, although some of the polymer may have desorbed from the surface. Particles coated with a conventional ligand such as citrate, or a hydrophilic polymer such as PAA, showed no change in γ, indicating that the particles were too hydrophilic to be interfacially active between oil and water. However when the aqueous phase contained a low concentration (0.27 % wt.) of PAA-*b*-PBA or PAA-*co*-PBA stabilized NPs γ was reduced by nearly one-half. The particles stabilized with the block copolymer with 26 PBA units produced the lowest γ. Upon adding additional PBA segments, γ increased monotonically. The large decrease in γ indicates that the amphiphilic polymer stabilizers caused the IO nanoclusters to adsorb strongly at the oil/water interface, unlike the particles coated with the hydrophilic PAA homopolymer coating. The observed increase in surface pressure $\gamma_o - \gamma$ as a function of the NP concentrations was far more pronounced than in previous studies. The surface pressure was calculated to be 25.2-30.3 mN/m for the PAA-*b*-PBA or PAA-*co*-PBA stabilized NPs, whereas previous studies using poly(styrenesulfonate) (PSS)-grafted silica particles reported much lower surface pressures ($\gamma_o - \gamma$ =15.5 mN/m)[10] with 1 % wt. or required larger NP concentration (2 % wt.) to achieve similar surface pressure ($\gamma_o - \gamma$ = 38 mN/m).[15] The significant decrease in γ observed with such low concentrations of PAA-*b*-PBA or PAA-*co*-PBA stabilized NPs reflected the ability of the amphiphilic polymer segments to efficiently interact with the oil and water on each side of the interface.[10,15]

While the block copolymer-coated particles lowered γ over a range of pH values from pH = 6 to 10, the behavior of the NPs with random copolymer shells at the dodecane/water interface was less robust. At lowered pH (pH = 6) these polymers were not completely soluble at a concentration of 0.27 % wt. and were unable to stabilize emulsions. Similarly at elevated pH (pH = 10) the random copolymers exhibited decreased solubility and were ineffective at stabilizing emulsions, likely because the ionic strength of the basic solution was too high for solvation of the hydrophobic PBA groups. However, at pH = 8, the polymer was fully soluble and at a concentration of 0.27 wt.% the γ measured for PAA_{133}-*co*-PBA_{44} NPs (γ = 28.2 mN/m) was similar to the value for the block copolymer with the closest homopolymer ratio, PAA_{114}-*b*-PBA_{38} (γ = 28.0 mN/m) (Table 6.2).

Having measured the interfacial tension of the series of nanoclusters, efforts were directed towards calculating the adsorption energy ΔE of one nanocluster at the dodecane-water interface to gain a better understanding of the interaction between the particles and the interface. The adsorption energy was determined from the measured decrease in interfacial tension upon addition of NPs, $\gamma - \gamma_o$ for a contact angle of 90° (Table 2) using Equation 6.1,

$$\Delta E = \frac{-(\gamma - \gamma_0)\pi a^2}{\eta} \qquad \text{Eq. 6.1}$$

where a is the particle radius and η is the 2-dimensional packing fraction. Given that the contact angle of the NP was unknown, we assumed a value of 90° based upon the approach of a previous study.[53] In this model, the adsorption energy is a function of the total interfacial area blocked by the NPs. For simplicity, we assumed a close-packed interface where η = 0.91. The resulting ΔE values may be corrected based on the approximated packing fraction, however the corrections are relatively modest.

Given the similar values of $\gamma - \gamma_0$ observed in the various copolymer-stabilized IO systems, we expected that differences in ΔE would result more significantly from the variation in particle radius, a. In all cases, the calculated ΔE values were large, indicating that the NPs adsorbed strongly to the interface and that their adsorption may be expected to be relatively irreversible. For the PAA_{114}-*b*-PBA_{26} stabilized nanoclusters, a value of $\Delta E = -3.9 \times 10^4\ k_BT$ for $a = 41$ nm was calculated, which was consistent with values reported previously for small NPs.[53] For larger nanoclusters stabilized with PAA_{133}-*co*-PBA_{44} where $a = 76$ nm, ΔE increased as expected to reach $\Delta E = -1.2 \times 10^5\ k_BT$ (Table 2). In comparison, Du et al. reported $\Delta E = -5.1\ k_BT$ for a Au NP with an extremely small radius ($a = 2.5$ nm), and $\Delta E = -9 \times 10^5\ k_BT$ for a large polystyrene sphere with $a = 1.05$ μm.[53] The experiments were performed with a constant concentration in the aqueous phase. However, this concentration is maintained only if only a small fraction of the NPs partitioned to the oil phase.

As the PBA length increased, it is possible that NPs may have been lost to the oil phase with the increase in lipophilicity. Future studies would be required to attempt to understand the detailed conformation of the various polymers on the NP surfaces and at the oil-water interface. Finally the results may be complicated by any desorption of polymer from the NP surface to the oil-water interface. One way to ensure that any desorption is prevented in the future would be to cross-link the polymer shells on the NPs surfaces, and studies of such cross-linked polymer shells are currently underway.[19] However, since no particle aggregation was observed, as would be expected if the polymer desorbed from the surface, we believe it is unlikely that significant polymer desorption occurred. Furthermore, since the total surface area between the NPs and water within one pendant drop was 6800 times larger than surface area between water and oil in the pendant drop, any desorbed polymer would likely diffuse into the water phase rather

than to the oil-water interface, and would not result in any additional interfacial tension lowering.

6.4 Properties of the NP-Stabilized Emulsions

In order to determine the partition coefficient of the polymer-coated IO NPs between the water and dodecane phases, experiments were performed with equal volumes of 0.27 % wt. aqueous solutions of IO particles and dodecane by gentle agitation, to avoid emulsification. For all polymer coatings in this study, the NPs favored the lower aqueous phase, to form a transparent colored dispersion, and the organic phase was colorless. When probe sonication was used, emulsions of dodecane and water (1:1 volume ratio) were formed with NP concentrations of only 0.27% Fe_3O_4 (w/v) in water for PAA-*b*-PBA or PAA-*co*-PBA-coated nanoclusters at pH = 8. Photographs of the colors and textures of the biphasic samples taken 24 hrs after probe sonication (Figure 6.4) indicated that the amphiphilic copolymer-coated particles formed a stable emulsion above an excess water phase. The aqueous phases below the emulsion phase were always colored by the presence of NPs indicating that an oil/water emulsion phase was present above the excess aqueous phase, which grew as the oil droplets creamed. According to the Bancroft rule, the continuous phase of the emulsions will be the phase favored by the NPs between bulk oil and water phases at equilibrium, without any shear or droplet formation. Thus, the presence of oil-in-water emulsions was consistent with the Bancroft rule.[54]

In contrast, when mixtures of dodecane and aqueous dispersions of PAA-coated nanoclusters were subjected to probe sonication, emulsification of the entire volume of the oil and water phases occurred, but the emulsion separated completely into oil and water phases after several hours and the NPs remained in the lower aqueous phase (Figure 6.4a). The lack of emulsion stability was in good agreement with the fact that γ

was not lowered for these hydrophilic particles (Table 6.2), as they partitioned too strongly to the aqueous phase.

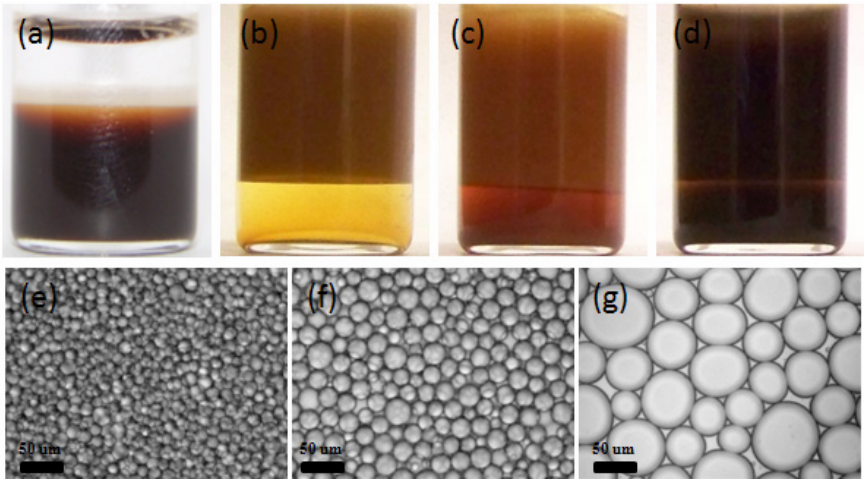

Figure 6.4: Photographs and microscopy images of oil-in-water emulsions formed between dodecane and aqueous dispersions of (a) PAA coated NPs, (b) (e) PAA_{114}-b-PBA_{26} coated NPs, (c) (f) PAA_{114}-b-PBA_{38} coated NPs, and (d) (g) PAA_{114}-b-PBA_{67} coated NPs. Images were acquired after 1 day at pH = 8 with equal volumes of oil and water phases.

NP Coating	**Average emulsion droplet size** (μm)		
	pH = 6	pH = 8	pH = 10
PAA_{114}-*b*-PBA_{26}	12.1	14.7	12.9
PAA_{114}-*b*-PBA_{38}	19.7	22.7	16.6
PAA_{114}-*b*-PBA_{67}	37.7	62.8	41.3
PAA_{133}-*co*-PBA_{44}	n/a	12.9	n/a

Table 6.3: Average emulsion droplet size by image analysis.

Analysis of microscopy images revealed that the emulsions stabilized by PAA-*b*-PBA-coated nanoclusters consisted of oil droplets ranging from 12.9 to 62.8 μm in diameter (Figure 6.4, Table 6.3). These emulsions only partially phase separated after 1 day leaving an excess water phase. For the three block copolymer shells, the intensity of

the color of the excess aqueous phase increased with increasing PBA block length, suggesting that more particles remained in the aqueous layer with increasing PBA content. The concentration of NPs in the excess water phase and the fraction of the total NPs in the upper emulsion phase (excluding the bottom excess water phase) are given in Table 6.4. The smallest oil droplets (14.7 μm) were formed with PAA_{114}-*b*-PBA_{26} stabilized nanoclusters above a light brown excess water phase, with 91% of the NPs in the emulsion phase. As the PBA block length increased, the droplet size increased and reached 22.7 μm for PAA_{114}-*b*-PBA_{38} with 76% of the NPs in the emulsion phase. The somewhat larger droplet size is consistent with the greater water resolution and lower NP concentration in the emulsion phase. In the emulsions stabilized by PAA_{114}-*b*-PBA_{67}-coated nanoclusters (Figure 6.4g) the excess aqueous phase was very dark and the droplet size reached 62.8 μm. The changes in the droplet size as a function of PBA length follow the same trends observed in γ and adsorption energy. The smaller droplet sizes observed with shorter PBA lengths are reflected by the lower γ and stronger adsorption of particles to oil/water interfaces.[54]

When dodecane/water emulsions were formed with NPs coated with the random copolymers at pH = 8, the lower aqueous phase was nearly clear and the NP concentration in the excess water phase was immeasurably low, indicating that most of the NPs had left the water phase and partitioned into the upper oil phase (Table 6.4). Additionally, the observed droplet sizes were smaller than those observed for the block copolymer-stabilized particles. However, at pH = 6 and pH = 10, the nanoclusters with random copolymer shells were incapable of stabilizing the emulsions, as may be expected given their low water solubility.

NP coating	Concentration of Excess Water Phase (% wt. of Fe)			Amount of NPs in oil phase (%)[a]		
	pH = 6	pH = 8	pH = 10	pH = 6	pH = 8	pH = 10
PAA$_{114}$-*b*-PBA$_{26}$	0.006	0.019	0.103	97.0	90.5	48.5
PAA$_{114}$-*b*-PBA$_{38}$	0.023	0.048	0.108	88.5	76.0	46.0
PAA$_{133}$-*co*-PBA$_{44}$	n/a	0 % wt.	n/a	n/a	100	n/a

Table 6.4: NP concentration in the oil and water phases.[a] Calculated by material balance given known concentration in the excess lower aqueous phase.

The interfacial surface area per NP, A, may be estimated from the NP radius, a, and the 2-dimensional packing fraction on an oil droplet, η, with the expression

$$A = \frac{\pi a^2}{\eta} \qquad \text{Eq. 6.2}$$

The total mass of particles in the emulsion phase, M, is used to estimate η with the expression

$$\eta = \frac{MR}{4V_{EP}\phi_c a \rho_p} \qquad \text{Eq. 6.3}$$

where R is the oil droplet radius, V is the volume of the emulsion phase, ϕ_c is the oil droplet volume fraction in the emulsion phase (assumed to be 0.74 for close packed spheres), and ρ_p is the nanocluster density (assumed to be half of the bulk IO density of 5.24 g/mL).[55] For example, when 1 mL of an aqueous dispersion (0.27% w/v) of IO particles coated with PAA$_{114}$-*b*-PBA$_{26}$ (a = 41 nm) was emulsified with 1 mL of dodecane to form 14 μm oil droplets in water, the resulting interfacial area per NP was calculated to be $A = 1.2 \times 10^5$ nm^2 (Table 6.5) at pH = 8. When the pH was varied, the changes in A were relatively small. The NP adsorption was on the order of 6-10 % of a monolayer. As the PBA block was increased to 38 units, A decreased significantly, and the adsorption reached 22% of a monolayer at pH = 8. Given the significant amount of NPs in the lower

aqueous phase, it appeared that the NP partitioning between phases reached a "quasi" equilibrium value. We use the term quasi as emulsions droplets are not in a state of thermodynamic equilibrium, but over time will phase separate. For the case of PAA_{133}-*co*-PBA_{44}, the interface was not saturated with NPs as the aqueous excess phase was clear (Figure 6.5). Here the interfacial area was much larger given the smaller droplets, such that the NPs only covered 4% of the interface (Figure 6.6, Table 6.5). Upon doubling the Fe_3O_4 concentration to 0.54% (w/v) the entire volume was emulsified and excess phase was not present even after 2 weeks.

NP Coating	**Monolayer coverage (%)**			**Interfacial area/Nanocluster (nm^2)**		
	pH = 6	pH = 8	pH = 10	pH = 6	pH = 8	pH = 10
PAA_{114}-*b*-PBA	7.04	10.02	6.09	1.4×10^5	1.2×10^5	1.8×10^5
PAA_{114}-*b*-PBA_{38}	17.87	22.15	10.09	9.2×10^4	8.5×10^4	1.4×10^5
PAA_{133}-*co*-PBA_{44}	n/a	4.12	n/a	n/a	5.1×10^5	n/a

Table 6.5: Estimate of percentage of full monolayer at oil/water interface. [a] Determined from material balance in Table 6.4.

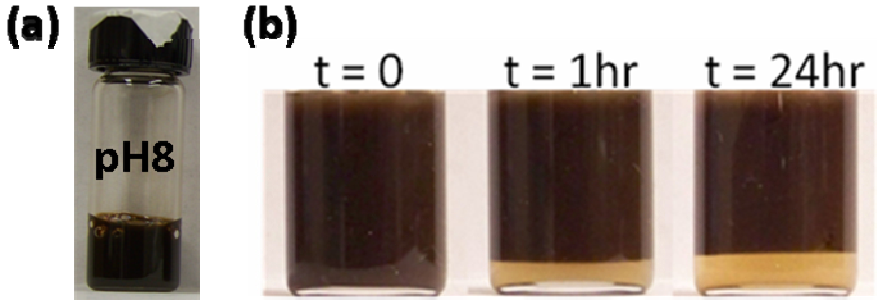

Figure 6.5: (a) Photographs of PAA_{133}-*co*-PBA_{44}-coated IO NP dispersions after 1 day at pH = 8. (b) Photographs of emulsions formed with equal volume fractions of dodecane and aqueous dispersion of 0.27 % wt. PAA_{133}-*co*-PBA_{44}-coated IO particles at pH = 8.

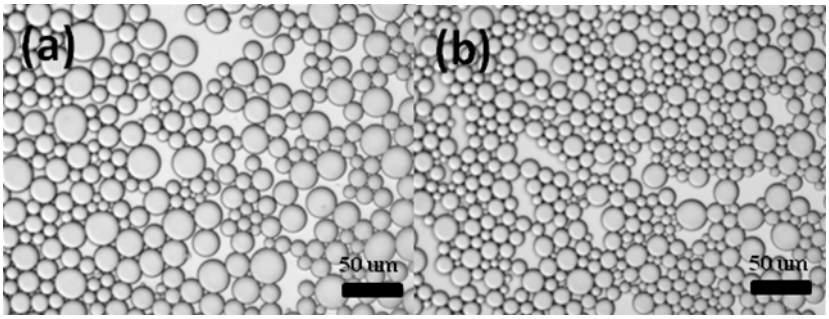

Figure 6.6: Optical micrographs of emulsions formed at pH = 8 at conditions in Figure 6.5. (a) PAA_{133}-*co*-PBA_{44}, 0 % wt. NaCl; (b) PAA_{133}-*co*-PBA_{44}, 3 % wt. NaCl. The optical micrographs were taken 24 h after emulsion formation.

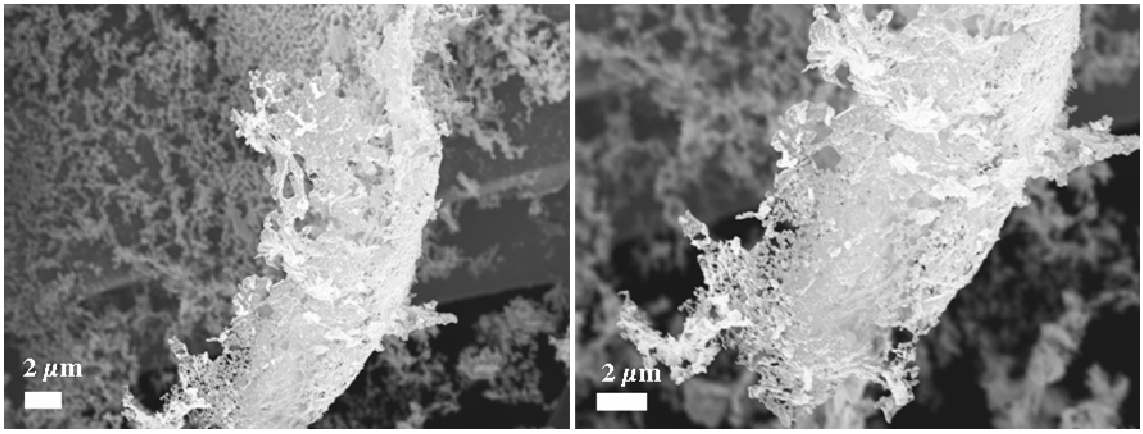

Figure 6.7: SEM images formed by freezing a droplet of the emulsion on a TEM grid pre-cooled in liquid nitrogen. The images (at two different magnifications) show the same single droplet of oil-in water-coated by much less than a monolayer of PAA_{114}-*b*-PBA_{26} coated NPs.

The SEM images in Figure 6.7 are consistent with Table 5 in that they show partial monolayers of the NPs on a 30~40 μm diameter oil droplet. These images provide direct evidence that the NPs adsorbed at the oil-water interface. The size of the oil droplet is comparable to that observed by optical microscopy. On the left hand side of the image, corresponding to the back of the spherical droplet, distinct large open spaces may be seen between the NPs. The surface coverage from SEM is only semi-quantitative given the various angles in the image and the fact that some rearrangement may have taken place during sample preparation. Clearly a tightly packed near full monolayer is not present as was the case in Binks et al,[56] as may be expected for the much lower NP concentration in the current study. The oil droplets were most likely stabilized by a bilayer patch of NPs that formed upon collision of two droplets at their contact point, which was consistent with previously reported results.[58]

The random copolymers were insufficiently solvated by water (too hydrophobic) to form a stable bilayer in the water channels of two approaching droplets at pH = 6, most likely due to the fact that at pH = 6 the acrylic acid groups were not sufficiently charged

given their proximity to PBA groups. At pH = 8, the zeta potentials were similar for the nanoclusters coated by random and block copolymers. The random copolymer chains that extend into water are more hydrophobic than those for the block copolymers, due to the distribution of the PBA groups throughout the polymer chain. Thus the NPs are less hydrophilic and essentially all the IO particles left the water phase and partitioned into the emulsion phase. Furthermore, these highly interfacially active NPs, based on the reduction in γ, stabilized the smallest droplets of any of the NPs tested. However at pH = 6 and pH = 10, where the random copolymer was not soluble and did not lower γ, emulsions could not be formed.

6.5 CONCLUSIONS

A series of sub-100 nm superparamagnetic IO nanoclusters stabilized by amphiphilic PAA-*b*-PBA and PAA-*co*-PBA copolymers were synthesized and shown to induce large reductions in the interfacial tension (high surface pressures) at the dodecane-water interface. During the NP synthesis, small amounts of copolymer coatings (< 20 % (w/w) by TGA) were adsorbed on the Fe_3O_4 particle surface and mediated the nucleation and growth of nanoclusters to control the nanocluster size, as evidenced by TEM and DLS measurements. The thin copolymer shells on IO played a key role in enabling high surface pressures at the oil-water interface as a function of the monomer ratio, although some of the effect may have been from desorbed polymer at the interface. Notably, large surface pressures were achieved at much lower NP concentrations than previously reported for homopolymer-coated NPs.[10] Sufficient adsorption of the NPs at the oil-water interface stabilized oil droplets as small as 12.1 μm in water at 24 hours, despite the low NP concentrations (0.27 % wt.), indicating high emulsification efficiency. Furthermore, the emulsion droplet formation was facilitated by the low interfacial tensions, which were

also shown to be dependent upon the polymer composition. The block copolymer coatings effectively stabilized emulsions over a broad range of pH values (pH = 6-10), while the random copolymer coatings were effective at pH = 8.

The adsorption of the nanoclusters at the oil-water interface was estimated from the concentration of nanoclusters in the excess phase and the interfacial surface area calculated using microscopy images. The most interfacially active was the block copolymer with 26 PBA units, which stabilized the emulsions with a lower fraction of monolayer coverage than with 38 PBA units. Collectively these results demonstrate that amphiphilic block copolymer shells on IO NPs promote high interfacial activity (large surface pressures), resulting in high emulsification efficiency and unusually small oil droplet sizes at low nanocluster concentrations. The ability to achieve significant adsorption at the oil/water interface and high surface pressures for NPs, including superparamagnetic nanoclusters with amphiphilic copolymer shells is expected to find utility in a wide variety of practical applications including magnetic imaging in biomedical and subsurface engineering and in enhanced oil recovery. Future studies of the conformation of the copolymers on the IO surface may be used to provide insight into the mechanism of the reduction of interfacial tension.

6.6 EXPERIMENTAL

6.6.1 Materials

All solvents were purchased from Fisher Scientific and used without further purification unless otherwise noted. *n*-Butyl acrylate (BA) and *t*-butyl acrylate (*t*BA) were filtered through a short plug of basic alumina to remove the 4-methoxyphenol (MEHQ) stabilizer. All other chemicals were purchase from commercial sources and

used without further purification. Dialysis tubing (Spectra/Por® 6; 50,000 MWCO; lot number 3246779) was purchased from Spectrum Laboratories, Inc., USA.

6.6.2 General Procedure for Synthesis of Polymer Coatings

The polymer coatings were prepared by atom transfer radical polymerization (ATRP) of *n*-butyl acrylate and *tert*-butyl acrylate followed by acidolysis to afford poly(acrylic acid-*co*-butyl acrylate). P*t*BA-*b*-PBA block copolymers were prepared by ATRP from P*t*BA macroinitiators. Generally, to an oven-dried 100 mL Schlenk flask with a magnetic stir bar was added copper(I) bromide, monomer (*n*-butyl acrylate and/or *tert*-butyl acrylate) and initiator (ethyl 2-bromoisobutyrate or macroinitiator P*t*BA) under an atmosphere of nitrogen. After one freeze-pump-thaw cycle, *N,N,N′,N′,N*-pentamethyldiethylenetriamine was added via a gas-tight syringe that had been purged with nitrogen. After three freeze-pump-thaw cycles, the reaction mixture was allowed to return to ambient temperature, and the reaction flask was backfilled with nitrogen, sealed and placed in an oil bath at 65 °C. The reaction mixture was allowed to stir for 2-4 h prior to quenching by immersion in liquid nitrogen. The reaction mixture was then taken up into THF and passed through a plug of neutral alumina to remove the Cu/ligand catalyst system. The polymer mixture was concentrated and precipitated three times into cold methanol/water mixture (1/1, v/v). After characterization by NMR spectroscopy and gel permeation chromatography, the isolated poly(*t*-butyl acrylate-*co*-*n*-butyl acrylate) was dissolved in dichloromethane in a round-bottom flask with a magnetic stir bar and excess trifluoroacetic acid was added. The reaction mixture was stirred at room temperature for 18 h, and the dichloromethane and trifluoroacetic acid were removed under reduced pressure. The residue was dissolved in DI water and dialyzed for 3 days against DI water.

P*t*BA$_{114}$: GPC: M_n = 14,650, M_w/M_n = 1.32. MW = 14,500 Da from ^{1}H NMR spectroscopy. Yield 16.6 g, 80%. ^{1}H NMR ($CDCl_3$, ppm): δ 4.05 (m, br), 2.30-2.10 (s, br), 1.88-1.68 (s, br), 1.65-1.30 (m, br).

P*t*BA$_{114}$-*b*-PBA$_{26}$: M_n = 18,830 Da from GPC, M_w/M_n = 1.38. MW = 18,000 Da from ^{1}H NMR spectroscopy. Yield 1.98 g, 88%. ^{1}H NMR ($CDCl_3$, ppm): δ 3.95 (m, br), 2.30-2.10 (m, br), 1.88-1.20 ((m, br), 0.80 (t, br).

P*t*BA$_{114}$-*b*-PBA$_{38}$: M_n = 21,490 Da from GPC, M_w/M_n = 1.39. MW = 19,500 Da from ^{1}H NMR spectroscopy. Yield 4.93 g, 75%. ^{1}H NMR ($CDCl_3$, ppm): δ 3.95 (m, br), 2.30-2.10 (m, br), 1.88-1.20 (m, br), 0.80 (t, br).

P*t*BA$_{114}$-*b*-PBA$_{67}$: M_n = 27,900 Da from GPC, M_w/M_n = 1.45. MW = 23200 Da from ^{1}H NMR spectroscopy. Yield 3.83 g, 82%. ^{1}H NMR ($CDCl_3$, ppm): δ 3.95 (m, br), 2.30-2.10 (m, br), 1.88-1.20 (m, br), 0.80 (t, br).

P*t*BA$_{133}$-*co*-PBA$_{44}$: M_n = 22,910 Da from GPC, M_w/M_n = 1.34. MW = 22,600 Da from ^{1}H NMR spectroscopy. Yield 13.8 g, 69%. ^{1}H NMR ($CDCl_3$, ppm): δ 4.12-3.95 (m, br), 2.42-2.08 (m, br), 1.92-1.70 (m, br), 1.65-1.20 (m, br), 0.80 (t, br).

6.6.3 NP Synthesis and Nanocluster Formation

The nanoclusters were formed by hydrolysis of iron chlorides under aqueous alkaline conditions by modifying well established synthetic approaches.[47-49] Briefly, in a three-necked flask $FeCl_2$ and $FeCl_3$ (1:2 molar ratio) and polymer (PAA, PAA-*b*-PBA, or PAA-*co*-PBA) were dissolved in 30 mL DI water and the solution was stirred vigorously with a magnetic stirrer for 30 minutes under an atmosphere of nitrogen. The weight ratio of polymer to total iron chloride was 1:4. The mixture was heated to 90 ^{o}C while stirring and 10 ml of 28 % wt. NH_4OH solution was added to the reaction mixture to nucleate and grow IO NPs. The reaction was further stirred and heated for 2 hours, then cooled to

room temperature. The stable dispersion was centrifuged at 9000 rpm for 10 minutes and the sediment was redispersed in 40 ml DI water by probe sonication. The final dispersion contained ~0.5 % wt. Fe as determined by flame atomic absorption spectroscopy (FAAS), and the pH value was measured to be 9.4. After probe sonication (Branson Sonifier® S-450A) the largest IO aggregates above ~400 nm were removed from the dispersion by centrifugation (6000 rpm for 5 min) and discarded. The clusters were redispersed in deionized (DI) water by probe sonication.

6.6.4 Characterization

Nuclear magnetic resonance (NMR) analysis was performed using a Varian Gemini (300 MHz or 400 MHz) spectrometer. Chemical shifts (δ) are expressed in parts per million (ppm) downfield from tetramethylsilane using the residual protic solvent as an internal standard ($CDCl_3$, 7.24 ppm). Gel permeation chromatography (GPC) was performed on a Viscotek system equipped with a VE 1122 pump, a VE 7510 degasser, two fluorinated polystyrene columns (IMBHW-3078 and I-MBLMW-3078) thermostated to 30 °C (using a ELDEX CH 150 column heater) and arranged in series, using refractive index (RI) detection. Molecular weight and polydispersity data are reported relative to polystyrene standards in tetrahydrofuran (THF).

Dynamic light scattering (DLS) analysis was performed at 90^o on a custom-built apparatus and the data were analyzed using a digital autocorrelator (Brookhaven BI-9000AT) and a non-negative least-squares (NNLS) routine (Brookhaven 9KDLSW32).[60] The suspension concentration was 0.05 mg/mL which gave a measured count rate of approximately 100-200 kcps. Measurements were made over a period of 2 min at least three times on each sample. Zeta potential measurements were performed in triplicate on the ZetaPlus dynamic light scattering apparatus (Brookhaven Instruments) at 90°

scattering angle and temperature of 25 °C. The zeta potential was determined from the electrophoretic mobility by assuming $\kappa a \ll 1$. The zeta potential in only an effective value because the polyelectrolyte on the particle surface is permeable.[61, 62]

Transmission electron microscopy (TEM) was used to observe the morphology of nanoclusters. The experiments were performed on a FEI TECNAI G2 F20 X-TWIN TEM using a high-angle annular dark field detector. The samples were prepared using a "flash-freezing" technique, in which a 200 mesh carbon-coated copper TEM grids were cooled using liquid nitrogen and then dipped into dilute aqueous nanocluster dispersion.[63] The sample was dried using a Virtis Advantage Tray Lyophilizer (Virtis Company, Gardiner, NY) with 2 hours of primary drying at -40ºC followed by a 12 hour ramp to 25ºC and then 2 hours of secondary drying at 25ºC. In this manner the aggregation of NPs caused by capillary forces during drying of the liquid on the TEM grid could be minimized. Scanning electron microscopy (SEM) was used to observe IO NPs at the interface. The experiments were performed using Zeiss Supra 40 VP field-emission SEM was operated at an accelerating voltage of 5 kV. SEM samples were prepared using a "flash-freezing" technique, which was dropping oil/water emulsion of IO nanoclusters onto 200 mesh carbon-coated copper TEM grids cooled using liquid nitrogen. The sample was dried into Virtis Advantage Tray Lyophilizer (Virtis Company, Gardiner, NY) with 2 hours of primary drying at -40ºC followed by a 12 hour ramp to 25ºC and then 2 hours of secondary drying at 25ºC. Thermogravimetric analysis (TGA) was used to determine the mass of adsorbed polymer on the iron nanoclusters. The experiments were performed using a Perkin–Elmer TGA 7 under nitrogen atmosphere at a gas flow rate of 20 mL/min. The powder samples were held at 100°C for 120 minutes to remove the remaining water and then heated at a constant rate of 20°C/min from 100°C to 800°C and held at 800°C for 30 minutes. Flame atomic absorption spectroscopy (FAAS) was used to determine the

iron concentration in the dispersion by using a GBC 908AA flame atomic absorption spectrometer (GBC Scientific Equipment Pty Ltd). All measurements were conducted at 242.8 nm using an air-acetylene flame. Superconducting quantum interference device (SQUID) magnetometer (Quantum Design MPMS) was used to measure the normalized saturation magnetization of the particles at 300 K.

The interfacial tension device analysis (software package CAM200 (KSV Ltd., Finland) with a pendant water droplet containing a known concentration of NPs in equilibrium with an excess oil phase, as described previously.[64] The average was taken of at least 10 measurements that were acquired every 10 s. The pendant drop was illuminated with a monochromatic light source and the digital images were recorded. The coordinates of the profiles were then analyzed through a computer program imbedded in a software package CAM200 (KSV Ltd., Finland) according to the Laplace equation.[64] For the emulsions, the images were analyzed to determine the droplet size using NIH Image J.

6.7 ACKNOWLEDGEMENTS

Portions of this chapter were reprinted with permission from Yoon, K. Y.; Li, Z.; Neilson, B. M.; Lee, W.; Huh, C.; Bryant, S. L.; Bielawski, C. W.; Johnston, K. P. *Macromolecules* **2012**, *45*, 5157-5166. Copyright 2012 American Chemical Society. I acknowledge my collaborators Ki Youl Yoon, Zicheng Li, and Wonjae Lee for their significant contributions to the NPs synthesis and characterization. I am grateful to Prof. Chun Huh, Prof. Steven L. Bryant, and Prof. Christopher Bielawski for their helpful discussions, and to principal investigator, Prof. Keith P. Johnston, for his help in writing the original manuscript. I also thank Ki Youl Yoon for his shared efforts in writing the original manuscript.

6.8 REFERENCES

[1] Binks, B. P. *Curr. Opin. Coll. Interf. Sci*. **2002**, *7*, 21-41.

[2] Hunter, T. N.; Pugh, R. J.; Franks, G. V.; Jameson, G. J. *Adv. Coll. Interf. Sci.* **2008**, *137*, 57-81.

[3 Binks, B. P. *Langmui*r **2004**, *20*, 1130-1137.

[4] Melle, S.; Lask, M.; Fuller, G. G. *Langmui*r **2005**, *21*, 2158-2162.

[5] Tcholakova, S.; Denkov, N. D.; Lips, A. *Phys. Chem. Chem. Phys*. **2008**, *10*, 1608–1627.

[6] Aveyard, R.; Clint, J. H.; Horozov, T. S. *Phys. Chem. Chem. Phys.* **2003**, *5*, 2398–2409.

[7] Schwartz, H.; Harel, Y.; Efrima, S. *Langmuir* **2001**, *17*, 3884-3892.

[8] Lin, Y.; Skaff, H.; Emrick, T.; Dinsmore, A. D.; Russell, T. P. *Science* **2003**, *299*, 226-229.

[9] Wang, W.; Zhou, Z.; Nandakumar, K.; Xu, Z.; Masliyah, J. H. *J. Colloid Interface Sci.* **2004**, *274*, 625–630.

[10] Saleh, N.; Sarbu, T.; Sirk, K.; Lowry, G. V.; Matyjaszewski, K.; Tilton, R. D. *Langmuir* **2005**, *21*, 9873-9878.

[11] Vignati, E.; Piazza, R. *Langmuir* **2003**, *19,* 6650-6656.

[12] Ma, H.; Luo, M.; Dai, L. L. *Phys. Chem. Chem. Phys.* **2008**, *10*, 2207-2213.

[13] Binks, B. P.; Rodrigues, J. A. *Langmuir* **2007**, *23*, 7436-7439.

[14] Stocco, A.; Drenckhan, W.; Rio, E.; Langevin, D.; Binks, B. P. *Soft Matter* **2009**, *5*, 2215–2222.

[15] Saigal, T.; Dong, H. C.; Matyjaszewski, K.; Tilton, R. D. *Langmuir* **2010**, *26*, 15200-15209.

[16] Saleh, N.; Phenrat, T.; Sirk, K.; Dufour, B.; Ok, J.; Sarbu, T.; Matyjaszewski, K.; Tilton, R. D.; Lowry, G. V. *Nano Lett.* **2005**, *5*, 2489-2494.

[7] Ditsch, A.; Laibinis, P. E.; Wang, D. I. C.; Hatton, T. A. *Langmuir* **2005**, *21*, 6006-6018.

[18] Kotsmar, C.; Yoon, K. Y.; Ingram, D. R.; Ryoo, S. Y.; Barth, J.; Shao, S.; Prodanovic´, M.; Milner, T.; Bryant, S. L.; Huh, C.; Johnston, K. P. *Ind. Eng. Chem. Res.* **2010**, *49*, 12435–12443.

[19] Yoon, K. Y.; Kotsmar, C.; Ingram, D. R.; Huh, C.; Bryant, S. L.; Milner, T. E.; Johnston, K. P. *Langmuir* **2011**, *27*, 10962-10969.

[20] Esser-Kahn, A. P.; Odom, S. A.; Sottos, N. R.; White, S. R.; Moore, J. S. *Macromolecules* **2011**, *44*, 5539–5553.

[21] Zhou, J.; Qiao, X.; Binks, B. P.; Sun, K.; Bai, M.; Li, Y.; Liu, Y. *Langmuir* **2011**, *27*, 3308–3316.

[22] Binks, B. P.; Kirkland, M. *Phys. Chem. Chem. Phys.* **2002**, *4*, 3727-3733.

[23 Lan, Q.; Liu, C.; Yang, F.; Liu, S.; Sun, D. *J. Colloid Interface Sci* **2007**, *310*, 260-269.

[24] Gupta, A. K.; Gupta, M. *Biomaterials* **2005**, *26*, 3995–4021.

[25] Oh, J.; Feldman, M. D.; Kim, J.; Condit, C.; Emelianov, S.; Milner, T. E. *Nanotechnology* **2006**, *17*, 4183-4190.

[26] Lattuada, M.; Hatton, T. A. *J. Am. Chem. Soc.* **2007**, *129*, 12878-12889.

[27] Lu, A.-H.; Salabas, E. L.; Schueth, F. *Angew. Chem. Int. Ed.* **2007**, *46*, 1222-1244.

[28] Ma, L. L.; Feldman, M. D.; Tam, J. M.; Paranjape, A. S.; Cheruku, K. K.; Larson, T. A.; Tam, J. O.; Ingram, D. R.; Paramita, V.; Villard, J. W.; Clarke, G. D.; Jenkins, J. T.; Asmis, R.; Sokolov, K.; Chandrasekar, B.; Milner, T. E.; Johnston, K. P. *ACS Nano* **2009**, *3*, 2686-2696.

[29] Sun, B.; Sun, M.-J.; Gu, Z.; Shen, Q.-D.; Jiang, S.-J.; Xu, Y.; Wang, Y. *Macromolecules* **2010**, *43*, 10348–10354.

[30] Adkins, S. S.; Gohil, D.; Dickson, J. L.; Webber, S. E.; Johnston, K. P. *Phys. Chem. Chem. Phys.* **2007**, *9*, 6333-6343.

[31] Yu, H.; Kotsmar, C.; Yoon, K. Y.; Ingram, D. R.; Johnston, K. P.; Bryant, S. L.; Huh, C. *17th SPE Improved Oil Recovery Symposium Tulsa*, *OK*; SPE: 2010; SPE 129887.

[32] Prodanovic, M.; Ryoo, S.; Rahmani, A. R.; Kuranov, R.; Kotsmar, C.; Milner, T. E.; Johnston, K. P.; Bryant, S. L.; Huh, C. *17th SPE Improved Oil Recovery Symposium Tulsa, OK*; SPE; 2010; SPE 129850.

[33] Prakash, A.; Zhu, H.; Jones, C. J.; Benoit, D. N.; Ellsworth, A. Z.; Bryant, E. L.; Colvin, V. L. *ACS Nano* **2009**, *3*, 2139-2146.

[34] Adkins, S. S.; Gohil, D.; Dickson, J. L.; Webber, S. E.; Johnston, K. P. *Phys. Chem. Chem. Phys.* **2007**, *9,* 6333-6343.

[35] Ryoo, S.; Rahmani, A. R.; Yoon, K. Y.; Prodanovic, M.; Kotsmar, C.; Milner, T. E.; Johnston, K. P.; Bryant, S. L.; Huh, C. *SPE Annual Meeting, Florence, Italy* SPE: 2010; SPE 134879.

[36] S.; Lask, M.; Fuller, G. G. *Langmuir* **2005**, *21*, 2158-2162.

[37] Ingram, D. R.; Kotsmar, C.; Yoon, K. Y.; Shao, S.; Huh, C.; Bryant, S. L.; Milner, T.; Johnston, K. P. *J. Colloid Interface Sci*. **2010**, *351*, 225-232.

[38] Massart, R.; Dubois, E.; Cabuil, V.; Hasmonay, E. *J. Magn. Magn. Mater.* **1995**, *149*, 1-5.

[39] Bacri, J.; Perzynski, R.; Salin, D.; Cabuil, V.; Massart, R. *J. Magn. Magn. Mater.* **1990**, *85*, 27.

[40] Kim, H. J.; Phenrat, T.; Tilton, R. D.; Lowry, G. V. *Environ. Sci. Technol.* **2008**, *43,* 3824-3830.

[41] Saleh, N.; Kim, H.-J.; Phenrat, T.; Matyjaszewski, K.; Tilton, R. D.; Lowry, G. V. *Environ. Sci. Technol.* **2008**, *42*, 3349-3355.

[42] Berret, J.-F. *Macromolecules* **2007**, *40*, 4260-4266.

[43] Berret, J.-F.; Schonbeck, N.; Gazeau, F.; El Kharrat, D.; Sandre, O.; Vacher, A.; Airiau, M. *J. Am. Chem. Soc.* **2006**, *128*, 1755-1761.

[44] Lin, C.-L.; Lee, C.-F.; Chiu, W.-Y. J. *Colloid Interface Sci.* **2005**, *291*, 411-420.

[45] Ge, J.; Hu, Y.; Biasini, M.; Beyermann, W. P.; Yin, Y. *Angew. Chem. Int. Ed.* **2007**, *46*, 4342-4345.

[46] Sondjaja, R.; Hatton, A. T.; Tam, M. K. C. *J. Magn. Magn. Mat.* **2009**, *321*, 2393-2397.

[47] Sahoo, Y.; Goodarzi, A.; Swihart, M. T.; Ohulchanskyy, T. Y.; Kaur, N.; Furlani, E. P.; Prasad, P. N. *J. Phys. Chem. B* **2005**, *109*, 3879–3885.

[48] Massart, R. *IEEE Trans. Magn.* **1981**, *17*, 1247-1248.

[49] Lyon, J. L.; Fleming, D. A.; Stone, M. B.; Schiffer, P.; Williams, M. E. *Nano Lett.* **2004**, *4*, 719-723.

[50] Jacquin, M.; Muller, P.; Talingting-Pabalan, R.; Cottet, H.; Berret, J. F.; Futterer, T.; Théodoly, O. *J. Colloid Interface Sci.* **2007**, *316*, 897–911.

[51] Campelj, S.; Makovec, D.; Drofenik, M. *J. Phys.: Condens. Matter* **2008**, *20*, 204101-204105.

[52] Berkowitz, A. E.; Lahut, J. A.; Sacobs, I. S.; Levinson, L. M.; Forester, D. W. *Phys. Rev.Lett.* **1975**, *34*, 594–597.

[53] Du, K.; Glogowski, E.; Emrick, T.; Russell, T. P.; Dinsmore, A. D. *Langmuir* **2010**, *26*, 12518-12522.

[54] Binks, B. P. *Curr. Opin. Coll. Interf. Sci.* **2002,** 7, 21-41.

[55] Golemanov, K.; Tcholakova, S.; Kralchevsky, P. A.; Ananthapadmanabhan, K. P.; Lips, A. *Langmuir* **2006,** 22, 4968-4977.

[56] Binks, B. P.; Kirkland, M.; Rodrigues, J. A. *Soft Mater.* **2008,** 4, 2373–2382.

[57] Ryoo, W.; Webber, S. E.; Johnston, K. P. *Ind. Eng. Chem. Res.* **2003,** *42*, 6348-6358.

[58] Ohshima, H. *Colloid Surface A* **1995,** 103, 249-255.

[59] Ohshima, H.; Makino, K *Colloid Surface A* **1996,** 109, 71-75.

[60] Tam, J. M.; Murthy, A. K.; Ingram, D. R.; Nguyen, R.; Sokolov, K. V.; P., J. K. *Langmuir* **2010,** *26*, 8988-8999.

[61] Chen, X.; Adkins, S. S.; Nguyen, Q. P.; Sanders, A. W.; Johnston, K. P. *J. Supercrit Fluid* **2010,** *55*, 712–723.

Chapter 7: Design and Synthesis of Sulfonated Copolymers for the Stabilization of Iron Oxide Nanoparticles

7.1 INTRODUCTION

Interest in nanotechnology for subsurface applications, including oil and gas recovery, reservoir imaging,[1] CO_2 sequestration[2] and environmental remediation,[3] has grown markedly over the last few years. Unfortunately, the high salinities (> 1 M) and often elevated temperatures (≤ 150 °C) found in subsurface reservoirs cause nanoparticle (NP) aggregation as well as excessive NP adsorption on mineral surfaces.[3,4] At low salinities small ligands, such as citrate, may be utilized to provide electrostatic repulsion over a relatively wide pH range.[5] At high ionic strength, extensive charge screening in very thin double layers weakens electrostatic repulsion between particles.[6] While ionic[3a,7] and zwitterionic[8] polymers have been shown to provide sufficient steric and electrosteric stabilization in aqueous NaCl up to 5 M[7] at ambient temperature, colloidal stabilization is unknown at elevated temperatures (50 - 150 °C), especially when concentrated divalent ions are present. At such high salinities, steric stabilization, which may be provided by polymer chains that extend from the surface, is often required to prevent flocculation.[6b,9] When charged polyelectrolytes are present on the particle surfaces, the stability can be further augmented by combined electrostatic and steric repulsion, known as "electrosteric" stabilization.[5d,3a,9b,10]

As a model metal oxide colloid, our efforts are focused on magnetic iron oxide (IO) NPs, which are of interest in numerous applications including biomedicine,[11] protein separation,[7a] water purification[12] and as contrast enhancement agents for imaging of subsurface oil reservoirs.[5f,7c] A wide array of polymers have been explored to stabilize IO dispersions at various salinities, including poly(ethylene glycol) (PEG),[5d,13]

polyacrylamide (poly(AM)),[14] poly(acrylic acid) (poly(AA)),[5d,15] poly(AA) copolymers[13b,7a,16] and a variety of sulfonated copolymers.[7]

In many cases, colloids coated with polymeric stabilizers flocculate under conditions (e.g., temperature, salinity, pH) similar to those that cause the pure polymer to phase separate in an aqueous medium.[6b] Flocculation and polymer phase separation each take place when the interactions between the polymer segments with the solvent are not strong enough relative to the segment-segment interactions. For polyelectrolytes, the solvation of the segments by the aqueous phase and the electrostatic repulsion between polymer segments are favored by dissociation of counterions.[17] These interactions are less favorable at high salinities as the double layer thickness decreases. Furthermore, although monovalent ions such as Na^+ and K^+ do not bind strongly to anionic polyacrylate ions,[18] divalent ions such as Ca^{2+} bind specifically and may induce gelation, as shown by solution behavior,[19] NMR studies[20] and calorimetry.[21] However, the binding constant for Ca^{2+} is weaker when the carboxylate groups are positioned further from the polymer backbone and even weaker for strongly acidic sulfonated polymers.[18,20] For example, while poly(vinylsulfonic acid) (poly(VS)) with short side chains clouded in aqueous $CaCl_2$ at 100 °C, poly(styrenesulfonic acid) (poly(SS)) and poly(2-acrylamido-2-methylpropanesulfonate) (poly(AMPS)) remained soluble.[18] Therefore, choice of the proper polymer composition by phase behavior studies at high salinity and temperature is expected to facilitate rapid screening of potential candidates for colloidal stabilization.[22]

Only a small number of studies have considered NP dispersions at high monovalent salinities (> 0.15 M) with either strong or weak polyelectrolyte stabilizers. Notably, latex particles (~50 nm) grafted with polymethacrylic acid (PMAA) were stabilized over a wide range of pH, salinity and grafting density at salt concentrations up to 3.5 M NaCl.[7b] Furthermore, ~100 nm IO nanoclusters were stabilized in up to 5 M

NaCl with copolymers composed of acrylic acid, styrene sulfonic acid and vinyl sulfonic acid.[7,22] Similarly, IO NPs synthesized in the presence of poly(styrene-*alt*-maleic acid) were stable in 8% NaCl (1.4 M NaCl).[7c] The addition of more strongly binding[18,19,23] divalent salts (> 0.1 M) such as Ca^{2+} adds an additional challenge to maintaining colloidal stability.[3c] However, such high Ca^{2+} levels are often encountered in natural sub-surface reservoirs of interest in oil recovery, and there is therefore a need for colloids that maintain stability under such conditions.[24,25] Both IO[13] and zero valent Fe[10d] NPs have been stabilized in up to 10% (or 0.9 M) $CaCl_2$ using adsorbed carboxylated[13] and/or sulfonated[10d] polyelectrolytes. Neither of those reports, however, provided explicit information on how long the particles were stable, and the former used relatively small NPs.

A further obstacle to achieving colloidal stabilization in high divalent salinity in sub-surface is encountered with elevated temperatures, up to 100 °C. While both CdSe quantum dots[13a] and IO NPs[13c] have been stabilized at up to 90 °C, only monovalent salts were tolerated and stabilities were short-lived. Given that sulfonated polymers such as poly(AMPS) and poly(SS) have been shown to be soluble in relatively concentrated solutions of divalent salts at elevated temperature,[18,20] we envisioned that such polymers with their highly acidic nature would be promising candidates to stabilize NP dispersions under similar conditions.

The same anionic polymers that provide repulsion between NPs also have the potential to minimize adsorption on negatively charged bulk surfaces (e.g., silica or mineral surfaces). However, studies of transport of polymer-stabilized NPs in porous media,[3] as well as NP adsorption isotherms[3b,26] have not examined high salinities, particularly with divalent ions. Here, charge screening weakens electrostatic repulsion between the particles and the substrate, and furthermore, divalent cations may bridge

anionic NPs to negatively charged silica. Given these extreme and unusual conditions, it is very unclear as to whether low NP adsorption levels would be possible.

Polymers that are good stabilizers in brine, such as PSS and PAMPS, interact weakly with multivalent cations including Fe, thus are expected to adsorb weakly on the surfaces of IO NPs. Therefore, to coat IO NP's with sulfonated polymers, anchor groups that bind strongly to Fe (e.g., acrylic acid) must be incorporated into the polymer structure. However, an anchor group such as acrylic acid would interact strongly with the dissolved divalent ions, leading to flocculation. Thus, the proper ratio of anchor groups to stabilizing groups must be chosen to strike a balance between sufficient polymer adsorption on the NP surface and polymer solvation by the brine. Furthermore, the amount of polymer adsorbed[5d,10d,7a] on IO NPs must be minimized to avoid lowering the magnetic weight fraction.[7b,27] Copolymers with sulfonate groups and carboxylate groups have been adsorbed on IO NPs during nucleation and growth of the NPs upon hydrolysis of various Fe precursors.[7,26] However, the IO NP morphology and magnetic properties may change with polymer structure, and it would thus be highly beneficial to devise novel methods to examine a variety of polymer stabilizers with varying functionality and molecular weights on pre-synthesized iron oxide cores with fixed properties.

Herein we report the development of random and block copolymer coatings on the surface of ~100 nm IO nanoclusters which provided colloidal stability in extremely concentrated brine composed of 8% wt. NaCl + 2% wt. $CaCl_2$ (API brine; 1.4 M NaCl + 0.2 M $CaCl_2$) and at an elevated temperature of 90 °C. A combinatorial materials chemistry approach was employed, which enabled the investigation of a large number of polymers on pre-synthesized IO nanoclusters. Only copolymers that were first found to be soluble in API brine at 90 °C were considered as stabilizers, and the synthesis of the IO NPs was completely separated from the copolymer adsorption on the NP surface.

Well-defined citrate-coated IO NPs with a fixed hydrodynamic diameter (D_H) of ~50 nm were developed, and a homologous series of poly(2-methyl-2-acrylamidopropanesulfonate-*co*-acrylic acid) (poly(AMPS-*co*-AA)) copolymers were adsorbed to provide electrosteric stabilization. In addition, a sulfonated block copolymer, poly(styrenesulfonate-*block*-acrylic acid) (poly(SS-*b*-AA)), and a sulfonated alternating copolymer, poly(styrenesulfonate-*alt*-maleic acid) (poly(SS-*alt*-MA)) were also investigated as stabilizers. The adsorption of the aforementioned polymers on iron oxide was facilitated by bridging of the carboxylate anchor groups to the like-charged citrate ligands on the IO nanoclusters with Ca^{2+}.[28] The success in coating of the polymer stabilizers on iron oxide was assessed by (i) colloidal stability in concentrated brine solutions at room temperature and 90 °C, (ii) measurement of the hydrodynamic volume (D_H) in API brine at ambient and elevated temperatures, (iii) zeta potential measurements over a range of salinities and (iv) quantification of the organic content by thermogravimetric analysis (TGA). Additionally, the adorption of the polymer-stabilized IO NPs on model SiO_2 microspheres was investigated to assess their utility for transport through porous media.

As an alternative to adsorption of the polymers on the IO NPs, for more permanent attachment, predesigned sulfonated copolymers with the desired composition and molecular weight were covalently attached to NP surface by the 'grafting to' technique.[8,11b,29] The polymer-grafted particles formed stable dispersions in API brine at 90 °C, and exhibited minimal adsorption on silica microparticles. The aforementioned copolymer, poly(AMPS-*co*-AA) (3:1), was designed to contain a high proportion of AMPS stabilizer groups to provide a low binding affinity for calcium ions as well as a proper fraction of AA anchor groups to enable multipoint covalent attachment.[30] The copolymer was covalently grafted to amine-functionalized IO NPs, which prevented

desorption from the IO surface even after a 40,000-fold serial dilution. The hydrodynamic diameter of the pure polymer, as measured by DLS, underwent little contraction at high salinity and elevated temperatures, reflecting weak interactions with Ca^{2+}. Consequently, favorable solvation of the extended poly(AMPS-*co*-AA) brushes on the IO surface enabled steric stabilization between NPs, and between NPs and the silica surfaces, resulting in extremely low NP adsorption (0.4% monolayer).

7.2 Synthesis and Phase Behavior of Sulfonated Copolymers

A variety of copolymers with carboxylate and sulfonate groups were identified as candidates for stabilizing IO nanoclusters (Figure 7.1a). Acrylic acid (AA) or maleic acid (MA) units were used as anchor groups to provide a means of attaching the polymers to the IO surface. Styrenesulfonate (SS) or 2-acrylamido-2-methylpropanesulfonate (AMPS) components were incorporated in varying mole fractions to offset the strong cation binding capability of the carboxylate groups and provide colloidal stability while minimizing adsorption of the IO on mineral surfaces (e.g. SiO_2). Specifically a series of poly(AMPS-*co*-AA) random copolymers ranging in molar monomer ratios from (1:8) through (3:1) were investigated. Additionally block and alternating copolymers containing styrenesulfonate, which has greater hydrophobicity, were studied to elucidate the effects of both the polymer backbone structure and the monomer structure. The random poly(AMPS-*co*-AA) copolymers with lower sulfonate content (AMPS:AA = 1:8, 1:6, 1:4) were commercially available, as was the alternating copolymer poly(SS-*alt*-MA). The poly(AMPS-*co*-AA) with higher sulfonate content, as well as the polymers containing SS were not available from commercial sources and were rationally designed and synthesized (Figure 7.1b-c).

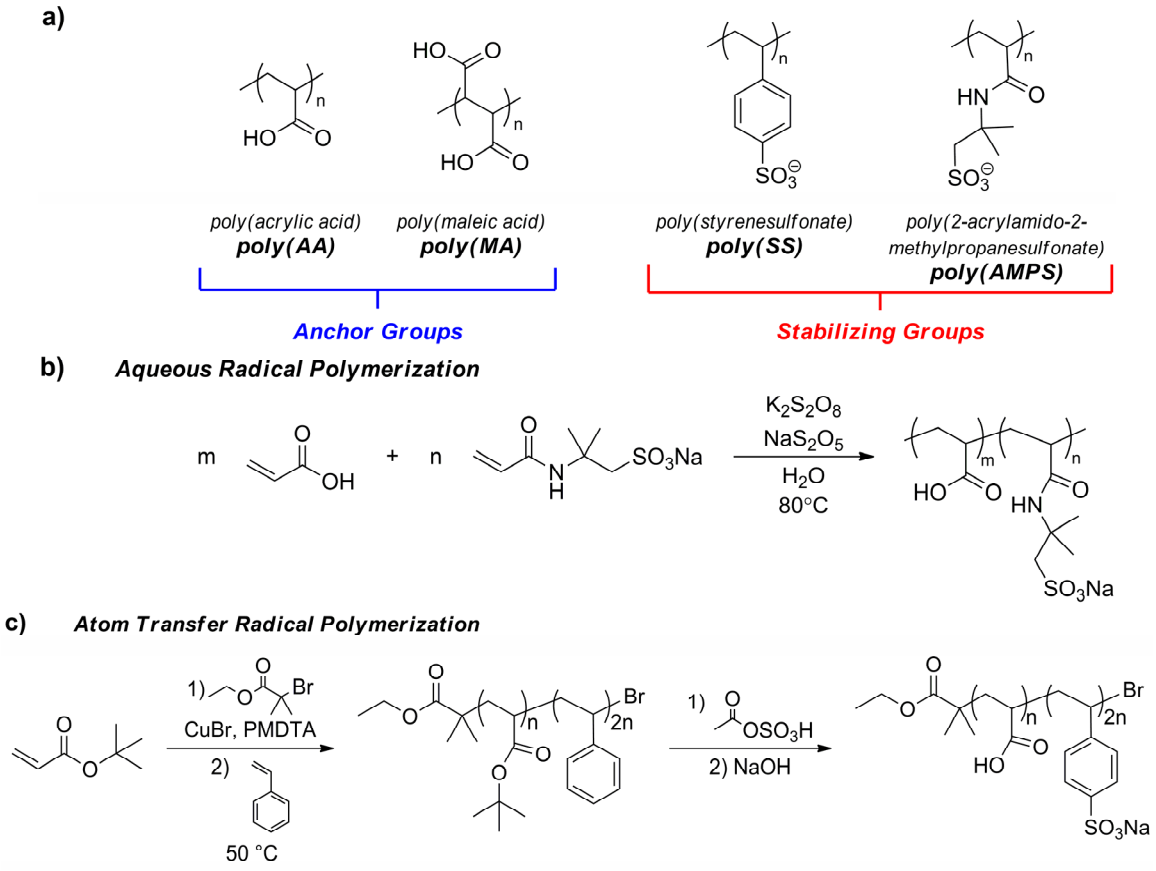

Figure 7.1: (a) Structures of polymer components: carboxylated units poly(acrylic acid) (AA) and poly(maleic acid) (MA) enabled attachment to IO surfaces; sulfonated units poly(styrenesulfonate) (SS) or poly(2-acrylamido-2-methylpropane sulfonate) (AMPS) provided electrosteric stabilization; poly(butylacrylate) was incorporated as a hydrophobic component. (b) Synthesis of poly(AMPS-*co*-AA) via aqueous radical polymerization. (c) Synthesis of poly(SS-*b*-AA) via ATRP followed by sulfonation. This method was also used to prepare poly((AA-*co*-BA)-*b*-SS).

The poly(AMPS-*co*-AA) copolymers were synthesized by aqueous free radical polymerization using the redox pair initiator $K_2S_2O_8/NaS_2O_5$,[31] and their compositions were confirmed to match the monomer feed ratio by ^{1}H NMR spectroscopy. The molecular weights (MW) of the synthesized poly(AMPS-*co*-AA) copolymers were estimated by correlating the hydrodynamic diameter (D_H) to the degree of polymerization

(DOP) of anionic copolymers of known MWs at pH = 8 in 1 M NaCl (Figure 7.2 and Table 7.1). At this high salinity, the polymer conformation can be approximated as a random coil; this assessment was confirmed by the size exponent of 0.48 from the polymer scaling law fit.[7,32] The block copolymer poly(SS-*b*-AA) was synthesized by atom transfer radical polymerization (ATRP) of *t*-butylacrylate and styrene followed by a one-pot sulfonation/deprotection using acetyl sulfate to afford poly(SS-*b*-AA). The MW of block copolymer poly(SS-*b*-AA) was calculated to be 40 kDa from the value measured by gel permeation chromatography (GPC) of its precursor polymer poly(*t*-butylacrylate-*b*-styrene) (in tetrahydrofuran versus polystyrene standards).

The phase behavior of the polymers (2% wt.) was studied in API brine at 25 and 90 °C (Table 7.1). With the exception of poly(AMPS-*co*-AA) (1:8) all investigated polymers were soluble under these conditions, which was consistent with previous phase behavior studies of related copolymers.[22,33] The cloudy appearance for the poly(AMPS-*co*-AA) (1:8) was attributed to the high acrylic acid content, as the carboxylate groups interact strongly with Ca^{2+}.[19] The strong Ca^{2+} binding of PAA via dehydration of the Ca^{2+} and COO^- groups results in the formation of a hydrophobic PAA-Ca^{2+} complex, leading to precipitation of the Ca^{2+}-bound polymer.[21,20] In contrast, polyaspartate (PAsp) which contains a hydrophilic amide backbone does not collapse in the presence of Ca^{2+}, due to both reduced Ca^{2+} binding and the more hydrophilic nature of the resulting Ca^{2+}-PAsp complex. It is likely that the hydrophilic amide bond in the AMPS structure (Figure 7.1) plays a similar role to reduce Ca^{2+} binding and chain collapse. McCormick and *co*-workers have demonstrated through viscosity and ^{23}Na NMR spectroscopy that AMPS polymers exhibit low binding affinities for Ca^{2+} and as a result remained soluble in $CaCl_2$ up to 100 °C.[18,20] The low affinity of AMPS for Ca^{2+} was attributed to the strong acidity of the AMPS group and the greater conformational freedom from the relatively long side

chains. Thus, in contrast with PAA, the stability of all other poly(AMPS-*co*-AA) copolymers with monomer ratios higher than 1:8 was primarily due to weak Ca^{2+} binding to the hydrophilic AMPS sulfonate group, which likely prevented dehydration of neighboring PAA groups.

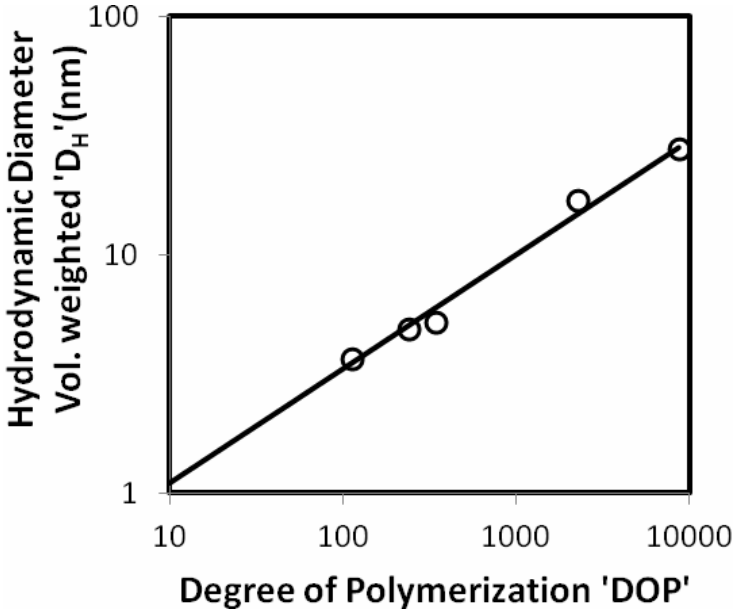

Figure 7.2: Volume-weighted hydrodynamic diameters (D_H) of (i) poly(styrenesulfonate-*co*-maleic acid) (3:1) – 20 kDa, (ii) poly(styrenesulfonate-*b*-acrylic acid) (2.4 : 1) – (40 kDa), (iii) poly(styrenesulfonate) (70 kDa), (iv) poly(acrylamide-*co*-acrylic acid) (1:3) – 200 kDa and (v) poly(2-acrylamido-2-methyl propanesulfonic acid) – 2 MDa, in 1 M NaCl at 25 °C correlated to their degree of polymerization (DOP) with a size exponent of 0.48.

Polymer Composition	D_H [b] (nm)	DOP[c]	MW[c] (kDa)	Source	Solubility in API brine[d]	
					25 °C	90 °C
poly(AMPS-*co*-AA) (1:8) [a]	4.7	206	22	SNF	Insoluble	Insoluble
poly(AMPS-*co*-AA) (1:6) [a]	6.5	406	46	Akzo Nobel	Soluble	Soluble
poly(AMPS-*co*-AA) (1:4) [a]	4.6	197	24	SNF	Soluble	Soluble
poly(AMPS-*co*-AA) (1:1) [a]	5.8	320	52	Synthesized	Soluble	Soluble
poly(AMPS-*co*-AA) (1:1) [a]	11.4	1310	212	Synthesized	Soluble	Soluble
poly(AMPS-*co*-AA) (3:1)	10	1000	200	Synthesized	Soluble	Soluble
Poly(SS-*b*-AA) (2.4:1) [a]	4.9	240[e]	40 [e]	Synthesized	Soluble	Soluble
Poly(SS-*alt*-MA) (3:1)	3.7	113[f]	20[f]	Sigma	Soluble	Soluble

Table 7.1: List of sulfonated copolymers, their hydrodynamic diameters (D_H), degrees of polymerization (DOP)/molecular weights (MW) and phase behavior in API brine (8 % wt. NaCl + 2 % wt. $CaCl_2$) after 1 day at room temperature and 90 °C. [a] Composition determined by ^{1}H NMR spectroscopy. [b] Vol. weighted hydrodynamic diameters collected in 1 M NaCl at 25 °C. [c] Degree of polymerization (DOP) and molecular weight (MW) estimated by fitting DH-DOP data to polymer scaling law as shown in Figure 7.2. [d] Phase behavior based on visual observation of 2% wt. IO. [e] MW and DOP determined by GPC. [f] MW and DOP obtained from the manufacturer.

The random copolymer (poly(AMPS-*co*-AA) (3:1) was expected to provide optimum Ca^{2+} tolerance due to its high sulfonate content, and was therefore identified as a candidate for covalent grafting to IO NPs as a stabilizer (see Section 7.4 below). Prior to covalent grafting to IO NPs, the phase behavior of (poly(AMPS-*co*-AA) (3:1) was studied in detail. In a manner analogous to the aforementionted poly(AMPS-*co*-AA), the 3:1 copolymer was synthesized by aqueous free radical polymerization, and its

composition was confirmed to match the monomer feed ratio by ^{1}H NMR spectroscopy. The molecular weight (MW) of the synthesized poly(AMPS-*co*-AA) was estimated by correlating the hydrodynamic diameter (D_H) to the degree of polymerization (DOP) of anionic copolymers of known MWs at pH = 8 in 1 M NaCl (Figure 7.2). The D_H of 10 nm for the poly(AMPS-*co*-AA) (3:1) translated to a DOP of approximately 1000 (750 AMPS:250 AA groups) and a MW of approximately 200 kDa (Table 7.1). A 2 mg/mL solution of poly(AMPS-*co*-AA) remained visually clear after 24 h at 90 °C in API brine and DLS analysis revealed a D_H of approximately 10 nm in API brine. Moreover, the poly(AMPS-*co*-AA) chains did not undergo significant aggregation or collapse, as evidenced by the minimal changes in D_H observed upon increasing the temperature from 25 to 90 °C. The observed maintenance of D_H at high temperature was not only consistent with the persistence of sufficient negative charge, but also was in good agreement with previous studies in which PSS and PAMPS copolymers in salt free solutions were shown to maintain their scattering profile in DI water up to 55 °C.[34] Additionally, macroscopically clear phases have been reported for poly(AMPS-*co*-acrylamide) copolymers in 3% $CaCl_2$ up to 100 °C.[18,22,33,35] Overall, the high acidity and hydrophilicity of the AMPS groups in poly(AMPS-*co*-AA) promoted hydration and reduced Ca^{2+}-affinity, providing excellent solvation even in the presence of PAA. The detailed characterization of poly(AMPS-*co*-AA) in highly concentrated API brine at 90 °C provided a basis for understanding its behavior as a stabilizer when grafted on NPs.

7.3 Ca^{2+}-Mediated Adsorption of Sulfonated Copolymers on IO

The copolymers poly(AMPS-*co*-AA) (1:6) were first adsorbed directly on the citrate coated IO nanoclusters. The acrylate functionalities are well known to form moderately strong charge transfer complexes with the Fe cations on the iron oxide

surface that are not covered with citrate ligands.[36] An excess of polymer (five-fold greater than IO concentration in % wt.) was used at pH = 7 to provide a sufficient driving force for polymer adsorption. Initially, we found that the adsorption levels of the copolymers on the iron oxide were quite low (~8% by weight by TGA). Thus, we introduced a method in which $CaCl_2$ was added to enhance the adsorption on the NPs, as shown in Figure 7.3a. Our hypothesis was that the divalent Ca^{2+} ions would bridge the acrylate anions to the like-charged citrate ligands on the IO surfaces (Figure 7.3a). To tune the extent of polymer adsorption, the amount of $CaCl_2$ added was varied while keeping the concentration of poly(AMPS-*co*-AA) (1:6) and IO clusters constant at 5% wt. and 1% wt., respectively (Figure 7.3b and Table 7.2). When the polymer was adsorbed in the absence of $CaCl_2$ and in 1% wt. $CaCl_2$, IO clusters were not stabilized in API brine (Figure 7.3b and Table 7.2), suggesting an insufficient amount of polymer on the surface. Thermogravimetric analysis (TGA) revealed that the organic content of IO clusters increased from 8% for citrate IO to only 13% with 1% $CaCl_2$ (Figure 7.3c-i, Table 7.2). To strengthen the binding of the polymer to the surface, the $CaCl_2$ concentration was increased to $\geq$2% wt. Quantitatively, the organic content reached 21% at 2% wt. $CaCl_2$ and to 32% at 10% wt. $CaCl_2$. These polymer levels were found to be sufficient for stabilization of the IO nanoclusters in API brine at pH values ranging from 2 through 10. To our knowledge, polymer-stabilized metal oxide particles in this size range have not previously been reported at high Ca^{2+} levels or in API brine. A plot of the organic content observed by TGA against the molar ratio of Ca^{2+} to acrylic acid content of polymer (poly(AMPS-*co*-AA) (1:6)) is shown in Figure 7.3c for two types of IO nanoclusters with either high or low citrate coverage. Each curve was fit with a Langmuir isotherm. The saturation percentages of organic material for the high and low citrate particles were calculated from the isotherm fits and were found to be 42.3 and 33.5%, respectively. The

corresponding equilibrium constants, K, were calculated to be K = 1.3 and 0.7, suggesting that a greater degree of polymer adsorption occurred with the high citrate level particles. The amount of polymer adsorbed was observed to increase rapidly up to $[Ca^{2+}]/[COO^{-}]_{poly}$ = 1 and eventually reached a plateau at higher concentrations. With greater quantities of Ca^{2+}, the amount of organic material adsorbed on the IO increased by up to a factor of 4. Furthermore, as shown in Figure 7.3b the aforementioned increase in added Ca^{2+} was necessary to overcome the repulsion between the polymer and IO to achieve sufficient polymer coating for stabilizing dispersions of the NPs in API brine. The adsorption increased markedly by bridging of Ca^{2+} ions to the carboxylate groups on the copolymer and citrate at high $[Ca^{2+}]/[COO^{-}]_{poly}$ ratios, as seen previously[28c,37] This bridging becomes stronger as the citrate density increases on the IO surface, for a given $[Ca^{2+}]/[COO^{-}]_{poly}$ ratio as shown in Figure 7.3. Thus, the presence of concentrated Ca^{2+} was essential for producing sufficient polymer coating.

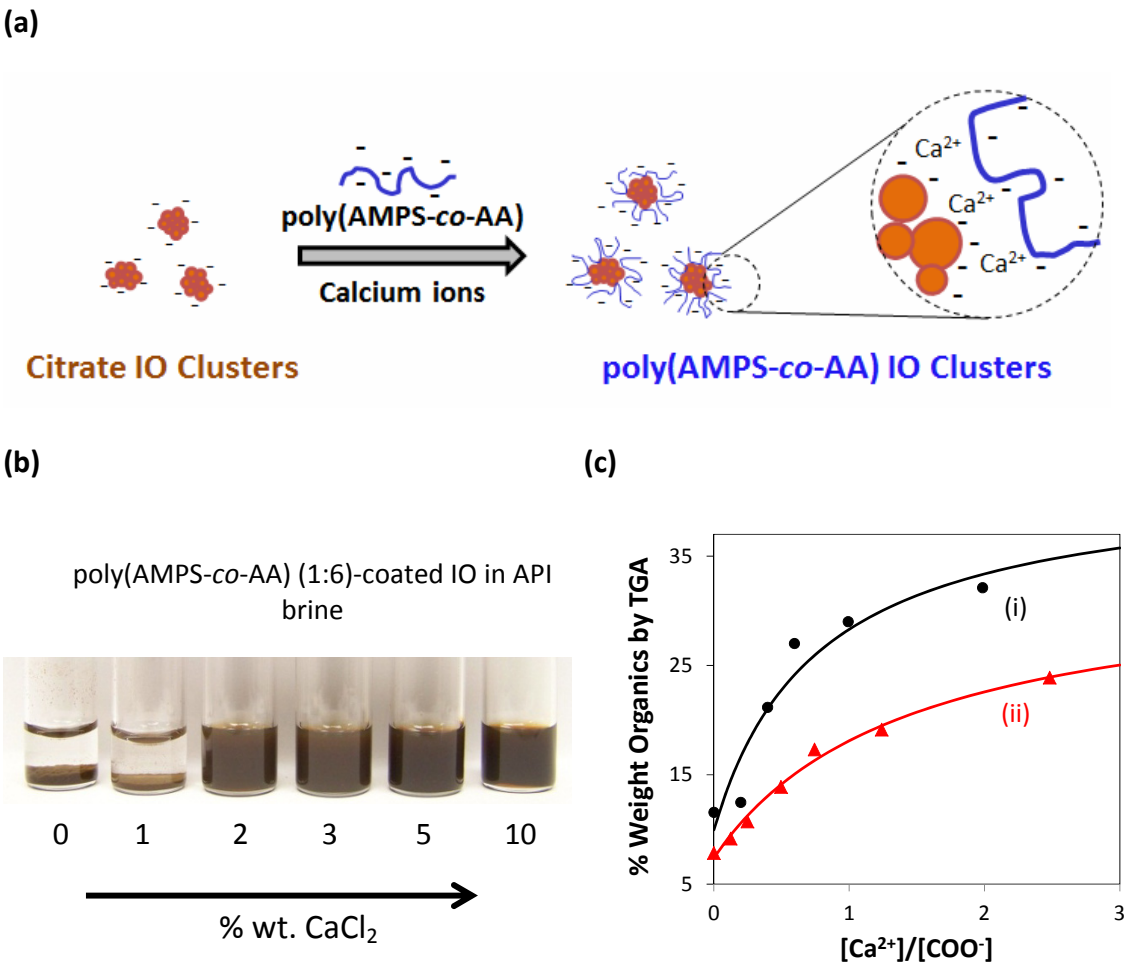

Figure 7.3: (a) Schematic of Ca^{2+}-mediated coating of anionic poly(AMPS-*co*-AA) polymers on negatively-charged citrate iron oxide (IO) nanoclusters. (b) Effect of the varying $CaCl_2$/poly(AMPS-*co*-AA) ratio during coating on the colloidal stability of IO clusters (0.2 % wt; pH = 8) in API brine after 1 day as evidenced by (c) Plot of % wt. organics measured by TGA versus the $[Ca^{2+}]/[COO^-]$ molar ratio for two different citrate IO particles: (i) high citrate (8% wt. TGA) and (ii) low citrate IO clusters (5% wt.TGA), fit to Langmuir isotherms.

The concept of adsorbing polymers using Ca^{2+} bridging was extended to a wide variety of poly(AMPS-*co*-AA) copolymers (Table 7.2) in addition to poly(AMPS-*co*-AA) (1:6). By varying the polymer and $CaCl_2$ concentrations when poly(AMPS-*co*-AA) (1:1)-212 kDa was used as a coating, adsorption of 16% - 22% wt. organic material was

observed, and led to stability in API brine. Eventually, when the organic content was reduced to 14%, the resulting dispersion was no longer stable. Under the same coating conditions (5, 1, and 5 % wt. polymer, iron oxide and $CaCl_2$, respectively) but with a lower MW poly(AMPS-*co*-AA) (1:1)-52, the organic content reached 25%, and stable dispersions were again formed. When a polymer of intermediate composition was used, poly(AMPS-*co*-AA) (1:4), an organic content of 21% wt. was sufficient to provide colloidal stability in API brine. However, when no Ca^{2+} was added, the polymer loading was again low and the particles did not form a stable dispersion, as was observed for the poly(AMPS-*co*-AA) (1:6) coating.

For a given coating condition (5% polymer, 1% IO, 5% $CaCl_2$) the amount of adsorbed polymer was expected to depend on the monomer ratio $[COO^-]/[SO_3^-]$ as well as the chain D_H (or the degree of polymerization) (Table 7.1), which together govern the number of acrylic acid attachment groups per polymer chain. As seen in Table 7.2, both poly(AMPS-*co*-AA) (1:1) polymers displayed lower adsorption (22% and 25% wt. organics) in comparison to poly(AMPS-*co*-AA) (1:6) (29% wt.). The poly(AMPS-*co*-AA) (1:4) exhibited even lower polymer adsorption (21% wt.) than the poly(AMPS-*co*-AA) (1:1) copolymers despite its greater $[COO^-]/[SO_3^-]$ ratio. However, with its small D_H the number of available COO^- groups per chain of poly(AMPS-*co*-AA) (1:4) was the lowest among all of the polymers investigated and therefore the polymer likely did not have enough attachment sites for favorable polymer adsorption.

Coating	Coating Conditions (% wt)			Stability in API at 25 °C	D_H[b] (nm)	% Organics[c]
	Polymer	Iron Oxide	$CaCl_2$			
Citrate	Before polymer coating			No	52[d]	8
poly(AMPS-*co*-AA) (1:6)	5	1	0	No	90	12
	5	1	1	No	228	13
	5	1	2	Yes	148	21
	5	1	3	Yes	177	27
	5	1	5	Yes	154[d]	29
	5	1	10	Yes	137	32
poly(AMPS-*co*-AA) (1:4)	5	1	0	No	73	-
	5	1	5	Yes	127[e]	21
poly(AMPS-*co*-AA) (1:1)-212	5	1	5	Yes	146[d]	22
	5	1	2	Yes	-	19
	2	1	0.8	Yes	-	16
	0.5	0.1	0.5	No	86	14
poly(AMPS-*co*-AA) (1:1)-52	5	1	5	Yes	98[e]	25

Table 7.2: Coating various poly(AMPS-*co*-AA) polymers on citrate-iron oxide (IO) nanoclusters, and their stability in API brine at 25 °C, hydrodynamic diameters (D_H) at 25 °C, and organic content by TGA. [a] Polymer adsorption conducted at pH = 7 and 90 °C for 60 minutes. [b] Hydrodynamic diameters were measured by DLS at 25 °C in DI water. [c] The percentage of organic content was measured by TGA. [d] The D_H was obtained from an average of 3 or more experiments. [e] The D_H was obtained from an average of 2 experiments.

To complement the experiments with AMPs containing copolymers, results are shown in Table 7.3 for a block copolymer poly(SS-*b*-AA) adsorbed onto low-citrate IO clusters. Adsorption of the copolymer in the absence of $CaCl_2$ did not increase the surface

organic content and unsurprisingly did not result in stable dispersions. Similarly, when an insufficient amount of polymer (0.2% wt.) was added during the coating process with $CaCl_2$ present, the resulting particles were unstable in API brine. However, higher poly(SS-*b*-AA) concentrations (0.5% and 2%) and the addition of 5% wt. $CaCl_2$ led to colloidal stability in API brine with 15% organic content adsorbed on the surface. For a commercial alternating copolymer poly(styrenesulfonate-*alt*-maleic acid) (poly(SS-*alt*-MA)) coating, the dispersions were always unstable in API brine, despite a reasonable organic content (24%). The observed instability with the poly(SS-*alt*-MA) coating was likely due to the phase behavior of maleic acid, which is more sensitive than acrylic acid to the presence of mono- and divalent cations as it is capable of chelation and thus displays a higher cation binding affinity.[38]

The strength of the Ca^{2+}-mediated adsorption was tested by dispersing IO clusters in concentrated NaCl brine, without any free Ca^{2+} ions in the solution. Remarkably, all of the IO dispersions were found to be stable in NaCl (8% wt.) and displayed D_{HS} that were close to those measured in API brine. Thus the Na^+ ions did not appear to break the Ca^{2+} bridges that held the polymer on the surface. As a further test to assess strength of polymer adsorption, a 2% wt. dispersion of poly(AMPS-*co*-AA) (1:6)-coated-IO was diluted to 0.01% wt. IO in 8% NaCl and equilibrated for a day in an attempt to drive polymer desorption. After separating IO clusters by ultracentrifugation and discarding the supernatant, IO nanoclusters were again subjected to the same equilibration (in 8% wt. NaCl) and separation (ultracentrifugation) procedure amounting to a 40,000-fold dilution. The resulting IO clusters were not only found to be stable in API brine, but retained most of the adsorbed polymer (80% of original organic content by TGA). In comparison, 57% of the polyacrylic acid attached directly to iron oxide NPs was lost after a similar desorption test[7b] without the use of Ca^{2+} bridging. The magnetic properties of the IO

clusters were preserved as evidenced by similar magnetization values (64 - 66 emu/g-Fe_3O_4) before and after polymer coating. These magnetization values are comparable with those for similar polymer-coated IO NPs prepared by the co-precipitation route.[7a]

Coating	**Coating Conditions** (% wt.)[a]		**Stability in API**	**% Organics**[b]
	Polymer	$CaCl_2$		
poly(SS-*b*-AA) (2.4:1)[c]	2	0	No	9
	2	5	Yes	15
	0.2	5	No	10
	0.2	10	No	11
	0.5	5	Yes	15
poly(SS-*alt*-MA) (3:1)	5	5	No	24
	5	2	No	---

Table 7.3: Coating for poly(SS-*b*-AA) (2.4:1) and poly(SS-*alt*-MA) (3:1) polymers on citrate-iron oxide (IO) nanoclusters, and their stability in API brine at room temperature and organic content. [a] Polymer adsorption conducted at pH = 9 and 90 °C for 60 minutes. [b] The percentage of organic content was measured by thermogravimetric analysis. [c] The experiments with poly(SS-*b*-AA) (2.4:1) were performed using low citrate platform IO particles.

7.4 COLAVENT GRAFTING OF SULFONATED COPOLYMERS TO IO NPS

To covalently attach the synthesized poly(AMPS-*co*-AA) copolymers to the surfaces of the IOs, we turned to the 'grafting-to' approach,[13f,29d,30b,39] which generally enables direct attachment of pre-formed copolymers with desired molecular weight and well-defined composition. This approach circumvents the limitations associated with 'grafting-from' approaches,[7b,29d,40] including the need for surface-grafted initiators, exogenous catalysts and, in many cases, inert atmospheres.[8] Poly(AMPS-*co*-AA) (3:1)

was grafted to amine-functionalized IO NPs by condensing the carboxylate groups on the polymer with the IO surface amine groups, as catalyzed by 1-ethyl-3-(3-dimethylaminopropyl)carbodiimide (EDC) (Figure 7.4a). The surface amine groups were installed by conjugation of pre-formed IO NPs with (3-aminopropyl)triethoxysilane (APTES) and confirmed by the following results: (i) a positive electrophoretic mobility of $+1.9 \times 10^{-8}$ $m^2/(V\text{-sec})$ at pH = 6 (Table 7.4), (ii) the presence of 7% wt. organics by thermogravimetric analysis (Table 7.4) and (iii) FTIR spectroscopy, which revealed the expected peaks corresponding to Si-O (1070 and 1150 cm^{-1}), N-H (1622, 1387, and 957 cm^{-1}) and C-H (2980 cm^{-1}) moieties. Analysis by transmission electron microscopy (TEM) revealed that ~50 nm diameter nanoclusters (APTES IO) were composed of primary IO NPs with a mean diameter of 8 nm (Figure 7.4b). Powder XRD patterns of both APTES and poly(AMPS-*co*-AA) grafted IO NPs (Figure 7.4c) matched well with magnetite crystal phase (ICDD card No. 19-0629) with a crystallite size of 8 nm by Scherrer analysis that agrees with the mean primary particle diameter by TEM.[41] A D_H of 55 nm was measured for the APTES IO (Figure 7.4d and Table 7.4), which was in good agreement with the cluster diameter observed by TEM and was consistent with the small size of the aminopropyl groups on the surface (< 1 nm).

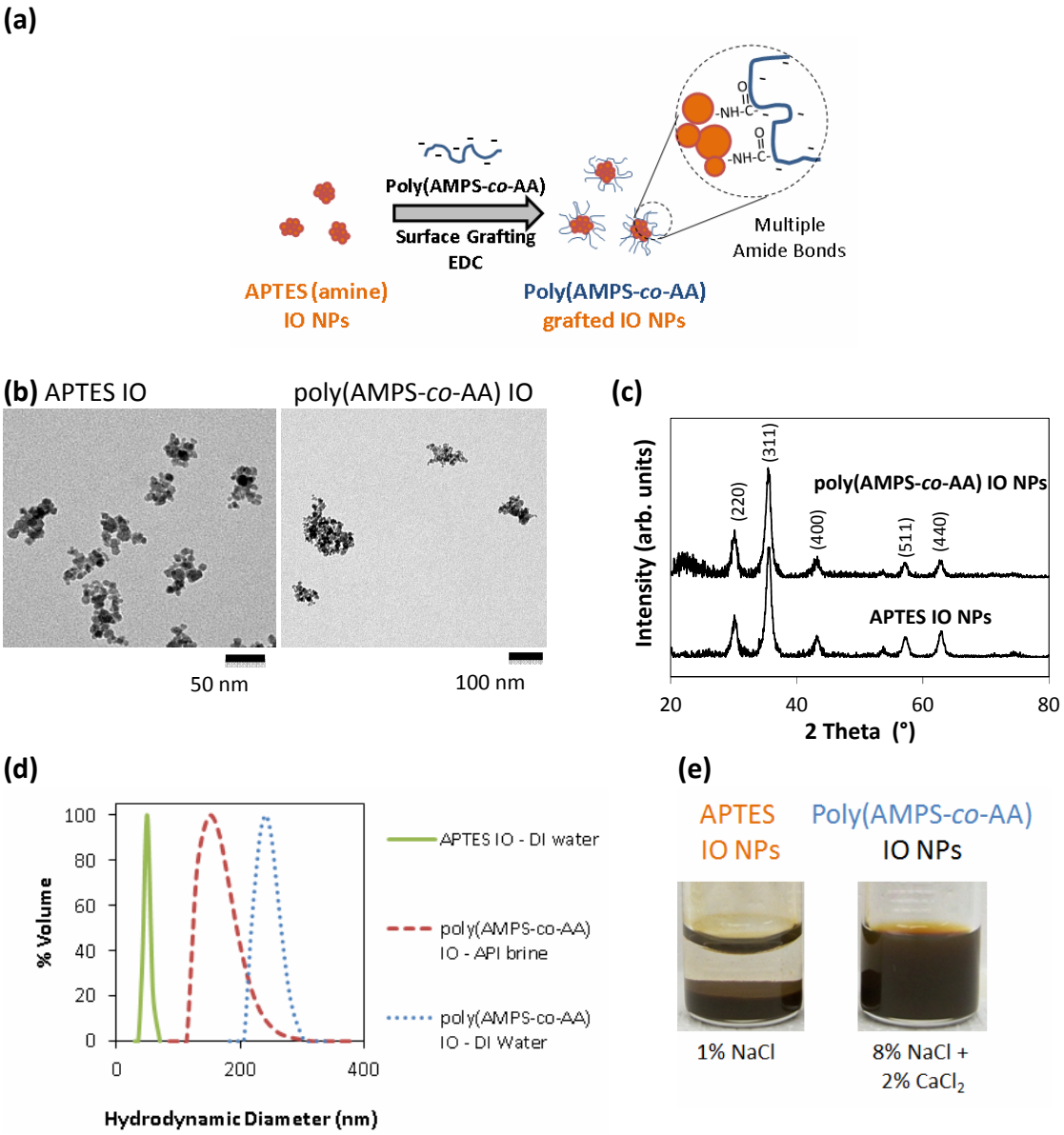

Figure 7.4: (a) Schematic of poly(AMPS-*co*-AA) multi-point grafting to APTES IO NPs via amidation. (b) TEM images of APTES IO NPs (left) and poly(AMPS-*co*-AA) grafted IO NPs (right); (c) Powder XRD pattern of poly(AMPS-*co*-AA) grafted IO and APTES IO NPs; (d) Volume weighted D_H distribution of APTES IO NPs in DI water, and poly(AMPS-*co*-AA) grafted IO NPs in DI water and API brine at pH = 8; (e) Photographs of dispersions of APTES IO in 1% NaCl and poly(AMPS-*co*-AA) grafted IO NPs in API brine.

Property	APTES IO NPs	poly(AMPS-*co*-AA) grafted IO NPs
Hydrodynamic diameter D_H [nm]	55 ± 7[a, b]	165 ± 24[a, c]
Electrophoretic mobility μ [10^{-8} m^2/(V-sec)]	+1.9 ± 0.3 [a] (pH = 6)	- 2.8 ± 0.2 [a] (pH = 8)
Magnetic Susceptibility of IO liquid dispersion at 700 Hz (SI units)	0.105 (2.1% wt. IO)	0.083 (1.7% wt. IO)
Magnetic Susceptibility/g-Fe (SI units)[d]	7.0	6.8

Table 7.4: Summary of colloidal and magnetic properties of IO nanoclusters before and after poly(AMPS-co-AA) grafting. [a] Reported value is the average of five independent experiments. [b] DH of APTES IOs measured in DI water. [c] DH of poly(AMPS-co-AA) grafted IOs measured in API brine. [d] Susceptibility of ~2% wt. IO dispersion measured in DI water and converted to SI units (/g-Fe).

The covalent grafting of the anionic poly(AMPS-*co*-AA) to the cationic amine surface at pH = 6 was expected to be favorable by the electrostatic attraction at low graft densities; however further grafting should be inhibited as the graft density increases the negative charge in the brush layer. The grafting procedure was therefore performed in the presence of NaCl to screen the charges. After grafting with anionic poly(AMPS-*co*-AA), the electrophoretic mobility was reversed to a negative value of -2.8×10^{-8} m^2/(V-sec) at pH = 8 and the organic content increased to 15% wt, as measured by TGA (Table 7.4). After grafting, the volume-based magnetic susceptibility of the liquid dispersion changed slightly (from 7 to 6.8 /g-Fe; Table 7.4), and the saturation magnetization was also essentially unchanged at ~90 emu/g-Fe, indicating that the magnetic properties of IO NPs were not significantly affected by the grafting process. Additionally, the D_H of the IO particles in DI water increased from 55 ± 7 to 258 ± 34 nm, as determined by DLS and TEM (Figure 7.4b,d). The increase was much larger than expected from the grafting of poly(AMPS-*co*-AA) with a D_H of only 10 nm. Presumably, the grafting process led to

aggregation of clusters, and/or to a process such as Ostwald ripening, whereby primary particles diffuse from smaller to larger clusters to lower the interfacial energy. Furthermore, the size of clusters may have been influenced by short-ranged attraction versus long-ranged repulsion between primary particles, which is generally mediated by the polymer.[42]

7.5 COLLOIDAL STABILITY OF COPOLYMER-STABILIZED IO NPS

7.5.1 Colloidal stability of IO NPs with adsorbed copolymers

To gain further insight into the structural properties and colloidal stability of the synthesized IO NPs, their D_Hs and zeta potentials were measured after coating under the standard condition (5% polymer, 1% IO and 5% $CaCl_2$), and are presented in Table 7.5. In DI water, the D_H of the clusters always increased significantly after polymer adsorption (Table 7.2 and Table 7.4). The observed increase in D_H was greater than the polymer D_H (Table 7.1) and thus indicated that aggregation of the IO clusters occurred during the coating process. For a given polymer composition of poly(AMPS-*co*-AA) (1:1), the size of the clusters increased with an increase in MW from 52 to 212 kDa significantly in DI water but only a small amount in API brine. The higher MW polymer may have increased the size by bridging flocculation. However, even for the lower MW 1:6 and 1:4 polymers, significant increases in size were observed indicating other growth mechanisms were operative. For example, the particles underwent massive flocculation during polymer coating, and the aggregates may not have fully reverted to individual particles upon sonication. Furthermore, given that only van der Waals forces hold the clusters together weakly before polymer adsorption, the clusters are dynamic[43] and the sizes may vary when the colloidal forces are perturbed by interactions with the polymer during the coating process. Once the polymer is adsorbed, it may help to bind the primary

particles together quench the cluster size and increase the cluster stability. The change in size may also reflect Ostwald ripening whereby primary particles migrated to a fraction of larger aggregates produced during the flocculation step upon polymer coating.[44]

Coating[a]	**Hydrodynamic Diameter D_H** (nm)		**Zeta Potential** (mV)[a]
	DI water	API brine	
Citrate	52 ± 12%	Unstable	- 31 ± 13%
poly(AMPS-*co*-AA) (1:6)	154 ± 16%	139 ± 5%	-37 ± 9%
poly(AMPS-*co*-AA) (1:4)	127 ± 46%	169 ± 35%	-36 ± 7%
poly(AMPS-*co*-AA) (1:1)-212kDa	146 ± 17%	126 ± 19%	- 42 ± 5%
poly(AMPS-*co*-AA) (1:1)-52kDa	98 ± 17%	110 ± 18%	- 25 ± 7%

Table 7.5: Summary of the colloidal properties of citrate IO clusters coated with poly(AMPS-*co*-AA) in aqueous media at room temperature. All listed poly(AMPS-*co*-AA) were adsorbed on IO under standard conditions : 5% wt. $CaCl_2$, 5% wt. polymer and 1% wt. IO at pH = 7, 90 °C for 60 minutes. [a] Zeta potential is reported at pH = 8 and 10 mM KCl.

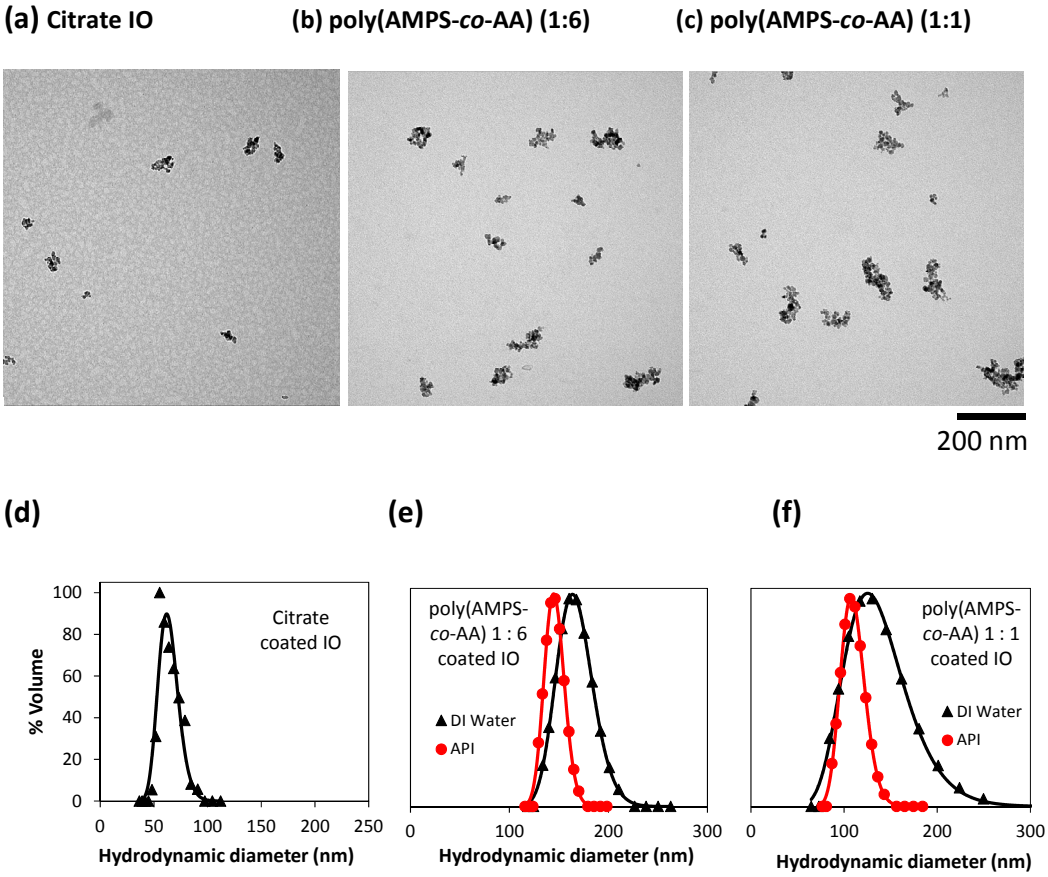

Figure 7.5: TEM images (a-c) and hydrodynamic diameter (D_H) distribution in DI water and API brine (d-f) of citrate IO, poly(AMPS-*co*-AA) (1:6)-coated and poly(AMPS-*co*-AA) (1:1)-212-coated IO. Average TEM size was determined by Image J software analysis for ~50 clusters by calculating circular diameters with equivalent surface area as the clusters. The vol. weighted TEM diameters were found to be 53 ± 10 nm, 75 ± 21 and 93 ± 22 nm, for citrate IO, poly(AMPS-*co*-AA) (1-6) and poly(AMPS-*co*-AA) (1-1)-212, respectively.

Despite the significant increase in D_H after polymer coating in DI water, the values were similar in DI water and API brine, essentially within experimental error (Table 7.5). Thus, the adsorbed polymers provided electrosteric stabilization against aggregation even at these extremely high salinity values. As expected due to differences in polymer size, the measured D_H was significantly smaller for the poly(AMPS-*co*-AA)

(1:1) 52 kDa than for the corresponding 212 kDa polymer. According to TEM images the volume-weighted core diameters of initial citrate IOs increased after coating with poly(AMPS-*co*-AA) (1:6) and poly(AMPS-*co*-AA) (1:1)-212 (Figure 7.5a-c). The measured mean D_{HS} therefore were subject to contributions both from changes in the core and from the thickness of the adsorbed polymer. The zeta potentials (measured in 10mM KCl at pH = 8) of all the polymer-coated IO clusters were between ζ = -36 and -42 mV, and were consistent with previously reported values for similar IO clusters[22], with the exception of poly(AMPS-*co*-AA) (1:1)-52 which was slightly less negative (ζ = -25 mV; Table 7.5).

The stability of the poly(AMPS-*co*-AA) coated IOs even in the presence of Ca^{2+} (API brine) is likely due to the solvation of the polymer chains in high $CaCl_2$ solutions.[18] The classic concept of Napper[6b] is that stability of polymer-coated colloids, namely the critical flocculation temperature or salinity may be correlated with the phase behavior of the polymer. Therefore, the poly(AMPS-*co*-AA) copolymers, which were found to be soluble in API brine, were extended on the surface of the nanoclusters and provided steric stabilization when adsorbed at sufficient surface coverages. The low Ca^{2+} binding affinity of AMPS prevented intrapolymer collapse, and translated to an extended conformation of PAMPS copolymers on particles, which allowed for steric stabilization of the IOs in API brine. As discussed earlier, the strong acidity of the AMPS group, the greater conformational freedom from the relatively longer side chain[18,20] and the hydrophillicity of AMPS (due to amide group)[21] contributed to its high tolerance to precipitation in the presence of Ca^{2+} ions.

Having demonstrated the stability of the IO NPs in API brine, efforts were directed towards testing the persistence of the same dispersions in extremely high NaCl and $CaCl_2$ concentrations (up to 20% wt.). Both poly(AMPS-*co*-AA) (1:6) and

poly(AMPS-*co*-AA) (1:1)-212 IOs were investigated at two pH values (pH = 5 and 8). These pH values were chosen to study the effect of protonated (pH = 5) and deprotonated (pH = 8) acrylic acid groups. Remarkably, both samples were stable in 20% wt. NaCl (3.4 M) at both pH = 5 and 8 for at least 3 months. Even the relatively small fraction of PAMPS in poly(AMPS-*co*-AA) (1:6) was sufficient for long term stability in 20% wt. NaCl. When analogous studies were conducted with $CaCl_2$, PAA homopolymer was also included as a coating to assess the need for the PAMPS component (Figure 7.6). The IO particles coated with PAA[7c] precipitated at both pH values and at all tested $CaCl_2$ concentrations, as expected, given the high binding affinity of PAA for Ca^{2+}. However, when poly(AMPS-*co*-AA) (1:1) was used as the coating, the IO clusters were stable in 20% wt. $CaCl_2$ at both pH = 5 and 8 for at least 3 months due to the high proportion of Ca^{2+}-tolerant AMPS.

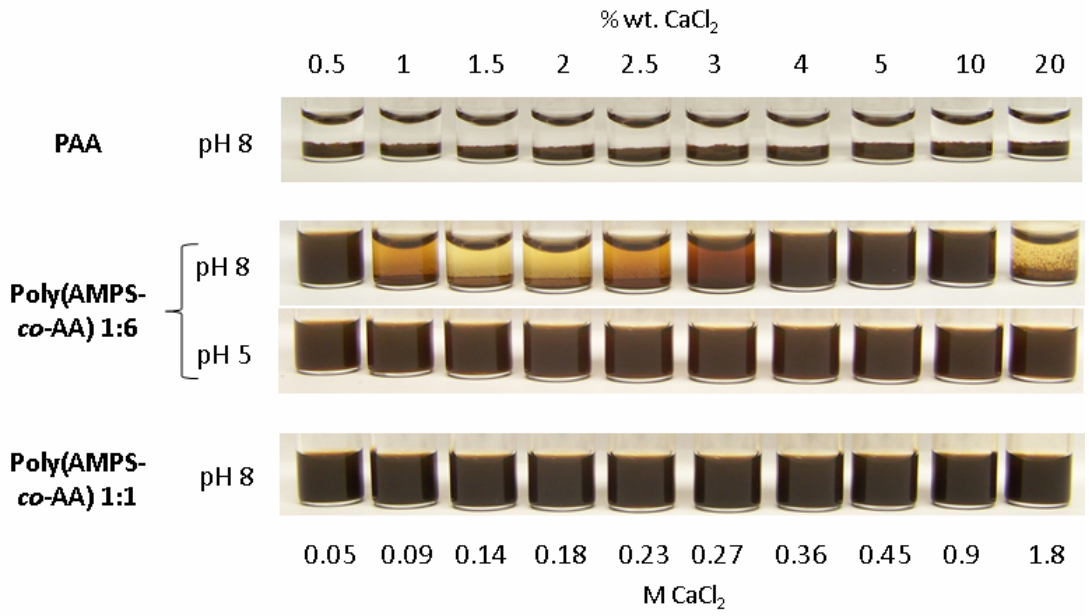

Figure 7.6: Stability of IO coated with PAA, poly(AMPS-*co*-AA) (1:6) and poly(AMPS-*co*-AA) (1:1)-212 after 1 day in $CaCl_2$ solutions of various concentrations (indicated) at the given pH values. Both PAA and poly(AMPS-*co*-AA) (1:1) coated IO clusters at pH = 5 (not shown) were similar to the above dispersions at pH = 8.

Given that the sulfonated copolymers adsorbed onto IO NPs provided room temperature stability in API brine and more concentrated $CaCl_2$ and NaCl brines, efforts shifted towards testing the dispersion stability in API brine at elevated temperatures. As shown in Figure 7.7a, all of the poly(AMPS-*co*-AA)-coated IO cluster dispersions were stable at room temperature in API brine, however only the poly(AMPS-*co*-AA) (1:1)-coated IOs were stable at 90 °C. Both poly(AMPS-*co*-AA) (1:6)- and poly(AMPS-*co*-AA) (1:4)-coated IOs precipitated in less than 30 min at 90 °C. The long term colloidal stability of poly(AMPS-*co*-AA) (1:1)-212-coated IO was tested in API brine at pH = 6 and 8 (Figure 7.7b). Dispersions kept at pH = 8 remained stable for up to 18 days, while those at pH = 6 were, remarkably, stable for up to one month. To the best of our knowledge this long term stability is unprecedented for a NP dispersion in such

concentrated brine at elevated temperature. The D_{HS} remained essentially unchanged at 140-150 nm over the measured period of 19 days (Figure 7.7c). Similar stability studies at 90 °C with lower MW poly(AMPS-*co*-AA) (1:1)-52-coated IOs (not shown here) resulted in stability for 10 days at pH = 6, and 8 days at pH = 8, after which the dispersions flocculated. Again, during the period of stability, the D_{HS} were maintained at ~ 100 nm. As an additional indicator of this long term stability, the D_{HS} of poly(AMPS-*co*-AA)(1:1)-212- and poly(AMPS-*co*-AA)(1:1)-52-coated IOs were measured in API brine at 74 °C (max. limit of Zeta PALS instrument). No significant change in the diameter was observed over the entire monitored duration of 1.5 h (Figure 7.7d), further confirming the excellent stability provided by poly(AMPS-*co*-AA) (1:1).

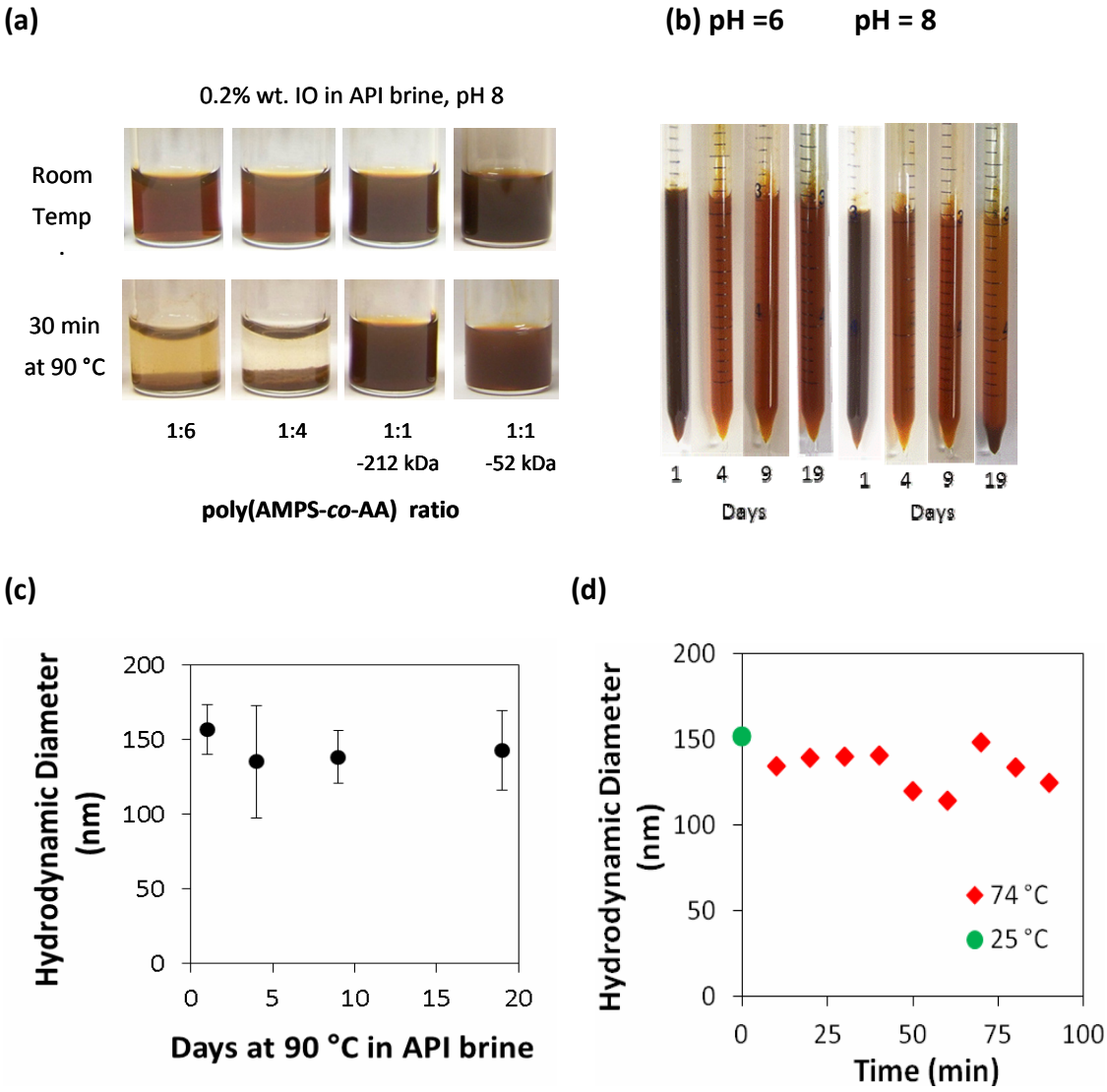

Figure 7.7: (a) Colloidal dispersions of IO clusters in API brine at room temperature and at 90 °C; (b) Long term colloidal stability of poly(AMPS-*co*-AA) (1:1)-212 coated IO at 90 °C in API brine at two pH values – pH = 6 and pH = 8; (c) Hydrodynamic diameters of of poly(AMPS-*co*-AA) (1:1)-212 coated IO at 90 °C in API brine at pH = 6; (d) Hydrodynamic diameters of poly(AMPS-*co*-AA) (1:1) 212-coated IO at 74 °C remained unchanged within experimental error.

As discussed above, the association of polyacrylic acid to Ca^{2+} is an entropically driven process due to release of water of hydration.[21] Therefore, it is not surprising that

with an increase in temperature the entropy driven association of acrylic acid to Ca^{2+} also increases,[45] causing precipitation of particles coated with PAA-containing polymers. For coatings with higher AA content such as poly(AMPS-*co*-AA) (1:6) and poly(AMPS-*co*-AA) (1:4) particle precipitation was more prevalent at higher temperatures due to intraparticle polymer collapse and interparticle Ca^{2+} bridging. The increased stability of the poly(AMPS-*co*-AA) (1:1) IOs relative to the poly(AMPS-*co*-AA) (1:6) IOs was largely due to the higher AMPS content. The high temperature solubility of AMPS in $CaCl_2$ ensured greater chain solvation and extended polymer conformation to favor stabilization. Finally, steric stabilization in API brine at 90 °C was also observed with the poly(SS-*b*-AA)-coated IO nanoclusters, which was consistent with previous observations that PSS is soluble in Ca^{2+} solutions at high temperatures.[18]

7.5.2 Colloidal stability of IO NPs with grafted copolymers

The poly(AMPS-*co*-AA) (3:1) grafted IO NPs were found to form stable dispersions in API brine at room temperature, whereas before grafting the APTES IO aggregated in only 1% NaCl (Figure 7.2e). Notably, the dispersions appeared uniform, visually stable and did not settle, thus demonstrating the first example of stabilization of polyelectrolyte coated inorganic NPs at high divalent salinity. Moreover, the dispersions maintained their stability at elevated temperature (90 °C), a feat which has only rarely been reported for metal oxide particles.[7a,14] The stability of the dispersions suggested that the polymer chains remained solvated in the brine and provided excellent steric stabilization. The exceptional stability was corroborated by measuring the D_H in API brine at room temperature and at 90 °C over an extended period of time (Figure 7.8). Notably, a decrease in D_H from 258 ± 34 nm in DI water to 165 ± 24 nm in API brine (Table 7.4) was observed, which may have been caused by an increased cluster density

due to weaker electrostatic repulsion between primary particles[40b] and/or reduced osmotic swelling.[46] Regardless, the D_H measured in API brine at 90 °C remained constant (D_H = 180-200 nm) over a period of 30 days, demonstrating that the clusters were exceptionally stable, and that only a negligible amount of aggregation occurred (Figure 7.8b). Together with the visual observations (Figure 7.8a), the high temperature DLS results confirmed that the grafted IO NPs exhibited remarkable colloidal stability in API brine at 90 °C for 1 month. To the best of our knowledge, this result is the first demonstration of long-term stability of inorganic NPs at elevated temperature and high divalent salinity.

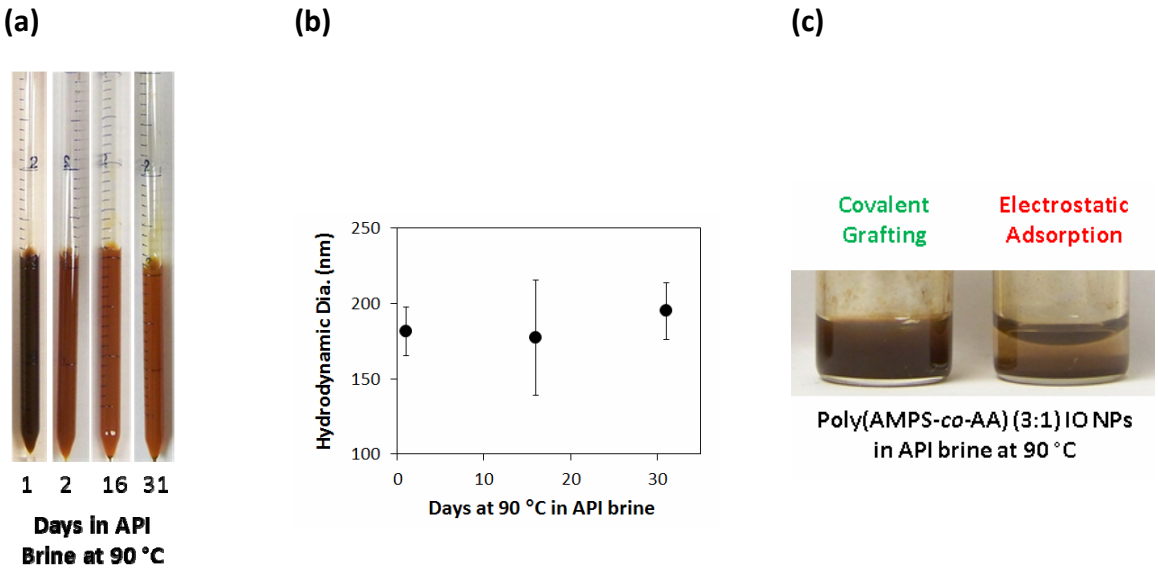

Figure 7.8: Poly(AMPS-*co*-AA) grafted APTES IOs were stable in API brine at 90 °C for 31 days, as evidenced by (a) visual inspection and (b) constant hydrodynamic diameters D_H in API brine. (c) After a 40,000-fold serial dilution in 1 M NaCl, poly(AMPS-*co*-AA) grafted APTES IO NPs remained stable at 0.2% wt. IO in API brine at 90 °C (left), whereas IO NPs with electrostatically attached poly(AMPS-*co*-AA) aggregated.

The remarkable stability of the poly(AMPS-*co*-AA) grafted IO NPs may be explained by established concepts in colloid chemistry. According to Napper[6b], the

colloidal stability of the poly(AMPS-*co*-AA) grafted IO NPs (Figure 7.8) at all salinities and temperatures may be anticipated given the limited collapse of the pure polymer. The total interaction potential between two polymer coated particles is a function of steric repulsion, electrostatic repulsion and van der Waals attraction. At high salinity (e.g., API brine), electrostatic interactions within the polyelectrolyte layer are screened by the ions and the brush may be considered as a neutral polymer.[7b,40c] The steric repulsion to the energy barrier comes from two distinct mechanisms: (i) osmotic repulsion between overlapping chains and (ii) entropy of elastic repulsion.[7b,47] Given that the morphology of the pure poly(AMPS-*co*-AA) did not significantly change in API brine, as observed by DLS, it is likely that the grafted chains on the IO nanoclusters were only partially collapsed, which made them especially effective at providing steric stabilization. Such steric stabilization has previously been reported with polyelectrolytes in NaCl brines at room temperature,[3a,7a,7b,48] however the resistance to divalent salts and high temperatures displayed by the poly(AMPS-*co*-AA) grafted IO NPs is unprecedented.

7.6 Adsorption of Copolymer-stabilized IO NPs on SiO_2

7.6.1 SiO_2 adsorption of IO NPs with adsorbed copolymers

The effects of the polymer coating (see Figure 7.1 for structures), nanocluster concentration, and pH on the equilibrium adsorption of IO nanoclusters on colloidal silica microspheres are summarized in Table 7.9. The % IO adsorbed quantifies the amount of adsorption relative to the initial concentration of IO in solution. When less than 10% of the initial IO was adsorbed, the uncertainty increased significantly given the small change measured in the supernatant. The equilibrium IO concentration and the specific adsorption are thermodynamic properties at equilibrium. The percent monolayer coverage

(% ML) is the adsorption level of nanoclusters compared to an ideal, 2-D close-packed monolayer of spheres.

The polymer coating on the nanoclusters provides steric repulsion between the nanoclusters and the silica as a barrier to adsorption, where more adsorbed polymer is expected to provide a larger barrier. Thermodynamically, this repulsion offsets the van der Waals and any specific attraction between the particles and the silica surface. The added steric repulsion with the polymer stabilizer is the key to minimizing adsorption of polymer-coated NPs at high salinity, despite the reduced double layer thickness.[7b] The polymer coatings were structurally varied in their constituent monomers, ratios of monomer units, and molecular weights, and each of these factors had an effect on the adsorption of the particles to silica. Overall, the poly(AMPS-*co*-AA) (1:1) 212 kDa polymer coating resulted in the highest silica adsorption with 2.58 mg-IO/m^2-silica at 0.085% w/v IO, representing a 1.3% ML (Table 7.9). Upon decreasing the IO concentration to 0.009% w/v IO, the lowest specific adsorption level was 0.16 mg-IO/m^2-silica displayed by the 77 kDa poly(AMPS-*co*-AA) (1:2)-coated clusters, which corresponded to 0.1% ML. A clear trend was not observed between the ratio of AMPS:AA at a fixed IO concentration (~0.01% w/v). However, the adsorption dropped from ~0.7 mg/m^2 for poly(AMPS-*co*-AA) (2:1)-coated nanoclusters to ~0.2 mg/m^2 for poly(AMPS-*co*-AA) (1:2) coated nanoclusters as the quantity of organics increased from 19% to 28%, respectively, which suggested to us that the amount of organic content on the particles was vital to minimizing adsorption. Furthermore, the specific adsorption at an IO concentration of approximately 0.2% w/v of the poly(AMPS-*co*-AA) (1:1) 52 kDa polymer which comprised 25% wt. of the IO was observed to be approximately 50% lower than that of the poly(AMPS-*co*-AA) (1:1) 212 kDa polymer which displayed a slightly lower polymer loading of 22% wt. The lower specific adsorption with the 52 kDa

polymer-coated nanoclusters also correlated with the smaller particle size (hydrodynamic diameter of 110nm vs. 142nm, respectively), which led to greater electrosteric repulsion relative to van der Waals attraction. However, the monolayer coverage of the two poly(AMPS-*co*-AA) (1:1)-coated particles was similar as the mass of particles constituting a monolayer is less for smaller diameter particles.

The poly(SS-*b*-AA) (2.4:1) coated particles that had a higher sulfonate content and a block copolymer architecture, but only 15% organic content (Table 7.9), displayed low levels of adsorption similar to poly(AMPS-*co*-AA) (1:1) (52 kDa), poly(AMPS-*co*-AA) (1:6) (46 kDa), and poly(AMPS-*co*-AA) (1:2) (77 kDa) at 0.01 % w/v IO in the initial solution. It is likely that in the block copolymer architecture, the sulfonate groups repelled the silica surface more effectively in high salinity, as they were separated from the more strongly adsorbing carboxylate groups. This structure places the stabilizing sulfonate groups towards the outer surface of the particles, which may reduce Ca^{2+} bridging of carboxylate groups, located near the iron oxide surface, to the silica surface. An increase in pH from pH = 8 to 10 resulted in nearly a 50% reduction in the adsorption of the 212 kDa poly(AMPS-*co*-AA) (1:1) coated particles by modifying the various ionic interactions between monomer groups, dissolved ions, and the silica surface.

Relatively few studies have examined NP adsorption on colloidal silica or glass beads. Wang et al. studied adsorption of bare 95 nm C_{60} fullerene aggregates on 360 μm diameter glass beads or Ottawa sand.[3b] The NP concentrations tested (0.0009-0.0012% w/v C_{60}) were two orders of magnitude lower than the highest NP concentration in this study (0.192 %w/v IO). The low adsorption of C_{60} in DI water (0.022-0.033 mg-C_{60}/m^2 or c.a. 0.03-0.04% ML) rapidly increased to 0.14-0.63 mg/m^2 or 0.18-0.79%ML in 1 mM $CaCl_2$ (ionic strength = 3 mM). In comparison, poly(AMPS-*co*-AA) (1:1)-212 coated IO nanoclusters displayed similar adsorption values 0.57-0.88 mg/m^2 (0.3-0.5%ML) with

600-fold higher salinity (API brine = 1.8 M ionic strength) at a higher 0.005-0.007% w/v IO due to the electrosteric stabilization provided by poly(AMPS-*co*-AA).

Coating	**Initial IO Conc.** (% w/v)	**% IO adsorbed**	**Equilibrium IO conc.** (% w/v)[a]	**Specific Adsorption of IO** (mg/m^2-silica)	**% Monolayer coverage**[b]
poly(AMPS-*co*-AA) (1:1), 212 kDa	0.01	33%	0.007	0.57	0.3%
	0.05	15%	0.043	1.27	0.7%
	0.05[5]	8%[c]	0.046[c]	0.71[c]	0.4%[c]
	0.10	15%	0.085	2.58	1.3%
	0.20	7%	0.185	2.56	1.3%
poly(AMPS-*co*-AA) (1:1), 52 kDa	0.01	12%	0.009	0.20	0.1%
	0.09	5%	0.087	1.72	1.5%
	0.20	4%	0.192	1.32	1.1%
poly(AMPS-*co*-AA) (1:6), 46 kDa	0.05	5%	0.047	0.46	0.2%
poly(AMPS-*co*-AA) (1:2), 77 kDa	0.01	10%	0.009	0.16	0.1%
poly(AMPS-*co*-AA) (2:1), 611 kDa	0.01	38%	0.006	0.66	0.3%
poly(SS-*b*-AA) (2.4:1), 40 kDa	0.01	20%	0.008	0.35	0.2%

Table 7.9: Adsorption at pH = 8 of a series of polymer-coated IO nanoclusters on colloidal silica microspheres in API brine (8% NaCl + 2% $CaCl_2$) before amine modification. [a] Observed experimental error in measured equilibruim IO conc. was ± 0.002 %w/v. [b] % monolayer coverage was calculated from specific adsorption (mg-IO/m^2) value by assuming: (i) 100% monolayer coverage to be equal to 2-D surface packing fraction of 0.74 (closest packed) of IO NP-clusters with hydrodynamic diamters (D_H) from Table 1 and (ii) IO volume fraction in the NPs is 50%. [c] Experiment performed at pH = 10.

Studies of NP adsorption using 1-D column flow experiments are more common than batch experiments, but very few have used high salinity brines. The retention of polymer-coated zero-valent iron (ZVI) NPs in brine (≤ 100mM NaCl or ≤ 40mM $CaCl_2$) on sandpacks was studied by Saleh et al.[49] and He et al..[50] Although a side-by-side comparison between column and batch adsorption data is complicated by additional particle removal mechanisms in a continuous flow configuration (e.g., hydrodynamic effects, pore-scale mechanisms), specific retention (mg/m^2) from the column studies will be compared qualitatively to adsorption from our batch study. Saleh et al.[48] studied ZVI particles coated with poly(methacrylic acid-*b*-methyl methacrylate-*b*-styrene sulfonate) copolymers on 300 μm silica sand at a low salinity of 100 mM NaCl and found specific retention of 0.029-0.035mg/m^2 with an injected iron concentration of 0.3% w/v. He et al.[49] studied ZVI particles coated with 90 kDa carboxymethyl cellulose (CMC) on 250-420 μm quartz sand at 40 mM $CaCl_2$ and found specific retention of 8.4 mg/m^2 with an injected iron concentration of 0.02 %w/v, which was much higher than the adsorption values in this study for unmodified polymer-coated IO nanoclusters. The high retention may be attributed in part to collapse of CMC chains due to high Ca^{2+} affinity of carboxylate groups in CMC that may be bridged to the substrate by strongly binding Ca^{2+}.

The same properties that facilitated colloidal stability of the IO NPs in API brine and at elevated temperature also resulted in low SiO_2 adsorption. The polymer chains likely exhibited an extended conformation from the IO surface due to high solubility of poly(AMPS-*co*-AA) in API brine. The extended chains, with a favorable Flory-Huggins parameter of < 0.5, provide electrosteric stabilization against IO nanocluster aggregation due to increased osmotic pressure when two polymer-coated IO nanoclusters approach each other. Similarly, the extended poly(AMPS-*co*-AA) chains also minimize adsorption

on silica, even at high salinity, given electrosteric repulsion with both osmotic and elastic contributions.[7,47]

7.6.2 SiO_2 adsorption of IO NPs with grafted copolymers

The batch adsorption technique allowed for rapid, high throughput measurement of equilibrium NP adsorption behavior relative to the measurement of NP retention in flow experiment in porous media,[3b] where additional effects of filtration[3a,48,51] and hydrodynamics may be present.[3c,52] The IO adsorption on silica microspheres was visually observed (Figure 7.9a) and quantified by measuring the change in IO concentration before and after equilibration (Figure 7.9b and Table 7.6). Experiments were conducted in either DI water or API brine, and after overnight equilibration at pH = 8, the settled silica microspheres were white in 0.05-0.1% w/v IO and lightly brown colored in 1.0% w/v IO. When measured in DI water, the difference between the initial and final concentration, reported as % IO adsorbed, was small (≤ 2%). Based on the volume of the solution and the surface area of silica, the calculated specific adsorption values were smaller than the experimental uncertainty and hence only upper bounds are reported. At the highest IO concentration (1% w/v) in DI water, the specific adsorption was < 1.1 mg-IO/m^2 silica. In API brine, the % IO adsorbed was modestly higher than in DI water. The calculated specific adsorption in API brine at the highest IO concentration of (1% w/v) was 1.0 ±2.1 mg/m^2 which corresponds to a very low NP monolayer coverage of 0.4%. In contrast, when the polymer was electrostatically adsorbed, 48% adsorption in API brine at 0.103% w/v IO equilibrium concentration was observed, which translated to a specific adsorption value of 16.6 mg/m^2 or 8.6% monolayer coverage.

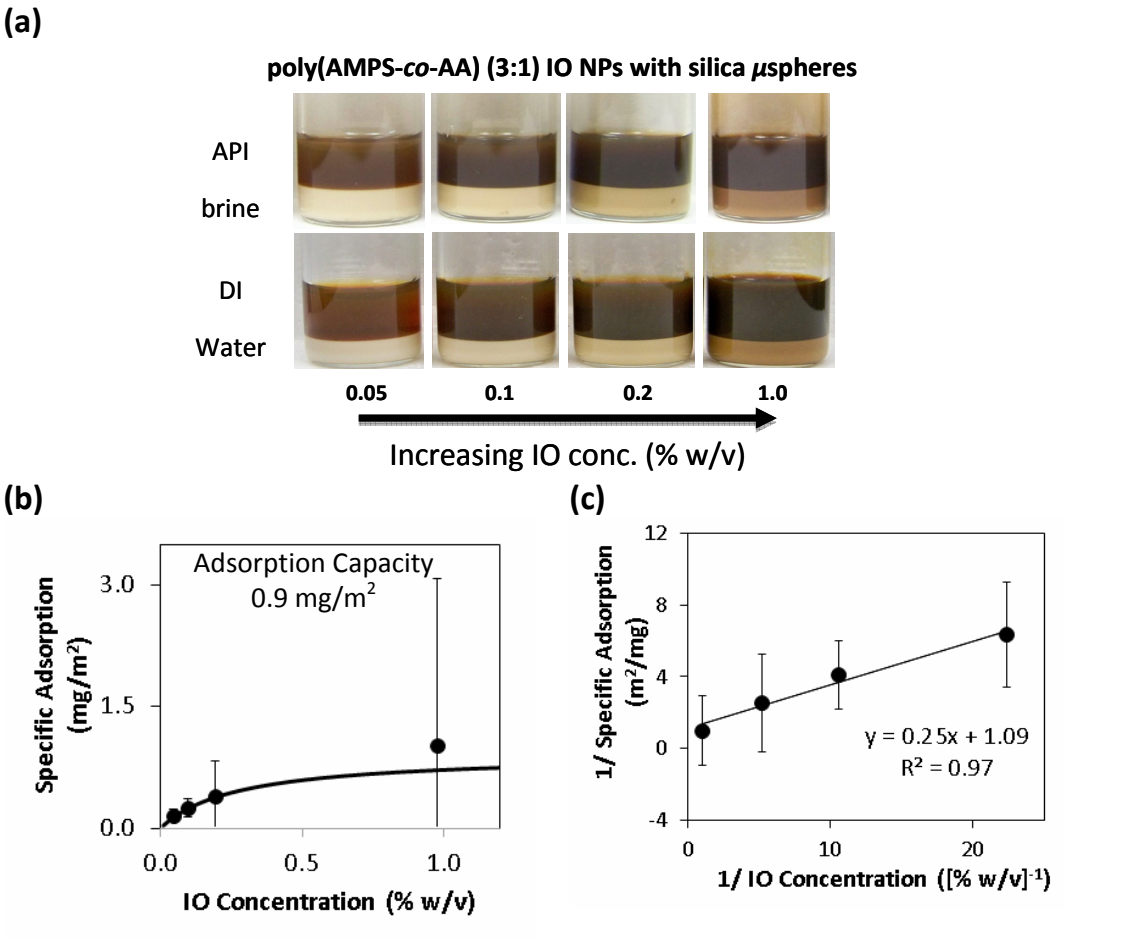

Figure 7.9: (a) Photographs of poly(AMPS-*co*-AA) grafted iron oxide (IO) nanoclusters in API brine (top) and DI water (bottom) displaying very low adsorption on silica at IO concentrations ranging from 0.05% to 1% w/v IO. Each sample vial contains 2 mL of IO dispersion at pH = 8 and 1 g of colloidal silica and was equilibrated for 16-20 h. IO adsorption isotherm data in API brine expressed (b) as fit to a Langmuir adsorption model in standard units and (c) inverse units.

Initial IO Conc. (% w/v)	**Medium**	**% IO Adsorbed**[b]	**Final Eq. IO Conc.** (% w/v)[b]	**Specific adsorption** (mg-IO/m^2)[b]	**% Monolayer**
0.1	DI water	2	0.098	< 0.04	< 0.03
0.2	DI water	2	0.197	< 0.11	< 0.05
1.0	DI water	1	1.00	< 1.1	< 0.4
0.05	API brine	7	0.047	0.16 ± 0.07	0.1
0.1	API brine	5	0.095	0.24 ± 0.11	0.1
0.2	API brine	4	0.192	0.4 ± 0.4	0.2
1.0	API brine	2	0.975	1.0 ± 2.1	0.4
0.2[c]	API brine	48[c]	0.103[c]	16.6 ± 1.3[c]	8.6[c]

Table 7.6: Adsorption of poly(AMPS-*co*-AA) IO nanoclusters on 8 μm colloidal silica microspheres in API brine and DI water at pH = 8 at varying IO concentrations. [a] The specific surface area of colloidal silica was measured to be ~0.58 m^2/g. [b] Average of four independent experiments; uncertainty in specific adsorption based on error propagation analysis. [c] Control sample data at 0.2% w/v initial IO conc. is also shown as an example of IOs with high adsorption where insufficient polymer grafting leads to poor stabilization. Adsorption was conducted with 0.2 g of silica and 2 mL of IO NP dispersion.

7.7 CONCLUSIONS

In summary, a variety of sulfonated copolymers have been developed as stabilizers for superparamagnetic IO NPs to prevent aggregation under harsh salinity and temperature conditions and minimize adsorption on SiO_2. The copolymers were attached to IO NPs via either Ca^{2+}-mediated adsorption on citrate-coated IO, or covalent grafting to amine-coated IO. Remarkable colloidal stability of ~100 nm iron oxide clusters in API brine (8% wt. NaCl + 2% wt. $CaCl_2$) at 90 °C for 1 month was achieved via Ca^{2+}-mediated adsorption of a sufficient level of (poly(AMPS-*co*-AA) copolymer on the IO

surface to provide electrosteric and steric stabilization. The stabilization was favored by the high content of AMPS, which has a low binding affinity for Ca^{2+} at high temperatures due to its strong acidity and hydrophilic nature. Steric and electrosteric stabilization were also present for dispersions at room temperature in even higher salinities (up to 20% wt. $CaCl_2$ and 20% wt. NaCl), even with very thin double layers. Similarly, IO NPs with permanently grafted poly(AMPS-*co*-AA) 3:1 copolymers exhibited long-term ($\leq$ 1 month) stabilization at high salinities and elevated temperatures (up to 90 ^{o}C). Furthermore, the AA anchor groups enabled robust multipoint polymer attachment, which prevented polymer desorption even after a 40,000 fold dilution of the covalently grafted NPs. In addition to their notably high tolerance to salinity and temperature, all of the IO NPs studied exhibited extremely low adsorption on silica surfaces (< 2.2 mg/m^2, < 1.1% of a monolayer) even at the extreme API brine salinity.

To the best of our knowledge this is the first example of colloidal stability and low mineral adsorption of superparamagnetic metal oxide NPs at such high ionic strength and elevated temperatures. We have, therefore, established guidelines on the amount of adsorbed polymer required to provide stabilization against the attractive van der Waal's forces that affect large (~50-90 nm) IO cores as a function of copolymer structure and MW. In addition, we have demonstrated a methodology to achieve a high level of adsorption of carboxylate containing copolymers on anionic citrate coated metal oxide surfaces by Ca^{2+} bridging, or on amine-coated surfaces by covalent amidation chemistry. These methodologies provided an efficient combinatorial materials chemistry approach to facilitate the investigation of a large number of copolymers on a given type of IO nanoclusters with high magnetization, by separating the NP synthesis step from the coating step. We envision that this materials chemistry approach may be extended to a wide variety of NPs and polymer stabilizers relevant to a vast array of applications,

including transport through sub-surface porous media for enhanced oil recovery, environmental remediation, CO_2 sequestration and electromagnetic imaging of hydrocarbon reservoirs.

7.8 EXPERIMENTAL

7.8.1 Materials and Methods

The reagents iron(II) chloride tetrahydrate, iron (III) chloride hexahydrate, citric acid monohydrate, 30% ammonium hydroxide, poly(styrenesulfonate) - 70 kDa, poly(acrylamide)-*co*-(acrylic acid) (1:3) - 200 kDa, poly(2-acrylamido-2-methyl propanesulfonic acid) - 2 MDa, poly(acrylic acid sodium salt) (2 kDa) and poly(styrenesulfonic acid-*alt*-maleic acid) sodium salt-20 kDa were obtained from Sigma-Aldrich. Aquatreat 546 (poly(AMPS-*co*-AA) 1:6) was a gift from Akzo Nobel. Flosperse 9037 CS (poly(AMPS-*co*-AA) 1:4) and Flosperse 9024 CS (poly(AMPS-*co*-AA) 1:8) were gifts from SNF. Calcium chloride dihydrate, sodium chloride, hydrochloric acid and sodium hydroxide were obtained from commercial sources and used as received. The monomers t-butyl acrylate (*t*BA) and styrene were purchased from commercial sources and filtered through a short plug of basic alumina to remove the 4-methoxyphenol (MEHQ) stabilizer and were degassed by bubbling with dry nitrogen for 15 min prior to use. N,N,N′,N′,N-pentamethyldiethylenetriamine, ethyl 2-bromoisobutyrate, acrylic acid, potassium persulfate, and sodium metabisulfite were obtained from commercial sources and used as received. The monomer 2-amino-2-methylpropanesulfonate (AMPS) was a gift from Lubrizol corporation and used as received. Deionized water from a Barnstead Nanopure system was used for experiments.

Synthesis of poly(2-acrylamido-3-methylpropanesulfonate-*co*-acrylic acid) (poly(AMPS-*co*-AA)). Generally, a three-necked round bottom flask equipped with a

magnetic stir bar, a nitrogen inlet and a reflux condenser was charged with AMPS monomer, potassium persulfate and sodium metabisulfite under an atmosphere of nitrogen. The flask was sealed with rubber septa and deionized water that was previously degassed by bubbling with nitrogen for 30 min was added via a nitrogen-purged syringe or a cannula to the reaction flask, such that the concentration of AMPS monomer was 1.0 M. With stirring, acrylic acid was added to the reaction flask via a nitrogen-purged syringe. The flask was placed in an oil bath and stirred at 80 °C for 16 h. The reaction mixture was then cooled to room temperature and the water was removed under reduced pressure. The resulting white solid was dried under reduced pressure until a constant mass was reached. Poly(AMPS-*co*-AA) (3:1): (^{1}H NMR (400 MHz, D_2O): δ 0.96 (m, br, 10H, backbone C*H*$_2$ of AMPS and AA, and C*H*$_3$ of AMPS), 1.60 (br, 2H, backbone C*H* of AMPS and AA), 2.83 (br, s, 2H, C*H*$_2$SO$_3$Na of AMPS). ^{13}C NMR (100 MHz, D_2O): δ 26.2 (*C*H_3 of AMPS), 34.4 (*C*H_2 of backbone), 42.0 (*C*H of backbone), 52.1 (*C*H_2SO_3Na of AMPS), 57.5 (*C*$CH_2(CH_3)_2NH$ of AMPS), 175.4 (*C*ONH of AMPS), 178.4 (*C*OOH of AA). IR (ATR): ν 2943.1, 1719.9, 1654.7, 1555.6, 1455.9, 1173.7, 1040.9, 884.4, 850.1.

Synthesis of poly(*t*-butyl acrylate)-*block*-(styrene) poly(*t*BA-*b*-SS). Under an atmosphere of nitrogen an oven-dried 50 mL Schlenk flask with a magnetic stir bar was charged with 300 mg (2.1 mmol) of copper(I) bromide. The flask was sealed with a rubber septum secured with copper wire and was evacuated and back-filled with nitrogen three times before 5 mL (34.1 mmol) of *tert*-butyl acrylate was added via a gas-tight syringe that had been purged with nitrogen. After one freeze-pump-thaw cycle, 0.5 mL (2.4 mmol) of *N,N,N′,N′,N*-pentamethyldiethylenetriamine was added via a nitrogen-purged gas-tight syringe. After a second freeze-pump-thaw cycle, 0.1 mL (0.68 mmol) of ethyl-2-bromoisobutyrate was added via a gas-tight syringe that had been purged with nitrogen. After two more freeze-pump-thaw cycles, the reaction mixture was allowed to

return to ambient temperature, and the reaction flask was backfilled with nitrogen and placed in an oil bath at 50 °C. The reaction mixture was allowed to stir for 3 h at the same temperature, after which an aliquot was removed from the reaction and analyzed by GPC (M_n = 5,500, M_w/M_n = 1.15) prior to addition of 7.4 mL (64.5 mmol) of styrene. The reaction mixture was allowed to stir for a further 18 h at 50 °C, then was cooled to room temperature. The mixture was then taken up into THF and passed through a plug of neutral alumina to remove the metal/ligand catalyst system. The resulting polymer solution was concentrated and purified by precipitation into a mixture of methanol and water (1/1, v/v). ^{1}H NMR (400 MHz, D_2O): δ 1.42-1.50 (m, br, 13H), 1.83 (br, 2H), 2.21 (br, s, 1H), 6.44-6.57 (br, d, 3H), 6.98-7.08 (br, d, 5H). GPC: M_n = 17,055 Da, M_w/M_n = 1.29.

Synthesis of poly(sytrenesulfonate-*block*-acrylic acid) poly(SS-*b*-AA) (2.4 : 1). A 1 L round bottom flask was charged with poly(tBA-*b*-SS) (prepared in the previous step) dissolved in 300 mL of chloroform. In a separate flask with a stir bar, a solution of 66 mL of acetic anhydride in 100 mL of chloroform was cooled to 0 °C. Concentrated sulfuric acid (37 mL) was added dropwise and the mixture was stirred at 0 °C for an additional 10 min before it was added to the flask containing the polymer solution. The reaction mixture was heated to 60 °C and stirred for 16 h, then was cooled to room temperature and slowly poured into methanol. The solution was neutralized by slow addition of 3.0 M NaOH, and the organic solvents were removed under reduced pressure. The resulting aqueous solution was loaded into dialysis tubing and dialyzed against DI H_2O for 3 days. After dialysis the desired polymer was isolated as an orange glassy solid by concentration and drying under reduced pressure (11.0 g, 46% yield over 2 steps). ^{1}H NMR (400 MHz, D_2O): δ 1.2-2.2 (m, br, 10H), 3.65 (br, 1H), 6.69 (br, s, 4H), 7.59 (br, s,

4H). IR (ATR): ν 3390.9, 2945.9, 1715.5, 1568.6, 1455.0, 1410.9 1221.1, 1132.5, 1049.5, 1006.2, 946.2, 775.4.

Synthesis of citrate-coated IO NPs. Citrate-coated iron oxide nanoclusters were prepared by coprecipitation of Fe(II) and Fe(III) chlorides in an alkaline solution.[53]

Synthesis of Amine-functionalized IO NPs. IO NPs were prepared by the coprecipitation of Fe(II) and Fe(III) chlorides in an alkaline solution.[53,54] Briefly, a mixture of 2.15 g $FeCl_2 \bullet 4H_2O$ and 5.87 g $FeCl_3 \bullet 6H_2O$ (1:2 mole ratio), and 0.125 g of citric acid were dissolved in 100 mL of DI water. The solution was heated to 90 °C with magnetic stirring followed by injection of 25 mL of 30 % wt. aqueous NH_4OH solution to nucleate the IO NPs. The NP growth was continued for 2 h at 90 °C. The mixture was then cooled to room temperature and centrifuged to recover 2.5 g of IO NPs that were dispersed in 50 mL of DI water with a Branson probe sonication microtip. Hydrolysis and condensation of APTES was conducted by mixing 12.5 mL of APTES in 125 g of a 5% wt. acetic acid solution. After 1 h of acid hydrolysis, which has been shown to form dimers and higher oligomers of APTES,[55] the pH was adjusted to pH = 8 using 1 N NaOH solution. The reaction mixture was further diluted with DI water followed by the addition of 50 mL of IO NP solution (2.5 g of IO) to reach a total volume of 500 mL and a final IO concentration of 0.5% w/v. The mixture was placed in a water bath at 65 °C and magnetically stirred for 24 h. The mixture was removed from the water bath and cooled to room temperature, then the NPs were separated with a strong magnet, the supernatant was discarded and the NPs were washed twice with 200 mL of DI water. Finally, the washed NPs were dispersed in 50 mL of DI water, the pH was adjusted to pH = 6 with 1 N HCl, and the NPs were probe sonicated for 30 mins then centrifuged at 4000 rpm for 10 min to remove large clusters. The amine-functionalized IOs (APTES IO) in

the supernatant were retained for grafting poly(AMPS-*co*-AA) polymer. The typical yield at the end of APTES functionalization was 60-70% IO.

Phase behavior of sulfonated copolymers. Solutions of the various copolymers (2% wt.) in API brine (8% wt. NaCl + 2% wt. $CaCl_2$) at pH = 8 were sealed in glass vials with Teflon tape and set in an oven at 90 °C. The solutions were observed visually for phase separation in terms of turbidity after a day.

Polymer coating of citrate-IO nanoclusters. Polymer coating on citrate-IO clusters was performed by preparation of polymer solution at pH = 7, followed by addition of 20% wt. $CaCl_2$ solution, dilution with DI water and then addition of the IO cluster stock solution. With the exception of a few specified cases, the citrate-coated IO nanoclusters with the higher citrate level were used. Most commonly, the final concentrations after mixing were 1% wt. IO, 5% wt. polymer and 5% wt. $CaCl_2$, although these concentrations were varied, as reported in the results section. Upon mixing the solutions, flocculated particles were formed and remained suspended while stirring. After adjusting the pH to 7, the mixture was transferred to a water bath and kept at 90 °C for 1 h. After cooling to room temperature, the coated NPs were separated by centrifugation, washed twice with DI water to remove excess polymer and $CaCl_2$, and redispersed in DI water by probe sonication to reach a final IO concentration of ~2% wt. The IO yield after coating ranged from 70-90%.

Grafting of poly(AMPS-*co*-AA) to APTES IO. Poly(AMPS-*co*-AA) was dissolved in 1 N NaOH to pH = 6, followed by addition of 20% wt. NaCl solution, DI water and APTES IO stock solution under vigorous magnetic stirring to reach a final concentration of 1% IO, 5% polymer and 3% NaCl. The pH was again adjusted to pH = 6, and after 5-10 minutes EDC (equimolar to PAA) was added to facilitate amide bond formation. The reaction was continued overnight at room temperature under constant

stirring. The polymer-coated iron oxide NPs were separated by centrifugation and washed with DI water twice to remove excess polymer and NaCl. The NPs were finally dispersed in DI water at ~2% w/v IO. The typical IO yield after this procedure was 70-90% IO. Electrostatically attached poly(AMPS-*co*-AA) IO NPs were prepared for the polymer desorption test by a similar procedure, except that EDC was not added.

Colloidal stability of polymer-coated IO nanoclusters. The colloidal stability was tested by mixing stock solutions of NaCl (20% wt.), CaCl2 (20% wt.), DI water and polymer-coated IO clusters to achieve a 0.2% wt. IO dispersion in API brine (8% wt. NaCl + 2% wt. CaCl2) or desired NaCl or CaCl2 concentration. The colloidal stability was assessed by visual observation and DLS measurements at room temperature and 90 °C. For long term stability tests in API brine at 90 °C, the solutions were sealed in glass pipettes with a butane torch. Pipettes were photographed and sacrificed periodically to measure the DH.

Adsorption of Polymer-Coated IO NPs on Silica. In a glass vial, 2 mL of aqueous dispersion of IO NPs was added to 1 g of silica. The initial concentration of IO ranged from 0.05% to 1% w/v. The glass vials were sealed and shaken overnight on a LW Scientific Model 2100A Lab Rotator at 200 rpm at room temperature, after which the mixture was left undisturbed to allow the silica adsorbent to gravimetrically sediment. The concentration of the IO NPs in the supernatant was determined by measuring the UV-vis absorbance at 575 nm after dilution of the samples, where necessary, such that the absorbance was below 2. The specific adsorption and monolayer coverage of IO nanoclusters to silica microspheres was calculated based on the difference in the supernatant concentrations and volumes before and after adsorption.

Polymer Desorption Test. The poly(AMPS-*co*-AA) grafted IO NPs were diluted 200-fold to 0.01% w/v IO in 1 M NaCl solution and left undisturbed to equilibrate for 24

hours to allow desorption of non-covalently attached polymer. The NPs were centrifuged at 15,000 g and dispersed in DI water after discarding the supernatant. The dilution and equilibration steps were repeated, which amounted to a 40,000-fold dilution of the initial IO solution, followed by NP separation by centrifugation and redispersion of the IO NPs in DI water by probe sonication. The final IO sample was tested for stability in API brine (8% wt. NaCl + 2% wt. $CaCl_2$) at 90 °C. As a control, a sample with electrostatically attached poly(AMPS-*co*-AA) on IO NPs (prepared without EDC) was subjected to an analogous dilution test followed by assessment of colloidal stability in API brine at 90 °C.

7.8.2 Characterization

Nucelar magnetic resonance spectroscopy (NMR). ^1H NMR spectra were recorded using a Varian 400 MHz spectrometer. Chemical shifts δ (in ppm) are referenced to tetramethylsilane using the residual solvent as an internal standard: $CDCl_3$, 7.24 ppm; D_2O, 4.79 ppm.

Infrared Spectroscopy (IR). IR spectra were recorded on a Thermo Scientific Nicolet iS5 spectrometer with an iD3 attenuated total reflectance (ATR) attachment (Ge crystal).

Gel permeation chromatography (GPC). GPC analysis was performed on a Viscotek system equipped with a VE 1122 pump, a VE 7510 degasser, two fluorinated polystyrene columns (IMBHW-3078 and I-MBLMW-3078) thermostated to 30 °C (using a ELDEX CH 150 column heater) and arranged in series, using refractive index (RI) detection. Molecular weight and polydispersity data are reported relative to polystyrene standards in tetrahydrofuran (THF).

Dynamic light scattering (DLS). D_{HS} were measured with Brookhaven ZetaPALS instrument with the BI-MAS option. Scattered light was collected with a 90° Avalanche photodiode detector and all data were fit with the CONTIN routine. Diameters of polymer solutions were measured at a conc. of ~2 mg/mL in 1 M NaCl, whereas IO cluster diameters were measured in DI water and API brine. High temperature D_{HS} were measured at 74 °C, which is the maximum limit of the instrument. All measurements were made over a period of 3 min and in triplicate.

Zeta potential. Electrophoretic mobility was measured with Brookhaven's ZetaPALS instrument at 15° scattering angle and 25 °C. Measurements were conducted in 10 mM KCl (Debye length λ_D^{-1} = 3 nm) and zeta potential was determined with Smoluchowski model (ζ_a >>1). For higher salinity measurements cycles were set at 20 Hz and voltage at 3 V to minimize polarization effects.

Transmission electron microscopy (TEM). The experiments were performed on a FEI TECNAI G2 F20 X-TWIN TEM. A dilute aqueous dispersion of the IO nanoclusters was deposited onto a 200 mesh carbon-coated copper TEM grid for imaging. The cluster diameters were obtained by ImageJ analysis. Cluster diameters were defined as equivalent circles of the same surface area as the clusters on the two dimensional TEM image. The size distribution was converted to volume-average diameters for comparison with volume-average DLS D_{HS}.

Thermogravimetric analysis (TGA). The organic content of citrate IO clusters and polymer-coated IO clusters were determined using a Mettler-Toledo TGA/SDTA851e instrument under an atmosphere of nitrogen at 5 °C/min from 25 to 800 °C. Washing steps ensured that excess ligands and polymers were removed from the sample prior to TGA analysis. The percentage mass loss was reported as the organic content in the particles.

Flame atomic absorption spectroscopy (FAAS). The concentration of Fe in the dispersion was determined on a GBC 908AA flame atomic absorption spectrometer (GBC Scientific Equipment Pty Ltd). All measurements were conducted at 242.8 nm using an air-acetylene flame.

7.9 ACKNOWLEDGEMENTS

Portions of this chapter were reprinted with permission from Bagaria, H. G.; Yoon, K. Y.; Neilson, B. M.; Cheng, V.; Lee, J. H.; Worthen, A. J.; Xue, Z.; Huh, C.; Bryant, S. L.; Bielawski, C. W.; Johnston, K. P. *Langmuir* **2013**, 3195-3206, and from Bagaria, H. G.; Xue, Z.; Neilson, B. M.; Worthen, A. J.; Yon, K. Y.; Nayak, S.; Cheng, V.; Lee, J. H.; Bielawski, C. W.; Johnston, K. P. *ACS Appl. Mater. Interfaces* **2013**, 3329-3339. Copyright 2013 American Chemical Society. Portions of this chapter were reprinted from the Journal of Colloid and Interface Science, Vol 398, Bagaria, H. G.; Neilson, B. M.; Worthen, A. J.; Zheng, X.; Yon, K. Y.; Cheng, V.; Lee, J. H.; Velagala, S.; Huh, C.; Bryant, S. L.; Bielawski, C. W.; Johnston, K. P. "Adsorption of Iron Oxide Nanoclusters Stabilized with Sulfonated Copolymers on Silica in Concentrated NaCl and $CaCl_2$ Brine," 217-226, Copyright 2013, with permission from Elsevier. I acknowledge my collaborators and co-authors Dr. Hitesh Bagaria, Ki Youl Yoon, Victoria Cheng, JaeHo Lee, Andrew J. Worthen, and Zheng Xue for their work on the synthesis and characterization of the polymer-coated iron oxide nanoparticles. I also thank Prof. Chun Huh, Prof. Steven L. Bryant, and Prof. Christopher Bielawski for helpful discussions, and principal investigator, Prof. Keith P. Johnston, for helping to write the original manuscript. I also thank Hitesh Bagaria, Andrew Worthen, and Zheng Xue for their shared efforts in writing the original manuscript.

7.10 REFERENCES

[1] Kanj, M. Y.; Rashid, M. H.; Giannelis, E. *SPE Middle East Oil and Gas Show and Conference*, Society of Petroleum Engineers, Manama, Bahrain **2011**.

[2] Jikich, S. A.; *J. Petrol. Technol*. **2012**, 28. (b) Javadpour, F. ; Nicot, J. P.; *Transport Porous Med.* **2011**, *89*, 265-284. (c) Worthen, A. J.; Bagaria, H. G.; Chen, Y.; Bryant, S. L.; Huh, C.; Johnston, K. P. *J. Coll. Interf. Sci.* **2012**, *391*, 142-151.

[3] Saleh, N.; Kim, H. J.; Phenrat, T.; Matyjaszewski, K.; Tilton, R. D.; Lowry, G. V.; *Environ. Sci. Technol.* **2008**, *42*, 3349-3355. (b) Wang, Y. G.; Li, Y. S.; Fortner, J. D.; Hughes, J. B.; Abriola, L.; M. Pennell, K. D. *Environ. Sci. Technol*. **2008**, *42*, 3588-3594. (c) Petosa, A. R.; Jaisi, D. P.; Quevedo, I. R.; Elimelech, M.; Tufenkji, N. *Environ. Sci. Technol*. **2010**, *44*, 6532-6549.

[4] (a) Kotsmar, C.; Yoon, K. Y.; Yu, H. Y.; Ryoo, S. Y.; Barth, J.; Shao, S.; Prodanovic, M.; Milner, T. E.; Bryant, S. L.; Huh, C.; Johnston, K. P. *Ind. Eng. Chem. Res.* **2010,** *49*, 12435-12443. (b) Berlin, J. M.; Yu, J.; Lu, W.; Walsh, E. E.; Zhang, L. L.; Zhang, P.; Chen, W.; Kan, A. T.; Wong, M. S.; Tomson, M. B.; Tour, J. M. *Energ. Environ. Sci.* **2011**, *4*, 505-509. (c) Ryoo, S.; Rahmani, A. R.; Yoon, K. Y.; Prodanovic, M.; Kotsmar, C.; Milner, T. E.; Johnston, K. P.; Bryant, S. L.; Huh, C. *J. Petrol. Sci. Eng.* **2012,** *81*, 129-144.

[5] (a) Jing, J. Y.; Zhang, Y.; Liang, J. Y.; Zhang, Q. B.; Bryant, E.; Avendano, C.; Colvin, V. L.; Wang, Y. D.; Li, W. Y.; Yu, W. W. *J. Nanopart. Res.* **2012,** *14*, DOI: 10.1007/s11051-012-0827-3. (b) Bacri, J. C.; Perzynski, R.; Salin, D.; Cabuil, V.; Massart, R. *J. Magn. Magn. Mater.* **1990,** *85*, 27-32. (c) Bee, A.; Massart, R.; Neveu, S. *J. Magn. Magn. Mater.* **1995,** *149*, 6-9. (d) Chanteau, B.; Fresnais, J.; Berret, J. F. *Langmuir* **2009,** *25*, 9064-9070. (e) Prakash, A.; Zhu, H. G.; Jones, C. J.; Benoit, D. N.; Ellsworth, A. Z.; Bryant, E. L.; Colvin, V. L. *ACS Nano* **2009,** *3,* 2139-2146. (f) Sahoo, Y.; Goodarzi, A.; Swihart, M. T.; Ohulchanskyy, T. Y.; Kaur, N.; Furlani, E. P.; Prasad, P. N. *J. Phys. Chem. B.* **2005,** *109*, 3879-3885.

[6] (a) Hiemenz, P. C.; Rajagopalan, R., *Principles of colloid and surface chemistry*. 3rd ed.; Marcel Dekker: New York, 1997; p 650. (b) Napper, D. H., *Polymeric stabilization of colloidal dispersions*. Academic Press: London ; New York, 1983; p 428. (c) Berg, J. C., *An introduction to interfaces & colloids : the bridge to nanoscience*. World Scientific: Singapore ; Hackensack, NJ, 2010; p 785.

[7] (a) Ditsch, A.; Laibinis, P. E.; Wang, D. I. C.; Hatton, T. A. *Langmuir* **2005**, *21*, 6006-6018. (b) Fritz, G.; Schadler, V.; Willenbacher, N.; Wagner, N. J. *Langmuir* **2002,** *18*, 6381-6390. (c) Yoon, K. Y.; Kotsmar, C.; Ingram, D. R.; Huh, C.; Bryant, S. L.; Milner, T. E.; Johnston, K. P. *Langmuir* **2011**, *27*, 10962-10969.

[8] Zhang, L.; Xue, H.; Gao, C. L.; Carr, L.; Wang, J. N.; Chu, B. C.; Jiang, S. Y. *Biomaterials* **2010**, *31*, 6582-6588.

[9] Sato, T.; Ruch, R., *Stabilization of colloidal dispersions by polymer adsorption*. Dekker: New York, 1980; p 155.

[10] (a) Lewis, J. A. *J. Am. Ceram. Soc.* **2000,** *83*, 2341-2359. (b) Biggs, S.; Healy, T. W. *J. Chem. Soc. Faraday T.* **1994,** *90*, 3415-3421.

[11] (a) Laurent, S.; Forge, D.; Port, M.; Roch, A.; Robic, C.; Elst, L. V.; Muller, R. N. *Chem. Rev.* **2008,** *108*, 2064-2110. (b) Amstad, E.; Textor, M.; Reimhult, E. *Nanoscale* **2011,** *3*, 2819. (c) Mahmoudi, M.; Sant, S.; Wang, B.; Laurent, S.; Sen, T. *Adv. Drug Deliv. Rev.* **2011,** *63*, 24-46. (d) Latham, A. H.; Williams, M. E. *Acc. Chem. Res.* **2008,** *41*, 411-420. (e) Jeong, U.; Teng, X. W.; Wang, Y.; Yang, H.; Xia, Y. N. *Adv. Mater.* **2007,** *19*, 33-60.

[12] (a) Yavuz, C. T.; Mayo, J. T.; Yu, W. W.; Prakash, A.; Falkner, J. C.; Yean, S.; Cong, L.; Shipley, H. J.; Kan, A.; Tomson, M.; Natelson, D.; Colvin, V. L. *Science* **2006,** *314*, 964-967. (b) Yavuz, C. T.; Prakash, A.; Mayo, J. T.; Colvin, V. L. *Chem. Eng. Sci.* **2009,** *64*, 2510-2521.

[13] (a) Yu, W. W.; Chang, E.; Falkner, J. C.; Zhang, J. Y.; Al-Somali, A. M.; Sayes, C. M.; Johns, J.; Drezek, R.; Colvin, V. L. *J. Am. Chem. Soc.* **2007,** *129*, 2871-2879. (b) Wan, S.; Zheng, Y.; Liu, Y.; Yan, H.; Liu, K. *J. Mater. Chem.* **2005,** *15*, 3424. (c) Amstad, E.; Gillich, T.; Bilecka, I.; Textor, M.; Reimhult, E. *Nano Lett.* **2009,** *9*, 4042-4048. (d) Na, H. B.; Palui, G.; Rosenberg, J. T.; Ji, X.; Grant, S. C.; Mattoussi, H. *ACS Nano* **2012,** *6*, 389-399. (e) Palui, G.; Na, H. B.; Mattoussi, H. *Langmuir* **2012,** *28*, 2761-2772. (f) Barrera, C.; Herrera, A. P.; Bezares, N.; Fachini, E.; Olayo-Valles, R.; Hinestroza, J. P.; Rinaldi, C. *J.Colloid Interf. Sci.* **2012,** *377*, 40-50.

[14] Jain, N.; Wang, Y.; Jones, S. K.; Hawkett, B. S.; Warr, G. G. *Langmuir* **2010,** *26*, 4465-4472.

[15] Golas, P. L.; Louie, S.; Lowry, G. V.; Matyjaszewski, K.; Tilton, R. D. *Langmuir* **2010,** *26*, 16890-16900.

[16] Sondjaja, R.; Hatton, A. T.; Tam, M. K. C. *J. Magn. Magn. Mater.* **2009,** *321*, 2393-2397.

[17] Manning, G. S. *Acc. Chem. Res.* **1979,** *12,* 443-449.

[18] McCormick, C. L.; Elliott, D. L. *Macromolecules* **1986,** *19*, 542-547.

[19] Schweins, R.; Huber, K. *Eur. Phys. J. E.* **2001,** *5*, 117-126.

[20] Newman, J. K.; Mccormick, C. L. *Macromolecules* **1994,** *27*, 5114-5122.

[21] Sinn, C. G.; Dimova, R.; Antonietti, M. *Macromolecules* **2004,** *37*, 3444-3450.

[22] (a) Rashidi, M.; Blokhus, A. M.; Skauge, A. *J. Appl. Polym. Sci.* **2011,** *119*, 3623-3629. (b) Levitt, D.; Pope, G. A. *SPE/DOE Symposium on Improved Oil Recovery*, Society of Petroleum Engineers: Tulsa, Oklahoma, USA, 2008.

[23] Radeva, T., *Physical chemistry of polyelectrolytes*. Marcel Dekker: New York, 2001; p 882.

[24] Halford, B. *Chemical & Engineering News* **2012**, *90*, 60-62.

[25] Chen, Y.; Elhag, A. S.; Poon, B. M.; Cui, L.; Ma, K.; Liao, S. Y.; Omar, A.; Worthen, A.; Hirasaki, G. J.; Nguyen, Q. P.; Johnston, K. P. *SPE Improved Oil Recovery Symposium*, Society of Petroleum Engineers: Tulsa, Oklahoma, USA, 2012.

[26] (a) Wagener, A. Schwenke, S. Barcikowski, *Langmuir* **2012**, *28*, 6132-6140. (b) Park, J. J.; Lacerda, S. H. D. P.; S. Stanley, K.; Vogel, B. M.; Kim, S.; Douglas, J. F. Raghavan, D.; Karim, A. *Langmuir* **2009**, *25*, 443-450.

[27] Yoon, K. Y.; Li, Z.; Neilson, B. M.; Lee, W.; Huh, C.; Bryant, S. L.; Bielawski, C. W.; Johnston, K. P. *Macromolecules* **2012**, *45*, 5157-5166.

[28] (a) Kirby, G. H.; Harris, D. J.; Li, Q.; Lewis, J. A. *J. Am. Ceram. Soc.* **2004**, *87*, 181-186. (b) Abraham, T.; Kumpulainen, A.; Xu, Z.; Rutland, M.; Claesson, P. M.; Masliyah, J. *Langmuir* **2001,** *17*, 8321-8327. (c) Turesson, M.; Labbez, C.; Nonat, A. *Langmuir* **2011,** *27*, 13572-13581.

[29] (a) Chanteau, B.; Fresnais, J.; Berret, J. F.; *Langmuir* **2009**, *25*, 9064-9070.(b) Barrera, C.; Herrera, A. P.; Bezares, N.; Fachini, E.; Olayo-Valles, R.; Hinestroza, J. P.; Rinaldi, C. *J. Colloid Interf. Sci.* **2012**, *377*, 40-50. (c) Lattuada, M.; Hatton, T. A.; *Langmuir* **2007**, *23*, 2158-2168. (d) Boyer, C.; Whittaker, M. R.; Bulmus, V.; Liu, J. Q.; Davis, T. P.; *NPG Asia Mater.* **2010**, *2*, 23-30. (e) Peng, J. X.; Liu, Q. X.; Xu, Z. H.; Masliyah, J.; *Adv. Funct. Mater.* **2012**, *22*, 1732-1740.

[30] (a) Ujiie, K.; Kanayama, N.; Asai, K.; Kishimoto, M.; Ohara, Y.; Akashi, Y.; Yamada, K.; Hashimoto, S.; Oda, T.; Ohkohchi, N.; Yanagihara, H.; Kita, E.; Yamaguchi, M.; Fujii, H.; Nagasaki, Y.; *Colloid Surface B* **2011**, *88*, 771-778. (b) Lopez-Cruz, A.; Barrera, C.; Calero-DdelC, V. L.; Rinaldi, C. *J. Mater. Chem.* **2009**, *19*, 6870-6876.

[31] Sarac, A. S. *Prog. Polym. Sci.* **1999**, *24*, 1149-1204.

[32] Reith, D.; Muller, B.; Muller-Plathe, F.; Wiegand, S. *J. Chem. Phys.* **2002,** *116*, 9100-9106.

[33] Hsieh, H. L.; Moradiaraghi, A.; Stahl, G. A.; Westerman, I. J. *Makromol. Chem.-M. Symp.* **1992,** *64*, 121-135.

[34] (a) Boue, F.; Cotton, J. P.; Lapp, A.; Jannink, G.; *J. Chem. Phys.* **1994**, *101*, 2562-2568. (b) Essafi, W.; Haboubi,; Williams, N. C.; Boue, F.; *J Phys Chem B* **2011**, *115*, 8951-8960.

[35] Levitt, D. B.; Slaughter, W.; Pope, G. A.; Jouenne, S.; *SPE Reserv. Eval. Eng*. **2011**, *14*, 287-298.

[36] Ge, J. P.; Hu, Y. X.; Biasini, M.; Dong, C. L.; Guo, J. H.; Beyermann, W. P.; Yin, Y. D. *Chem. Eur. J.* **2007,** *13*, 7153-7161.

[37] (a) Kriwet, B.; Kissel, T. Interactions *Int. J. Pharmaceut.* **1996,** *127*, 135-145. (b) David, C.; Companys, E.; Galceran, J.; Garces, J. L.; Mas, F.; Rey-Castro, C.; Salvador, J.; Puy, J. *J. Phys. Chem. B.* **2007,** *111*, 10421-10430.

[38] Kawaguchi, S.; Toui, S.; Onodera, M.; Ito, K.; Minakata, A. *Macromolecules* **1993,** *26*, 3081-3085.

[39] Zdyrko, B.; Luzinov, I.; *Macromol. Rapid Comm.* **2011**, *32*, 859-869.

[40] (a) Saleh, N.; Sarbu, T.; Sirk, K.; Lowry, G. V.; Matyjaszewski, K.; Tilton, R. D.; *Langmuir* **2005**, *21*, 9873-9878. (b) Mei, Y.; Ballauff, M.; *Eur. Phys. J. E* **2005**, *16*, 341-349. (c) Lozsan, A. E.; Romero-Cano, M. S.; *J. Colloid. Interf. Sci.* **2011**, *354*, 70-75.

[41] Yathindranath, V.; Rebbouh, L.; Moore, D. F.; Miller, D. W.; van Lierop, J. Hegmann, T. *Adv. Funct. Mater.* **2011**, *21*, 1457-1464.

[42] (a) Johnston, K. P.; Maynard, J. A.; Truskett, T. M.; Borwankar, A. U.; Miller, M. A.; Wilson, B. K.; Dinin, A. K.; Khan, T. A.; Kaczorowski, K. J. *ACS Nano* **2012**, *6*, 1357-1369. (b) Tam, J. M.; Murthy, A. K.; Ingram, D. R.; Nguyen, R.; Sokolov, K. V.; Johnston, K. P. *Langmuir* **2010**, *26*, 8988-8999.

[43] Xia, Y. S.; Nguyen, T. D.; Yang, M.; Lee, B.; Santos, A.; Podsiadlo, P.; Tang, Z. Y.; Glotzer, S. C.; Kotov, N. A. *Nature Nanotech.* **2011,** *6*, 580-587.

[44] Voorhees, P. W. *J. Stat. Phys.* **1985,** *38*, 231-252.

[45] Lages, S.; Lindner, P.; Sinha, P.; Kiriy, A.; Stamm, M.; Huber, K. *Macromolecules* **2009,** *42*, 4288-4299.

[46] (a) Ballauff, M.; Borisov, O.; *Curr Opin Colloid In.* **2006**, *11*, 316-323. (b) Dobrynin, A. V.; Rubinstein, M.; *Prog Polym Sci.* **2005**, *30*, 1049-1118. (c) Rubinstein, M.; Papoian, G. A.; *Soft Mater.* **2012**, *8*, 9265-9267.(d) Israels, R.; Leermakers, F. A. M. G.; Fleer, J.; Zhulina, E. B.; *Macromolecules* **1994**, *27*, 3249-3261.

[47] Phenrat, T.; Saleh, N.; Sirk, K.; Kim, H. J.; Tilton, R. D.; Lowry, G. V.; *J. Nanopart. Res.* **2008**, *10*, 795-814.

[48] Guo, X.; Ballauff, M.; *Phys. Rev. E.* **2001**, *64*.

[49]Saleh, N.; Sirk, K.; Liu, Y.; Phenrat, T.; Dufour, B.; Matyjasewski, K.; Tilton, R. D.; Lowry, G. V. *Environ. Eng. Sci.* **2007**, *24*, 45-47.

[50] He, F.; Zhang, M.; Qian, T.; Zhao, D. *J. Colloid Interf. Sci.* **2009**, *334,* 96-102.

[51] Jaisi, D. P.; Saleh, N. B.; Blake, R. E.; Elimelech, M. *Environ. Sci. Technol.* **2008**, *42*, 8317-8323.

[52] (a) Zhang, M.; Akbulut, M. *Langmuir* **2011**, *27*, 12550-12559. (b) Mays, D. C.; Hunt, J. R. *Environ. Sci. Technol.* **2005**, *39*, 577-584.

[53] (a) Massart, R. *IEEE Trans. Magn.* **1981,** 17, 1247-1248. (b) Lyon, J. L.; Fleming, D. A.; Stone, M. B.; Schiffer, P.; Williams, M. E. *Nano Lett.* **2004,** 4, 719-723. (c) Sahoo, Y.; Goodarzi, A.; Swihart, M. T.; Ohulchanskyy, T. Y.; Kaur, N.; Furlani, E. P.; Prasad, P. N. *J. Phys. Chem. B* **2005,** 109, 3879–3885.

[54] Bee, A.; Massart, R.; Neveu, S. *J Magn. Magn. Mater.* **1995**, *149*, 6-9.

[55] (a) Feng, B.; Hong, R. Y.; Wang, L. S.; Guo, L.; Li, H. Z.; Ding, J.; Zheng, Y.; Wei, D. G. *Colloid Surface A* **2008**, *328*, 52-59. (b) Salon, M. C. B.; Belgacem, M. N.; *Colloid Surface A* **2010**, *366*, 147-154.(c) Paquet, O.; M. Salon, C. B.; Zeno, E.; Belgacem, M. N.; *Mat. Sci. Eng. C-Mater.* **2012**, *32*, 487-493.

Appendices

APPENDIX A: X-RAY CRYSTALLOGRAPHY FOR CHAPTER 2

A.1 X-ray Crystallography Experimental Details for 1o.

Crystals of **1o** were grown as colorless laths by slow evaporation from benzene. The data crystal was cut from a larger crystal and had approximate dimensions: 0.58 × 0.12 × 0.04 mm. The data were collected on a Rigaku SCX-Mini diffractometer with a Mercury CCD using a graphite monochromator with MoKα radiation (λ = 0.71073Å). A total of 1080 frames of data were collected using ω-scans with a scan range of 0.5° and a counting time of 23 seconds per frame. The data were collected at 223 K using a Rigaku Tech50 low temperature device. Details of crystal data, data collection and structure refinement are listed in Table A1. Data reduction was performed using the Rigaku Americas Corporation's Crystal Clear version 1.40. The structure was solved by direct methods using SIR97[1] and refined by full-matrix least-squares on F^2 with anisotropic displacement parameters for the non-H atoms using SHELXL-97.[2] The hydrogen atoms on carbon were calculated in ideal positions with isotropic displacement parameters set to 1.2 × U_{eq} of the attached atom (1.5 × U_{eq} for methyl hydrogen atoms). The function, $\Sigma w(|F_o|^2 - |F_c|^2)^2$, was minimized, where $w = 1/[(\sigma(F_o))^2 + (0.0771 \times P)^2 + (0.2977 \times P)]$ and $P = (|F_o|^2 + 2|F_c|^2)/3$. $R_w(F^2)$ refined to 0.137, with R(F) equal to 0.0489 and a goodness of fit, S, = 1.05. Definitions used for calculating R(F), $R_w(F^2)$ and the goodness of fit, S, are given below in Table A1. The data were checked for secondary extinction effects but no correction was necessary. Neutral atom scattering factors and values used to calculate the linear absorption coefficient are from the International Tables for X-ray Crystallography.[3]

A.2 X-ray Crystallography Experimental Details for 1c.

Crystals of **1c** were grown as colorless plates by slow evaporation from pentane in the dark. The data crystal had approximate dimensions: 0.22 × 0.18 × 0.14 mm. The data were collected on a Nonius Kappa CCD diffractometer using a graphite monochromator with MoKα radiation (λ = 0.71073Å). A total of 433 frames of data were collected using ω-scans with a scan range of 0.8° and a counting time of 116 seconds per frame. The data were collected at 153 K using an Oxford Cryostream low temperature device. Details of crystal data, data collection and structure refinement are listed in Table A1. Data reduction were performed using DENZO-SMN.[4] The structure was solved by direct methods using SIR97[1] and refined by full-matrix least-squares on F^2 with anisotropic displacement parameters for the non-H atoms using SHELXL-97.[2] The hydrogen atoms were calculated in ideal positions with isotropic displacement parameters set to 1.2 × U_{eq} of the attached atom (1.5 × U_{eq} for methyl hydrogen atoms).

The methyl groups on the cyclohexadiene portion of the molecule were disordered. The disorder affected the methyl groups, C14 and C15, and the associated ring atoms, C6 and C7 (Figure A1). The disorder was modeled by assigning the variable *x* to the site occupancy factors for one component composed of atoms, C6, C7, C14 and C15. The variable (1 - *x*) was assigned to the site occupancy factors of the alternate component composed of atoms, C6a, C7a, C14a and C15a. A common isotropic displacement parameter was refined for the rings atoms, C6, C7, C6a and C7a while refining *x*. A second isotropic displacement parameter was refined for the methyl carbon atoms, C14, C15, C14a and C15a while simultaneously refining the variable *x*. The geometry of the two orientations was restrained to be equivalent while refining the site occupancy factor, *x*. In this way, the site occupancy for the major component consisting of C6, C7, C14 and C15 refined to 55(2)%. These atoms were refined anistropically with

their displacement parameters restrained to be approximately isotropic in the final refinement model. The geometric restraints on the carbon atoms were removed in the final refinement cycles.

The two different orientations represent different enantiomers. The molecule containing C6, C7, C14 and C15 has the *S,S* configuration at C6 and C7, respectively (Figure A1). The molecule containing C6a, C7a, C14a and C15a has the *R,R* configuration at C6a and C7a, respectively. The function, $\Sigma w(|F_o|^2 - |F_c|^2)^2$, was minimized, where $w = 1/[(\sigma(F_o))^2 + (0.021 \times P)^2 + (4.1805 \times P)]$ and $P = (|F_o|^2 + 2|F_c|^2)/3$. $R_w(F^2)$ refined to 0.185, with R(F) equal to 0.0943 and a goodness of fit, S, = 1.12. Definitions used for calculating R(F),$R_w(F^2)$ and the goodness of fit, S, are given below. The data were checked for secondary extinction but no correction was needed. Neutral atom scattering factors and values used to calculate the linear absorption coefficient are from the International Tables for X-ray Crystallography (1992).[3] All figures were generated using SHELXTL/PC.[5]

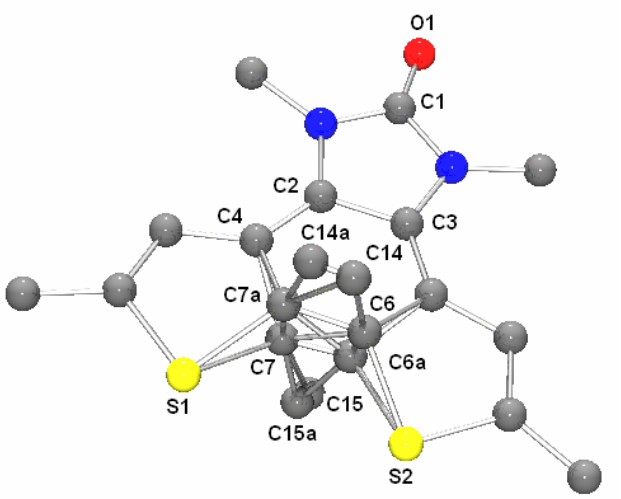

Figure A1: POV-ray representations of urea **1c** showing the two superimposed enantiomers, with ellipsoids at 50% probability. Hydrogen atoms have been omitted for clarity.

	1o	**1c**
CCDC number	821251	821252
Empirical formula	C_{17} H_{20} N_2 O S_2	C_{17} H_{20} N_2 O S_2
Formula weight	332.47	332.47
Crystal system	Triclinic	monoclinic
Space group	P-1	P21/c
Crystal size (mm)	0.58 × 0.12 × 0.04	0.22 × 0.18 × 0.14
a (Å)	7.529(2)	14.097(3)
b (Å)	8.949(2)	9.195(2)
c (Å)	13.633(3)	14.255(3)
α (deg)	97.796(5)	90.00
β (deg)	101.116(5)	119.229(2)
γ (deg)	107.984(5)	90.00
Volume ($Å^3$)	838.3(3)	1612.5(6)
Z	2	4
ρ (calculated), (Mg/m^3)	1.317	1.370
μ (mm^{-1})	0.321	0.333
F(000)	352	704
θ range (deg)	3.11 to 27.48	1.66 to 24.99
Reflections collected	8945	4753
Independent reflections	3768	2803
Completeness to θ = 27.48° (%)	97.8	98.9
Data / restraints / parameters	3768 / 0 / 205	2803 / 48 / 243
Goodness-of-fit on F^2	1.050	1.198
R_1[a] (all data)	0.0489 (0.0586)	0.0955 (0.1681)
wR_2 (all data)	0.1272 (0.1369)	0.1644 (0.2116)
Largest diff. peak, hole (e $Å^{-3}$)	0.367, -0.507	0.264, -0.253

Table A1: Crystal Data, Data Collection, and Refinement Parameters for **1o** and **1c**. [a] $R_w(F^2) = \{\Sigma_w(|F_o|^2 - |F_c|^2)^2/\Sigma_w(|F_o|)^4\}^{1/2}$ where w is the weight given each reflection. $R(F) = \Sigma(|F_o| - |F_c|)/\Sigma|F_o|\}$ for reflections with $F_o > 4(\sigma(F_o))$. $S = [\Sigma_w(|F_o|^2 - |F_c|^2)^2/(n - p)]^{1/2}$, where n is the number of reflections and p is the number of refined parameters.

A.3 References

[1] SIR97. (1999), A program for crystal structure solution: A. Altomare, M. C. Burla, Camalli, G. L. Cascarano, C. Giacovazzo, A.Guagliardi, A. G. G. Moliterni, G. Polidori, Spagna *J. Appl. Cryst.* **1999**, 32, 115-119.

[2] Sheldrick, G. M. SHELXL97, Program for the Refinement of Crystal Structures. University of Gottingen, (Germany) **1994**.

[3] International Tables for X-ray Crystallography. Vol. C, Tables 4.2.6.8 and 6.1.1.4, A. (Ed.: J. C. Wilson) Kluwer Academic Press, Boston, **1992**.

[4] DENZO-SMN. (1997): Z. Otwinowski, W. Minor in *Methods in Enzymology, 276: Macromolecular Crystallography, part A*, (Eds.: C. W. Carter, Jr., R. M. Sweets) Academic Press, **1997**, 307 – 326.

[5] Sheldrick, G. M. SHELXTL/PC (Version 5.03). Siemens Analytical X-ray Instruments, Inc., Madison, Wisconsin, **1994**.

APPENDIX B: SECOND ORDER KINETIC ANALYSES FOR CHAPTER 3

The condensation reactions between allyl alcohol and vinyl acetate or between ethyl acetate and aminoethanol catalyzed by NHC precatalyst **1** may be represented as:

$$A + B \longrightarrow P$$

Assuming no side reactions, the two reactants will always be present in equimolar quantities. As such, the above equation may be simplified to:

$$2A \longrightarrow P$$

The above equation may be expressed as the following rate law:

$$\frac{d[P]}{dt} = k[A]^2$$

The integrated form of the above equation is as follows:

$$\frac{1}{[A]} = kt + \frac{1}{[A]_0}$$

Rearranging the integrated rate law and substituting the initial concentration of 0.1 M for $[A]_0$ gives:

$$\frac{1}{[A]} - 10 = kt$$

Thus, plotting (1/[A]-10) (M) vs. *t* (s) should give a linear plot where *k* is equal to the slope of the line, as shown below in Figures A2 – A4 for selected examples. Each reported rate constant (k_{vis}, k_{UV}, *k*) was obtained from the average of at least three separate experiments.

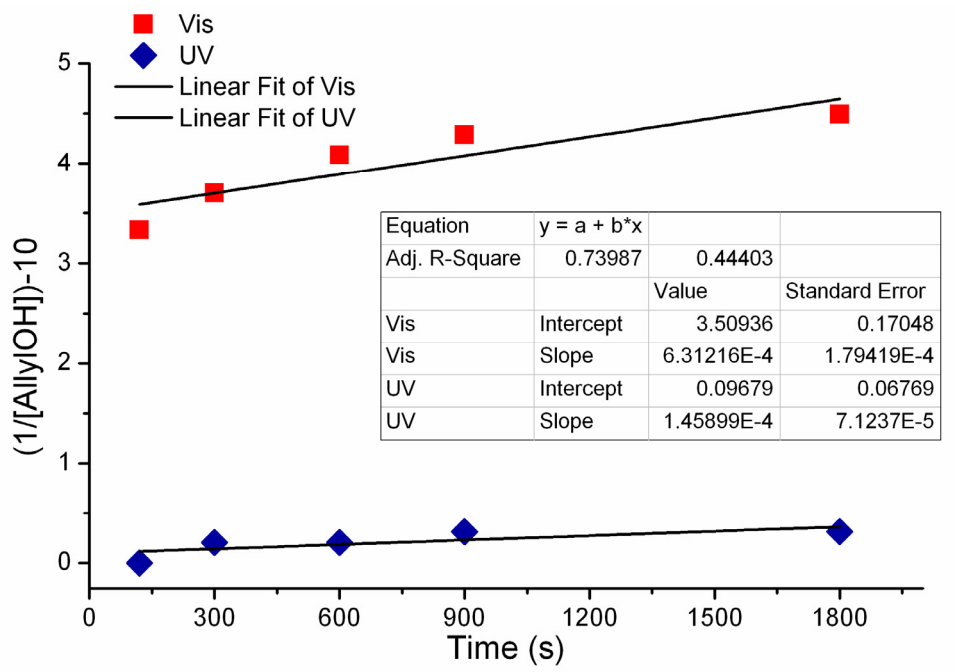

Equation	y = a + b*x		
Adj. R-Square	0.73987	0.44403	
		Value	Standard Error
Vis	Intercept	3.50936	0.17048
Vis	Slope	6.31216E-4	1.79419E-4
UV	Intercept	0.09679	0.06769
UV	Slope	1.45899E-4	7.1237E-5

Figure A2: Plot of (1/[allyl alcohol])-10 (M) vs. time (s) for the NHC catalyzed reaction between allyl alcohol and vinyl acetate. Two reactions were run concurrently with one exposed to UV light (λ_{irr} = 313 nm) for 1 h prior to substrate addition (♦) and one kept under ambient light (■).

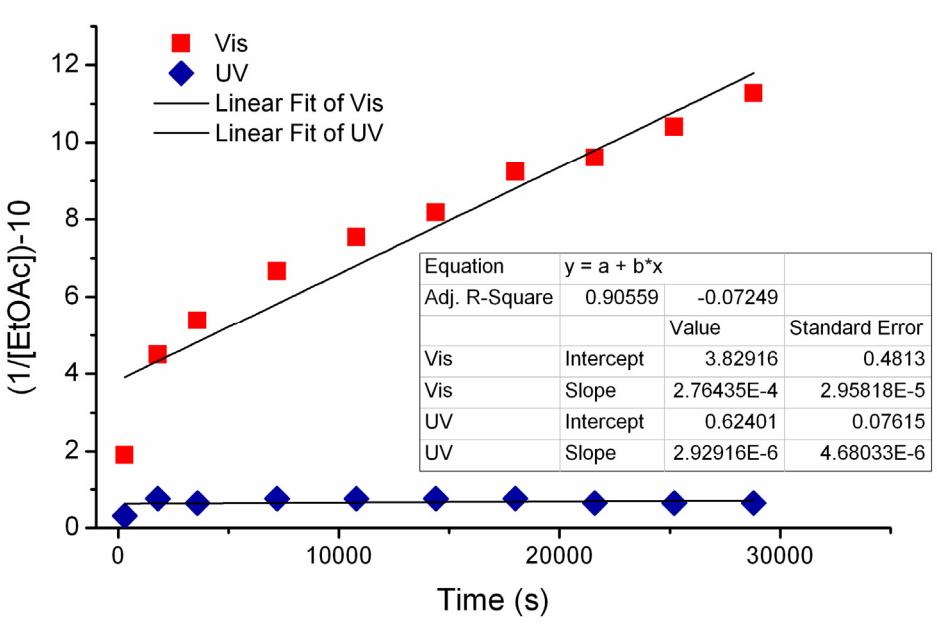

Figure A3: Plot of (1/[ethyl acetate])-10 (M) vs. time (s) for the NHC catalyzed reaction between 2-aminoethanol and ethyl acetate. Two reactions were run concurrently with one exposed to UV light (λ_{irr} = 313 nm) for 1 h prior to substrate addition (♦) and one kept under ambient light (■).

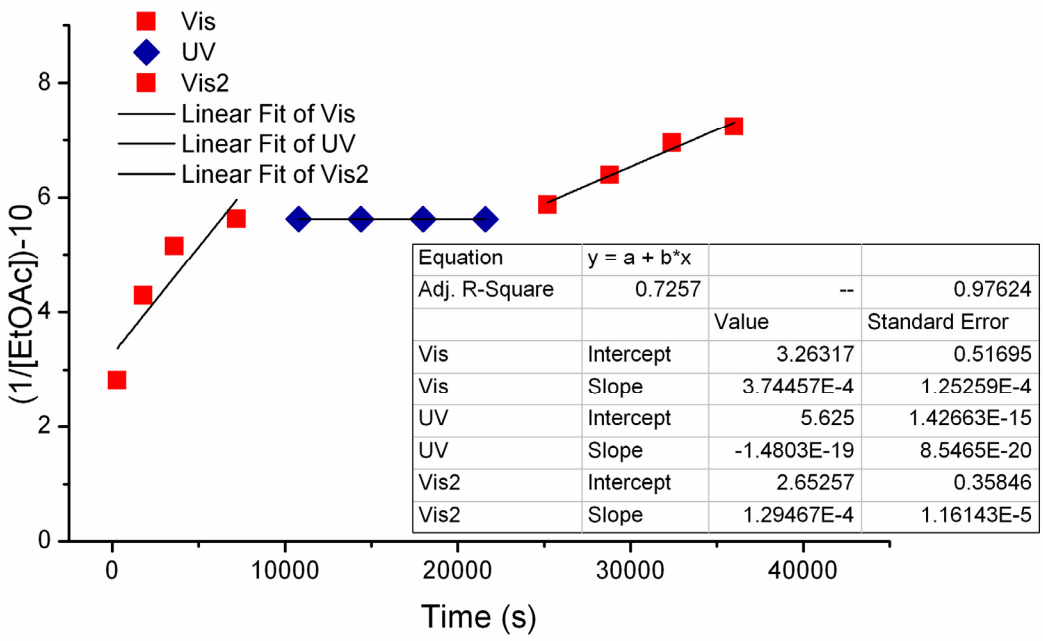

Equation	y = a + b*x		
Adj. R-Square	0.7257	--	0.97624
		Value	Standard Error
Vis	Intercept	3.26317	0.51695
Vis	Slope	3.74457E-4	1.25259E-4
UV	Intercept	5.625	1.42663E-15
UV	Slope	-1.4803E-19	8.5465E-20
Vis2	Intercept	2.65257	0.35846
Vis2	Slope	1.29467E-4	1.16143E-5

Figure A4: Plot of (1/[ethyl acetate])-10 (M) vs. time (s) for the NHC catalyzed reaction between 2-aminoethanol and ethyl acetate. A single reaction was allowed to react under ambient light for 3 h (■), then irradiated with UV light (λ_{irr} = 313 nm) for 1 h and kept in the dark for a further 3 h (♦) prior to exposure to visible light (■) (λ_{irr} > 500 nm).

APPENDIX C: ^{1}H AND ^{13}C NMR FOR PHOTOCHEMICAL REACTIONS IN CHAPTER 3

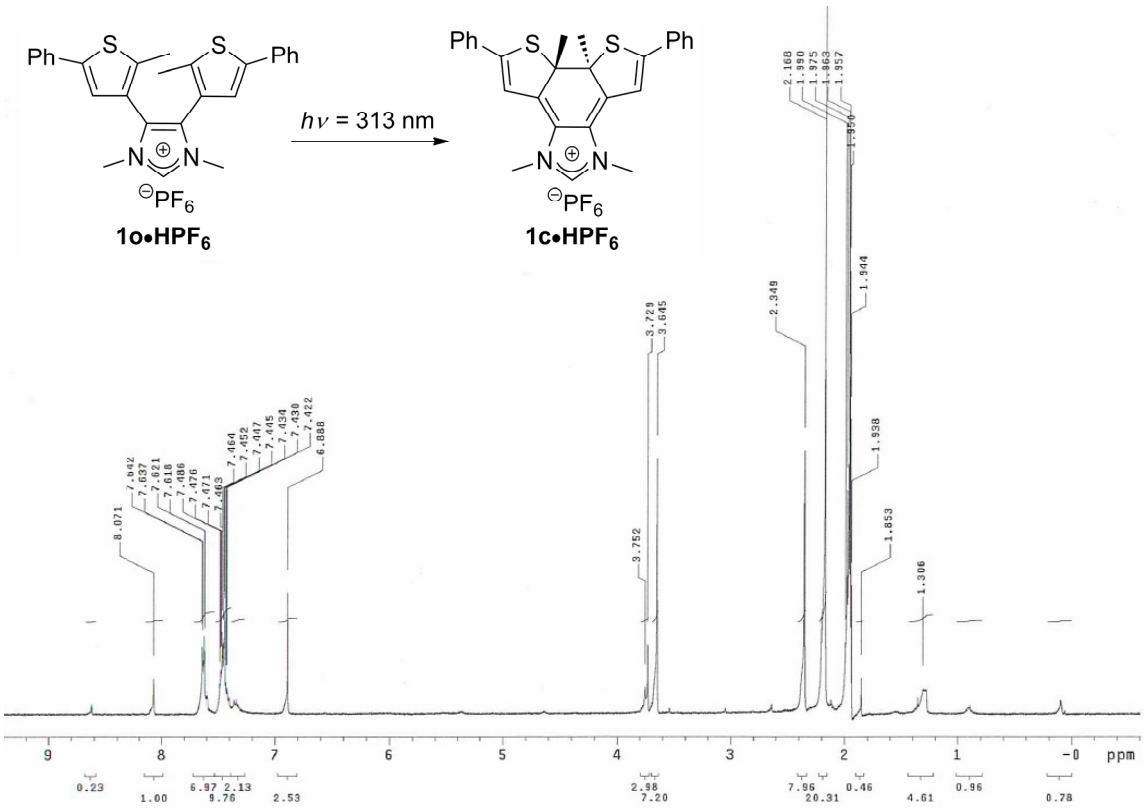

Figure A5: ^{1}H NMR spectrum of the mixture of **1o•HPF$_6$** and **1c•HPF$_6$** obtained after the irradiation of **1o•HPF$_6$** ([**1o•HPF$_6$**]$_0$ = 1 × 10^{-3} M) for 45 min (λ_{irr} = 313 nm) (CD_3CN).

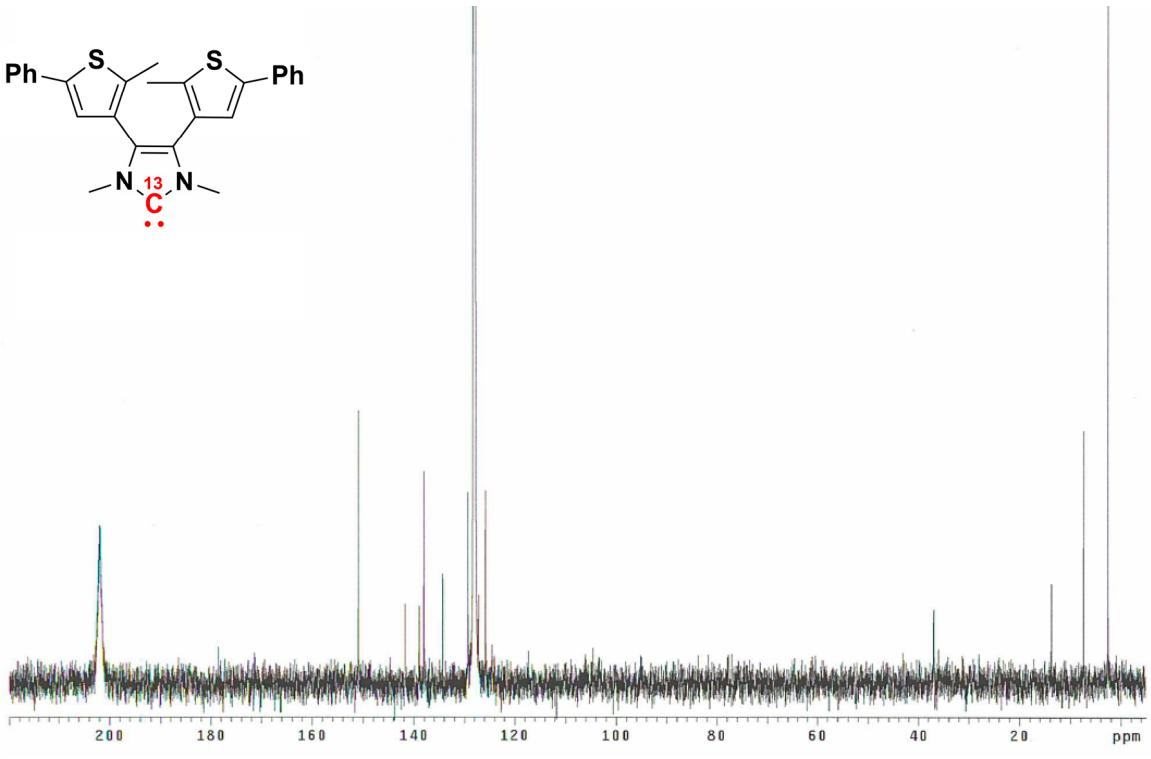

Figure A6: ^{13}C NMR spectrum of **1o*** (C_6D_6).

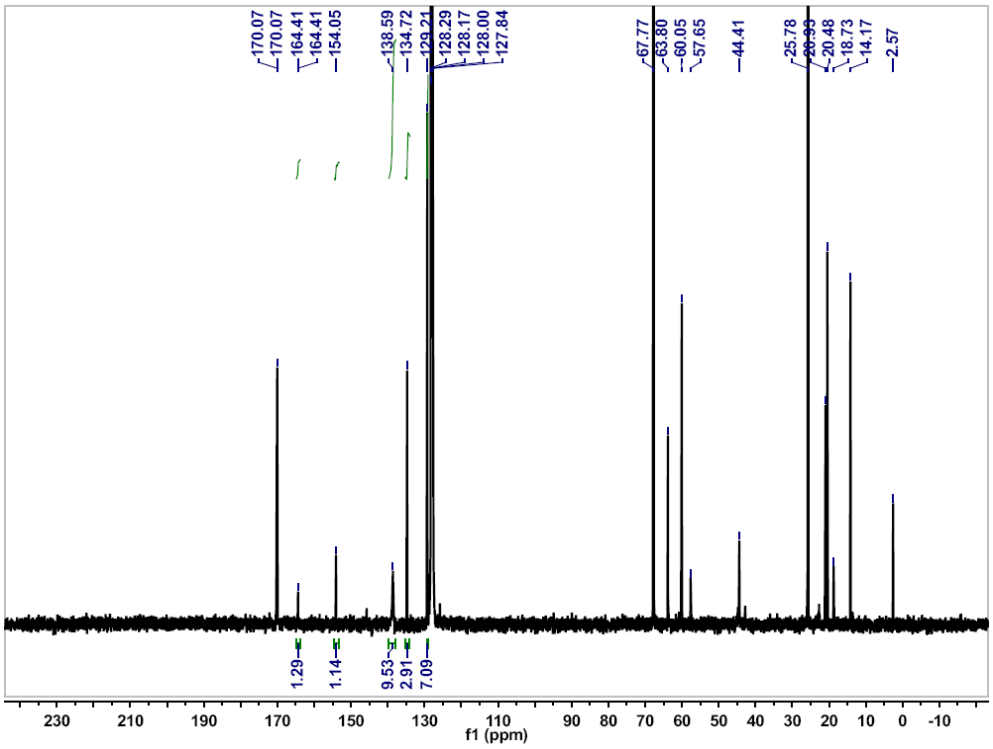

Figure A7: Quantitative ^{13}C NMR spectrum of the adduct obtained after the addition of 2-aminoethanol (0.4 mmol) and ethyl acetate (0.4 mmol) to **1o*** ($[\mathbf{1o^*}]_0$ = 0.01 mmol) with *p*-xylene (0.08 mmol) added as an internal standard (2% v/v THF in C_6D_6).

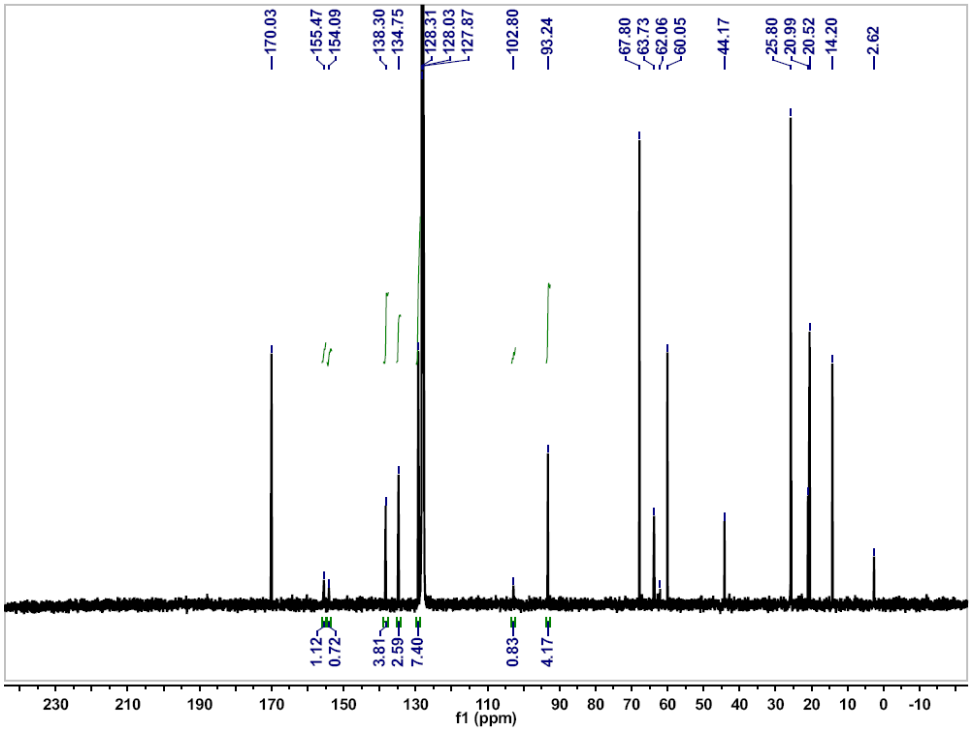

Figure A8: Quantitative ^{13}C NMR spectrum of the adduct obtained after the addition of 2-aminoethanol (0.4 mmol) and ethyl acetate (0.4 mmol) to **1o*** ($[\mathbf{1o^*}]_0$ = 0.01 mmol) and subsequent irradiation ($[\mathbf{1o^*}] = 1 \times 10^{-3}$ M) for 1 h (λ_{irr} = 313 nm) with *p*-xylene (0.08 mmol) added as an internal standard (2% v/v THF in C_6D_6).

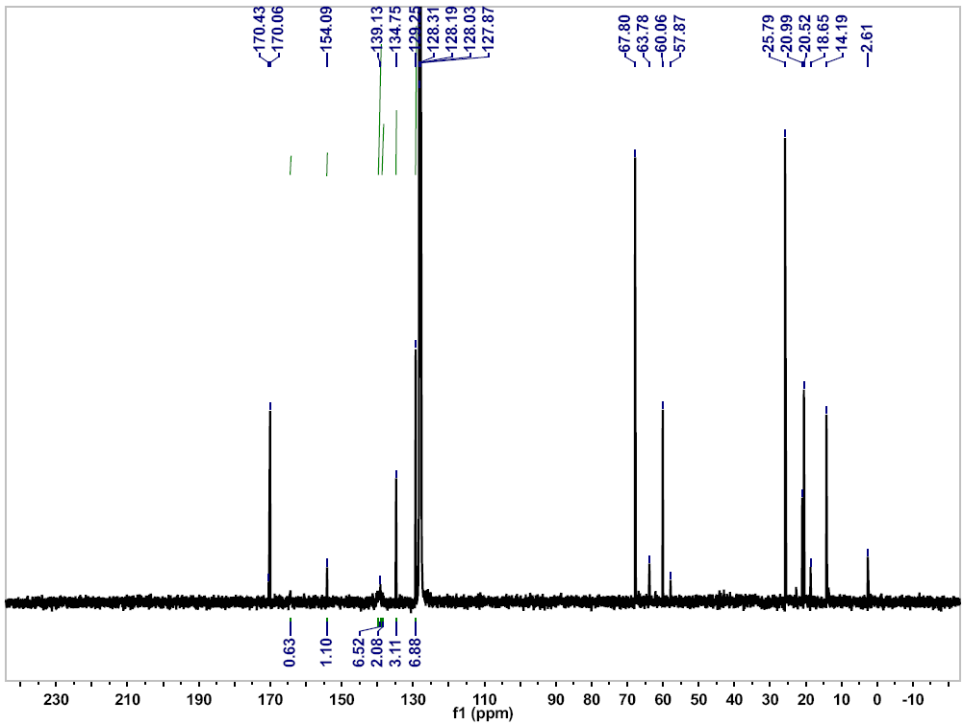

Figure A9: Quantitative ^{13}C NMR spectrum of the cycloreverted adduct of **1o*** in the presence of 2-aminoethanol (0.4 mmol) and ethyl acetate (0.4 mmol) obtained after UV irradiation of **1o*** ($[\mathbf{1o^*}]_0 = 1 \times 10^{-3}$ M) for 1 h (λ_{irr} = 313 nm) followed by visible light irradiation for 2 h ($\lambda_{irr} > 500$ nm) with *p*-xylene (0.08 mmol) as an internal standard (2% v/v THF : C_6D_6).

APPENDIX D: PSEUDO FIRST ORDER KINETIC ANALYSES FOR CHAPTER 4

The ring-opening polymerization of valerolactone initiated by benzyl alcohol and catalyzed by NHC precatalyst **1** may be represented as:

$$A + B \longrightarrow P$$

Assuming no side reactions, the valerolactone (*A*) will always be present in a large excess over the benzyl alcohol (*B*) quantities. As such, pseudo-first order kinetics may be assumed, and the following rate law applies:

$$\frac{d[P]}{dt} = k[A][B]_0 = k[A]$$

The integrated form of the above equation is as follows:

$$\ln[A] = \ln[A]_0 - kt$$

Rearranging the integrated rate law and substituting the initial concentration of 2.0 M for $[A]_0$ gives:

$$\ln\left(\frac{[A]}{[A]_0}\right) = \ln\left(\frac{[A]}{2.0}\right) = -kt$$

Thus, plotting $\ln([A]_0/[A])$ vs. *t* (s) should give a linear plot where $-k$ is equal to the slope of the line, as shown below in Figures A10 – A13 for selected examples.

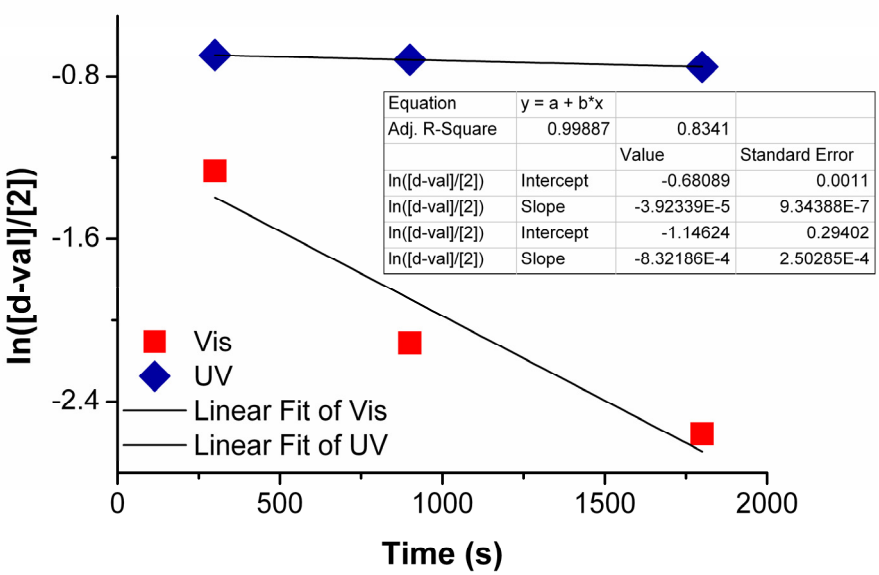

Figure A10: Plot of ln([δ-valerolactone]/2.0) vs. time (s) for the ring opening polymerization of δ-valerolactone catalyzed by **1**. Two reactions were run concurrently with one exposed to UV light (λ_{irr} = 313 nm) for 1 h prior to substrate addition (♦) and one kept under ambient light (■).

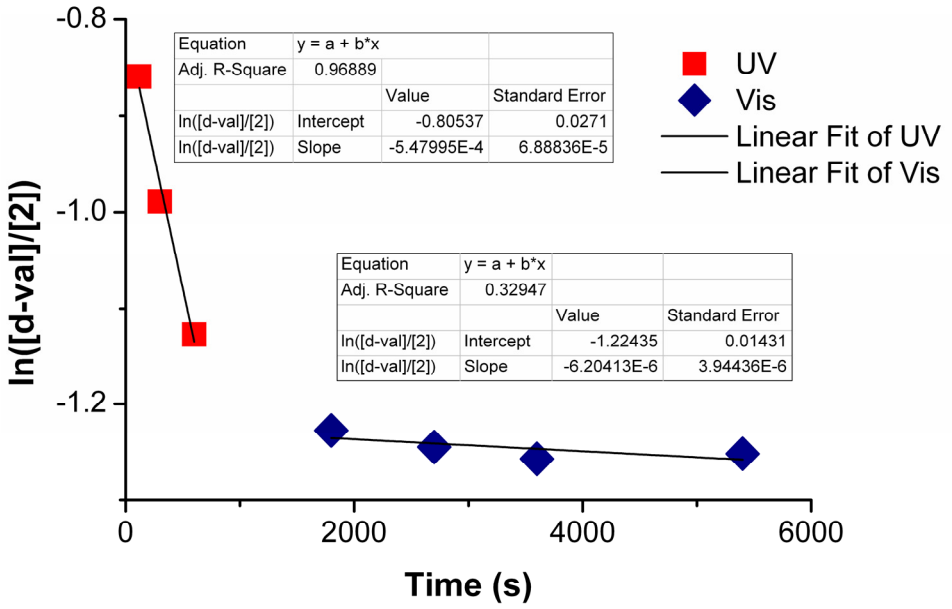

Figure A11: Plot of ln([δ-valerolactone]/2.0) vs. time (s) for the ring opening polymerization of δ-valerolactone catalyzed by **1**. A single reaction was allowed to react under ambient light for 10 min (■), then irradiated with UV light (λ_{irr} = 313 nm) for 80 min (♦).

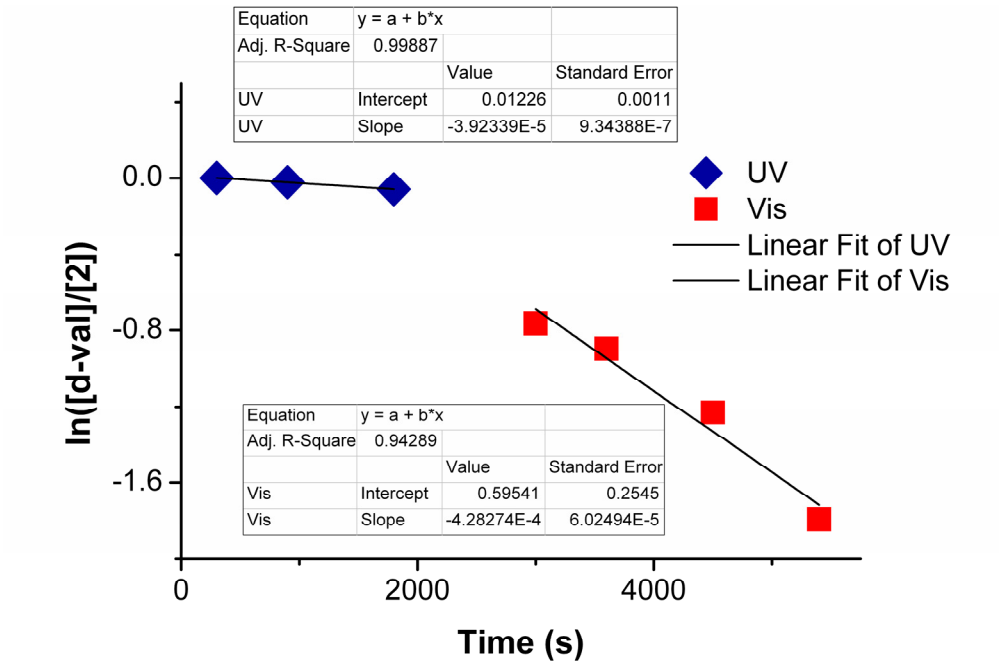

Figure A12: Plot of ln([δ-valerolactone]/2.0) vs. time (s) for the ring opening polymerization of δ-valerolactone catalyzed by **1**. A single reaction was exposed to UV irradiation (λ_{irr} = 313 nm) for 1 h prior to substrate addition and was kept under UV irradiation for a further 30 min (♦). The reaction was subsequently exposed to visible irradiation (λ_{irr} > 500 nm) for a further 1 h (■).

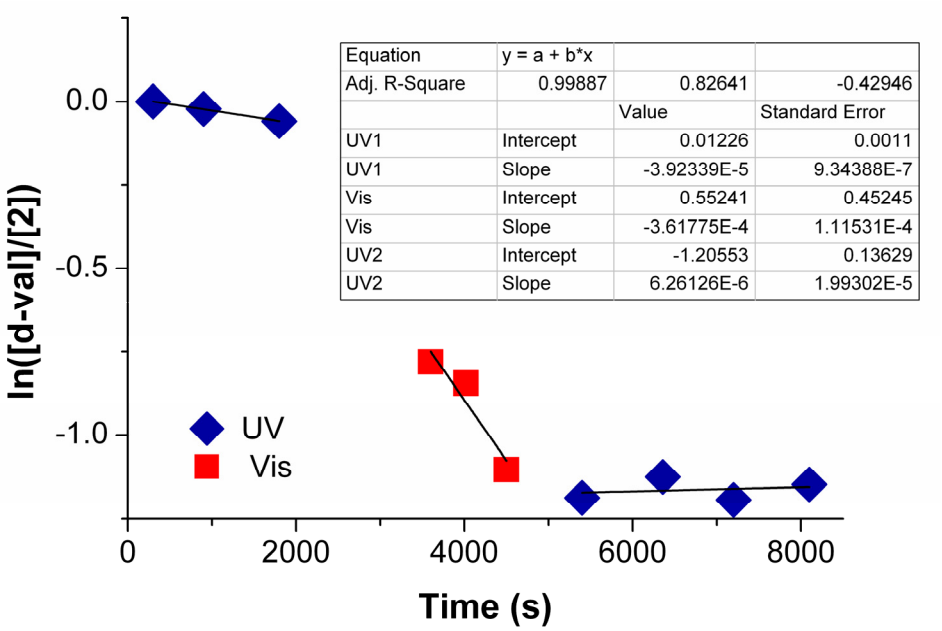

Figure A13: Plot of ln([δ-valerolactone]/2.0) vs. time (s) for the ring opening polymerization of δ-valerolactone catalyzed by **1**. A single reaction was exposed to UV irradiation (λ_{irr} = 313 nm) for 1 h prior to substrate addition and was kept under UV irradiation for a further 30 min (♦). The reaction was then exposed to visible irradiation (λ_{irr} > 500 nm) for 1 h (■), followed by subsequent UV irradiation for a further 1.25 h.

APPENDIX E: SECOND ORDER KINETIC ANALYSES FOR CHAPTER 5

The reactions between 1-octene, styrene or *t*-butylacetyelene and pinacolborane may be represented as:

$$A + B \longrightarrow P$$

Assuming no side reactions, the two reactants will always be present in equimolar quantities. As such, the above equation may be simplified to:

$$2A \longrightarrow P$$

This reaction equation may be expressed as the following rate law:

$$\frac{d[P]}{dt} = k[A]^2$$

The integrated form of the above equation is as follows:

$$\frac{1}{[A]} = kt + \frac{1}{[A]_0}$$

Rearranging the integrated rate law and substituting the initial concentration of 0.1 M for $[A]_0$ gives:

$$\frac{1}{[A]} - 10 = kt$$

Thus, plotting (1/[A]-10) (M) vs. *t* (s) gives a linear plot where *k* is equal to the slope of the line, as shown below in Figures A14 – A19 for selected examples. Each reported rate constant (k_{vis}, k_{UV}, k) was obtained from the average of at least three separate experiments.

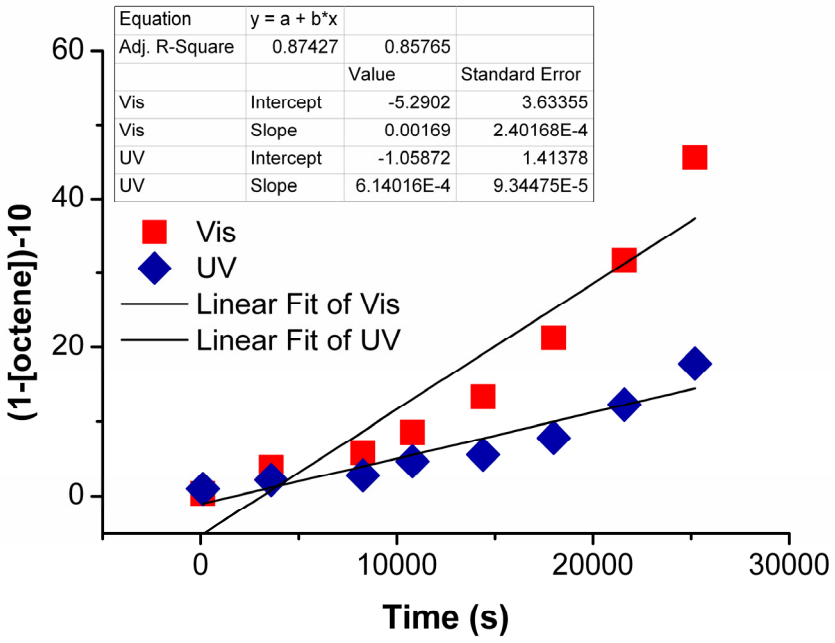

Figure A14: Plot of (1/[octene])-10 (M) vs. time (s) for the hydroboration reaction between 1-octene and pinacolborane catalyzed by **1**. Two reactions were run concurrently with one exposed to UV light (λ_{irr} = 313 nm) for 2 h prior to substrate addition (♦) and one kept under ambient conditions (■).

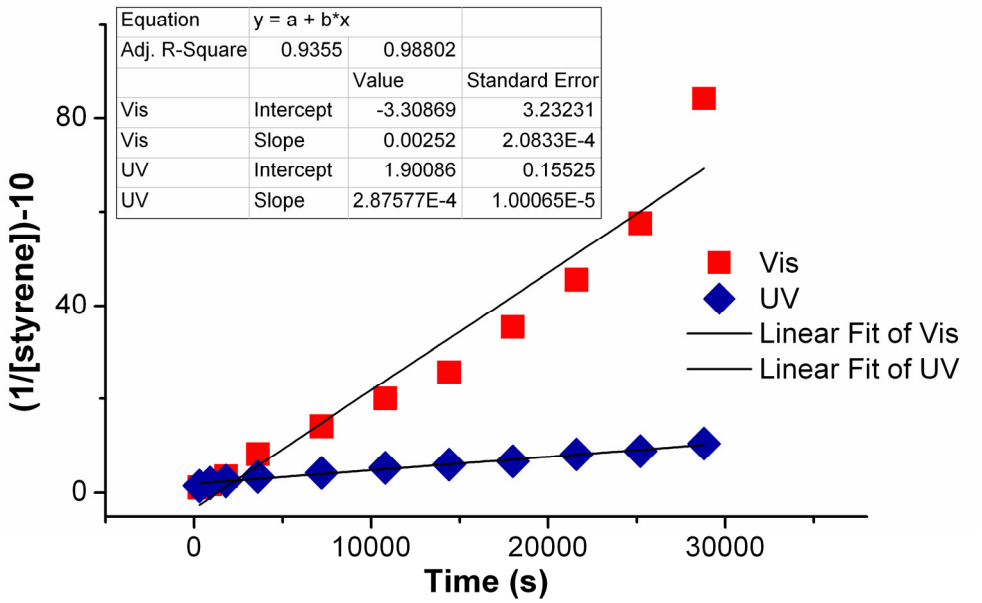

Figure A15: Plot of (1/[styrene])-10 (M) vs. time (s) for the hydroboration reaction between styrene and pinacolborane catalyzed by **1**. Two reactions were run concurrently with one exposed to UV light (λ_{irr} = 313 nm) for 2 h prior to substrate addition (♦) and one kept under ambient conditions (■).

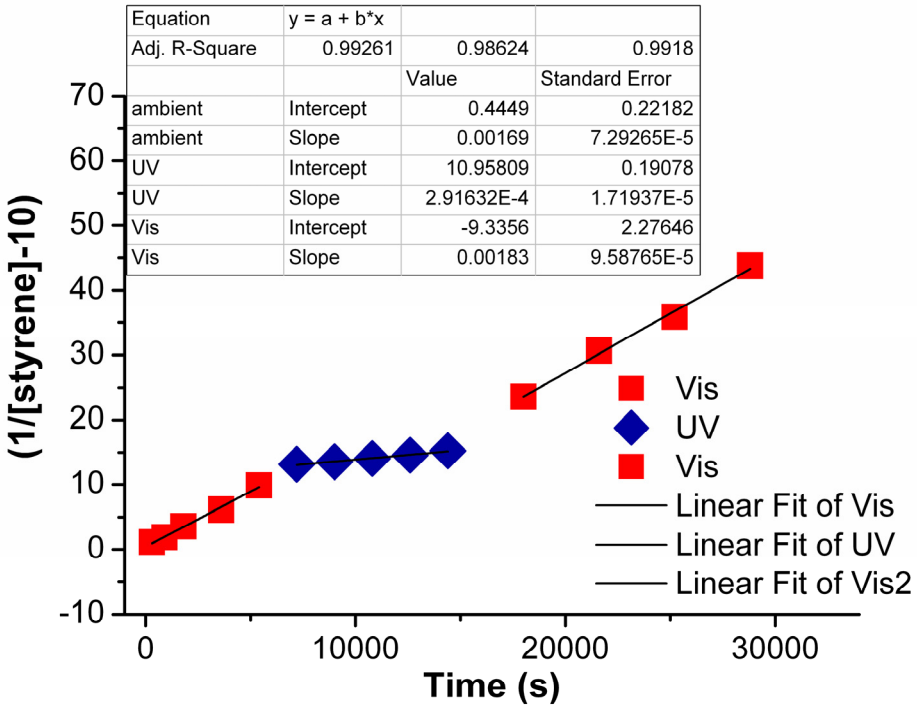

Figure A16: Plot of (1/[styrene])-10 (M) vs. time (s) for the hydroboration reaction between styrene and pinacolborane catalyzed by **1**. The reaction was started in ambient light (■), then exposed to UV light (λ_{irr} = 313 nm) (♦) after 1 h prior to subsequent exposure to visible light (λ_{irr} > 500 nm) (■) after 2 h to restore reactivity.

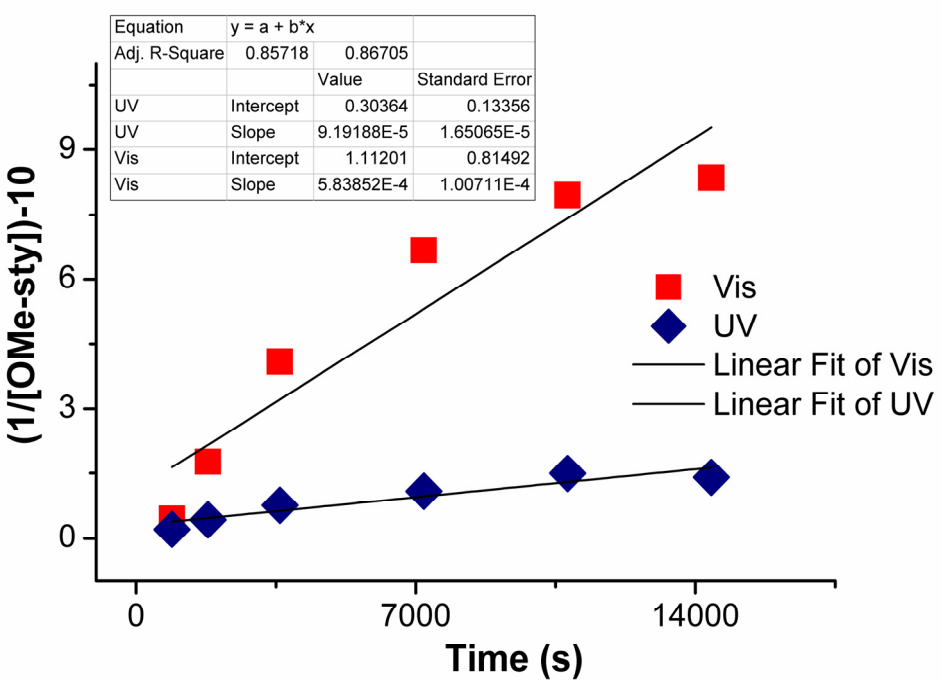

Figure A17: Plot of (1/[OMe-styrene])-10 (M) vs. time (s) for the hydroboration reaction between 4-methoxystyrene and pinacolborane catalyzed by **1**. Two reactions were run concurrently with one exposed to UV light (λ_{irr} = 313 nm) for 2 h prior to substrate addition (♦) and one kept under ambient conditions (■).

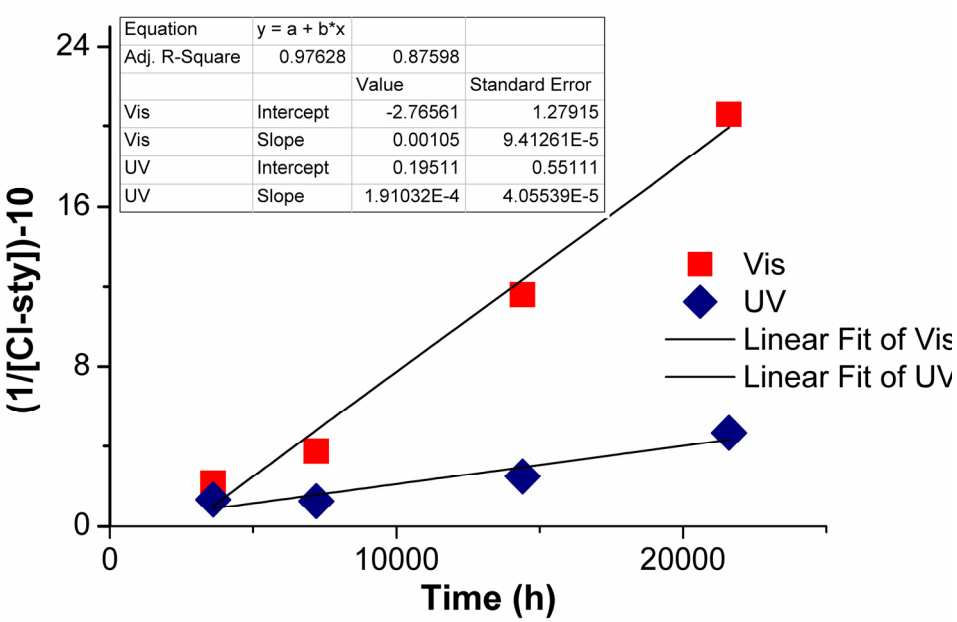

Figure A18: Plot of (1/[Cl-styrene])-10 (M) vs. time (s) for the hydroboration reaction between 4-chlorostyrene and pinacolborane catalyzed by **1**. Two reactions were run concurrently with one exposed to UV light (λ_{irr} = 313 nm) for 2 h prior to substrate addition (♦) and one kept under ambient conditions (■).

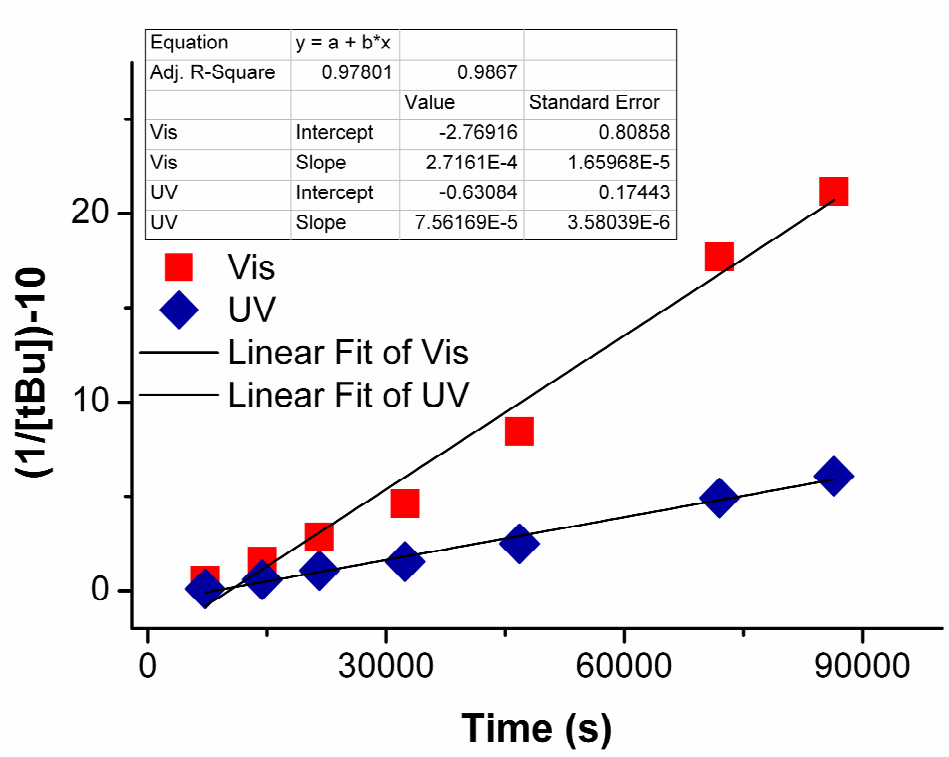

Figure A19: Plot of (1/[*t*-butylacetylene])-10 (M) vs. time (s) for the hydroboration reaction between *t*-butylacetylene and pinacolborane catalyzed by **1**. Two reactions were run concurrently with one exposed to UV light (λ_{irr} = 313 nm) for 2 h prior to substrate addition (♦) and one kept under ambient conditions (■).

APPENDIX E: ^{1}H AND ^{13}C NMR FOR PHOTOCHEMICAL REACTIONS IN CHAPTER 5

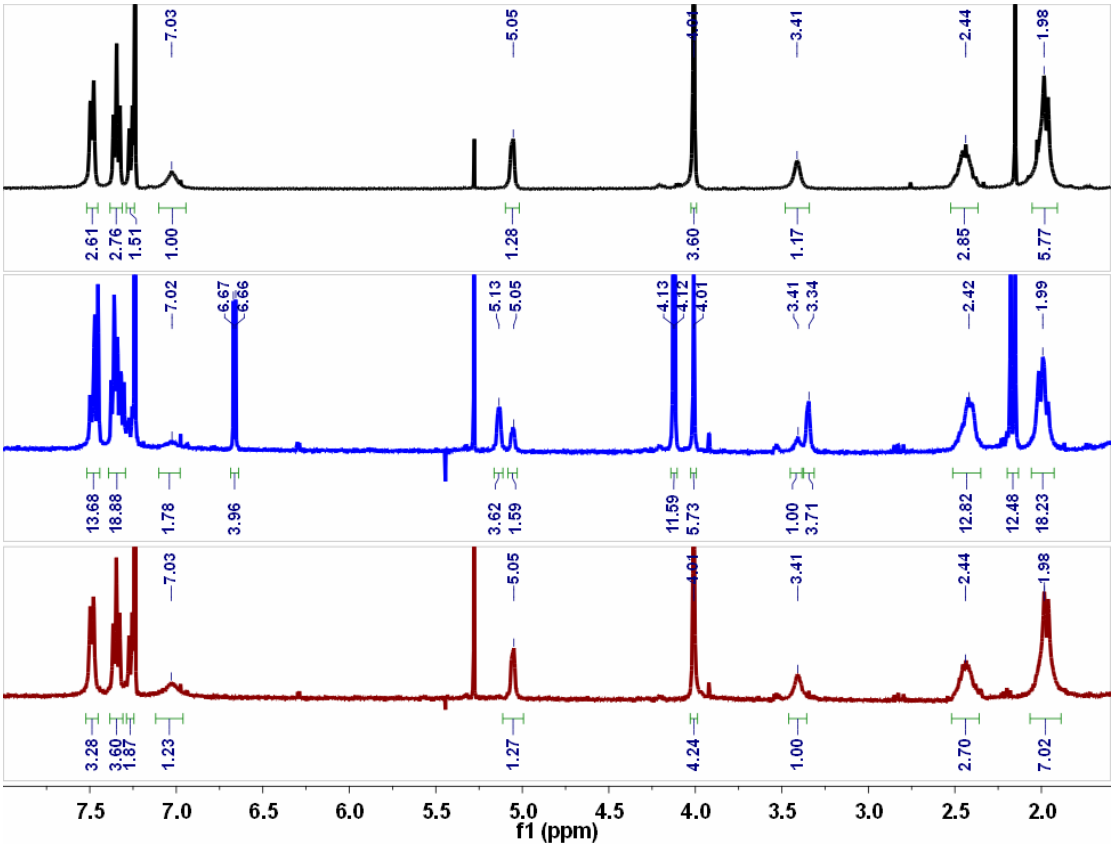

Figure A20: ^{1}H NMR spectra ($CDCl_3$) of (top) **1o**, (middle) the mixture of **1o** and **1c** after UV irradiation (λ_{irr} = 313 nm) of **1o** ($[\mathbf{1o}]_0 = 1 \times 10^{-3}$ M) in cyclohexane for 1 h, (bottom) and the mixture after visible irradiation (λ_{irr} > 500 nm) for 2 h.

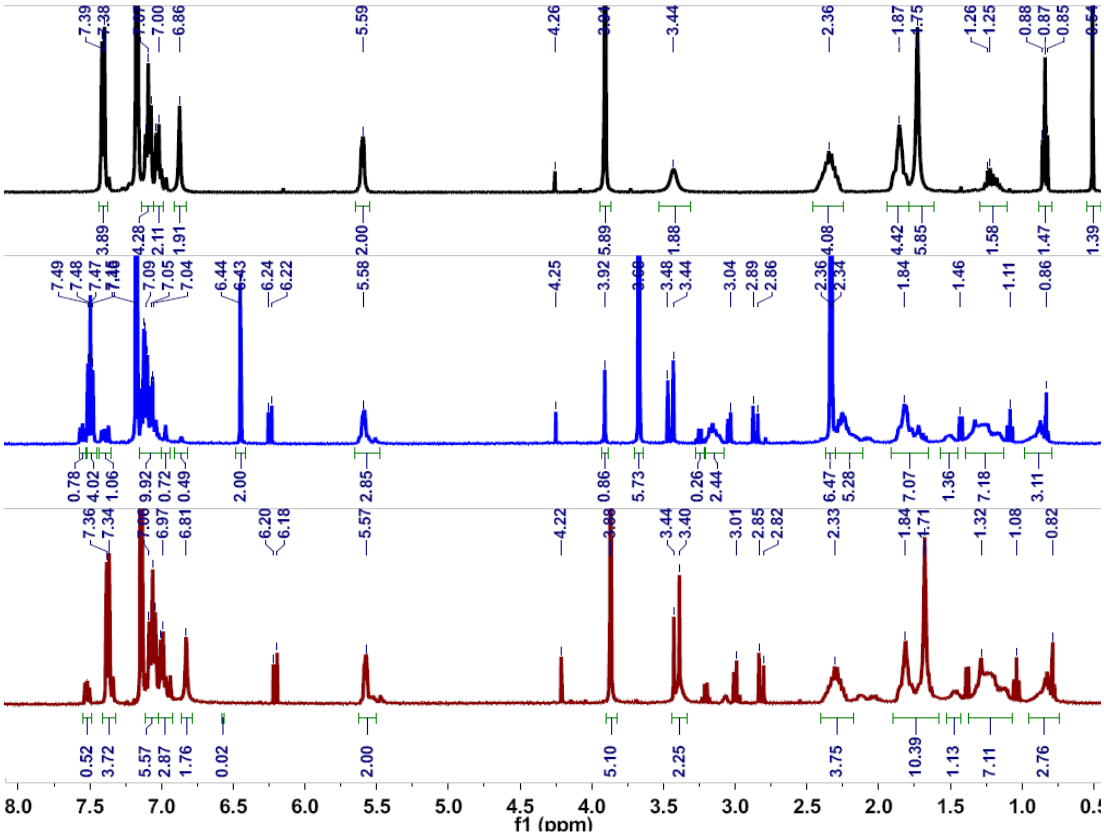

Figure A21: ^{1}H NMR spectra (C_6D_6) of (top) **1o**, (middle) the mixture of **1o** and **1c** after UV irradiation (λ_{irr} = 313 nm) of **1o** ([**1o**]$_0$ = 1 × 10^{-3} M) in C_6H_6 for 2 h, and (bottom) the mixture after visible irradiation (λ_{irr} > 500 nm) for 2 h.

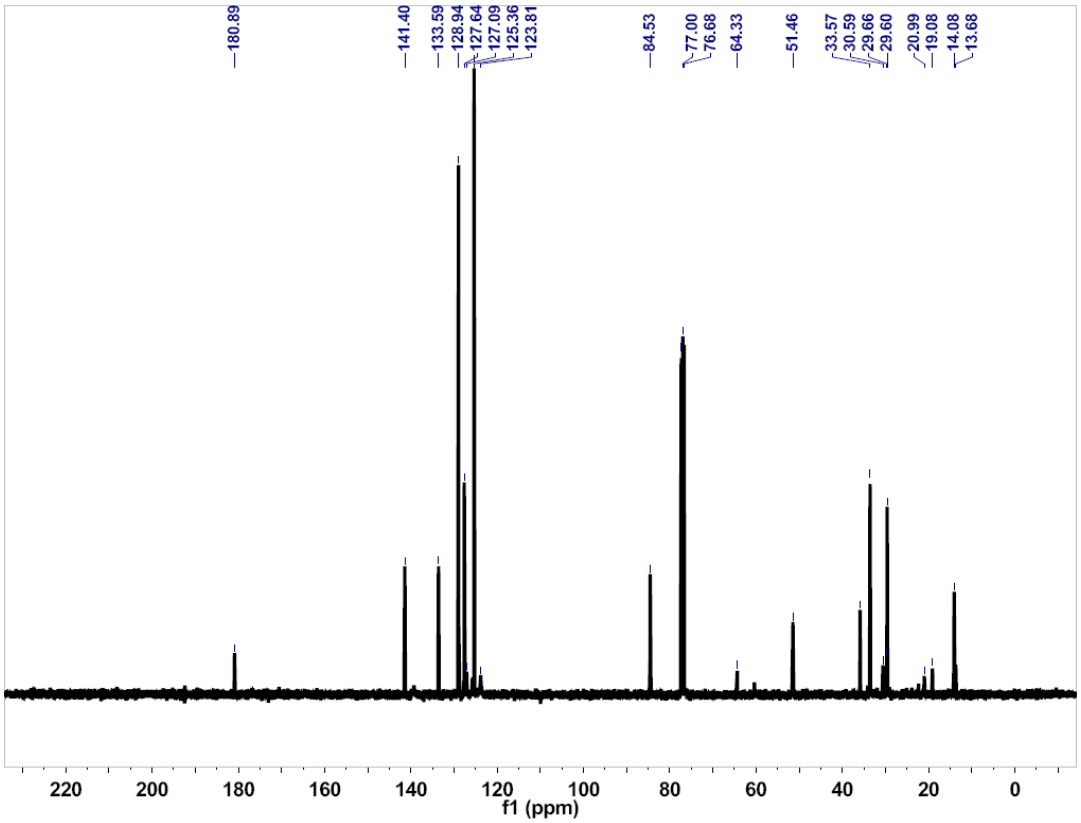

Figure A22: ^{13}C NMR spectrum of **1o** ($CDCl_3$).

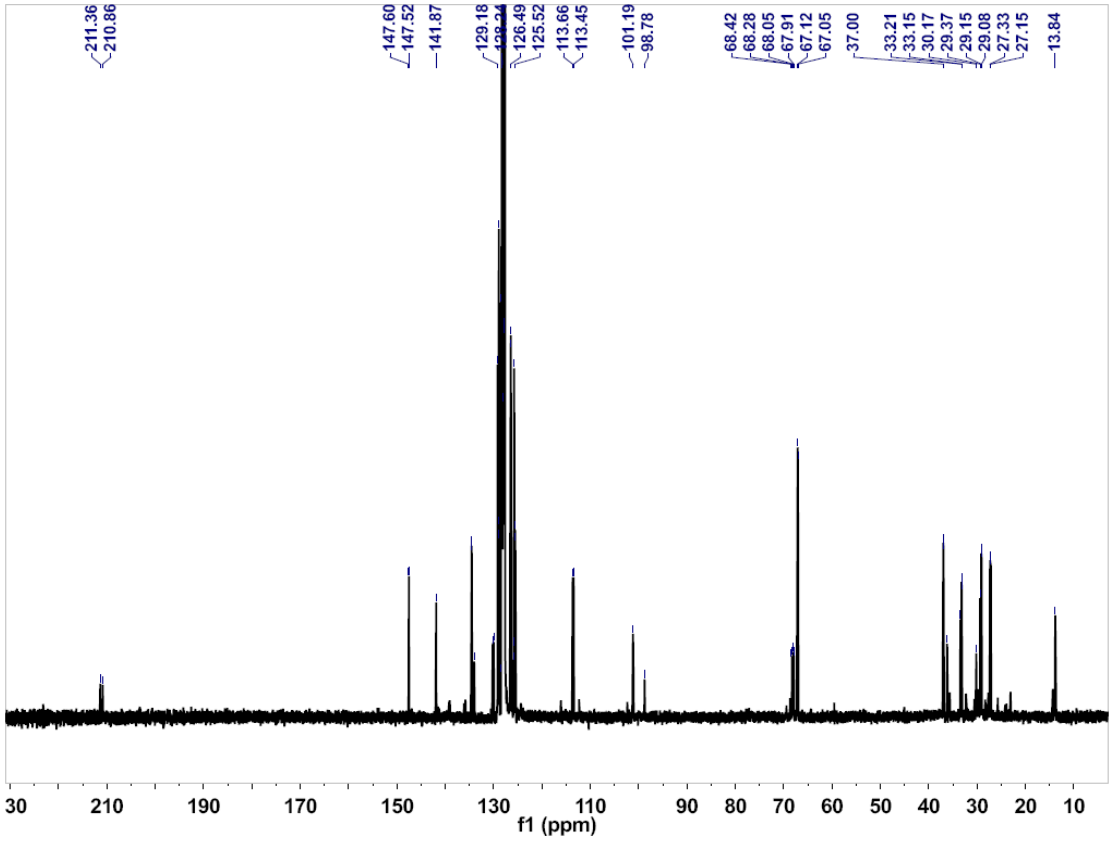

Figure A23: ^{13}C NMR spectra (C_6D_6) the mixture of **1o** and **1c** after UV irradiation (λ_{irr} = 313 nm) of **1o** ($[\mathbf{1o}]_0 = 1 \times 10^{-3}$ M) in C_6H_6 for 2 h.

Bibliography

Abraham, T.; Kumpulainen, A.; Xu, Z.; Rutland, M.; Claesson, P. M.; Masliyah, J. *Langmuir* **2001,** *17*, 8321-8327.

Adkins, S. S.; Gohil, D.; Dickson, J. L.; Webber, S. E.; Johnston, K. P. *Phys. Chem. Chem. Phys.* **2007**, *9*, 6333-6343.

Akita, M. *Organometallics* **2011**, *30*, 43-51.

Allgeier, A. M.; Mirkin, C. A. *Angew. Chem. Int. Ed.* **1998**, *37*, 894-908.

Amstad, E.; Gillich, T.; Bilecka, I.; Textor, M.; Reimhult, E. *Nano Lett.* **2009,** *9*, 4042-4048.

Amstad, E.; Textor, M.; Reimhult, E. *Nanoscale* **2011,** *3*, 2819.

Anjos, T.; Charlton, A.; Coles, S. J.; Croft, A. K.; Hurshouse, M. B.; Kalaji, M.; Murphy, P. J.; Roberts-Bleming, S. J. *Macromolecules*, **2009**, *42*, 2505-2515.

Aveyard, R.; Clint, J. H.; Horozov, T. S. *Phys. Chem. Chem. Phys.* **2003**, *5*, 2398–2409.

Bacri, J.; Perzynski, R.; Salin, D.; Cabuil, V.; Massart, R. *J. Magn. Magn. Mater.* **1990**, *85*, 27.

Bagaria, H. G.; Neilson, B. M.; Worthen, A. J.; Xue, Z.; Yoon, K. Y. Cheng, V.; Lee, J. H.; Velagala, S.; Huh, C.; Bryant, S. L.; Bielawski, C. W.; Johnston, K. P. *J. Colloid. Interf. Sci.* **2013**, *398*, 217-226.

Bagaria, H. G.; Yoon, K. Y.; Neilson, B. M.; Cheng, V.; Lee, J. H.; Worthen, A. J.; Xue, Z.; Huh, C.; Bryant, S. L.; Bielawski, C. W.; Johnston, K. P. *Langmuir* **2013**, 3195-3206.

Bagaria, H. G.; Xue, Z.; Neilson, B. M.; Worthen, A. J.; Yon, K. Y.; Nayak, S.; Cheng, V.; Lee, J. H.; Bielawski, C. W.; Johnston, K. P. *ACS Appl. Mater. Interfaces* **2013**, 3329-3339.

Ballauff, M.; Borisov, O.; *Curr Opin Colloid In.* **2006**, *11*, 316-323.

Balof, S. L. P'Pool, S. J. Berger, N. J. Valente, E. J. Shiller, A. M. Schanz, H.-J. *Dalton Trans.* **2008**, *42*, 5791-5799.

Balof, S. L. Yu, B. Lowe, A. B. Ling, Y. Zhang, Y. Schanz, H.-J. *Eur. J. Inorg. Chem.* **2009**, *13*, 1717-1722.

Bandara, H. M. D.; Burdette, S. C. *Chem. Soc. Rev.* **2012**, *41*, 1809-1825.

Barrera, C.; Herrera, A. P.; Bezares, N.; Fachini, E.; Olayo-Valles, R.; Hinestroza, J. P.; Rinaldi, C. *J.Colloid Interf. Sci.* **2012,** *377*, 40-50.

Belen'kii, L. I.; Shirinyan, V. Z.; Gromova, G. P.; Kolotaev, A. V.; Strelenko, Y. A.; Tandura, S. N.; Shumskii, A. N.; Krayushkin, M. M.; *Chem. Het. Cmpds.* **2003**, *39*, 1570-1578.

Beletskaya, I.; Pelter, A. *Tetrahedron* **1997**, *53*, 4957-5026.

Benac, B. L.; Burgess, E. M.; Arduengo, A. J. *Org. Synth.* **1986**, *64*, 92.

Ben-Asuly, A.; Aharoni, A.; Diesendruck, C. E.; Vidavsky, Y.; Goldberg, I.; Straub, B. F.; Lemcoff, N. G. *Organometallics* **2009**, *28*, 4652-4655.

Benhamou, L.; Vujkovic, N.; César, V.; Gornitzka, H.; Lugan, N.; Lavigne, G. *Organometallics* **2010**, *29*, 2616-2630.

Berg, J. C., *An introduction to interfaces & colloids : the bridge to nanoscience*. World Scientific: Singapore ; Hackensack, NJ, 2010; p 785.

Berkovic, G.; Krongauz, V.; Weiss, V. *Chem. Rev.* **2000**, *100*, 1741-1753.

Berkowitz, A. E.; Lahut, J. A.; Sacobs, I. S.; Levinson, L. M.; Forester, D. W. *Phys. Rev.Lett.* **1975**, *34*, 594–597.

Berlin, J. M.; Yu, J.; Lu, W.; Walsh, E. E.; Zhang, L. L.; Zhang, P.; Chen, W.; Kan, A. T.; Wong, M. S.; Tomson, M. B.; Tour, J. M. *Energ. Environ. Sci.* **2011**, *4*, 505-509.

Berret, J.-F. *Macromolecules* **2007**, *40*, 4260-4266.

Berret, J.-F.; Schonbeck, N.; Gazeau, F.; El Kharrat, D.; Sandre, O.; Vacher, A.; Airiau, M. *J. Am. Chem. Soc.* **2006**, *128*, 1755-1761.

Biggs, S.; Healy, T. W. *J. Chem. Soc. Faraday T.* **1994,** *90*, 3415-3421.

Biju, A. T.; Kuhl, N.; Glorius, F. *Acc. Chem. Res.* **2011**, *44*, 1182-1195.

Binks, B. P. *Curr. Opin. Coll. Interf. Sci.* **2002,** 7, 21-41.

Binks, B. P. *Langmui*r **2004**, *20*, 1130-1137.

Binks, B. P.; Kirkland, M. *Phys. Chem. Chem. Phys.* **2002**, *4*, 3727-3733.

Binks, B. P.; Kirkland, M.; Rodrigues, J. A. *Soft Mater.* **2008,** 4, 2373–2382.

Binks, B. P.; Rodrigues, J. A. *Langmuir* **2007**, *23*, 7436-7439.

Blanco, V.; Carlone, A.; Hänni, K. D.; Leigh, D. A.; Lewandowski, B. *Angew. Chem. Int. Ed.* **2012**, *51*, 5166-5169.

Boue, F.; Cotton, J. P.; Lapp, A.; Jannink, G.; *J. Chem. Phys.* **1994**, *101*, 2562-2568.

Bourissou, D.; Guerret, O.; Gabbaï, F. P.; Bertrand, G.; *Chem. Rev.* **2000**, *100*, 39-91.

Boyer, C.; Whittaker, M. R.; Bulmus, V.; Liu, J. Q.; Davis, T. P.; *NPG Asia Mater*. **2010**, *2*, 23-30.

Broderick, E. M.; Guo, N.; Vogel, C. S.; Xu, C.; Sutter, J. R.; Miller, J. T.; Meyer, K.; Mehrkhodavandi, P.; Diaconescu, P. L. *J. Am. Chem. Soc.* **2011**, *133*, 9278.

Broderick, E. M.; Guo, N.; Wu, T.; Vogel, C. S.; Xu, C.; Sutter, J.; Miller, J. T.; Meyer, K.; Cantat, T.; Diaconescu, P. L. *Chem. Commun.* **2011**, *47*, 9897.

Burgess, K.; Ohlmeyer, M. J. *Chem. Rev.* **1991**, *91*, 1179-1191.

Burgess, K.; van der Donk, W. A.; Jarstfer, M. B.; Ohlmeyer, M. J. *J. Am. Chem. Soc.* **1991**, *113*, 6139-6144.

Cacciapaglia, R.; Di Stefano, S.; Mandolini, L. *J. Am. Chem. Soc.* **2003**, *125*, 2224-2227.

Campelj, S.; Makovec, D.; Drofenik, M. *J. Phys.: Condens. Matter* **2008**, *20*, 204101-204105.

Caputo, C.; Nobile, C.; Kipp, T.; Blasi, L.; Grillo, V.; Carlino, E.; Manna, L.; Cingolani, R.; Cozzoli, P. D.; Athanassiou, A. *J. Phys. Chem. C.* **2008**, *112*, 701-714.

Carroll, A.-M.; O'Sullivan, T. P.; Guiry, P. J. *Adv. Synth. Catal.* **2005**, *347*, 609-631.

Chan, C.; Heid, R.; Zheng, S.; Guo, J.; Zhou, B.; Furuuchi, T.; Danishefsky, S. J. *J. Am. Chem. Soc.* **2005**, *127*, 4596-4598.

Chanteau, B.; Fresnais, J.; Berret, J. F. *Langmuir* **2009,** *25*, 9064-9070.

Chen, X.; Adkins, S. S.; Nguyen, Q. P.; Sanders, A. W.; Johnston, K. P. *J. Supercrit Fluid* **2010,** *55*, 712–723.

Chen, Y.; Elhag, A. S.; Poon, B. M.; Cui, L.; Ma, K.; Liao, S. Y.; Omar, A.; Worthen, A.; Hirasaki, G. J.; Nguyen, Q. P.; Johnston, K. P. *SPE Improved Oil Recovery Symposium*, Society of Petroleum Engineers: Tulsa, Oklahoma, USA, 2012.

Chianese, A. R.; Li, X.; Janzen, M. C.; Faller, J. W.; Crabtree, R. H. *Organometallics*, **2003**, *22*, 1663-1667.

Choi, H.; Lee, H.; Kang, Y.; Kim, E.; Kang, S.-O.; Ko, J. *J. Org. Chem.* **2005**, *70*, 8291-8297.

Clayden, J.; Moran, W.; *Angew. Chem. Int. Ed.* **2006**, *45*, 7118-7120.

Coleman, A. W.; Hithcock, P. B.; Lappert, M. F.; Maskell, R. K.; Müller, J. H. *J. Organomet. Chem.* **1985**, *296*, 173-196.

Connor, E. F.; Nyce, G. W.; Myers, M.; Möck, A.; Hedrick, J. L. *J. Am. Chem. Soc.* **2002**, *124*, 914-915.

Crudden, C. M.; Edwards, D. *Eur. J. Org. Chem.* **2003**, *24*, 4695-4712.

Crudden, C. M.; Hleba, Y. B.; Chen, A. C. *J. Am. Chem. Soc.* **2004**, *126*, 9200-9201.

Csihony, S.; Culkin, D. A.; Sentman, A. C.; Dove, A. P.; Waymouth, R. M.; Hedrick, J. L. *J. Am. Chem. Soc.* **2005**, *127*, 9079-9084.

David, C.; Companys, E.; Galceran, J.; Garces, J. L.; Mas, F.; Rey-Castro, C.; Salvador, J.; Puy, J. *J. Phys. Chem. B.* **2007,** *111*, 10421-10430.

Davies, M.; Jones, J.; *J. Chem. Soc.* **1958**, 955-958.

DENZO-SMN. (1997): Z. Otwinowski, W. Minor in *Methods in Enzymology, 276: Macromolecular Crystallography, part A*, (Eds.: C. W. Carter, Jr., R. M. Sweets) Academic Press, **1997**, 307 – 326.

Díez-González, S.; Marion, N.; Nolan, S. P.; *Chem. Rev.* **2009**, *109*, 3612-3676.

Ditsch, A.; Laibinis, P. E.; Wang, D. I. C.; Hatton, T. A. *Langmuir* **2005**, *21*, 6006-6018.

Dobrynin, A. V.; Rubinstein, M.; *Prog Polym Sci.* **2005**, *30*, 1049-1118.

Dröge, T.; Glorius, F.; *Angew. Chem. Int. Ed*. **2010**, *49*, 6940-6952.

Du, K.; Glogowski, E.; Emrick, T.; Russell, T. P.; Dinsmore, A. D. *Langmuir* **2010**, *26*, 12518-12522.

Duan, G. Zhu, N.; Yam, V. W.-W. *Chem. Eur. J.* **2010**, *16*, 13199-13209.

Durr, H. Bouas-Laurent, H. Eds. *Photochromism: Molecules and Systems*; Elsevier: Amsterdam, The Netherlands, **2003**.

Enders, D.; Niemeier, O.; Henseler, A.; *Chem. Rev.* **2007**, *107*, 5606-5655.

Essafi, W.; Haboubi,; Williams, N. C.; Boue, F.; *J Phys Chem B* **2011**, *115*, 8951-8960.

Esser-Kahn, A. P.; Odom, S. A.; Sottos, N. R.; White, S. R.; Moore, J. S. *Macromolecules* **2011**, *44*, 5539–5553.

Evans, D. A.; Fu, G. C. *J. Org. Chem.* **1990**, *55*, 2280-2282.

Evans, D. A.; Fu, G. C.; Anderson, B. A. *J. Am. Chem. Soc.* **1992**, *114*, 6679-6685.

Fagnoni, M.; Dondi, D.; Ravelli, D.; Albini, A. *Chem. Rev.* **2007**, *107*, 2725-2756.

Feng, B.; Hong, R. Y.; Wang, L. S.; Guo, L.; Li, H. Z.; Ding, J.; Zheng, Y.; Wei, D. G. *Colloid Surface A* **2008**, *328*, 52-59.

Feng, X.-J.; Zhai, J.; Lian, L. *Angew. Chem. Int. Ed.* **2005**, *44*, 5115-5118.

Fogg, D. E.; dos Santos, E. N. *Coord. Chem Rev.* **2004**, *248*, 2365-2379

Fors, B. P.; Hawker, C. J. *Angew. Chem. Int. Ed.* **2012**, *51*, 8850-8853.

Fritz, G.; Schadler, V.; Willenbacher, N.; Wagner, N. J. *Langmuir* **2002,** *18*, 6381-6390.

Fruk, L.; Rajendran, V.; Spengler, M.; Niemeyer, C. M. *ChemBioChem.* **2007**, *8*, 2195-2198.

Fürstner, A.; Alcarazo, M.; Krause, H.; Lehmann, C. W.; *J. Am. Chem. Soc.* **2007**, *129*, 12676-12677.

Ge, J. P.; Hu, Y. X.; Biasini, M.; Dong, C. L.; Guo, J. H.; Beyermann, W. P.; Yin, Y. D. *Chem. Eur. J.* **2007,** *13*, 7153-7161.

Ge, J.; Hu, Y.; Biasini, M.; Beyermann, W. P.; Yin, Y. *Angew. Chem. Int. Ed.* **2007**, *46*, 4342-4345.

Gil, W.; Lis, T.; Trzeciak, A. M.; Ziółkowski, J. J. *Inorg. Chim. Acta* **2006**, *359*, 2835-2841.

Gil, W.; Trzeciak, A. M. *Coord. Chem. Rev.* **2011**, *255*, 473-483.

Golas, P. L.; Louie, S.; Lowry, G. V.; Matyjaszewski, K.; Tilton, R. D. *Langmuir* **2010,** *26*, 16890-16900.

Goldberg, Y.; Alper, H. *J. Chem. Soc. Chem. Commun.* **1994**, 1209-1210.

Golemanov, K.; Tcholakova, S.; Kralchevsky, P. A.; Ananthapadmanabhan, K. P.; and Lips, A. *Langmuir* **2006,** 22, 4968-4977.

Graff, J. L.; Sanner, R. D.; Wrighton, M. S. . *J. Am. Chem. Soc.* **1979**, *101*, 273-275.

Grasa, G. A.; Güveli, T.; Singh, R.; Nolan. S. P. *J. Org. Chem.* **2003**, *68*, 2812-2819.

Grasa, G. A.; Kissling, R. M.; Nolan. S. P. *Org. Lett.* **2002**, *4*, 3583-3586.

Grasa, G. A.; Moore, Z.; Martin, K. L.; Stevens, E. D.; Nolan, S. P.; Paquet, V.; Lebel, H. *J. Organomet. Chem.* **2002**, *658*, 126-131.

Gregson, C.; Gibson, K. A.; V. C.; Long, N. J.; Marshall, E. L.; Oxford, P. J.; White, A. J. P. *J. Am. Chem. Soc.* **2006**, *128*, 7410.

Guerchais, V.; Ordronneau, L.; Bozec, H. L. *Coord. Chem. Rev.* **2010**, *254*, 2533-2545.

Guo, X.; Ballauff, M.; *Phys. Rev. E.* **2001**, *64*.

Gupta, A. K.; Gupta, M. *Biomaterials* **2005**, *26*, 3995–4021.

Hafner, A.; Mühlebach A.; van der Schaaf, P. *Angew. Chem. Int. Ed.* **1997**, *36*, 2121-2124.

Hahn, F. E.; Jahnke, M. C.; *Angew. Chem. Int. Ed.* **2008**, *47*, 3122-3172.

He, F.; Zhang, M.; Qian, T.; Zhao, D. *J. Colloid Interf. Sci.* **2009**, *334,* 96-102.

Hennig, H. *Coord. Chem. Rev.* **1999**, *182*, 101-123.

Herder, M.; Pätzel, M.; Grubert, L.; Hecht, S. *Chem. Commun.* **2011**, *47*, 460-462.

Herrmann, W. A.; *Angew. Chem. Int. Ed.* **2002**, *41*, 1290-1309.

Herrmann, W. A.; Elison, M.; Fischer, J.; Köcher, C.; Artus, G. R. J. *Chem. Eur. J.* **1996**, *2*, 772-780.

Herrmann, W. A.; Köcher, C. *Angew. Chem. Int. Ed.* **1997**, *36*, 2162-2187.

Hiemenz, P. C.; Rajagopalan, R., *Principles of colloid and surface chemistry*. 3rd ed.; Marcel Dekker: New York, 1997; p 650.

Hirose, T.; Irie, M.; Matsuda, K. *Adv. Mat.* **2008**, *20*, 2137-2141.

Hirose, T.; Matsuda, K.; Irie, M. *J. Org. Chem.* **2006**, *71*, 7499-7508.

Hsieh, H. L.; Moradiaraghi, A.; Stahl, G. A.; Westerman, I. J. *Makromol. Chem.-M. Symp.* **1992,** *64*, 121-135.

Hudnall, T. W.; Bielawski, C. W. *J. Am. Chem. Soc.* **2009**, *131*, 16039-16041.

Hudnall, T. W.; Moerdyk, J. P.; Bielawski, C. W. *Chem. Comm.* **2010**, *46*, 4288-4290.

Hudnall, T. W.; Tennyson, A. G.; Bielawksi, C. W.; *Organometallics*, **2010**, *29*, 4569-4578.

Hunter, T. N.; Pugh, R. J.; Franks, G. V.; Jameson, G. J. *Adv. Coll. Interf. Sci.* **2008**, *137*, 57-81.

Imahori, T.; Yamaguchi, R.; Kurihara, S. *Chem. Eur. J.* **2012**, *18*, 10802-10807.

Ingram, D. R.; Kotsmar, C.; Yoon, K. Y.; Shao, S.; Huh, C.; Bryant, S. L.; Milner, T.; Johnston, K. P. *J. Colloid Interface Sci*. **2010**, *351*, 225-232.

International Tables for X-ray Crystallography. Vol. C, Tables 4.2.6.8 and 6.1.1.4, A. (Ed.: J. C. Wilson) Kluwer Academic Press, Boston, **1992**.

Irie, M.; Lifka, T.; Kobatake, S.; Kato, N. *J. Am. Chem. Soc.* **2000**, *122*, 4871-4876.

Irie, M. *Chem Rev*. **2000**, *100*, 1685-1716.

Irie, M.; Kobatake, S.; Horichi, M. *Science*, **2001**, *291*, 1769-1772.

Israels, R.; Leermakers, F. A. M. G.; Fleer, J.; Zhulina, E. B. *Macromolecules* **1994**, *27*, 3249-3261.

Iwamoto, O.; Sugiyama, H.; Hara, T. Fulgimide Derivatives. U. S. Patent 5,359,085, October 25, 1994.

Jacquin, M.; Muller, P.; Talingting-Pabalan, R.; Cottet, H.; Berret, J. F.; Futterer, T.; Théodoly, O. *J. Colloid Interface Sci.* **2007**, *316*, 897–911.

Jain, N.; Wang, Y.; Jones, S. K.; Hawkett, B. S.; Warr, G. G. *Langmuir* **2010,** *26*, 4465-4472.

Jaisi, D. P.; Saleh, N. B.; Blake, R. E.; Elimelech, M. *Environ. Sci. Technol.* **2008**, *42*, 8317-8323.

Javadpour, F.; Nicot, J. P.; *Transport Porous Med.* **2011**, *89*, 265-284.

Jeong, U.; Teng, X. W.; Wang, Y.; Yang, H.; Xia, Y. N. *Adv. Mater.* **2007,** *19*, 33-60.

Jikich, S. A.; *J. Petrol. Technol*. **2012**, 28.

Jing, J. Y.; Zhang, Y.; Liang, J. Y.; Zhang, Q. B.; Bryant, E.; Avendano, C.; Colvin, V. L.; Wang, Y. D.; Li, W. Y.; Yu, W. W. *J. Nanopart. Res.* **2012,** *14*, DOI: 10.1007/s11051-012-0827-3.

Johnston, K. P.; Maynard, J. A.; Truskett, T. M.; Borwankar, A. U.; Miller, M. A.; Wilson, B. K.; Dinin, A. K.; Khan, T. A.; Kaczorowski, K. J. *ACS Nano* **2012**, *6*, 1357-1369.

Kamber, N. E.; Jeong, W.; Gonzalez, S.; Hedrick, J. L.; Waymouth, R. M. *Macromolecules* **2009**, *42*, 1634-1649.

Kamber, N. E.; Jeong, W.; Waymouth, R. M.; Pratt, R. C.; Lohmeijer, B. G. G.; Hedrick, J. L. *Chem. Rev.* **2007**, *107*, 5813-5840.

Kanj, M. Y.; Rashid, M. H.; Giannelis, E. *SPE Middle East Oil and Gas Show and Conference*, Society of Petroleum Engineers, Manama, Bahrain **2011**.

Karthikeyan, S.; Potisek, S. L.; Piermattei, A.; Sijbesma, R. P. *J. Am. Chem. Soc.* **2008**, *130*, 14968-14969.

Kawaguchi, S.; Toui, S.; Onodera, M.; Ito, K.; Minakata, A. *Macromolecules* **1993,** *26*, 3081-3085.

Kawai, S. H.; Gilat, S. L.; Lehn, J. M. *Eur. J. Org. Chem.* **1999**, 2359-2366.

Keitz, B. K.; Grubbs, R. H. *J. Am. Chem. Soc.* **2009**, *131*, 2038-2039.

Kelly III, R. A.; Clavier, H.; Giudice, S.; Scott, N. M.; Stevens, E. D. Bordner, I Samardjiev, Hoff, J. C. D.; Cavallo, L.; Nolan, S. P.; *Organometallics*, **2008**, *27*, 202-210.

Khramov, D. M.; Lynch, V. M.; Bielawski, C. W. *Organometallics* **2007**, *26*, 6042-6049.

Khramov, D. M.; Rosen, E. L.; Er, J. A. V.; Vu, P. D.; Lynch, V. M.; Bielawski, C. W.; *Tetrahedron*, **2008**, *64*, 6853-6862.

Kim, H. J.; Phenrat, T.; Tilton, R. D.; Lowry, G. V. *Environ. Sci. Technol.* **2008**, *43,* 3824-3830.

Kirby, G. H.; Harris, D. J.; Li, Q.; Lewis, J. A. *J. Am. Ceram. Soc.* **2004**, *87*, 181-186.

Kishimoto, Y.; Miyatake, T.; Ikariya, T.; Noyori, R. *Macromolecules* **1996**, *29*, 5054-5055.

Klajn, R.; Bishop, K. J. M.; Gryzbowski, B. A. *P. Natl. Acad. Sci. USA*, **2007**, *104*, 10305-10309.

Klajn, R.; Wesson, P. J.; Bishop, K. J. M.; Gryzbowski, B. A. *Angew. Chem. Int. Ed.* **2009**, *48*, 7035-7039.

Ko, C.-C.; Yam, V.-W.-W. *J. Mater. Chem.* **2010**, *20*, 2063-2070.

Kobatake, S. Shibata, K. Uchida, Irie, K. M. *J. Am. Chem. Soc.* **2000**, *122*, 12135-12141.

Kobatake, S.; Irie, M. *Annu. Rep. Prog. Chem., Sect. C.* **2003**, *99*, 277-313.

Kobatake, S.; Yamada, M.; Yamada, T.; Irie, M. *J. Am. Chem. Soc.* **1999**, *121*, 8450-8456

Kodani, T.; Matsuda, K.; Yamada, T.; Kobatake, S.; Irie, M. *J. Am. Chem. Soc.* **2000**, *122*, 9631-9637.

Kotsmar, C.; Yoon, K. Y.; Ingram, D. R.; Ryoo, S. Y.; Barth, J.; Shao, S.; Prodanovic´, M.; Milner, T.; Bryant, S. L.; Huh, C.; Johnston, K. P. *Ind. Eng. Chem. Res.* **2010**, *49*, 12435–12443.

Krausz, P.; Garnier, F.; Dubois, J. E. *J. Am. Chem. Soc.* **1975**, *97*, 437-438.

Krayushkin, M. M.; Ivanov, S. N.; Martynkin, A. Y.; Lichitsky, B. V.; Dudinov, A. A.; Vorontsova, L. G.; Starikova, Z. A.; Uzhinov, B. M.; *Russ. Chem. Bull. Int. Ed*., **2002**, *51*, 1731-1736.

Kriwet, B.; Kissel, T. *Int. J. Pharmaceut.* **1996,** *127*, 135-145.

Kuma, S.; Nishihara, H. *Dalton Trans.* **2008**, 3260-3271.

Kwak, Y.; Matyjaszewski, K. *Macromolecules*, **2010**, *43*, 5180-5183.

Lages, S.; Lindner, P.; Sinha, P.; Kiriy, A.; Stamm, M.; Huber, K. *Macromolecules* **2009,** *42*, 4288-4299.

Lan, Q.; Liu, C.; Yang, F.; Liu, S.; Sun, D. *J. Colloid Interface Sci* **2007**, *310*, 260-269.

Latham, A. H.; Williams, M. E. *Acc. Chem. Res.* **2008,** *41*, 411-420.

Lattuada, M.; Hatton, T. A. *J. Am. Chem. Soc.* **2007**, *129*, 12878-12889.

Lattuada, M.; Hatton, T. A.; *Langmuir* **2007**, *23*, 2158-2168.

Laurent, S.; Forge, D.; Port, M.; Roch, A.; Robic, C.; Elst, L. V.; Muller, R. N. *Chem. Rev.* **2008,** *108*, 2064-2110.

Lee, P. H.-M.; Ko, C.-C.; Zhu, N.; Yam, V. W.-W. *J. Am. Chem. Soc.* **2007**, *129*, 6058-6059.

Lee, W.-S.; Ueno, A. *Macromol. Rapid Commun.* **2001**, *22*, 448–450.

Leibfarth, F. A.; Mattson, K. M.; Fors, B. P. Collins, H. A.; Hawker, C. J. *Angew. Chem. Int. Ed.* **2013**, *52*, 199-210.

Lemieux, V.; Gauthier, S.; Branda, N. R. *Angew. Chem. Int. Ed.* **2006**, *45*, 6820-6824.

Lemieux, V.; Spantulescu, D. M.; Baldridge, K. K.; Branda, N. R. *Angew. Chem. Int. Ed.* **2008**, *120*, 5112-5115.

Levitt, D. B.; Slaughter, W.; Pope, G. A.; Jouenne, S.; *SPE Reserv. Eval. Eng*. **2011**, *14*, 287-298.

Levitt, D.; Pope, G. A. *SPE/DOE Symposium on Improved Oil Recovery*, Society of Petroleum Engineers: Tulsa, Oklahoma, USA, 2008.

Lewis, J. A. *J. Am. Ceram. Soc.* **2000,** *83*, 2341-2359.

Lin, C.-L.; Lee, C.-F.; Chiu, W.-Y. J. *Colloid Interface Sci.* **2005**, *291*, 411-420.

Lin, Y.; Skaff, H.; Emrick, T.; Dinsmore, A. D.; and Russell, T. P. *Science* **2003**, *299*, 226-229.

Lopez-Cruz, A.; Barrera, C.; Calero-DdelC, V. L.; Rinaldi, C. *J. Mater. Chem.* **2009**, *19*, 6870-6876.

Lorkovic, I. M.; Duff, R. R.; Wrighton, M. S. *J. Am. Chem. Soc.* **1995**, *117*, 3617.

Lozsan, A. E.; Romero-Cano, M. S.; *J. Colloid. Interf. Sci.* **2011**, *354*, 70-75.

Lu, A.-H.; Salabas, E. L.; Schueth, F. *Angew. Chem. Int. Ed.* **2007**, *46*, 1222-1244.

Lüning, U. *Angew. Chem. Int. Ed.* **2012**, *51*, 8163-8165.

Lyon, J. L.; Fleming, D. A.; Stone, M. B.; Schiffer, P.; Williams, M. E. *Nano Lett.* **2004**, *4*, 719-723.

Ma, H.; Luo, M.; Dai, L. L. *Phys. Chem. Chem. Phys.* **2008**, *10*, 2207-2213.

Ma, L. L.; Feldman, M. D.; Tam, J. M.; Paranjape, A. S.; Cheruku, K. K.; Larson, T. A.; Tam, J. O.; Ingram, D. R.; Paramita, V.; Villard, J. W.; Clarke, G. D.; Jenkins, J. T.; Asmis, R.; Sokolov, K.; Chandrasekar, B.; Milner, T. E.; Johnston, K. P. *ACS Nano* **2009**, *3*, 2686-2696.

Mahmoudi, M.; Sant, S.; Wang, B.; Laurent, S.; Sen, T. *Adv. Drug Deliv. Rev.* **2011**, *63*, 24-46.

Männig, D.; Nöth, H. *Angew. Chem. Int. Ed.* **1985**, *24*, 878-879.

Manning, G. S. *Acc. Chem. Res.* **1979,** *12,* 443-449.

Marion, N.; Díez-González, S.; Nolan, S. P. *Angew. Chem. Int. Ed.* **2007**, *46*, 2988-3000.

Massart, R. *IEEE Trans. Magn.* **1981**, *17*, 1247-1248.

Massart, R.; Dubois, E.; Cabuil, V.; Hasmonay, E. *J. Magn. Magn. Mater.* **1995**, *149*, 1-5.

Matsuda, K.; Irie, M. *J. Photochem. Photobio. C: Photochem Rev.* **2004**, 169.

Mays, D. C.; Hunt, J. R. *Environ. Sci. Technol.* **2005**, *39*, 577-584.

McCormick, C. L.; Elliott, D. L. *Macromolecules* **1986,** *19*, 542-547.

Mei, Y.; Ballauff, M. *Eur. Phys. J. E* **2005**, *16*, 341-349.

Melle, S.; Lask, M.; Fuller, G. G. *Langmui*r **2005**, *21*, 2158-2162.

Melle, S.; Lask, M.; Fuller, G. G. *Langmuir* **2005**, *21*, 2158-2162.

Moerdyk, J. P.; Bielawski, C. W. *Organometallics* **2011**, *30*, 2278-2284.

Morimoto, M.; Irie, M. *J. Am. Chem. Soc.* **2010**, *132*, 14172-14178.

Morimoto, M.; Kobatake, S.; Irie, M. *Chem. Eur. J.* **2003**, *9*, 621-627.

Morimoto, M.; Kobatake, S.; Irie, M. *Photochem. Photobiol. Sci.* **2003**, *2*, 1088-1094.

Mosnáček, J.; Ilčíková, M. *Macromolecules*, **2012**, *45*, 5859-5865.

Motoyama, K.; Koike, T.; Akita, M. *Chem. Commun.* **2008**, 5812-5314.

Movassaghi, M.; Schmidt, M. A. *Org. Lett.* **2005**, *7*, 2453-2456.

Murata, M.; Watanabe, S.; Masuda, Y. *Tetrahedron Lett.* **1999**, *40*, 2585-2588.

Musaev, D. G.; Mebel, A. M.; Keiji, M. *J. Am. Chem. Soc.* **1994**, *116*, 10693-10702.

Na, H. B.; Palui, G.; Rosenberg, J. T.; Ji, X.; Grant, S. C.; Mattoussi, H. *ACS Nano* **2012,** *6*, 389-399.

Nair, V.; Menon, R. S.; Biju, A. T.; Sinu, C. R.; Paul, R. R.; Jose, A.; Vellalath, S. *Chem. Soc. Rev.* **2011**, *40*, 5336-5346.

Nair, V.; Vellalath, S.; Babu, B. P. *Chem. Soc. Rev.* **2008**, *37*, 2691-2698.

Nakashima, T.; Goto, M.; Kawai, S.; Kawai, T. *J. Am. Chem. Soc.* **2008**, *130*, 14570-14575.

Napper, D. H., *Polymeric stabilization of colloidal dispersions*. Academic Press: London; New York, 1983.

Narayanam, J. M. R.; Stephenson, C. R. J. *Chem. Soc. Rev.* **2011**, *40*, 102-113.

Neilson, B. M.; Bielawksi, C. W. *J. Am. Chem. Soc.* **2012**, *134*, 12693-12699.

Neilson, B. M.; Lynch, V. M.; Bielawski, C. W. *Angew. Chem. Int. Ed.* **2011**, *50*, 10322-10326.

Newman, J. K.; Mccormick, C. L. *Macromolecules* **1994,** *27*, 5114-5122.

Niazov, T.; Shlyahovsky, B.; Willner, I. *J. Am. Chem. Soc.* **2007**, *129*, 6374-6375.

Niu, F.; Zhai, J.; Jiang, L.; Song, W.-G. *Chem. Commun.* **2009**, 4738-4740.

Nyce, G. W.; Glauser, T.; Connor, E. F.; Möck, A.; Waymouth, R. M.; Hedrick, J. L. *J. Am. Chem. Soc.* **2003**, *125*, 3046-3056.

Nyce, G. W.; Lamboy, J. A.; Connor, E. F.; Waymouth, R. M.; Hedrick, J. L. *Org. Lett.* **2002**, *4*, 3587-3590.

O'Brien, C. J.; Kantchev, E. A. B.; Chass, G. A.; Niloufar, H.; Hopkinson, A. C.; Organ, M. G., Setiadi, D. H.; Tang, T.; Fan, D. *Tetrahedron,* **2005**, 61, 9723-9735.

Odo, Y.; Matsuda, K.; Irie, M. *Chem. Eur. J.* **2006**, *12*, 4283-4288.

Oh, J.; Feldman, M. D.; Kim, J.; Condit, C.; Emelianov, S.; Milner, T. E. *Nanotechnology* **2006**, *17*, 4183-4190.

Ohmura, T.; Yamamoto, Y.; Miyaura, N. *J. Am. Chem. Soc.* **2000**, *122*, 4990-4991.

Ohshima, H. *Colloid Surface A* **1995,** 103, 249-255.

Ohshima, H.; Makino, K *Colloid Surface A* **1996,** 109, 71-75.

P'Pool, S. J.; Schanz, H.-J. *J. Am. Chem. Soc.* **2007**, *129*, 14200-14212.

Palui, G.; Na, H. B.; Mattoussi, H. *Langmuir* **2012,** *28*, 2761-2772.

Papper, V.; Likhtenshtein, G. I. *J. Photoch. Photobio. A* **2001**, *140*, 39-52.

Paquet, O.; M. Salon, C. B.; Zeno, E.; Belgacem, M. N.; *Mat. Sci. Eng. C-Mater.* **2012**, *32*, 487-493.

Park, J. J.; Lacerda, S. H. D. P.; S. Stanley, K.; Vogel, B. M.; Kim, S.; Douglas, J. F. Raghavan, D.; Karim, A. *Langmuir* **2009**, *25*, 443-450.

Parnom, V. N. *Catal. Today* **1997**, *39*, 137-144.

Peeck, L. H.; Leuthäusser, S.; Plenio, H. *Organometallics* **2010**, *29*, 4339-4345.

Peng, J. X.; Liu, Q. X.; Xu, Z. H.; Masliyah, J. *Adv. Funct. Mater.* **2012**, *22*, 1732-1740.

Pereira, S.; Srebnik, M. *J. Am. Chem. Soc.* **1996**, *118*, 909-910.

Pereira, S.; Srebnik, M. *Tet. Lett.* **1996**, *37*, 3283-3286.

Peters, M. V.; Stoll, R. S.; Kühn, A.; Hecht, S. *Angew. Chem. Int. Ed.* **2008**, *47*, 5968-5972.

Petosa, A. R.; Jaisi, D. P.; Quevedo, I. R.; Elimelech, M.; Tufenkji, N. *Environ. Sci. Technol*. **2010**, *44*, 6532-6549.

Phenrat, T.; Saleh, N.; Sirk, K.; Kim, H. J.; Tilton, R. D.; Lowry, G. V. *J. Nanopart. Res.* **2008**, *10*, 795-814.

Photocatalysis; Bignozzi, C. A., Ed.; Topics in Current Chemistry 303; Springer: Berlin, Germany, 2011.

Pignataro, L.; Papalia, T.; Slawin, A. M. Z.; Goldup, S. M. *Org. Lett.* **2009**, *11*, 1643-1646.

Poater, A.; Cosenza, B.; Correa, A.; Giudice, S.; Ragone, F.; Scarano, V.; Cavallo, L. *Eur. J. Inorg. Chem.* **2009**, *13*, 1759-1766.

Praetorius, J. M.; Crudden, C. M. *Dalton Trans.* **2008**, 4079-4094.

Prakash, A.; Zhu, H.; Jones, C. J.; Benoit, D. N.; Ellsworth, A. Z.; Bryant, E. L.; Colvin, V. L. *ACS Nano* **2009**, *3*, 2139-2146.

Prodanovic, M.; Ryoo, S.; Rahmani, A. R.; Kuranov, R.; Kotsmar, C.; Milner, T. E.; Johnston, K. P.; Bryant, S. L.; Huh, C. *17th SPE Improved Oil Recovery Symposium Tulsa, OK*; SPE; 2010; SPE 129850.

Radeva, T., *Physical chemistry of polyelectrolytes*. Marcel Dekker: New York, 2001; p 882.

Rao, C. N. R. *Chemical Applications of Infrared Spectroscopy*, Academic Press: New York, **1963**, pp 298-303.

Rashidi, M.; Blokhus, A. M.; Skauge, A. *J. Appl. Polym. Sci.* **2011,** *119*, 3623-3629.

Ravelli, D.; Dondi, D.; Fagnoni, M.; Albini, A. *Chem. Soc. Rev.* **2009**, *38*, 1999-2011.

Reith, D.; Muller, B.; Muller-Plathe, F.; Wiegand, S. *J. Chem. Phys.* **2002,** *116*, 9100-9106.

Rosen, E. L.; Varnado Jr., C. D.; Tennyson, A. G.; Khramov, D. M.; Kamplain, J. W.; Sung, D. H.; Cresswell, P. T.; Lynch, V. M.; Bielawski, C. W. *Organometallics*, **2009**, *28*, 6695-6706.

Rubinstein, M.; Papoian, G. A.; *Soft Mater.* **2012**, *8*, 9265-9267.

Russew, M.-M.; Hecht, S. *Adv. Mat.* **2010**, *22*, 3348-3360.

Ryoo, S.; Rahmani, A. R.; Yoon, K. Y.; Prodanovic, M.; Kotsmar, C.; Milner, T. E.; Johnston, K. P.; Bryant, S. L.; Huh, C. *SPE Annual Meeting, Florence, Italy* SPE: 2010; SPE 134879.

Ryoo, S.; Rahmani, A. R.; Yoon, K. Y.; Prodanovic, M.; Kotsmar, C.; Milner, T. E.; Johnston, K. P.; Bryant, S. L.; Huh, C. *J. Petrol. Sci. Eng.* **2012,** *81*, 129-144.

Ryoo, W.; Webber, S. E.; Johnston, K. P. *Ind. Eng. Chem. Res.* **2003,** *42*, 6348-6358.

Sahoo, Y.; Goodarzi, A.; Swihart, M. T.; Ohulchanskyy, T. Y.; Kaur, N.; Furlani, E. P.; Prasad, P. N. *J. Phys. Chem. B* **2005**, *109*, 3879–3885.

Saigal, T.; Dong, H. C.; Matyjaszewski, K.; Tilton, R. D. *Langmuir* **2010**, *26*, 15200-15209.

Sakaki, S.; Sumimoto, M.; Fukuhara, M.; Sugimoto, M.; Fujimoto, H.; Matsuzaki, S. *Organometallics*, **2002**, *21*, 3788-3802.

Saleh, N.; Kim, H.-J.; Phenrat, T.; Matyjaszewski, K.; Tilton, R. D.; Lowry, G. V. *Environ. Sci. Technol.* **2008**, *42*, 3349-3355.

Saleh, N.; Phenrat, T.; Sirk, K.; Dufour, B.; Ok, J.; Sarbu, T.; Matyjaszewski, K.; Tilton, R. D.; Lowry, G. V. *Nano Lett.* **2005**, *5*, 2489-2494.

Saleh, N.; Sarbu, T.; Sirk, K.; Lowry, G. V.; Matyjaszewski, K.; Tilton, R. D. *Langmuir* **2005**, *21*, 9873-9878.

Saleh, N.; Sirk, K.; Liu, Y.; Phenrat, T.; Dufour, B.; Matyjasewski, K.; Tilton, R. D.; Lowry, G. V. *Environ. Eng. Sci.* **2007**, *24*, 45-47.

Salomon, R. G. *Tetrahedron*, **1983***, 39*, 485-575.

Salon, M. C. B.; Belgacem, M. N. *Colloid Surface A* **2010**, *366*, 147-154.

Samachetty, H. D.; Branda, N. R. *Chem. Commun.* **2005**, 2840-2842.

Samachetty, H. D.; Branda, N. R. *Pure Appl. Chem.* **2006**, *78*, 2351-2359.

Samachetty, H. D.; Lemieux, V.; Branda, N. R. *Tetrahedron*, **2008**, *64*, 8292-8300.

Sanderson, M. D.; Kamplain, J. W.; Bielawski, C. W. *J. Am. Chem. Soc.* **2006**, *128*, 12614-15615.

Sarac, A. S. *Prog. Polym. Sci.* **1999**, *24*, 1149-1204.

Sashuk, V.; Peeck, L. H.; Plenio, H. *Chem. Eur. J.* **2010**, *16*, 3983-3993.

Sato, T.; Ruch, R. *Stabilization of colloidal dispersions by polymer adsorption*. Dekker: New York, 1980; p 155.

Schmittel, M.; De, S.; Pramanik, S. *Angew. Chem. Int. Ed.* **2012**, *51*, 3822-3826.

Schroeder, M. A.; Wrighton, M. S. *J. Am. Chem. Soc.* **1976**, *98*, 551-558.

Schwartz, H.; Harel, Y.; Efrima, S. *Langmuir* **2001**, *17*, 3884-3892.

Schweins, R.; Huber, K. *Eur. Phys. J. E.* **2001,** *5*, 117-126.

Serpone, N.; Salinaro, A.; Emeline, A.; Ryabchuk, V. *J. Photochem. Photobiol. A* **2000**, *130*, 83-94.

Sheldrick, G. M.; SHELXL97, Program for the Refinement of Crystal Structures. University of Gottingen, (Germany) **1994**.

Sheldrick, G. M.; SHELXTL/PC (Version 5.03). Siemens Analytical X-ray Instruments, Inc., Madison, Wisconsin, **1994**.

Shindoh, N.; Takemoto, Y.; Takasu, K. *Chem. Eur. J.* **2009**, *15*, 12168-12179.

Shirai, M.; Tsunooka, M. *Prog. Polym. Sci.* **1996**, *21*, 1-45.

Siamaki, A. R.; Black, D. A.; Arndtsen, B. A. *J. Org. Chem.* **2008**, *73*, 1135-1138.

Singer, M.; Jäschke, A. *J. Am. Chem. Soc.* **2010**, *132*, 8372-8277.

Singh, R.; Kissling, R. M.; Letellier, M.-A.; Nolan. S. P. *J. Org. Chem.* **2004**, *69*, 209-212.

Sinn, C. G.; Dimova, R.; Antonietti, M. *Macromolecules* **2004,** *37*, 3444-3450.

SIR97. (1999), A program for crystal structure solution: A. Altomare, M. C. Burla, Camalli, G. L. Cascarano, C. Giacovazzo, A.Guagliardi, A. G. G. Moliterni, G. Polidori, Spagna *J. Appl. Cryst.* **1999**, 32, 115-119.

Sondjaja, R.; Hatton, A. T.; Tam, M. K. C. *J. Magn. Magn. Mater.* **2009**, *321*, 2393-2397.

Special Issue: "Photochromism: Memories and Switches" (Ed. M. Irie), *Chem Rev.* **2000**, *100*, 1683.

Stocco, A.; Drenckhan, W.; Rio, E.; Langevin, D.; Binks, B. P. *Soft Matter* **2009**, *5*, 2215–2222.

Stoll, R. S.; Hecht, S. *Angew. Chem. Int. Ed.* **2010**, *49*, 5054-5075.

Stoll, R. S.; Hecht, S. *Org. Lett.* **2009**, *11*, 4790-4793.

Stoll, R. S.; Peters, M. V.; Kühn, A.; Heiles, S.; Goddard, R.; Bühl, M.; Thiele, C. M.; Hecht, S. *J. Am. Chem. Soc.* **2009**, *131*, 357-367.

Structure Determination of Organic Compounds: Tables of Spectral Data, 4th ed., Springer-Verlag: Berlin, Germany, **2009,** pp 310-324.

Sud, D.; McDonald, R.; Branda, N. R. *Inorg. Chem.* **2005**, *44*, 5060-5962.

Sud, D.; Norsten, T. B.; Branda, N. R. *Angew. Chem. Int. Ed.* **2005**, *44*, 2019-2021. (e)

Sud, D.; Wigglesworth, T. J.; Branda, N. R. *Angew. Chem. Int. Ed.* **2007**, *46*, 8017-8019.

Sugimoto, H.; Kimura, T.; Inoue, S. *J. Am. Chem. Soc.* **1999**, *121*, 2325-2326.

Sun, B.; Sun, M.-J.; Gu, Z.; Shen, Q.-D.; Jiang, S.-J.; Xu, Y.; Wang, Y. *Macromolecules* **2010**, *43*, 10348–10354.

Sun, X.; Gao, J. P.; Wang, Z. Y. *J. Am. Chem. Soc.* **2008**, *130*, 8130-8131.

Sun, X.; Gao, J. P.; Wang, Z. Y. *J. Am. Chem. Soc.* **2008**, *130*, 8130-8131.

Süβner, M.; Plenio, H. *Angew. Chem. Int. Ed.* **2005**, *44*, 6885-6888.

Süβner, M.; Plenio, H. *Chem. Commun.* **2005**, *43*, 5417-5419.

Szostak, M.; Yao, L.; Day, V. W.; Powell, D. R.; Aubé, J. *J. Am. Chem. Soc.* **2010**, *132*, 8836-8837.

Tabata, M.; Yang, W.; Yokota, K. *Polym. J.* **1990**, *22*, 1105-1107.

Tam, J. M.; Murthy, A. K.; Ingram, D. R.; Nguyen, R.; Sokolov, K. V.; Johnston, K. P. *Langmuir* **2010,** *26*, 8988-8999.

Tan, W.; Zhou, J.; Li, F.; Yi, T.; Tian, H. *Chem. Asian. J.* **2011**, *6*, 1263-1268.

Tanabe, M.; Vandermeulen, G. W. M.; Chan, W. Y.; Cyr, P. W.; Vanderark, L.; Rider, D. A.; Manners, I. *Nature Chem.* **2006**, *6*, 467-470.

Tanaka, Y.; Inagaki, A.; Akita, M. *Chem. Commun.* **2007**, 1169-1171.

Tanaka, Y.; Ishisaka, T.; Inagaki, A.; Koike, T.; Lapinte, C.; Akita, M. *Chem. Eur. J.* **2010**, *16*, 4762-4776.

Tani, K.; Stoltz, B. M. *Nature*, **2006**, *441*, 731-734;

Tcholakova, S.; Denkov, N. D.; Lips, A. *Phys. Chem. Chem. Phys*. **2008**, *10*, 1608–1627.

Tennyson, A. G.; Lynch, V. M.; Bielawski, C. W. *J. Am. Chem. Soc.* **2010**, *132*, 9420-9429.

Tennyson, A. G.; Wiggins, K. M.; Bielawski, C. W. *J. Am. Chem. Soc.* **2010**, *132*, 16631-16636.

Tian, H.; Wang, S. *Chem. Commun.* **2007**, 781.

Tian, H.; Yang, S. *Chem. Soc. Rev.* **2004**, *33*, 85.

Toda, F.; Tanaka, K.; Tange, H. *J. Chem. Soc. Perkin Trans. I*, **1989**, 1555-1556.

Tolman, C. A. *Chem. Rev.* **1977**, *77*, 313-348.

Trnka, T. M.; Morgan, J. P.; Sanford, M. S.; Wilhelm, T. E.; Scholl, M.; Choi, T.-L.; Ding, S.; Day, M. W.; Grubbs, R. H. *J. Am. Chem. Soc.* **2003**, *125*, 2546-2558.

Turesson, M.; Labbez, C.; Nonat, A. *Langmuir* **2011,** *27*, 13572-13581.

Uchida, K.; Inagaki, A.; Akita, M. *Organometallics*, **2007**, *26*, 5030-5041.

Ueno, A.; Takahashi, K.; Osa, T. *J. Chem. Soc., Chem. Commun*. **1981**, *3*, 94–96.

Ujiie, K.; Kanayama, N.; Asai, K.; Kishimoto, M.; Ohara, Y.; Akashi, Y.; Yamada, K.; Hashimoto, S.; Oda, T.; Ohkohchi, N.; Yanagihara, H.; Kita, E.; Yamaguchi, M.; Fujii, H.; Nagasaki, Y.; *Colloid Surface B* **2011**, *88*, 771-778.

van der Schaaf, P.; Hafner, A. *Angew. Chem. Int. Ed.* **1996**, *35*, 1845-1847.

Veige, A. S. *Polyhedron*, **2008**, *27*, 3177-3189.

Vignati, E.; Piazza, R. *Langmuir* **2003**, *19,* 6650-6656.

Voorhees, P. W. *J. Stat. Phys.* **1985,** *38*, 231-252.

Wagener, A. Schwenke, S. Barcikowski, *Langmuir* **2012**, *28*, 6132-6140.

Wan, S.; Zheng, Y.; Liu, Y.; Yan, H.; Liu, K. *J. Mater. Chem.* **2005,** *15*, 3424.

Wang, D.; Wurst K.; Knolle, W.; Decker, U.; Prager, L.; Naumov, S.; Buchmeiser, M. R. *Angew. Chem. Int. Ed.* **2008**, *47*, 3267-3270.

Wang, H. M. J.; Lin, I. J. B.; *Organometallics*, **1998**, *17*, 972-975.

Wang, J.; Feringa, B. L. *Science* **2011**, *331*, 1429-1432.

Wang, R.; Hashimoto, A.; Fujishima, M.; Chikuni, M.; Kojima, E.; Kitamura, A.; Shimohigoshi, M.; Watanabe, T.; *Nature*, **1997**, *388*, 431-432.

Wang, W.; Zhou, Z.; Nandakumar, K.; Xu, Z.; Masliyah, J. H. *J. Colloid Interface Sci.* **2004**, *274*, 625–630.

Wang, Y. G.; Li, Y. S.; Fortner, J. D.; Hughes, J. B.; Abriola, L.; M. Pennell, K. D. *Environ. Sci. Technol*. **2008**, *42*, 3588-3594.

Wasilke, J.-C.; Obrey, S. J.; Baker, R. T.; Bazan, G. S. *Chem Rev.* **2005***, 105*, 1001-1020.

Wei, Y.; Han, S.; Kim, J.; Soh, S.; Grzybowski, B. A. *J. Am. Chem. Soc.* **2010**, *132*, 11018-11020.

Widauer, C.; Grüntzmacher, H.; Ziegler, T. *Organometallics* **2000**, *19*, 2097-2107.

Wiggins, K. W.; Hudnall, T. W.; Tennyson, A. G.; Bielawski, C. W. *J. Mater. Chem.* **2011**, *21*, 8355-8359.

Woodward, R. B.; Hoffman, R. *The Conservation of Orbital Symmetry*, Verlag Chemie GmbH: Weinheim, **1970**.

Worthen, A. J.; Bagaria, H. G.; Chen, Y.; Bryant, S. L.; Huh, C.; Johnston, K. P. *J. Coll. Interf. Sci.* **2012**, *391*, 142-151.

Würthner, F.; Rebek Jr., J. *Angew. Chem. Int. Ed.* **1995**, *34*, 446-448.

Würthner, F.; Rebek Jr., J. *J. Chem. Soc. Perkin Trans. 2*, **1995**, *9*, 1727-1734.

Xia, Y. S.; Nguyen, T. D.; Yang, M.; Lee, B.; Santos, A.; Podsiadlo, P.; Tang, Z. Y.; Glotzer, S. C.; Kotov, N. A. *Nature Nanotech.* **2011,** *6*, 580-587.

Yam, V. W.-W.; Lee, J. K.; Ko, C.; Zhu, N. *J. Am. Chem. Soc.* **2009**, *131*, 912-913.

Yang, D.; Long, Y.; Wang, H.; Zhang, Z. *Org. Lett.* **2008**, *10*, 4723-4726.

Yathindranath, V.; Rebbouh, L.; Moore, D. F.; Miller, D. W.; van Lierop, J. Hegmann, T. *Adv. Funct. Mater.* **2011**, *21*, 1457-1464.

Yavuz, C. T.; Mayo, J. T.; Yu, W. W.; Prakash, A.; Falkner, J. C.; Yean, S.; Cong, L.; Shipley, H. J.; Kan, A.; Tomson, M.; Natelson, D.; Colvin, V. L. *Science* **2006,** *314*, 964-967.

Yavuz, C. T.; Prakash, A.; Mayo, J. T.; Colvin, V. L. *Chem. Eng. Sci.* **2009,** *64*, 2510-2521.

Yoon, H. J.; Junpei, K.; Kim, J.-H.; Mirkin, C. A. *Science* **2010**, *330*, 66-69.

Yoon, K. Y.; Kotsmar, C.; Ingram, D. R.; Huh, C.; Bryant, S. L.; Milner, T. E.; Johnston, K. P. *Langmuir* **2011**, *27*, 10962-10969.

Yoon, K. Y.; Li, Z.; Neilson, B. M.; Lee, W.; Huh, C.; Bryant, S. L.; Bielawski, C. W.; Johnston, K. P. *Macromolecules* **2012**, *45*, 5157-5166.

Yu, H.; Kotsmar, C.; Yoon, K. Y.; Ingram, D. R.; Johnston, K. P.; Bryant, S. L.; Huh, C. *17th SPE Improved Oil Recovery Symposium Tulsa*, *OK*; SPE: 2010; SPE 129887.

Yu, W. W.; Chang, E.; Falkner, J. C.; Zhang, J. Y.; Al-Somali, A. M.; Sayes, C. M.; Johns, J.; Drezek, R.; Colvin, V. L. *J. Am. Chem. Soc.* **2007,** *129*, 2871-2879.

Yun, C.; You, J. ; Kim, J.; Huh, J.; Kim, E. *J. Photochem. Photobio. C: Photochem Rev.* **2009**, *10*, 111-129.

Zdyrko, B.; Luzinov, I. *Macromol. Rapid Comm.* **2011**, *32*, 859-869.

Zeitler, K. *Angew. Chem. Int. Ed.* **2005**, *44*, 7506-7510.

Zhang, G.; Song, I. Y.; Ahn, K. H.; Park, T.; Choi, W. *Macromolecules*, **2011**, *44*, 7594-7599.

Zhang, L.; Xue, H.; Gao, C. L.; Carr, L.; Wang, J. N.; Chu, B. C.; Jiang, S. Y. *Biomaterials* **2010**, *31*, 6582-6588.

Zhang, M.; Akbulut, M. *Langmuir* **2011**, *27*, 12550-12559.

Zheng, X.; Yue, M.; Yang, P.; Li, Qi, Yang, W. *Polym. Chem.* **2012**, *3*, 1982-1986.

Zhou, H.; Johnson, J. A. *Angew. Chem. Int. Ed.* **2013**, *52*, 2235-2238.

Zhou, J.; Qiao, X.; Binks, B. P.; Sun, K.; Bai, M.; Li, Y.; Liu, Y. *Langmuir* **2011**, *27*, 3308–3316.

Zhu, L.; Yan, H.; Ang, C. Y.; Nguyen, K. T.; Li, M.; Zhao, Y. *Chem. Eur. J.* **2012**, *18*, 13979-13983.

Vita

Bethany M. Neilson was born in Fort Worth, TX where she developed an early interest in chemistry while working in labs of Prof. Patty Wisian-Neilson at Southern Methodist University and Robert Neilson at Texas Christian University. She earned a B.S. degree in chemistry in 2008 from Duke University in Durham, NC. While at Duke, she was fortunate to conduct research in novel stimuli-responsive materials under the guidance of Prof. Stephen Craig. In the fall of 2008 she moved back to Texas and matriculated into the chemistry Ph.D. program at the University of Texas at Austin, where she joined Prof. Christopher Bielawski's research group. Her graduate research focused on the development of novel photoswitchable catalysts, as well as the synthesis of functional co-polymers and nanoparticles for oil-field applications. She is currently a chemist at the Dow Chemical Company.

Permanent address (or email): bneilson@cm.utexas.edu

This dissertation was typed by the author.